Metallic quantum ferromagnets

M. Brando[*]

Max Planck Institute for Chemical Physics of Solids, Nöthnitzer Strasse 40, D-01187 Dresden, Germany

D. Belitz[†]

Department of Physics, and Institute of Theoretical Science, and Materials Science Institute, University of Oregon, Eugene, Oregon 97403, USA

F. M. Grosche[‡]

University of Cambridge, Cavendish Laboratory, CB3 0HE Cambridge, United Kingdom

T. R. Kirkpatrick[§]

Institute for Physical Science and Technology, and Department of Physics, University of Maryland, College Park, Maryland 20742, USA

(published 31 May 2016; corrected 22 June 2016)

An overview of quantum phase transitions (QPTs) in metallic ferromagnets, discussing both experimental and theoretical aspects, is given. These QPTs can be classified with respect to the presence and strength of quenched disorder: Clean systems generically show a discontinuous, or first-order, QPT from a ferromagnetic to a paramagnetic state as a function of some control parameter, as predicted by theory. Disordered systems are much more complicated, depending on the disorder strength and the distance from the QPT. In many disordered materials the QPT is continuous, or second order, and Griffiths-phase effects coexist with QPT singularities near the transition. In other systems the transition from the ferromagnetic state at low temperatures is to a different type of long-range order, such as an antiferromagnetic or a spin-density-wave state. In still other materials a transition to a state with glasslike spin dynamics is suspected. The review provides a comprehensive discussion of the current understanding of these various transitions and of the relation between experiment and theory.

DOI: 10.1103/RevModPhys.88.025006

CONTENTS

I. Introduction 2
A. General remarks on quantum phase transitions 3
B. Quantum ferromagnetic transitions in metals 4
II. Experimental Results 6
A. General remarks 6
B. Systems showing a discontinuous transition 7
1. Transition-metal compounds 7
a. MnSi 7
b. $ZrZn_2$ 8
c. CoS_2 9
d. Ni_3Al 10
2. Uranium-based compounds 10
a. UGe_2 10
b. U_3P_4 11
c. URhGe and UCoGe 11
d. UCoAl 12
e. URhAl 13
3. Lanthanide-based compounds 14
a. $La_{1-x}Ce_xIn_2$ 14
b. $SmNiC_2$ 14
c. Yb-based systems 14
d. CePt 14
4. Strontium ruthenates 14
a. $Sr_{1-x}Ca_xRuO_3$ (bulk ceramic samples) 14
b. $Sr_3Ru_2O_7$ 15
5. Discussion, and comparison with theory 15
C. Systems showing a continuous transition 16
1. Weakly disordered systems 16
a. Ni_xPd_{1-x} 16
b. $Ni_3Al_{1-x}Ga_x$ and $(Ni_{1-x}Pd_x)_3Al$ 17
c. UIr 18
d. $UNiSi_2$ 19
e. $(Cr_{1-x}Fe_x)_2B$ 19
f. $Zr_{1-x}Nb_xZn_2$ 19
g. $Sr_{1-x}Ca_xRuO_3$ (bulk powder samples) 20
h. $SrCo_2(Ge_{1-x}P_x)_2$ 20
i. $CeSi_x$ 20
j. $CePd_{1-x}Ni_x$ 21
k. $(Sc_{1-x}Lu_x)_{3.1}In$ 21
l. $U_4Ru_7Ge_6$ and $U_4(Ru_{1-x}Os_x)_7Ge_6$ 21
2. Strongly disordered systems 21
a. $LaV_xCr_{1-x}Ge_3$ 21

[*]brando@cpfs.mpg.de
[†]dbelitz@uoregon.edu
[‡]fmg12@cam.ac.uk
[§]tedkirkp@umd.edu

 © 2016 American Physical Society

b. $URu_{2-x}Re_xSi_2$ 21
c. $URh_{1-x}Ru_xGe$ 22
d. $UCo_{1-x}Fe_xGe$ 22
e. $Th_{1-x}U_xCu_2Si_2$ 22
3. Quasi-one-dimensional systems 22
a. $YbNi_4P_2$ 22
b. $YbNi_4(P_{1-x}As_x)_2$ 23
4. Discussion, and comparison with theory 23
D. Systems changing to spin-density-wave or antiferromagnetic order 24
1. Simple ferromagnets 24
a. An itinerant magnet: $Nb_{1-y}Fe_{2+y}$ 24
b. An induced-moment magnet: PrPtAl 25
2. Ferromagnetic Kondo-lattice systems: CeTPO 26
a. CeRuPO 26
b. $CeFeAs_{1-x}P_xO$ 27
c. $CeRu_{1-x}Fe_xPO$ 28
3. Other Kondo-lattice systems 29
a. $CeAgSb_2$ 29
b. $CeRu_2Ge_2$ and $CeRu_2(Ge_{1-x}Si_x)_2$ 29
c. $YbRh_2Si_2$ and $Yb(Rh_{1-x}Co_x)_2Si_2$ 30
4. Discussion, and comparison with theory 31
E. System showing glasslike behavior, short-range order, or other strong-disorder effects 31
1. Systems with glasslike features 32
a. $CePd_{1-x}Rh_x$ 32
b. $CePt_{1-x}Rh_x$ 34
c. $Ni_{1-x}V_x$ 34
d. $UNi_{1-x}Co_xSi_2$ 34
2. Other systems showing effects of strong disorder 35
a. $U_{1-x}Th_xNiSi_2$ 35
b. $CeTi_{1-x}V_xGe_3$ 35
3. A thin-film system: $Sr_{1-x}Ca_xRuO_3$ (thin-film samples) 36
4. A system showing short-range order: CeFePO 36
5. Discussion and comparison with theory 37
III. Theoretical Results 37
A. Soft modes in metals 37
1. Why we should care about soft modes 37
2. Goldstone modes in metals 39
a. Goldstone modes in a Fermi gas 39
b. Goldstone modes in a Fermi liquid 40
c. Goldstone modes in a disordered Fermi liquid: Diffusons 41
B. Effects of fermionic soft modes: Simple physical arguments 41
1. Renormalized Landau theory 41
2. Clean systems 42
3. Disordered systems 43
C. Effects of order-parameter fluctuations, and comparison with experiment 45
1. Coupled field theory for soft modes 45
2. Clean systems 45
a. Hertz's action, and relation to spin-fluctuation theory 46
b. Scaling analysis of the preasymptotic regime 47
c. First- and second-order transitions, tricritical behavior, and quantum-critical points 48
d. Quantum-critical points at the wing tips 49
e. Comparison with experiment 49
3. Disordered systems 49
a. Effective soft-mode action 50
b. Hertz's action 50
c. Fixed-point action 51
d. Fixed points, and their stability 51
e. Asymptotic critical behavior 52
f. Preasymptotic behavior 53
g. Summary of critical exponents in the disordered case 54
h. Relation to experiment 54
4. Exponent relations 54
D. Rare-region effects in disordered systems 54
1. Quantum Griffiths effects 54
2. Disordered local moments 56
3. Interacting rare regions 56
4. The size of Griffiths effects 57
E. Textured phases as a way to avoid a quantum-critical point 58
F. Other mechanisms for a first-order transition 58
1. Band-structure effects 58
2. Magnetoelastic effects 58
a. Classical magnets 59
b. Quantum magnets 59
IV. Summary, Discussion, and Outlook 59
A. Summary and discussion 59
B. Open problems 61
Acknowledgments 63
Appendix A: List of Acronyms 63
Appendix B: Definitions of Critical Exponents 63
References 63

I. INTRODUCTION

Metallic ferromagnets have been studied since ancient times, as this class of materials includes elemental iron, which gave ferromagnetism its name. Detailed studies in the early 1900s led to one of the first examples of mean-field theory (Weiss, 1907). A more elaborate mean-field theory by Stoner (1938) explained how a nonzero magnetization can arise from a spontaneous splitting of the conduction band. When it became clear, 30 years later, that mean-field theory does not correctly describe the behavior close to the phase transition, ferromagnetism became one of the testing grounds for the theory of critical phenomena (Stanley, 1971; Wilson and Kogut, 1974). More recently metallic ferromagnets with low Curie temperatures, ranging from tens of degrees to a few degrees, or even lower, have attracted much attention. Many of these materials allow for decreasing the Curie temperature even further, by applying pressure or by changing the chemical composition. This makes possible the study of the quantum phase transition (QPT) that occurs at zero temperature and for fundamental reasons must be quite different in nature from the thermal phase transition observed at a nonzero Curie temperature. Over the years it again became clear that the quantum version of mean-field theory does not correctly describe the behavior close to the transition, contrary to early suggestions.

This review summarizes the experimental and theoretical understanding of this quantum phase transition. Our discussion of experimental results is restricted to materials where an instability of a ferromagnetic phase at low temperatures is clearly observed and reasonably well characterized. In parallel to this discussion we describe the relevant theoretical ideas and the extent to which they explain, and in some cases predict, the experimental observations. In this section we start

with some general remarks about quantum phase transitions and then turn to the one in metallic ferromagnets.

A. General remarks on quantum phase transitions

QPTs have been discussed for many years and remain a subject of great interest (Hertz, 1976; Sachdev, 1999). Whereas classical or thermal phase transitions occur at a nonzero transition temperature and are driven by thermal fluctuations, QPTs occur at zero temperature, $T = 0$, as a function of some nonthermal control parameter (typical examples are pressure, composition, or an external magnetic field) and are driven by quantum fluctuations. The ways in which the description of QPTs differs from that of their classical counterparts are subtle and took a long time to understand. Early on it was realized that at a mean-field level the description is the same for both quantum and classical phase transitions. Indeed, the earliest theory of a QPT was the Stoner theory of ferromagnetism (Stoner, 1938). Stoner considered the case of itinerant ferromagnets, where the conduction electrons are responsible for the ferromagnetism,[1] and developed a mean-field theory that describes both the classical and the quantum ferromagnetic transition.

Important mathematical developments were the Trotter formula (Trotter, 1959), and the coherent-state formalism (Casher, Lurié, and Revzen, 1968), which proved useful for representing the partition function of quantum spin systems in terms of a functional integral (Suzuki, 1976a, 1976b). It implied, at least for certain spin models, that a quantum phase transition in a system with d spatial dimensions could be described in terms of the corresponding classical phase transition in an effective dimension $d_{\text{eff}} = d + 1$. An example is the Ising model in a transverse field (DeGennes, 1963; Stinchcombe, 1973). The crucial observation was that the functional-integral representation of the partition function contains an integration over an auxiliary variable (usually referred to as imaginary time) that extends from zero to the inverse temperature $1/T$. At $T = 0$, this integration range becomes infinite and mimics an additional spatial integration in the thermodynamic limit. If space and time scale in the same way, then $d_{\text{eff}} = d + 1$ follows. For the classical Ising model, in particular, the upper critical dimension, above which mean-field theory provides an exact description of the transition, is $d_c^+ = 4$. It follows that the critical behavior of the quantum Ising model in a transverse field in $d > 3$ is mean field like (Suzuki, 1976a). More generally, the statics and the dynamics are intrinsically coupled at QPTs, unlike the case of classical phase transitions, where the dynamic critical phenomena are decoupled from the statics (Ferrell *et al.*, 1967, 1968; Halperin and Hohenberg, 1967, 1969; Hohenberg and Halperin, 1977).

This leads to the following general point: For classical critical phenomena, the dynamic universality classes are much smaller (and therefore more numerous) than the static ones. Physically, this is due to the fact that the order-parameter fluctuations that determine the universality class can be conserved (such as in, e.g., a ferromagnet) or nonconserved (such as in, e.g., an antiferromagnet), and they can couple to any number of other slow or soft modes or excitations, with each of these cases realizing a different universality class (Hohenberg and Halperin, 1977). By the same argument one expects quantum phase transitions in metals to be different from those in insulators because the respective dynamical processes are very different.[2]

Hertz (1976), in an important paper, among other things, generalized the Trotter-Suzuki formulation to the case where space and time do not scale the same way.[3] He showed that if the slow order-parameter time scale t_ξ at a continuous QPT diverges as $t_\xi \propto \xi^z$, with ξ the correlation length and z the dynamical scaling exponent (which in general is not equal to unity), then the imaginary-time integral is analogous to a spatial integration over an additional z spatial dimensions. For such a class of problems the critical behavior at the continuous QPT is equivalent to that at the corresponding classical transition in $d_{\text{eff}} = d + z$ dimensions. At this point it seemed that QPTs were, in fact, not fundamentally different from their classical counterparts. The statics and the dynamics couple, leading to an effective dimension different from the physical spatial dimension, and the number of universality classes is different, but the technical machinery that had been developed to solve the classical phase-transition problem (Wilson and Kogut, 1974; Ma, 1976; Fisher, 1983) could be generalized to treat QPTs as well and map them onto classical transitions in a different dimension.[4]

These considerations assume that the phase transition separates an ordered phase from a disordered one, with the ordered phase characterized by a local order parameter. For the ferromagnetic transition that is the subject of this review, this is indeed the case. It should be mentioned, however, that there are very interesting phase transitions, both classical and quantum, that do not allow for a description in terms of a local order parameter. One example is provided by spin liquids (Balents, 2010), others by the quantum Hall effects (von Klitzing, Dorda, and Pepper, 1980; Tsui, Stormer, and Gossard, 1982) and topological insulators (Hasan and Kane, 2010; Qi and Zhang, 2011). Other interesting cases are the Anderson and Anderson-Mott metal-insulator

[1]We refer to systems where the conduction electrons are the sole source of the magnetization as "itinerant ferromagnets," and to ones where part or all of the magnetization is due to localized spins as "localized-moment ferromagnets." The theory reviewed in Secs. III.B and III.C is valid for both.

[2]To date, no comprehensive classification of QPTs, at a level of the classification of classical critical dynamics given by Hohenberg and Halperin (1977), exists.

[3]Initially, mathematical results for specific spin models that yielded $z = 1$ had been applied more broadly than their validity warranted, which led to considerable confusion.

[4]There are important QPTs that have no classical analogs; examples include various metal-insulator transitions in disordered electron systems with or without the electron-electron interaction taken into account (Anderson, 1958; Finkelstein, 1984; Lee and Ramakrishnan, 1985; Kramer and MacKinnon, 1993; Belitz and Kirkpatrick, 1994; Evers and Mirlin, 2008). While they do not allow for a mapping onto a classical counterpart, their theoretical descriptions still use the same concepts that were developed for classical transitions.

transitions (see footnote [4]). It was proposed that for these transitions, and indeed for all QPTs, the von Neumann entanglement entropy S_e is a useful concept since it displays nonanalyticities characteristic of the QPT (Kopp, Jia, and Chakravarty, 2007). S_e tends to scale with the area of the subsystem rather than its volume and provides interesting connections between correlated electrons, quantum information theory, and the thermodynamics of black holes (Eisert, Cramer, and Plenio, 2010).

B. Quantum ferromagnetic transitions in metals

Hertz's prime example was the same as Stoner's, namely, an itinerant ferromagnet. Here the magnetization serves as an order parameter, and Hertz (1976) derived a dynamical Landau-Ginzburg-Wilson (LGW) functional for this transition by considering a model of itinerant electrons that interact only through a contact potential in the particle-hole spin-triplet channel. He analyzed this LGW functional by means of renormalization-group (RG) methods. He concluded that in this case the dynamical critical exponent has the value $z = 3$, and that the QPT for an itinerant Heisenberg ferromagnet hence maps onto the corresponding classical transition in $d_{\text{eff}} = d + 3$ dimensions. Since the upper critical dimension for classical ferromagnets is $d_c^+ = 4$, this seemed to imply that Stoner theory for the critical behavior was exact in the physical spatial dimensions $d = 2$ and 3. This in turn implied that the transition was generically continuous or second order, with mean-field static critical exponents. Preceding Hertz's work, Moriya and collaborators in the early 1970s had developed a description of itinerant quantum ferromagnets that one would now classify as a self-consistent one-loop theory [historically, it was often referred to as self-consistently renormalized (SCR) or spin-fluctuation theory]; this work was summarized by Moriya (1985). Millis (1993) used Hertz's RG framework to study the behavior at low but nonzero temperature and the crossover between the quantum and classical scaling behaviors. Most of the explicit results confirmed the earlier results of the spin-fluctuation theory. This combined body of work is often referred to as Hertz-Millis-Moriya or Hertz-Millis theory. We will discuss its basic features and results in Sec. III.C.2.

A related but separate line of investigations dealt with quantitative issues regarding the strength of the magnetism, and the properties of the ordered phase, in itinerant ferromagnets. It was realized early on that Stoner theory and its extension to finite temperature (Edwards and Wohlfarth, 1968) leaves key questions unanswered, especially for metals with low Curie temperatures T_C: First, why is the exchange energy, which can be extracted from band-structure probes or from careful analysis of the magnetic equation of state, typically at least an order of magnitude larger than $k_B T_C$? If the order was destroyed solely by a thermal smearing of the Fermi function, the two would be expected to be of similar magnitude. Second, why is the ordered moment in the low-temperature limit only a small fraction of the fluctuating moment as extracted from the Curie constant in the temperature dependent susceptibility? Third, why is the temperature dependence of the magnetization at low temperature proportional to T^2 rather than $T^{3/2}$, as would be expected from including spin-wave excitations?

The key to answering these questions, and to achieving a quantitative description of itinerant ferromagnets with low ordering temperatures, was to include the effect of fluctuations of the local magnetization, as demonstrated by Murata and Doniach (1972). More comprehensive models were developed in the 1970s by Moriya and collaborators (Moriya, 1985) in the spin-fluctuation-theory work already mentioned. As inelastic neutron scattering became feasible, which demonstrated the existence of magnetic fluctuations and allowed for their quantitative parametrization (Ishikawa *et al.*, 1982; Bernhoeft *et al.*, 1983), it became possible to accurately model key material properties such as T_C, the low-temperature ordered moment, and its temperature dependence, as well as the temperature dependence of the magnetic susceptibility and the associated fluctuating moment, in a further development of the SCR spin-fluctuation approach (Lonzarich and Taillefer, 1985).

Returning to the statistical-mechanics description of the phase transition itself, a key result of both the SCR theories and Hertz's RG description of clean metallic ferromagnets was the value of the dynamical exponent $z = 3$. This can be made plausible independent of the technical details of Hertz's theory, and, more importantly, independent of whether or not the conduction electrons themselves are responsible for the magnetism. In the absence of soft modes other than the order-parameter fluctuations, the bare order-parameter susceptibility χ_{OP} at criticality as a function of the frequency ω and the wave number k has the form (Hohenberg and Halperin, 1977)

$$\chi_{\text{OP}}^{-1}(k,\omega) = -i\omega/\gamma + k^2, \tag{1.1a}$$

if the order parameter is not a conserved quantity, or

$$\chi_{\text{OP}}^{-1}(k,\omega) = -i\omega/\lambda k^2 + k^2, \tag{1.1b}$$

if it is, with γ and λ kinetic coefficients. At $T > 0$, or at $T = 0$ in the presence of quenched disorder, γ and λ are weakly k dependent and approach constants as $k \to 0$. However, in clean systems at $T = 0$ these coefficients do not exist in the limit of zero frequency and wave number, and in metallic systems their effective behavior is $\gamma \propto \lambda \propto 1/k$. For a nonconserved order parameter this leads to $z = 1$, as in the case of a quantum antiferromagnet (Chakravarty, Halperin, and Nelson, 1989), or an Ising model in a transverse field (Suzuki, 1976a). For a ferromagnet, where the order parameter is conserved, we find from Eq. (1.1b) $z = 3$ in the clean case, and $z = 4$ in the disordered case. This is consistent with Hertz's explicit calculation for a specific model. Equations (1.1) do not get qualitatively changed by renormalizations, provided $d_{\text{eff}} = d + z$ is greater than the upper critical dimension: The coupling between the statics and the dynamics ensures that the critical exponent[5] η is zero and the exponents in Eqs. (1.1) remain unchanged. Simple mean-field arguments, including Eqs. (1.1), are therefore self-consistently valid for all $d > d_c^+ - z$, the static critical behavior is mean field like, and the dynamical critical exponent is the one that follows from Eqs. (1.1). However, all of these considerations are valid only under the assumption that there are no other soft modes that couple to the order parameter. In metallic

[5]For a definition of critical exponents, see Appendix B.

ferromagnets this assumption is not valid as explained in detail in Sec. III.

The experimental situation through the 1990s was confusing: In some materials a second-order transition was observed, but many others showed a first-order transition. Within mean-field theory, the standard explanation for a first-order transition is that the coefficient of the quartic term in the Landau expansion happens to be negative (Landau and Lifshitz, 1980). While this can always be the case in some specific materials, for reasons related to the band structure, there is no reason to believe that it will be the case in whole classes of materials. A much more general mechanism for a first-order transition was proposed in 1999, when two of the present authors, together with Thomas Vojta, showed theoretically that the QPT in two-dimensional and three-dimensional metallic systems from a paramagnetic (PM) phase to a homogeneous ferromagnetic one is generically first order, provided the material is sufficiently clean (Belitz, Kirkpatrick, and Vojta, 1999, referred to as BKV). The physical reason underlying this universal conclusion is a coupling of the magnetization to electronic soft modes that exist in any metal, which leads to a fluctuation-induced first-order transition. The same conclusion was reached by other groups (Chubukov, Pépin, and Rech, 2004; Maslov, Chubukov, and Saha, 2006; Rech, Pépin, and Chubukov, 2006). This theoretical work was later generalized to include the effects of an external magnetic field, which leads to tricritical wings in the phase diagram (Belitz, Kirkpatrick, and Rollbühler, 2005). Since the role of the electronic soft modes diminishes with increasing temperature, this theory predicts that in clean systems there necessarily exists a tricritical point in the phase diagram, i.e., a temperature that separates a line of first-order transitions at low temperatures from a line of second-order transitions at higher temperatures as the control parameter is varied. In addition, BKV showed that nonmagnetic quenched disorder suppresses the tricritical temperature, and that the transition remains second order down to zero temperature if the disorder strength exceeds a critical value.

An important generalization of the theory was the realization that it is equally valid for localized-moment ferromagnets as for itinerant ones (Kirkpatrick and Belitz, 2012a); the previous focus on itinerant magnets was historically rooted and not necessary. In addition, it applies to systems where the magnetic order is ferrimagnetic (Kirkpatrick and Belitz, 2012a) or magnetic nematic (Kirkpatrick and Belitz, 2011) rather than ferromagnetic.

Many experiments are consistent with these predictions, and over time experiments on cleaner samples, or at lower temperatures, or both, showed a first-order transition even in cases where previously a continuous transition had been found. The predicted tricritical point and associated tricritical wings have also been observed in many systems. For a representative example of this type of phase diagram, showing a tricritical point (TCP), the tricritical wings, and "quantum critical end points" (QCEPs)[6] at the wing tips, see Fig. 1.

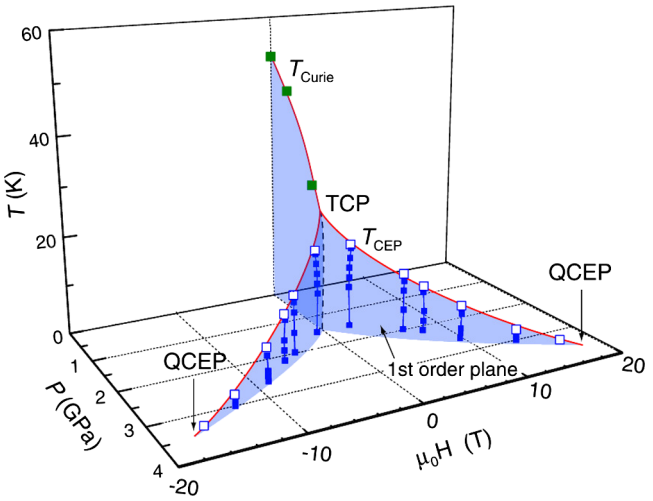

FIG. 1. Observed phase diagram of UGe_2 in the space spanned by temperature (T), pressure (P), and magnetic field (H). Solid red curves represent lines of second-order transitions, and blue planes represent first-order transitions. Also shown are the tricritical point (TCP), and the extrapolated "quantum-critical end points" (QCEP) at the wing tips. From Kotegawa, Taufour *et al.*, 2011.

Strongly disordered materials, on the other hand, almost always show a continuous transition, also in agreement with the theoretical prediction. There are, however, exceptions from these general patterns, which are discussed in Sec. II.C.1.

These predictions and observations are for systems where the transition is to a homogeneous ferromagnetic state; the schematic phase diagrams for the discontinuous and continuous cases, respectively, are shown in Figs. 2(a) and 2(b). In other materials, magnetic order of a different kind is found to compete with homogeneous ferromagnetism at low temperatures, as schematically illustrated in Fig. 2(c). In strongly disordered systems, spin-glass freezing and quantum Griffiths effects may occur at low temperatures and augment or compete with critical behavior; see Fig. 2(d). These effects are discussed in detail in Secs. II.D, II.E, III.D, and III.E.

The striking difference between the predictions of BKV and Hertz theory is due to a coupling of the order-parameter fluctuations to electronic degrees of freedom. Hertz theory treats this coupling in too simple an approximation to capture all of its qualitative effects. In metals at $T = 0$ there are soft or gapless two-fermion excitations that couple to the magnetic order-parameter fluctuations in important ways. In effect, the combined fermionic and bosonic (order-parameter) fluctuations determine the quantum universality class in all spatial dimensions $d < 3$. As a result of this coupling, the upper critical dimension is $d_c^+ = 3$, rather than $d_c^+ = 1$ as predicted by Hertz theory, and the transition is first order, rather than continuous with mean-field exponents. The mechanism behind this phenomenon is similar to what is known as a fluctuation-induced first-order transition in classical phase transitions (Halperin, Lubensky, and Ma, 1974; Chen, Lubensky, and Nelson, 1978), but it is different in at least one crucial way; cf. Secs. III.B.2 and IV.A. Two well-known classical examples of a fluctuation-induced first-order transition are the superconducting Bardeen-Cooper-Schrieffer

[6]A critical end point (CEP) is defined as a point where a line of second-order transitions terminates at a line of first-order transitions, with the first-order line continuing into an ordered region; see, e.g., Chaikin and Lubensky (1995) and references therein. In the recent literature the term CEP is often misused.

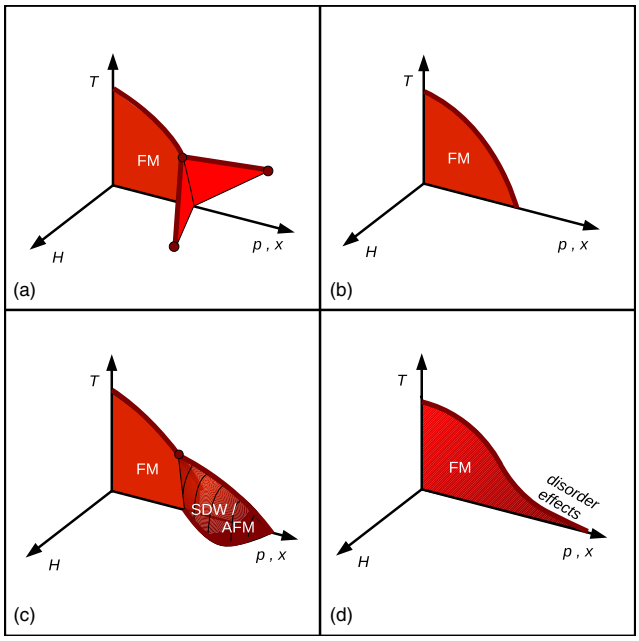

FIG. 2. Schematic phase diagrams observed in ferromagnetic (FM) systems that show, at the lowest temperatures realized, (a) a discontinuous transition and tricritical wings in a magnetic field, (b) a continuous transition, (c) a change to spin-density-wave (SDW) or antiferromagnetic (AFM) order, and (d) a continuous transition in strongly disordered systems that may be accompanied by quantum Griffiths effects or spin-glass freezing in the tail of the phase diagram.

transition, and the nematic-to-smectic-*A* transition in liquid crystals.[7]

We now add some remarks about the relative strength of fluctuations at second-order and certain first-order transitions. At a second-order transition above the upper critical dimension, treating the fluctuations in a Gaussian approximation suffices to obtain the exact critical behavior; this is what Hertz theory concluded for the ferromagnetic QPT. At a critical point below the upper critical dimension this is not true; fluctuations are strong enough to modify the critical exponents, although they do not change the continuous nature of the transition. At a fluctuation-induced first-order transition, the combined effects of order-parameter fluctuations and other soft modes are so strong that they change the order of the transition predicted by mean-field theory.[8] The prediction of BKV was that this will happen at the ferromagnetic QPT in clean systems.

[7]In liquid crystals it took a long time until the weakly first-order transition was observed (Anisimov *et al.*, 1990). We discuss in Secs. III.B.2 and IV.A why the fluctuation-induced first-order transition in quantum ferromagnets is so much more robust.

[8]It is often thought that at first-order transitions, as opposed to second-order ones, fluctuations are not important. In the case of a fluctuation-induced first-order transition this notion is obviously misleading. Less obviously, all first-order transitions can be understood as a limiting case of second-order transitions where the critical exponents (including $\beta = 0$) can be determined exactly (Nienhuis and Nauenberg, 1975; Fisher and Berker, 1982).

The continuous quantum ferromagnetic transition in disordered metals, in systems where the disorder is strong enough to suppress the tricritical temperature to zero, has also been studied in detail theoretically (Kirkpatrick and Belitz, 1996; Belitz *et al.*, 2001a, 2001b). In this case the itinerant electrons are moving diffusively, rather than ballistically. Because this is a slower process, there is an effective enhancement of the exchange interaction that causes ferromagnetism, and some crucial signs are changed compared to the clean case. The net result is that the second-order transition predicted by Hertz theory becomes, so to speak, even more continuous by the coupling to the electronic soft modes: For example, the theory predicts that in $d = 3$ the critical exponent (see footnote [5]) β is equal to 2, compared to $\beta = 1/2$ in Hertz theory.[9] This large value of β may give the impression of a "smeared transition," even though there still is a sharp critical point. This, as well as the predicted values of other exponents, is consistent with numerous experiments in disordered systems, as we will discuss. In related developments, much work has been done on Griffiths singularities and Griffiths phases in disordered metallic magnets. Depending on the nature and symmetry of the order parameter, these theories predict that in some systems the Griffiths-phase effects are very weak, while in others they lead to strong power-law singularities with continuously varying exponents, and in yet others they completely destroy the sharp quantum phase transition [for a review, see Vojta (2010)]. If these effects are important, they will be superimposed on the critical behavior.

Finally, there are theories that suggest that in some metallic systems an inhomogeneous magnetic phase may form in between the paramagnetic and the homogeneous ferromagnetic state at low T. This was first suggested by Belitz, Kirkpatrick, and Vojta (1997), and has been explored in detail by others. Spiral phases, spin nematics, and spin-density waves have been proposed to appear between the uniform ferromagnet and the paramagnetic phase (Chubukov, Pépin, and Rech, 2004; Maslov, Chubukov, and Saha, 2006; Rech, Pépin, and Chubukov, 2006; Efremov, Betouras, and Chubukov, 2008; Chubukov and Maslov, 2009; Conduit, Green, and Simons, 2009; Karahasanovic, Krüger, and Green, 2012). We discuss these and related theories in Sec. III.E.

II. EXPERIMENTAL RESULTS

Here we discuss experimental results organized with respect to the observed phase diagrams as shown in Fig. 2.

A. General remarks

During the last two decades a large number of FM metals have been found that (1) have a low Curie temperature, and (2) can be driven across a ferromagnet-to-paramagnet QPT. The control parameter is often either hydrostatic pressure or uniaxial stress, but the transition can also be triggered by composition, or an external magnetic field. The initial motivation was to look for a ferromagnetic quantum-critical

[9]The asymptotic critical behavior in this case actually consists of power laws multiplied by log-normal terms; see Sec. III.C.3.

point (QCP), and possibly novel states of matter in its vicinity, as had been found in many antiferromagnetic (AFM) metals (Grosche *et al.*, 1996; Mathur *et al.*, 1998; Park *et al.*, 2006; von Löhneysen *et al.*, 2007; Gegenwart, Si, and Steglich, 2008). It soon became clear, however, that the FM case is quite different from the AFM one. Instead of displaying a quantum-critical point, many systems were found to undergo a first-order QPT, with a tricritical point in the phase diagram separating a line of second-order transitions at relatively high temperatures from a line of first-order transitions at low temperatures. In several of these materials the existence of a tricritical point was confirmed by the observation of tricritical wings upon the application of an external magnetic field H, as shown schematically in Fig. 2(a). Some systems, such as $ZrZn_2$, were initially reported to have a QCP, but with increasing sample quality the transition at low temperatures was found to be first order. The first-order transition occurs in a large variety of materials, including $3d$ transition metals as well as $4f$- and $5f$-electron systems; see Tables I and II. Some systems do show a continuous QPT to the lowest temperatures observed; see Tables III, IV, and V and Fig. 2(b). Several of these are either strongly disordered, as judged by their residual resistivities,[10] or their crystal structure makes them quasi one dimensional. Finally, the expectation of additional phases was borne out. In some systems the long-range order changes from ferromagnetic to modulated spin-density-wave (SDW) or AFM order [see Fig. 2(c)], and strongly disordered systems often show a spin-glass-like phase in the tail of the phase diagram; see Fig. 2(d). Accordingly, we distinguish four categories of metallic quantum ferromagnets, namely, (1) systems that display a first-order QPT; (2) systems that display, or are suspected to display, a QCP; (3) systems that undergo a phase transition to a different type of magnetic order before the FM quantum phase transition is reached; and (4) systems with spin-glass-like characteristics or other manifestations of strong disorder at low temperatures. This phenomenological classification, which is independent of the microscopical origin of the magnetism, is reflected in Fig. 2 and Tables I–VII. For each of these categories we discuss a number of representative materials in which the QPT has been reasonably well characterized. This list of materials is not exhaustive.

We also mention that superconductivity has been found to coexist with itinerant ferromagnetism in four U-based FM metals: UGe_2 (Saxena *et al.*, 2000), URhGe (Aoki *et al.*, 2001; Yelland *et al.*, 2011), UCoGe (Huy, Gasparini, Klaasse *et al.*, 2007), and UIr (Kobayashi *et al.*, 2006). While very interesting, this topic is outside the scope of this review and will be mentioned only in passing. For a related review, see Pfleiderer (2009). Another interesting class of materials that we do not cover are ferromagnetic semiconductors which have recently been reviewed by Jungwirth *et al.* (2006).

B. Systems showing a discontinuous transition

We first discuss systems in which there is strong evidence for a first-order transition at low temperatures. These include the transition-metal compounds MnSi and $ZrZn_2$, several uranium-based compounds, and some other materials; their properties are summarized in Tables I and II. The widespread pattern of first-order transitions near the QPT is consistent with fundamental arguments such as the BKV theory (Belitz, Kirkpatrick, and Vojta, 1999; Belitz, Kirkpatrick, and Rollbühler, 2005), which for clean ferromagnets predicted a first-order quantum phase transition at $T = 0$, a tricritical point in the phase diagram, and associated tricritical wings in an external magnetic field. This theory is reviewed in Sec. III, where we give a detailed discussion of the relation between theory and experiment.

1. Transition-metal compounds

a. MnSi

MnSi is a very well-studied material in which the search for a FM QCP resulted in the observation of a first-order quantum phase transition. The transition temperature at ambient pressure is $T_C \approx 29.5$ K,[11] and the application of hydrostatic pressure suppresses T_C to zero at a critical pressure $p_c \approx 14.6$ kbar (Pfleiderer, MeMullan, and Lonzarich, 1994; Pfleiderer *et al.*, 1997). This compound is actually a weak helimagnet (Ishikawa *et al.*, 1976) with a complicated phase diagram [see Mühlbauer *et al.* (2009) and references therein]. However, the long wavelength of the helix, about 180 Å, allows one to approximate the system as a ferromagnet. The helical order implies that the transition should be very weakly first order even at ambient pressure (Bak and Jensen, 1980). This has indeed been observed (Stishov *et al.*, 2007, 2008; Janoschek *et al.*, 2013).[12] Pfleiderer *et al.* (1997) found evidence of a strongly first-order transition for pressures $p^* < p < p_c$ with $p^* \approx 12$ kbar. The tricritical temperature (i.e., the transition temperature at $p = p^*$) is $T_{tc} \approx 12$ K.[13] These results were later corroborated by the observation of tricritical wings (Pfleiderer, Julian, and Lonzarich, 2001) (see Fig. 3), and by μSR data that show, for $p^* < p < p_c$, phase separation indicative of a first-order transition (Uemura *et al.*, 2007);

[10] We use the residual resistivity, denoted by ρ_0, as a measure of quenched disorder. We note that ρ_0 is a very rough and incomplete measure of disorder, that many transport theories make simple assumptions regarding the scattering process, and that relating the measured value of ρ_0 to theoretical considerations can therefore be difficult. Also, different manifestations of disorder may affect ρ_0 differently than they affect magnetism. This may be relevant for certain systems that are nominally rather clean, such as Ni_xPd_{1-x}; see Sec. II.C.1.a. Unfortunately, more extensive characterizations of disorder are rarely available.

[11] We denote the ferromagnetic transition temperature by T_C irrespective of the order of the transition. In parts of Sec. III, where we want to emphasize that a transition is second order, we denote the critical temperature by T_c.

[12] The first-order transition at ambient pressure was found by Janoschek *et al.* (2013) to be of a type that was first predicted by Brazovskiĭ (1975) for different systems. It differs slightly from the type predicted by Bak and Jensen (1980) for helical magnets.

[13] Since the transition is likely to be weakly first order for all $p < p^*$, the observed apparent tricritical point separates a very weakly first-order transition from one that is more strongly first order.

TABLE I. Systems showing a first-order transition I: transition-metal and uranium-based compounds. FM = ferromagnetism, SC = superconductivity, T_C = Curie temperature, T_{tc} = tricritical temperature, ρ_0 = residual resistivity, and n.a. = not available.

System	Order of transition[a]	T_C/K[b]	Magnetic moment/μ_B[c]	Tuning parameter	T_{tc}/K	Wings observed	Disorder[d] ($\rho_0/\mu\Omega$cm)	Comments
MnSi	1st[1,2]	29.5[3]	0.4[3]	Pressure[1]	≈10[e,1]	Yes[4]	0.33[4]	Weak helimagnet[5,6]
$ZrZn_2$	1st[7]	28.5[7]	0.17[7]	Pressure[7]	≈5[7]	Yes[7]	≥0.31[8]	Long history[9]
CoS_2	1st[10,11]	122[10]	0.84[12]	Pressure[10]	≈118[10]	(Yes)[f]	0.2–0.6[13]	High T_C and T_{tc}
Ni_3Al	(1st?)[g]	41–15[h]	0.075[i]	Pressure[14]	n.a.	No	0.84[15]	First-order transition suspected
UGe_2	1st[16,17]	52[18]	1.5[18]	Pressure[18,19]	24[20]	Yes[18,20]	0.2[19]	Easy-axis FM coex. FM + SC[19]
U_3P_4	1st[21]	138[22]	1.34[j, 23]	Pressure[21]	32[21]	Yes[k, 21]	4[l, 21]	Canted easy-axis FM
URhGe	1st[17,24]	9.5[25]	0.42[25]	$\perp B$ field[24,26]	≈1[24]	Yes[24]	8[27]	Easy-plane FM coex. FM + SC[25]
UCoGe	1st[17,28]	2.5[28]	0.03[29]	None	> 2.5?[m]	No	12[29]	Very weak FM coex. FM + SC[29]
UCoAl	1st[n, 30]	≈0[o, 30,31]	0[o,30,31]	Pressure[30,31]	> 11 K[30]	Yes[30]	24[30]	Easy-axis FM
URhAl	1st[33]	34 − 25[32,33]	≈0.9[32,33]	Pressure[33]	≈11[33]	Yes[33]	≈65[33]	Weakly first order

[a]At the lowest temperature achieved.
[b]A single value of T_C at the default value of the tuning parameter (ambient pressure, zero field) is given if T_{tc} has also been measured; a range of T_C for a range of control parameters in all other cases.
[c]Per formula unit unless otherwise noted.
[d]For the highest-quality samples.
[e]Disputed by Stishov *et al.* (2007); see the text.
[f]Metamagnetic behavior in first-order region indicative of wings.
[g]Suspected first-order transition near $p = 80$ kbar (Niklowitz *et al.*, 2005; Pfleiderer, 2007).
[h]For pressures $p = 0$–60 kbar.
[i]Per Ni at $p = 0$ (Niklowitz *et al.*, 2005).
[j]Per U.
[k]Via a metamagnetic transition; wings have not been mapped out.
[l]At the critical pressure $p_c \approx 4$ GPa.
[m]Pressure decreases T_C (Slooten *et al.*, 2009); TCP is not accessible. T_C increases nonmonotonically upon doping with Rh (Sakarya *et al.*, 2008); order of transition for $URh_xCo_{1-x}Ge$ not known except for $x = 1$ (second order with $T_C = 9.5$ K).
[n]Inferred from existence of tricritical wings.
[o]PM at zero pressure. Uniaxial pressure induces FM, so does doping; see Ishii *et al.* (2003) and references therein.

[1]Pfleiderer *et al.* (1997). [2]Uemura *et al.* (2007). [3]Ishikawa *et al.* (1985). [4]Pfleiderer, Julian, and Lonzarich (2001). [5]Ishikawa *et al.* (1976). [6]Mühlbauer *et al.* (2009). [7]Uhlarz, Pfleiderer, and Hayden (2004). [8]Sutherland *et al.* (2012). [9]Pfleiderer (2007). [10]Goto *et al.* (1997). [11]Goto, Fukamichi, and Yamada (2001). [12]Adachi, Sato, and Takeda (1969). [13]Sidorov, Krasnorussky *et al.* (2011). [14]Niklowitz *et al.* (2005). [15]Steiner *et al.* (2003). [16]Huxley *et al.* (2001). [17]Aoki, Hardy *et al.* (2011). [18]Kotegawa, Taufour *et al.* (2011). [19]Saxena *et al.* (2000). [20]Taufour *et al.* (2010). [21]Araki *et al.* (2015). [22]Trzebiatowski and Troć (1963). [23]Wiśniewski, Gukasov, and Henkie (1999). [24]Huxley *et al.* (2007). [25]Aoki *et al.* (2001). [26]Levy *et al.* (2005). [27]Miyake, Aoki, and Flouquet (2009). [28]Hattori *et al.* (2010). [29]Huy, Gasparini, de Nijs *et al.* (2007). [30]Aoki, Combier *et al.* (2011). [31]Ishii *et al.* (2003). [32]Veenhuizen *et al.* (1988). [33]Shimizu *et al.* (2015b).

see Fig. 4. Moreover, this has been confirmed by neutron Larmor diffraction experiments under pressure (Pfleiderer *et al.*, 2007). Conversely, data presented by Stishov *et al.* (2007), Petrova *et al.* (2009), and Petrova and Stishov (2012) suggest that the quantum phase transition at $p = p_c$ is either continuous or very weakly first order. Although the evidence for a pressure induced first-order transition appears convincing in the purest crystals, no agreement has been reached (Otero-Leal *et al.*, 2009a, 2009b; Stishov, 2009).

For $p < p_c$ the properties of MnSi are in good agreement with the SCR theory (Pfleiderer *et al.*, 1997). Specifically, $T_C^{4/3}$ is a linear function of the pressure. This agreement fails at $p \to p_c$ due to the presence of the first-order transition. Also, a striking $T^{3/2}$ power law for the resistivity was observed in a broad range of $p \gtrsim p_c$ (Pfleiderer *et al.*, 2001), where one would expect Fermi-liquid T^2 behavior. The physics behind this non-Fermi-liquid (NFL) behavior, which seems to be common in itinerant magnets near their QPT (cf. Sec. IV.B), is still unclear.

b. $ZrZn_2$

$ZrZn_2$ crystallizes in the cubic C15 structure and is a true ferromagnet (Matthias and Bozorth, 1958; Pickart *et al.*, 1964) with a small magnetic anisotropy and an ordered moment of $0.17\mu_B$ per formula unit (Uhlarz, Pfleiderer, and Hayden, 2004). The material can be tuned across the transition by means of hydrostatic pressure. While early experiments (Smith, Mydosh, and Wohlfarth, 1971; Huber, Maple, and Wohlleben, 1975; Grosche *et al.*, 1995) suggested the existence of a quantum-critical point, an increase in sample quality led to the realization that the transition becomes first order near the critical pressure $p_c \approx 16.5$ kbar (Uhlarz, Pfleiderer, and Hayden, 2004). The transition temperature at ambient pressure is $T_C \approx 28.5$ K, and the tricritical temperature is $T_{tc} \approx 5$ K. The phase diagram is qualitatively the same as that shown in Fig. 3; the observation of tricritical wings by Uhlarz, Pfleiderer, and Hayden (2004) confirmed an earlier suggestion by Kimura *et al.* (2004). The first-order nature of the QPT was confirmed by Kabeya *et al.* (2012, 2013), who also studied

TABLE II. Systems showing a first-order transition II: lanthanide-based compounds and strontium ruthenates. T_C = Curie temperature, T_{tc} = tricritical temperature, ρ_0 = residual resistivity, and n.a. = not available.

System	Order of transition[a]	T_C/K	Magnetic moment/μ_B[b]	Tuning parameter	T_{tc}/K	Wings observed	Disorder[c] ($\rho_0/\mu\Omega$cm)	Comments
$La_{1-x}Ce_xIn_2$	1st[1]	22–19.5[d,1]	n.a.	Composition[1]	>22?[e]	No	n.a.	Third phase?[1]
$SmNiC_2$	1st[2]	17–15[f,2]	0.32[2]	Pressure[2]	>17?	No	2	Other phases[2]
$YbCu_2Si_2$	1st[3]	$4.7-3.5$[g,3,2]	0.16–0.42[h,3]	Pressure[3,4,5]	n.a.	No	<0.5[6]	Strong Ising anisotropy[3]
$YbIr_2Si_2$	1st[7]	$2.3-1.3$[i]	n.a.	Pressure[7]	n.a.	No	≈22[j]	FM order suspected[7]
CePt	(1st?)[8]	$5.8-0$[9,8]	n.a.	Pressure[8]	n.a.	No	≈11[9]	First-order transition suspected
$Sr_{1-x}Ca_xRuO_3$	1st[10]	$160-0$[k]	$0.8-0$[k]	Composition[10]	n.a.	No	n.a.	Ceramic samples
$Sr_3Ru_2O_7$	1st[l]	0[m]	0[m]	Pressure[m]	n.a.	Yes[11]	<0.5[11]	Foliated wings, exotic phase[11]

[a]At the lowest temperature achieved.
[b]Per formula unit unless otherwise noted.
[c]For the highest-quality samples.
[d]For $x = 1.0$–0.9.
[e]First order for $x = 1$, TCP not accessible.
[f]For $p = 0$–2 GPa.
[g]For pressures $p \approx 11.5 - 9.4$ GPa.
[h]For pressures $p = 9.4$–11.5 GPa.
[i]For pressures $p \approx 10 - 8$ GPa.
[j]For a magnetic sample at pressures $p \approx 8$–10 GPa. Samples with ρ_0 as low as 0.3 $\mu\Omega$ cm at ambient pressure have been prepared (Yuan *et al.*, 2006).
[k]For $x = 0$ to $x \gtrsim 0.7$.
[l]Phase diagram not mapped out completely; the most detailed measurements show tips of wings. See Wu *et al.* (2011).
[m]Paramagnetic at ambient pressure. Hydrostatic pressure drives the system away from FM, and uniaxial stress drives it toward FM. See Wu *et al.* (2011) and references therein, especially Ikeda *et al.* (2000).

[1]Rojas *et al.* (2011). [2]Woo *et al.* (2013). [3]Tateiwa *et al.* (2014). [4]Winkelmann *et al.* (1999).
[5]Fernandez-Pañella *et al.* (2011). [6]Colombier *et al.* (2009). [7]Yuan *et al.* (2006). [8]Larrea *et al.* (2005).
[9]Holt *et al.* (1981). [10]Uemura *et al.* (2007). [11]Wu *et al.* (2011).

crossover phenomena above the tricritical wings. However, the transition is weakly first order and, for $p < p_c$, $ZrZn_2$ can be reasonably well understood within the SCR theory (Grosche *et al.*, 1995; Smith *et al.*, 2008). The resistivity exponent shows an abrupt change from 5/3 for $p < p_c$ to 3/2 at $p > p_c$ and remains 3/2 up to higher pressures (about 25 kbar). As in MnSi (Sec. II.B.1.a), this NFL behavior is not understood.

c. CoS_2

Cobalt disulphide crystallizes in a cubic pyrite structure. It is an itinerant ferromagnet with $T_C \approx 124$ K, an ordered moment of $0.84\mu_B$/Co, and an effective moment of $1.76\mu_B$/Co(Jarrett *et al.*, 1968; Adachi, Sato, and Takeda, 1969). Density-functional calculations concluded that CoS_2 is a half-metallic ferromagnet (Zhao, Callaway, and Hayashibara, 1993; Mazin, 2000). The spin polarization is high at about 56% (Wang, Chen, and Leighton, 2004), and the transport coefficients and the thermal expansion coefficient show unusual behavior in the vicinity of the transition (Yomo, 1979; Adachi and Ohkohchi, 1980). Magnetization measurements indicate that the transition is almost first order at ambient pressure (Wang, Chen, and Leighton, 2004). Hydrostatic pressure decreases T_C, and at a pressure of about 0.4 GPa the nature of the transition changes from second order to first order, with a tricritical temperature $T_{tc} \approx 118$ K (Goto *et al.*, 1997). A much lower value for the tricritical pressure was found by Otero-Leal *et al.* (2008); however, this analysis depended on a specific model equation of state. Sidorov, Krasnorussky *et al.* (2011) confirmed a strongly first-order QPT at a critical pressure of about 4.8 GPa. T_C is also suppressed if selenium is substituted for sulfur, and the transition again becomes first order at a small selenium concentration, with 1% of selenium roughly equivalent to a pressure of 1 GPa (Hiraka and Endoh, 1996).

Two groups have investigated the p-T phase diagram at higher pressures up to the QPT: Barakat *et al.* (2005) observed a monotonically decreasing T_C with increasing pressure. They inferred a first-order quantum phase transition at $p_c \approx 6$ GPa from a change of the temperature dependence of the resistivity $[\rho(T) = \rho_0 + AT^n]$ from $n = 2$ in the FM phase to $n \approx 1.6$ for $p > p_c$. Their samples had a residual resistivity $\rho_0 \approx 2$ $\mu\Omega$ cm and a residual resistance ratio (RRR) of about 60. Sidorov, Krasnorussky *et al.* (2011) performed experiments on a cleaner sample ($\rho_0 \approx 0.7$ $\mu\Omega$ cm) and concluded that $p_c = 4.8$ GPa. They found that the temperature dependence of the resistivity does not change across the transition, with $n = 2$ both below and above p_c, while the residual resistivity drops by about a factor of 3 as the transition is crossed.

These discrepancies notwithstanding, all experiments agree on the first-order nature of the quantum phase transition. This makes the phase diagrams of CoS_2, $ZrZn_2$, and MnSi qualitatively the same.

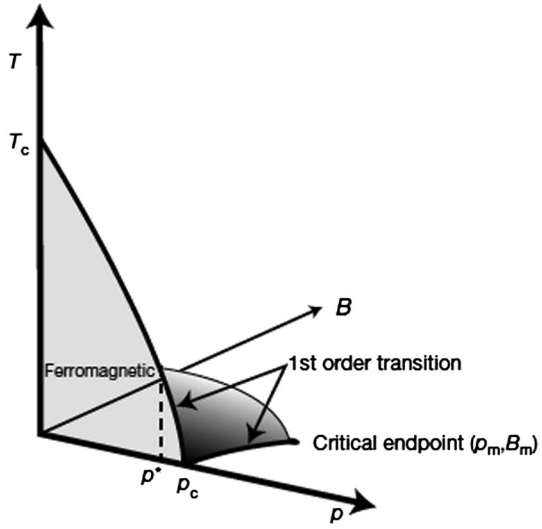

FIG. 3. Phase diagram of MnSi. In the temperature-pressure (T-p) plane the transition temperature drops from $T_C = 29.5$ K at ambient pressure and changes from second to first order at $p^* = 12$ kbar, where $T_C \approx 12$ K. T_C vanishes at $p_c = 14.6$ kbar. In the magnetic field, pressure (B-p) plane at $T = 0$, and everywhere across the shaded wing, the transition is first order up to a "critical end point" (see footnote [6]) estimated to be located at $B_m = 0.6$ T and $p_m = 17$ kbar. From Pfleiderer, Julian, and Lonzarich, 2001.

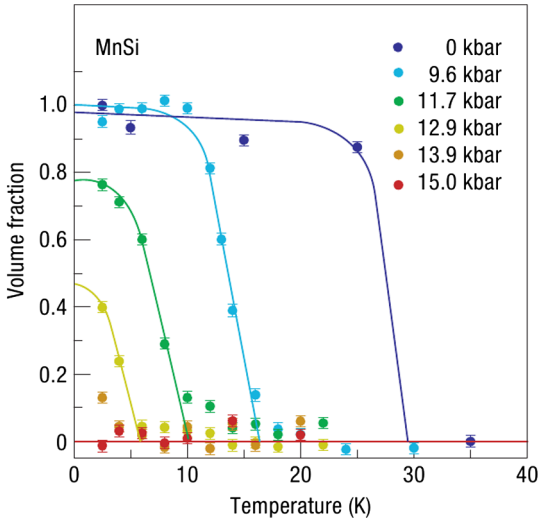

FIG. 4. μSR results for the volume fraction with static magnetic order. The nonzero volume fraction less than unity at $T = 0$ for intermediate pressures indicates phase separation, which in turn is indicative of a first-order transition. From Uemura *et al.*, 2007.

d. Ni_3Al

Ni_3Al crystallizes in the simple cubic Cu_3Au structure. Its magnetic properties depend on the exact composition; the stoichiometric compound at ambient pressure is a ferromagnet with $T_C = 41$ K and a small ordered moment of $0.075\mu_B$/Ni (de Boer *et al.*, 1969; Niklowitz *et al.*, 2005). T_C decreases upon the application of hydrostatic pressure and vanishes at a critical pressure of 8.1 GPa (Niklowitz *et al.*, 2005). The resistivity of stoichiometric Ni_3Al shows a pronounced NFL temperature dependence on either side of the transition, $\Delta\rho \propto T^n$, with n somewhere between 3/2 and 5/3 (Fluitman *et al.*, 1973; Steiner *et al.*, 2003; Pfleiderer, 2007). At ambient pressure and in zero magnetic field Steiner *et al.* (2003) found $n = 1.65$ for temperatures between about 0.5 and 3.5 K. The prefactor is comparable with that of the $T^{3/2}$ behavior of the resistivity in $ZrZn_2$ (Pfleiderer *et al.*, 2001; Yelland *et al.*, 2005).

The transition at ambient pressure is second order, and the overall form of the phase diagram is consistent with the results of the spin-fluctuation theory described in Sec. III.C.2, as is the logarithmic temperature dependence of the specific heat (Sato, 1975; Niklowitz *et al.*, 2005; Yang *et al.*, 2011). However, studies of the temperature dependence of the resistivity under pressure suggest that the QPT at the critical pressure is first order (Niklowitz *et al.*, 2005; Pfleiderer, 2007). This is analogous to the behavior of MnSi; see Sec. II.B.1.a.

T_C also decreases upon doping Ni_3Al with Pd (Sato, 1975) or Ga (Yang *et al.*, 2011); these systems are discussed in Sec. II.C.1.b.

2. Uranium-based compounds

Ferromagnetism with a first-order transition at low temperatures has been observed in the uranium-based heavy-fermion (HF) compounds UGe_2 (Huxley, Sheikin, and Braithwaite, 2000; Taufour *et al.*, 2010; Kotegawa, Taufour *et al.*, 2011), URhGe (Huxley *et al.*, 2007), and UCoGe (Hattori *et al.*, 2010). UCoAl is paramagnetic at ambient pressure, but very close to a first-order QPT (Aoki, Combier *et al.*, 2011). The ferromagnetism is due to $5f$ electrons. The extent to which these electrons are localized or itinerant, and the consequences for neutron scattering observations, have been investigated in some detail (Yaouanc *et al.*, 2002; Fujimori *et al.*, 2012; Chubukov, Betouras, and Efremov, 2014). Coexistence of ferromagnetism and superconductivity was found in UGe_2 (Saxena *et al.*, 2000; Huxley *et al.*, 2001), URhGe (Aoki *et al.*, 2001), and UCoGe (Huy, Gasparini, de Nijs *et al.*, 2007); for a recent overview, see Aoki and Flouquet (2014).

a. UGe_2

UGe_2 crystallizes in an inversion-symmetric orthorhombic structure, and the best samples have residual resistivities as low as 0.2 $\mu\Omega$ cm (Saxena *et al.*, 2000). Taufour *et al.* (2010) found the residual resistivity to be strongly pressure dependent. The Curie temperature at ambient pressure is $T_C \approx 52$ K (Saxena *et al.*, 2000; Aoki *et al.*, 2001; Huxley *et al.*, 2001; Aoki and Flouquet, 2012). T_C decreases with increasing hydrostatic pressure and vanishes at $p \approx 16$ kbar, which coincides with the pressure where the superconductivity disappears. Within the ferromagnetic phase a further transition is observed, across which the magnitude of the magnetic moment changes discontinuously. The associated transition line starts near the peak in the superconducting transition temperature, ends at a critical point at a temperature of about 4 K, and is replaced by a crossover at higher temperatures (Huxley *et al.*, 2007; Taufour *et al.*, 2010); see Fig. 5. The tricritical temperature has been measured to be $T_{tc} \approx 24$ K

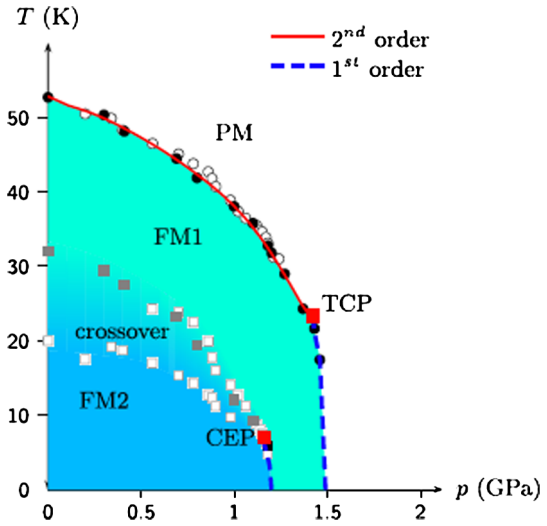

FIG. 5. Phase diagram of UGe_2 in the temperature-pressure plane. Shown are the paramagnetic (PM) phase, two ferromagnetic phases (FM1 and FM2), and the tricritical point (TCP). The critical point marked CEP (see footnote [6]) is related to the transition between the phases FM1 and FM2. From Taufour *et al.*, 2010.

(Taufour *et al.*, 2010; Kotegawa, Taufour *et al.*, 2011), but values as high as $T_{tc} \approx 31$ K have been reported (Huxley *et al.*, 2007) with a tricritical pressure $p_{tc} \approx 13$ kbar. Kabeya *et al.* (2010) found a somewhat smaller value of ≈12.5 kbar from measurements of the linear thermal expansion coefficient. The tricritical wings have been mapped out in detail; see Fig. 1.

b. U_3P_4

U_3P_4 at ambient pressure is a ferromagnet with $T_C = 138$ K (Trzebiatowski and Troć, 1963). It crystallizes in a bcc structure with no inversion symmetry, and the magnetic structure is canted with a FM component along ⟨111⟩ (Heimbrecht, Zumbusch, and Biltz, 1941; Zumbusch, 1941; Burlet *et al.*, 1981; Wiśniewski, Gukasov, and Henkie, 1999). Pressure reduces T_C until a QPT is reached at $p_c \approx 4$ GPa. From measurements of the resistivity and the magnetic susceptibility at $p \approx 1.5$ GPa, Araki *et al.* (2015) concluded that the transition changes from second order to first order with a tricritical temperature $T_{tc} = 32$ K. Consistent with this, the pressure dependence of T_C changes from a Hertz-type $T_C \propto (p - p_c)^{3/4}$ behavior to $T_C \propto (p - p_c)^{1/2}$. In a magnetic field, metamagnetic behavior has been observed that is indicative of tricritical wings, although the wings have not been mapped out.

c. URhGe and UCoGe

Both of these materials belong to the ternary UTX intermetallic U- compounds where T is one of the late transition metals and X is a *p*-electron element. They crystallize in the orthorhombic TiNiSi structure (space group P_{nma}). For lattice parameters, see Troć and Tran (1988) and Canepa *et al.* (1996). Because the $5f$ electrons, which carry the magnetic moments, are partially delocalized in these materials, the ordered moment is often reduced compared to the free ion value and an enhanced electronic specific heat is observed. In addition, they are characterized by a strong Ising anisotropy (Sechovsky and Havela, 1998). Two main mechanisms control the delocalization of the $5f$ electrons and thus the magnetism: the direct overlap of neighboring U $5f$ orbitals, and their hybridization with the *d* electrons. For inter-U distances smaller than the Hill limit ($d_{U-U} \approx 3.4$–3.6 Å) (Hill, 1970), the strong overlap of the $5f$ orbitals results in a nonmagnetic ground state. Larger values yield a FM or AFM ordered ground state. For values close to this limit the $f - d$ hybridization strength controls the magnetic properties. There is a clear tendency of these systems to show magnetic order with increasing *d*-electron filling of the *T* element (Sechovsky and Havela, 1998). The strongest electronic correlations are therefore found in UTX compounds with intermediate values of d_{U-U} and *d*-electron filling.

URhGe has a $d_{U-U} = 3.5$ Å close to the Hill limit. It is ferromagnetic with a Curie temperature $T_C = 9.5$ K and an ordered moment of $0.42\mu_B$, oriented along the *c* axis. A magnetic field parallel to the *b* axis suppresses T_C and leads to a tricritical point at $T \approx 1$ K and $H_b \approx 12$ T (Huxley *et al.*, 2007). With an additional field in the *c* direction, tricritical wings appear; see Fig. 6. The superconductivity that is observed in zero field (Aoki *et al.*, 2001) is absent at intermediate fields, but reappears at low temperatures in the vicinity of the tricritical wings (Levy *et al.*, 2005; Huxley *et al.*, 2007).

The nature of the magnetic order in UCoGe, ferromagnetic or otherwise, was initially unclear. This, together with the observation that URhGe is ferromagnetic, prompted the study of $URh_{1-x}Co_xGe$ alloys (Sakarya *et al.*, 2008), and the final conclusion was that UCoGe is indeed a weak ferromagnet with a Curie temperature near 3 K and a small ordered moment of $0.03\mu_B$ (Huy, Gasparini, de Nijs *et al.*, 2007). The transition was found to be weakly first order by means of nuclear quadrupole resonance measurements (Hattori *et al.*, 2010). Hydrostatic pressure decreases T_C (Hassinger *et al.*, 2008; Slooten *et al.*, 2009) which vanishes near the maximum of the superconducting dome; see Fig. 7. A tricritical point must appear as T_C increases upon doping with Rh, see Fig. 8, but the order of the transition has not been studied as a

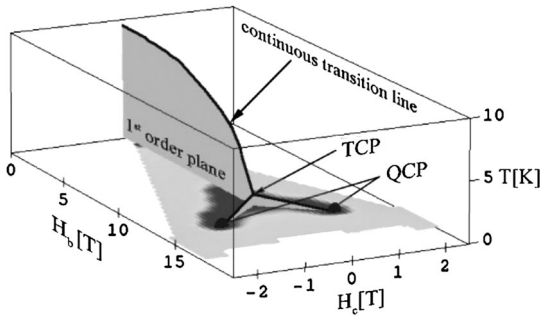

FIG. 6. Phase diagram of URhGe in the space spanned by temperature and magnetic fields in the *b* and *c* directions. The dark shaded regions indicate the presence of superconductivity. From Huxley *et al.*, 2007.

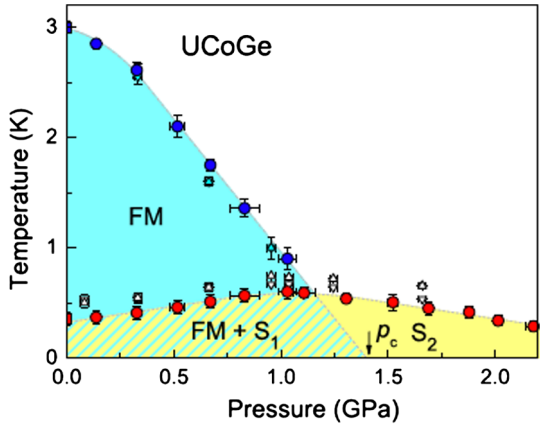

FIG. 7. Phase diagram of UCoGe in the temperature-pressure plane, showing the ferromagnetic and superconducting phases. The magnetic transition is first order for all pressure values (Hattori *et al.*, 2010). From Slooten *et al.*, 2009.

function of the Rh concentration. Similarly, in pure UCoGe tricritical wings should appear in a magnetic field, analogously to what is observed in UCoAl, see Fig. 10. A recent study reported that T_C is suppressed by doping with Ru, with an extrapolated critical Ru concentration of about 31% (Vališka *et al.*, 2015). The order of the transition has not been determined.

UCoGe displays the coexistence of superconductivity and ferromagnetism below 0.8 K (Huy, Gasparini, de Nijs *et al.*, 2007; Slooten *et al.*, 2009). In contrast to both UGe_2 and URhGe the superconductivity is observed in both the ferromagnetic and paramagnetic phases; see Fig. 7.

d. UCoAl

At ambient pressure and zero field, UCoAl is a paramagnet with a strong uniaxial magnetic anisotropy (Sechovsky *et al.*, 1986). It crystallizes in the hexagonal ZrNiAl structure consisting of U-Co and Co-Al layers that alternate along the c axis. The inter-U distance is $d_{U-U} \approx 3.5$ Å (the same value as in URhGe, see II.B.2.c), but a large d filling leads to UCoAl being paramagnetic (Sechovsky and Havela, 1998). Its

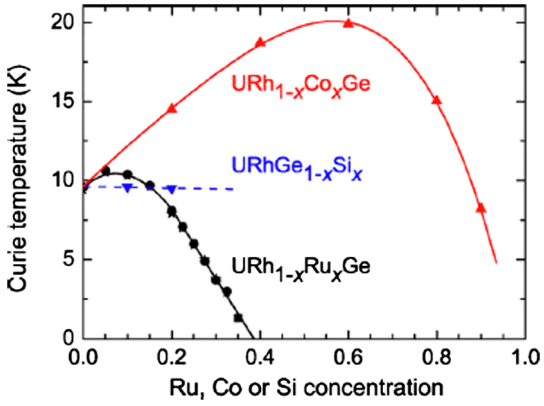

FIG. 8. Curie temperature of URhGe doped with Co, Si, or Rh as a function of the dopant concentration. The transition in pure URhGe is second order, and in pure UCoGe, first order. From Sakarya *et al.*, 2008.

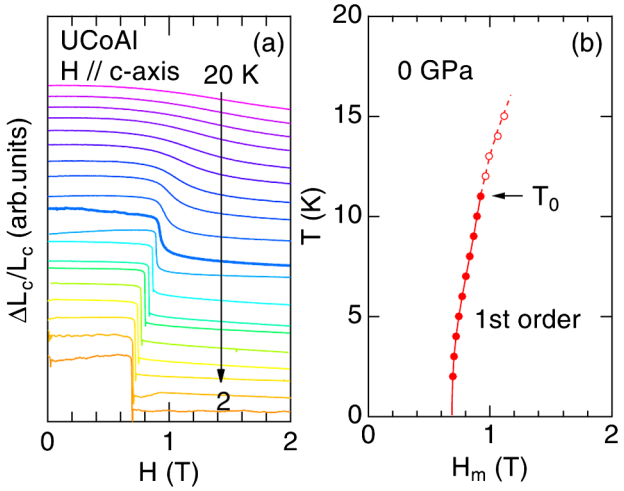

FIG. 9. (a) Magnetostriction measured along the c axis with $H \| c$ for temperatures between 2 and 21 K (every 1 K). (b) Temperature vs field evolution of the metamagnetic transition which changes from first order to a crossover for $T > T_0 = 11$ K. From Aoki, Combier *et al.*, 2011.

isoelectronic analog URhAl is ferromagnetic with $d_{U-U} \approx 3.63$ Å (cf. Sec. II.B.2.e). These observations suggest that UCoAl is close to a FM instability, which is indeed the case: Application of a magnetic field along the easy magnetization axis (the crystallographic c axis) induces a first-order metamagnetic phase transition at $H_m \approx 0.7$ T at low temperature with an induced moment of about $0.3\mu_B$ (Andreev *et al.*, 1985; Mushnikov *et al.*, 1999). Moreover, uniaxial stress induces ferromagnetism (Ishii *et al.*, 2003; Shimizu, Salce *et al.*, 2015). The susceptibility shows Curie-Weiss behavior for $T > 40$ K with a fluctuating moment of about $1.6\mu_B$, much larger than the induced moment of $0.3\mu_B$ (Havela *et al.*, 1997). The magnetism is believed to be itinerant with the U $5f$ electrons providing the main contribution (Eriksson, Johansson, and Brooks, 1989; Wulff *et al.*, 1990; Mushnikov *et al.*, 1999); polarized-neutron diffraction experiments have found the magnetic moment exclusively at the U sites with the orbital moment being twice as large as (and antiparallel to) the spin moment (Wulff *et al.*, 1990; Javorský *et al.*, 2001).

Studies of the magnetostriction, magnetoresistivity (Aoki, Combier *et al.*, 2011), nuclear magnetic resonance (Karube *et al.*, 2012), and thermopower (Palacio-Morales *et al.*, 2013) indicate that the field-induced first-order transition terminates in a critical point at a temperature $T_0 = 11$ K at ambient pressure, as illustrated in Fig. 9: $\Delta L(H)/L$ shows a steplike jump at H_m for $T < T_0$ which becomes smooth for $T \geq T_0$. A determination of critical exponents suggests that the transition at T_0 is in the 3-d Ising universality class (Karube *et al.*, 2012). H_m increases with pressure and each wing terminates in a quantum-critical point (denoted by QCEP in the figure) at $P \approx 1.5$ GPa and $\mu_0 H \approx 7$ T. At the wing-tip point a pronounced enhancement of the effective mass (derived from the coefficient of the T^2 term in the electrical resistivity) is observed (Aoki, Combier *et al.*, 2011).

The resulting T-P-H semischematic phase diagram is shown in Fig. 10, which demonstrates the presence of

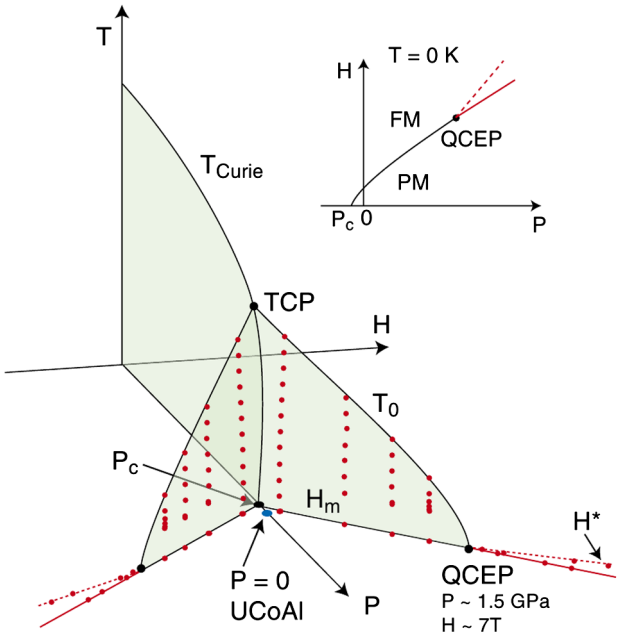

FIG. 10. T-P-H phase diagram of UCoAl. The tricritical wings are determined by the observation of a first-order metamagnetic transition at H_m (red dots); they are bounded by lines of second-order transitions at T_0 and end in quantum "critical end points" (QCEPs) (see the explanation in the Fig. 1 caption). The critical pressure P_c is negative and the tricritical point (TCP) is not accessible. From Aoki, Combier *et al.*, 2011.

tricritical wings in UCoAl. The red dots represent the experimental values for H_m determined by magnetoresistivity (with $J \perp H$) and magnetostriction measurements. Since $T_0 =$ 11 K at the ambient pressure, the tricritical point (TCP) must be located at $T > 11$ K. At pressures higher than 1.5 GPa, the first-order character of the metamagnetic transition disappears and new features in the form of kinks in the magnetoresistivity and Hall effect are observed at H_m and H^* (Combier *et al.*, 2013). Investigations of the transverse and longitudinal resistivities and of the magnetization under pressure (Combier, 2013) point to a much richer phase diagram, where the exact location of the QCEP remains uncertain, with possible changes of the Fermi surface as well as the appearance of new phases around the QCEP.

The substitution of Fe for Co was found to lead to a FM ground state in zero field and ambient pressure by Karube *et al.* (2015). By nuclear quadrupole resonance measurements they found a first-order transition in $U(Co_{1-x}Fe_x)Al$ with a T_C of about 10 and 17 K for $x = 0.1$ and 0.02, respectively.

e. URhAl

URhAl belongs to the same UTX compound family as URhGe, UCoGe, and UCoAl. It has the same layered hexagonal ZrNiAl-type crystal structure as UCoAl, but with $d_{U-U} = 3.63$ Å, larger than the Hill limit (cf. Sec. II.B.2.c). Consistent with this, and contrary to UCoAl which has a nonmagnetic ground state, URhAl orders ferromagnetically via a second-order transition. Values of T_C between 27 and 34 K have been reported, with strong Ising-like ordered moments of $0.9\mu_B$/U along the c axis (Veenhuizen *et al.*, 1988; Combier, 2013; Shimizu *et al.*, 2015b).

The itinerant versus localized nature of magnetism in URhAl is controversial, as it is in many other UTX compounds. A peak at 380 meV in inelastic neutron scattering experiments (Hiess *et al.*, 1997) was interpreted as indication of an intermultiplet transition, suggesting $5f$-electron localization. X-ray magnetic circular dichroism experiments also indicate a high degree of localization of the $5f$ orbitals (Grange *et al.*, 1998). On the other hand, polarized-neutron studies point to a rather strong delocalization of the $5f$ electrons (Paixao *et al.*, 1992). Moreover, band-structure calculations based on an itinerant approach can reproduce most of the experimental findings (Kučera *et al.*, 1998; Kuneš *et al.*, 2001).

Pressure experiments were performed on a rather clean single crystal with a RRR ≈ 14 and $T_C = 28$ K (Combier, 2013). At ambient pressure the phase transition is mean field like characterized by a single peak in C/T and a kink in the thermal expansion ratio $\Delta L/L$. The magnetization with $H \| c$ shows a clear hysteresis at 2 K with a remanent magnetization of $0.9\mu_B$/U. Transport experiments on moderately disordered samples ($\rho_0 \approx 65$ $\mu\Omega$ cm near the transition) have mapped out the phase diagram in more detail (Shimizu *et al.*, 2015a, 2015b). The QPT at a critical pressure $p_c \approx 5.2$ GPa is weakly first order, allowing strong spin fluctuations to be observed in

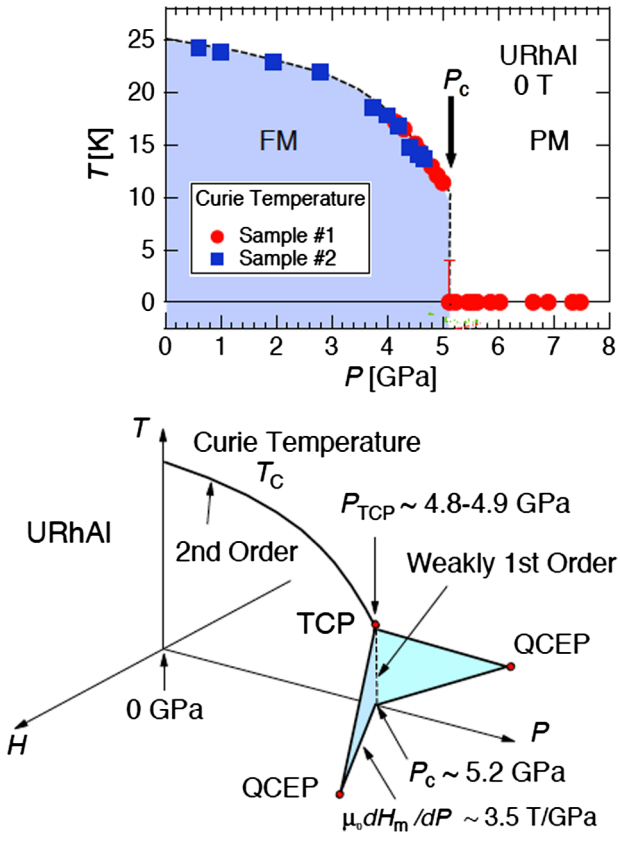

FIG. 11. Upper panel: Temperature-pressure phase diagram of URhAl in zero field determined from resistivity measurements. Lower panel: Temperature-pressure-field diagram inferred from metamagnetic behavior observed in an external field. From Shimizu *et al.*, 2015b.

transport and thermodynamic properties. Metamagnetic signatures in a magnetic field imply the existence of tricritical wings; see Fig. 11.

3. Lanthanide-based compounds

a. $La_{1-x}Ce_xIn_2$

$CeIn_2$ crystallizes in the orthorhombic $CeCu_2$ structure and undergoes a first-order transition to a FM state at $T_C = 22$ K (Rojas *et al.*, 2009). This conclusion on the basis of discontinuities at T_C in the resistivity, the thermal expansion, and the magnetic entropy was later corroborated by μSR measurements (Rojas *et al.*, 2011). Application of hydrostatic pressure increases T_C (Mukherjee, Iyer, and Sampathkumaran, 2012), but upon doping with lanthanum T_C decreases, to about 19.4 K in $La_{1-x}Ce_xIn_2$ with $x = 0.9$, and the transition remains first order (Rojas *et al.*, 2011). The same μSR measurements indicated the existence of a second magnetic phase with long-range order in between the FM and PM phases. The nature of this phase is not known. Doping with Ni decreases T_C sharply, and the transition in $Ce(In_{1-x}Ni_x)_2$ has been reported to be second order to a FM for $x = 0.025$, 0.05, and 0.15 (Rojas, Espeso, and Fernández, 2013). However, an earlier experiment by Sung *et al.* (2009) concluded that the ground state for $x = 0.15$ is AFM.

b. $SmNiC_2$

The ferromagnetic charge-density-wave (CDW) compound $SmNiC_2$ has a T_C of about 17 K which is weakly susceptible to pressure (Woo *et al.*, 2013). The polycrystalline samples measured had a residual resistivity of less than 2 $\mu\Omega$ cm for pressures below about 3 GPa. The PM-FM transition is first order and remains first order as the pressure is increased from 0 to 2 GPa, with T_C dropping to 15 K. At higher pressure, there is a second-order or weakly first-order transition from the FM to a phase of unclear nature, and at least two other phases appear at low temperature. Since the nonmagnetic phase in this material is a CDW state below $T \approx 150$ K, the phase diagram may fall outside the classification provided by Fig. 2 and the first-order transition may be of different origin than in other materials; see Sec. III.F.

c. Yb-based systems

$YbCu_2Si_2$ crystallizes in the body-centered $ThCr_2Si_2$ structure and does not order magnetically at ambient pressure. A transition to a magnetically ordered phase under pressure was suggested on the basis of transport measurements (Alami-Yadri and Jaccard, 1996; Alami-Yadri, Wilhelm, and Jaccard, 1998), and later confirmed by means of Mössbauer data (Winkelmann *et al.*, 1999). Fernandez-Pañella *et al.* (2011) concluded from susceptibility measurements that the nature of the order is FM, and the transition is likely first order (Winkelmann *et al.*, 1999; Colombier *et al.*, 2009; Fernandez-Pañella *et al.*, 2011). The FM nature of the ordered phase was confirmed by Tateiwa *et al.* (2014), who also found evidence for phase separation indicative of a first-order transition.

$YbIr_2Si_2$ crystallizes in either the $ThCr_2Si_2$ structure or the *P*-type $CaBe_2Ge_2$ structure, depending on the synthesis conditions (Hossain *et al.*, 2005). The former is magnetically (presumably AFM) ordered below 0.7 K, whereas the latter is a paramagnet at ambient pressure. Yuan *et al.* (2006) found that by applying pressure the system in its *P*-type structure undergoes a first-order QPT to an ordered phase at a critical pressure $p_c \approx 8$ GPa. The nature of the ordered phase is suspected to be FM, but additional investigations are needed. Recent measurements of the resistivity under hydrostatic pressure as high as 15 GPa found NFL behavior in a pressure range $3 \leq p \leq 8$ GPa, and confirmed the sudden appearance of magnetic order at 8.3 GPa, suggesting a first-order QPT (Macovei, 2010). The transition temperature shifts to higher values and shows a weak maximum around 11 GPa, a behavior very similar to that of $YbRh_2Si_2$ under pressure (Mederle *et al.*, 2001; Knebel *et al.*, 2006). $YbRh_2Si_2$ evolves from an AFM to a FM ordered state under chemical pressure (Co substitution) (Lausberg *et al.*, 2013) and possibly even under hydrostatic pressure (Knebel *et al.*, 2006). This suggests that the nature of the magnetic ordered phase in $YbIr_2Si_2$ could also be AFM, but more investigations are needed.

d. CePt

CePt under pressure has been reported to display a FM QPT at $p_c \approx 12.1$ GPa (Larrea *et al.*, 2005). The transition at $p = 0$ is second order (Holt *et al.*, 1981). No magnetization measurements have been performed under pressure. The FM signature is strongly weakened under pressure well before p_c and transport experiments indicate a sudden drop of the phase boundary line close to p_c, suggesting the presence of a first-order transition.

4. Strontium ruthenates

The perovskite ruthenates, which include Sr_2RuO_4 and $Sr_4Ru_3O_{10}$ in addition to $SrRuO_3$ and $Sr_3Ru_2O_7$, belong to the Ruddlesden-Popper series; for a historical overview, see Mackenzie and Grigera (2004). In $SrRuO_3$ a QPT can be triggered by means of doping with calcium, whereas the phase diagram of $Sr_3Ru_2O_7$ has been explored by applying pressure and an external magnetic field. In $Sr_{1-x}Ca_xRuO_3$ a variety of very different behaviors has been observed, which is likely due to different sample preparation methods (bulk ceramic, bulk powder, and thin films). We therefore discuss this material both in the present section and in Secs. II.C.1 and II.E.3.

a. $Sr_{1-x}Ca_xRuO_3$ *(bulk ceramic samples)*

$Sr_{1-x}Ca_xRuO_3$ is a metallic system that crystallizes in an orthorhombically distorted perovskite structure. $SrRuO_3$ is an itinerant ferromagnet with a second-order transition at $T_C \approx 160$ K (Kim *et al.*, 2003) and an ordered moment of about $1\mu_B$/Rh, while $CaRuO_3$ is a strongly exchange-enhanced Pauli paramagnet with no sign of metamagnetism and a Fermi-liquid ground state with an anomalously low coherence scale (Schneider *et al.*, 2014). Long-range FM order disappears for a Ca concentration around $x_c \approx 0.7$, and nuclear magnetic resonance (NMR) experiments established the presence of FM spin fluctuations for all concentrations, the Curie-Weiss behavior of the susceptibility with a Weiss

temperature that changes sign at x_c notwithstanding (Yoshimura *et al.*, 1999). This and the large effective moment (compared to the ordered one) of about $3\mu_B$/Ru seemed to make $Sr_{1-x}Ca_xRuO_3$ a good candidate for the SCR theory of itinerant ferromagnetism (cf. Sec. I.B). However, a μSR study by Uemura *et al.* (2007) of ceramic samples with $x = 0.65$ and 0.7 found a finite volume fraction of ferromagnetic order and a suppression of the critical dynamics at smaller values of x. These results are similar to the corresponding ones in MnSi (Fig. 4) and are indicative of a first-order transition. No information about the disorder strength in these samples is available. For bulk powder samples and epitaxial thin films of the same material rather different results have been obtained; see Secs. II.C.1.g and II.E.3, respectively.

b. $Sr_3Ru_2O_7$

Very clean samples of $Sr_3Ru_2O_7$ have been prepared, with residual resistivities of less than 0.25 $\mu\Omega$ cm (Perry and Maeno, 2004). The ground state in zero field and at ambient pressure is PM close to a FM instability (Ikeda *et al.*, 2000). In the generic phase diagram of Fig. 2(a) this places the system between the tricritical wings (see Fig. 12), as is the case for UCoAl, Fig. 10. A magnetic field applied in the magnetically easy *ab* plane takes the system through the metamagnetic wings at about 5 T if the temperature is low enough; see Fig. 12, inset (i). Hydrostatic pressure and uniaxial stress drive the system away from and toward ferromagnetism, respectively (Ikeda *et al.*, 2001, 2004; Chiao *et al.*, 2002; Wu *et al.*, 2011). Wu *et al.* (2011) investigated the ac susceptibility under pressure across the metamagnetic transition. They found a QCP (denoted by QCEP in Fig. 12) (see the explanation in the Fig. 1 caption) at $p_c \approx 13.6$ kbar, but no divergence of the susceptibility at this point as would be expected for the generic model of quantum-critical metamagnetism (Millis *et al.*, 2002), implying that the metamagnetism cannot solely be explained by field-induced ferromagnetism.

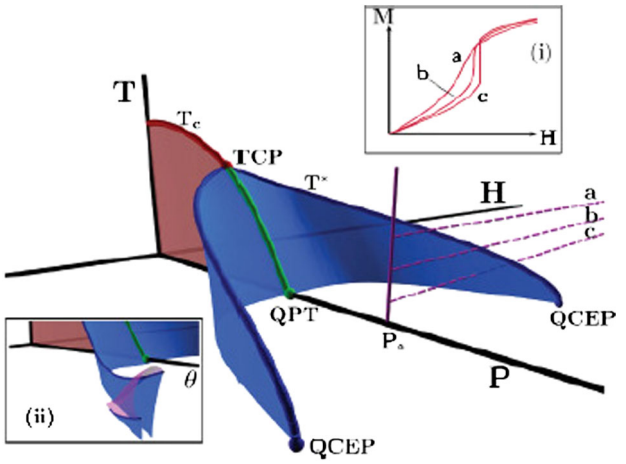

FIG. 12. Schematic phase diagram of $Sr_3Ru_2O_7$ in the space spanned by temperature (T), hydrostatic pressure (P), and magnetic field (H), with $H \perp c$. Ambient pressure (P_0) is indicated by the solid purple line. The tricritical point (TCP) is not accessible, but the tricritical wings are observed by sweeping the magnetic field at fixed temperature [dashed purple lines and inset (i)]. The critical temperature T^* can be tuned by rotating the magnetic field by an angle θ out of the magnetically easy *ab* plane. As T^* decreases, the wing tips split and a phase displaying a strong transport anisotropy is found in between two sheets, with a second-order phase boundary on top [inset (ii) and Fig. 13]. From Wu *et al.*, 2011.

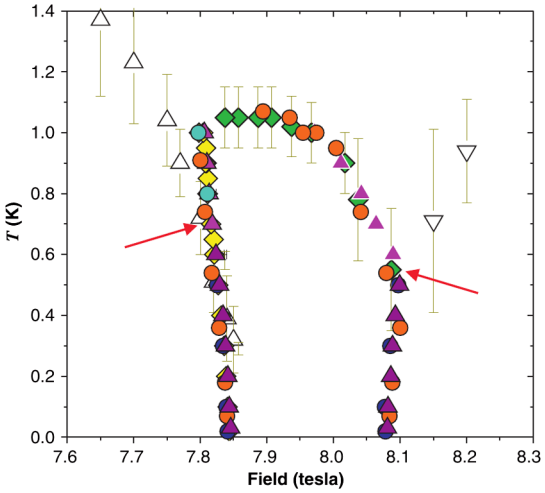

FIG. 13. T-H phase diagram of $Sr_3Ru_2O_7$ at ambient pressure with $H \| c$. The near-vertical lines are the two sheets of the tricritical wings, with the novel phase in between. The transition below (above) the red arrows is first (second) order. From Grigera *et al.*, 2004.

Another way to navigate the phase diagram is to change the field direction out of the magnetically easy *ab* plane: Changing the field tilt angle θ allows one to follow the wings and suppress the critical temperature T^* that marks the top of the wing (Grigera *et al.*, 2001, 2003). As T^* goes to zero, a second sheet of the wing appears, and instead of the QCP that is observed in simpler systems (see Sec. II.B.2) a more complicated phase structure emerges (Grigera *et al.*, 2004; Perry *et al.*, 2004; Rost *et al.*, 2011). The observed bifurcation of the wings has been modeled phenomenologically by means of a Landau theory (Green *et al.*, 2005). The phase between the two sheets, which is observed with field tuning but not with pressure tuning (Wu *et al.*, 2011), has been interpreted as a magnetic nematic (i.e., a non-*s*-wave FM) (Grigera *et al.*, 2004; Borzi *et al.*, 2007; Raghu *et al.*, 2009; Rost *et al.*, 2011; Stingl *et al.*, 2011), or an inhomogeneous phase analogous to the Fulde-Ferrell-Larkin-Ovchinnikov phase in superconductors (Berridge *et al.*, 2009, 2010), but the details are not well understood. Magnetic neutron scattering experiments have identified an incommensurate SDW order with an ordered moment of about $0.1\mu_B$/Ru and wave vector $\boldsymbol{q} = (0.233, 0, 0)$ in the phase between the sheets, and an additional phase at slightly higher magnetic fields with a different ordering wave vector $\boldsymbol{q} = (0.218, 0, 0)$ (Lester *et al.*, 2015).

5. Discussion, and comparison with theory

A striking aspect of the phase diagrams discussed in this section is their universality. As illustrated in Tables I and II and discussed in that context, phase diagrams that are qualitatively the same as the one shown in Fig. 1 are observed in a wide variety of systems with very different electronic

structures and different symmetries of the order parameter. Their only commonality is that they are metallic ferromagnets with rather small amounts of disorder (see footnote [10]). This universal behavior calls for an equally universal explanation of the first-order nature of the QPT. Although quantitative modeling of the phase diagram is still lacking, the theory described in Sec. III.B.2 can explain the phase diagram qualitatively in terms of a fluctuation-induced first-order transition, with generic soft modes in the conduction-electron system playing the role of the extraneous (to the order parameter) soft modes that drive the transition first order.

There are large quantitative differences between the systems listed in Tables I and II. Sang, Belitz, and Kirkpatrick (2014) showed that the sizes of the tricritical wings, which vary dramatically from material to material, correlate with the saturation magnetization as expected from the theory discussed in Sec. III.B.2. Regarding the shape of the wings, theory and all experiments agree that the wings point in the "forward" direction, i.e., the wing tips are located at a larger value of the control parameter than the first-order transition in zero field. However, the curvature of the wings is not expected to be universal; it depends on the relation between the experimental control parameter and the theoretical one (i.e., the mass term in a LGW theory), which in turn depends on microscopic details. For instance, the wings in UGe_2, Fig. 1, have a pronounced curvature, whereas the ones in UCoAl, Fig. 10, are almost flat. Similarly, the shape of the lines that connect the tricritical point with the wing tips is not universal. Wysokiński, Abram, and Spałek (2014, 2015) considered a model containing f electrons in addition to conduction electrons and achieved good agreement with the shape of the wings in UGe_2. The physical mechanism that leads to a first-order QPT in their theory is the same as the one discussed in Sec. III.B.2.

There also is a clear correlation between the size of the ordered moment and the value of T_{tc}; see Tables I and II. This is consistent with the theory, which predicts that T_{tc} is proportional to the ordered magnetic moment (for given microscopic temperature and magnetic-moment scales, which one would expect to be similar for systems that are chemically similar) (Belitz, Kirkpatrick, and Rollbühler, 2005). For instance, within the uranium-based systems there is a rough correlation between T_{tc} and the ordered moment. A U-based system in which no first-order transition has been found is UIr; see Sec. II.C.1 and Table III. Since the ordered moment in the phase FM3 of UIr, from which the QPT to the PM phase occurs, is smaller than the one in UGe_2 by more than a factor of 30, and smaller than the one in URhGe by a factor of more than 10 (Kobayashi *et al.*, 2006), one expects T_{tc} to be smaller by a similar factor. This would put T_{tc} well below 1 K, and possibly lower than 100 mK, which is less than the lowest T_C observed in UIr. Similarly, in the first group of materials in Tables I and II T_{tc} correlates with the size of the ordered moment: CoS_2 has the largest moment and the highest T_{tc}, while in Ni_3Al, which has the smallest moment, a first-order transition at very low temperatures is suspected but has not yet been convincingly observed. More generally, it is conceivable that T_{tc} in several weakly disordered systems is rather low and has not been observed so far. A related issue is the robustness of the first-order transition discussed in Secs. III.B.2 and IV.A.

C. Systems showing a continuous transition

We now discuss systems that show a continuous transition at low temperatures; their properties are summarized in Tables III, IV, and V. Most of these materials are composition tuned, which introduces various amounts of disorder, and they can be classified with respect to the disorder strength. The first group is known or suspected to be relatively weakly disordered as judged by the residual resistivity (see footnote [10]); see Table III. Consistent with this, their phase diagrams have the shape shown in Fig. 2(b). In the second group, Table IV, the disorder is strong, and the phase diagrams are of the form shown in Fig. 2(d). $YbNi_4P_2$ falls into a separate category due to its quasi-one-dimensional electronic structure which sets it apart from all other materials we discuss; see Table V.

1. Weakly disordered systems

a. Ni_xPd_{1-x}

NiPd alloys, which crystallize in an fcc structure, form a series of solid solutions whose composition can be varied continuously from pure Pd to pure Ni. The alloying procedure can produce very little disorder as measured by the residual resistivity ρ_0, which has been reported not to exceed 0.1 $\mu\Omega$ cm for any concentration (Ikeda, 1987). A small concentration (about 2.5%) of Ni induces FM order (Murani, Tari, and Coles, 1974). This composition-induced QPT was studied by Nicklas *et al.* (1999) by means of heat capacity, electrical resistivity, and magnetization measurements. For Ni concentrations up to 10% above the critical concentration $x_c \approx 0.026$ they found $T_C \propto (x - x_c)^{3/4}$ and a $T \ln T$ contribution to the specific heat down to 0.3 K. The T dependence of the resistivity shows a power-law behavior

$$\rho(T \to 0) = \rho_0 + AT^n. \tag{2.1}$$

The exponent n displays a sharp minimum of $n = 5/3$ near x_c, while the prefactor A shows an equally sharp maximum. These results are all consistent with the predictions of Hertz-Millis-Moriya theory; cf. Sec. III.C.2.

The lowest T_C achieved in these experiments was $T_C \approx 7$ K at $x - x_c \approx 0.002$; see Fig. 14. This is on the same order as the temperature above which, e.g., MnSi displays behavior consistent with Hertz theory even though the behavior at low T is very different. Subsequent ac susceptibility and zero-field-cooled and field-cooled magnetization measurements on the same samples at temperatures as low as 2 K found evidence for spin-glass freezing in a small region of the phase diagram ($0.025 \leq x \leq 0.028$) (Nicklas, 2000). To corroborate this observation a measurement of the thermal expansion was performed on the same $x = 0.024$ polycrystal studied by Nicklas *et al.* (1999). Küchler *et al.* (2006) found that the Grüneisen ratio (i.e., the thermal expansion coefficient divided by the specific heat) does not increase with decreasing T, but remains constant below 3 K, in contrast to what is expected at a QCP (Küchler *et al.*, 2006). Single-crystalline samples investigated by Franz *et al.* (2010) showed similar transport

TABLE III. Systems showing a second-order transition: Weakly disordered bulk systems. T_C = Curie temperature, ρ_0 = residual resistivity, FM = ferromagnetism, SC = superconductivity, and n.a. = not available.

System	Order of Transition[a]	T_C/K	Magnetic moment/μ_B[b]	Tuning parameter	Disorder ($\rho_0/\mu\Omega$cm)[c]	Comments
Ni_xPd_{1-x}	2nd[1]	$600-7$[d]	0.2–2.45[e]	Composition[1]	1.5 (?)[f]	Low-T behavior unclear
$(Ni_{1-x}Pd_x)_3Al$	2nd[2]	$42-4$[g]	$0.075-0$[h]	Composition[2]	10[i,2]	Moderate disorder
$Ni_3Al_{1-x}Ga_x$	2nd[3]	$41-5$[j,3]	$0.075-0.02$[j,3]	Composition[3]	n.a.	Disorder unknown
UIr	2nd[4]	$46-1$[4]	0.5[4]	Pressure[4]	n.a.[k]	Three FM phases, coex. FM + SC
$UNiSi_2$	2nd[5]	95[5,6,7]	1.2[6]	Pressure[5]	≈ 25[5]	Two FM phases
$(Cr_{1-x}Fe_x)_2B$	2nd[8]	$45-8$[l,8]	$1.4-0.25$[l]	Composition	35[8]	Moderate disorder
$Zr_{1-x}Nb_xZn_2$	2nd[9]	$18-0$[m,9]	$0.08-0$[m,9]	Composition[9]	n.a.	Disorder unknown
$Sr_{1-x}Ca_xRuO_3$	2nd[10]	$160-0$[n]	$0.8-0$[n]	Composition	n.a.	Bulk powder samples
$SrCo_2(Ge_{1-x}P_x)_2$	2nd[11]	$35-2$[o,11]	$0.1-0.02$[o,11]	Composition[11]	n.a.	FM induced by dimer breaking
$CeSi_{1.81}$	2nd[12]	$9.5-3$[p,12]	$0.2-0$[q,12]	Pressure	12 (30)[r]	Moderate disorder
$CePd_{1-x}Ni_x$	2nd[13]	$10.5-6.1$[s,13]	n.a.	Composition[13]	≈ 15[13]	T_C nonmonotonic
$U_4Ru_7Ge_6$	2nd[14]	$11.2-3$[t]	0.2[u]	Pressure[14]	58[t]	Intermediate disorder
$U_4(Ru_{1-x}Os_x)_7Ge_6$	n.a.	$12-1$[v]	0.2[u]	Composition[15]	n.a.	Disorder unknown
$(Sc_{1-x}Lu_x)_{3.1}In$	2nd[16]	$4-1$[w]	$0.13-0$[w]	Composition[16]	n.a.	Quasi-1-d chains of Sc-In

[a]At the lowest temperature achieved.
[b]Per formula unit unless otherwise noted.
[c]For the highest-quality samples.
[d]For $x = 1-0.027$ (Nicklas *et al.*, 1999).
[e]For $0.018 \lesssim x \lesssim 0.1$ (Nicklas *et al.*, 1999).
[f]Nicklas (2000) and Tari and Coles (1971); Ikeda (1987) reported ρ_0 as small as 0.01 $\mu\Omega$ cm for the relevant Ni concentrations.
[g]For $x = 0$–0.9.
[h]For $x = 0$ (Niklowitz *et al.*, 2005) to $x = 0.1$ (Sato, 1975).
[i]For $x = 0.1$.
[j]For $x = 0$–0.33.
[k]RRR up to 250 (Kobayashi *et al.*, 2006).
[l]For $x = 0.05-0.02$.
[m]For $x = 0$–0.08.
[n]For $x = 0-x \gtrsim 0.7$.
[o]Per Co for $x = 0.55-0.35$.
[p]For $p = 0$–13 kbar.
[q]At $T = 1.7$ K for $p = 0$–14 kbar.
[r]For $CeSi_{1.86}$ at $p = 0$ with a current in the a (c) direction (Sato *et al.*, 1988).
[s]For $x \approx 0.5-0.94$.
[t]For $p = 0$–2 GPa.
[u]Per U.
[v]For $x = 0$–0.3 (Colineau *et al.*, 2001).
[w]For $x = 0$–0.03.
[1]Nicklas *et al.* (1999). [2]Sato (1975). [3]Yang *et al.* (2011). [4]Kobayashi *et al.* (2006). [5]Sidorov, Tobash *et al.* (2011). [6]Das *et al.* (2000). [7]Pikul and Kaczorowski (2012). [8]Schoop *et al.* (2014). [9]Sokolov *et al.* (2006). [10]Itoh, Mizoguchi, and Yoshimura (2008). [11]Jia *et al.* (2011). [12]Drotziger *et al.* (2006). [13]Kappler *et al.* (1997). [14]Hidaka *et al.* (2011). [15]Colineau *et al.* (2001). [16]Svanidze *et al.* (2015).

and thermodynamic properties as those seen in polycrystals studied by Nicklas *et al.* (1999), but a detailed analysis of the magnetization indicates that at low fields and low temperatures the behavior is not consistent with either a mean-field QCP or a first-order transition. Considering that neutron-depolarization imaging experiments showed that polycrystalline samples are much more homogeneous than the single-crystalline samples (Pfleiderer *et al.*, 2010), these results raise the question of disorder present in the samples. The strength of the disorder, or how to characterize it, is not quite clear. The data obtained by Ikeda (1987) suggested a residual resistivity $\rho_0 \approx 5$ $\mu\Omega$ cm for x around the critical concentration. Tari and Coles (1971) reported a low-temperature (< 4.2 K) resistivity of about 1 $\mu\Omega$ cm for a sample with $x = 0.025$. ρ_0 for the samples studied by Nicklas (2000) is about 0.5 $\mu\Omega$ cm for pure Pd (RRR = 40) and for $x = 0.1$, 1.5 $\mu\Omega$ cm for $x \approx x_c$, and it reaches a maximum of 3 $\mu\Omega$ cm at $x \approx 0.04$. These results suggest that there is a substantial amount of disorder even in the best samples. It would be desirable to revisit the QPT in NiPd, while carefully characterizing the amount of disorder in the samples. A ρ_0 of 1 $\mu\Omega$ cm would put the sample marginally in the intermediate regime II of the theory discussed in Sec. III.B.3, where the theory predicts a continuous transition with effectively mean-field exponents. However, if the spin-glass effects found by Nicklas (2000) were to be corroborated this theory would be inapplicable and the system would have to be classified with the materials discussed in Sec. II.E.

b. $Ni_3Al_{1-x}Ga_x$ *and* $(Ni_{1-x}Pd_x)_3Al$

The FM order in Ni_3Al with $T_C = 41$ K (see Sec. II.B.1.d) can be suppressed by substitution of Pd for Ni (Sato, 1975), or by doping with Ga (Yang *et al.*, 2011). In the former system, a QCP is reached at $x \approx 0.095$, at which concentration the samples measured by Sato (1975) had a residual resistivity

TABLE IV. Systems showing a second-order transition: strongly disordered bulk systems. T_C = Curie temperature, ρ_0 = residual resistivity, FM = ferromagnetism, SC = superconductivity, and n.a. = not available.

System	Order of transition[a]	T_C/K	Magnetic moment/μ_B[b]	Tuning parameter	Disorder ($\rho_0/\mu\Omega$ cm)[c]	Comments
$LaV_xCr_{1-x}Ge_3$	n.a.	$55-20$[d]	1.4[e]	comp + press[1]	100[f]	Lowest T_C rather high
$URu_{2-x}Re_xSi_2$	2nd[2,3]	$25-2$[g]	$0.4-0.03$[3]	Composition[2]	≈100[h]	Strong disorder
$URh_{1-x}Ru_xGe$	2nd[4]	$\approx 10-0$[i,4]	$\approx 0.1-0$[i,4]	Composition[4]	n.a.[j]	Disorder unclear
$Th_{1-x}U_xCu_2Si_2$	2nd[5]	$101-12$[k]	$0.92-0.09$[k]	Composition[5]	235[l]	Disorder unclear
$UCo_{1-x}Fe_xGe$	2nd[6]	$8.5-3$[m]	$0.1-0.02$[m]	Composition[6]	430[n]	Extremely high ρ_0

[a]At the lowest temperature achieved.
[b]Per formula unit unless otherwise noted.
[c]For the highest-quality samples.
[d]For $x = 0.16$ and $p = 0$–3 GPa.
[e]For $x = 0$.
[f]For $x = 0.16$.
[g]For $x = 0.6 - 0.2$ (Butch and Maple, 2009).
[h]For $x = 0.1$ (Butch and Maple, 2010).
[i]For $x = 0$–0.4 (Huy, Gasparini, Klaasse *et al.*, 2007).
[j]Large nominal $\rho_0 \approx 200 - 300$ $\mu\Omega$ cm due to cracks; not indicative of the intrinsic disorder (Huy, Gasparini, Klaasse *et al.*, 2007).
[k]For $x = 1 - 0.15$.
[l]High ρ_0 due to microcracks.
[m]For $x \approx 0.75 - 0.22$.
[n]For $x = 0.22$.
[1]Lin *et al.* (2013). [2]Bauer *et al.* (2005). [3]Butch and Maple (2009). [4]Huy, Gasparini, Klaasse *et al.* (2007).
[5]Lenkewitz *et al.* (1997). [6]Huang *et al.* (2013).

TABLE V. Systems showing a second-order transition: Quasi-one-dimensional (1D) materials. T_C = Curie temperature, ρ_0 = residual resistivity, and n.a. = not available.

System	Order of Transition[a]	T_C/K	Magnetic moment/μ_B[b]	Tuning parameter	Disorder ($\rho_0/\mu\Omega$ cm)[c]	Comments
$YbNi_4P_2$	2nd[1]	0.14[2]	≈0.035[2]	None	2.6[1]	Quasi-1D
$YbNi_4(P_{1-x}As_x)_2$	2nd[3]	$0.15-0.025$[d,3]	≈0.05[3]	Composition	≈5.5, 15[e,3]	Quasi-1D, disordered

[a]At the lowest temperature achieved.
[b]Per formula unit unless otherwise noted.
[c]For the highest-quality samples.
[d]For $x = 0$–0.08 (Steppke *et al.*, 2013).
[e]5.5 for $J \| c$, 15 for $J \perp c$ (Steppke *et al.*, 2013).
[1]Krellner *et al.* (2011). [2]Spehling *et al.* (2012). [3]Steppke *et al.* (2013).

$\rho_0 \approx 10$ $\mu\Omega$ cm, indicating moderate disorder. The observed critical behavior is consistent with the Hertz-Millis-Moriya theory, as one would theoretically expect for systems in this disorder regime; see Sec. III.B.3.

T_C also decreases monotonically upon doping with Ga, leading to a QPT in $Ni_3Al_{1-x}Ga_x$ at $x_c \approx 0.34$ (Yang *et al.*, 2011); Ni_3Ga is paramagnetic (Hayden, Lonzarich, and Skriver, 1986). The disorder strength in these samples is not known, but assuming the same moderate disorder as in $(Ni_{1-x}Pd_x)_3Al$ one would expect Hertz-type critical behavior according to the theoretical analysis reviewed in Sec. III.B.3. This is indeed borne out by the experiment (see Fig. 15): The temperature-concentration phase diagram obeys Eq. (3.51), the susceptibility at the critical concentration diverges as $T^{-4/3}$, Eq. (3.55), and the magnetization as a function of temperature near T_C obeys Eq. (3.59). The first result reflects the combination of critical exponents $\nu z/(1+2\nu) = 3/4$; see Eq. (3.47). The second one reflects the exponent $\gamma_T = 4/3$, and if combined with the first one it also implies $\gamma = 1$, in agreement with Eq. (3.47), since $\chi \sim T^{-4/3} \sim |x - x_c|^{-1}$. The third one reflects $\beta = 1/2$ in addition to the combination $\nu z/(1+2\nu)$. See Appendix B for the definitions of the critical exponents, and Sec. III.C.2.b for the scaling considerations underlying the above statements. As emphasized in Sec. III, this behavior is expected to hold, strictly speaking, only in a preasymptotic regime. However, for moderate disorder strengths the true asymptotic regime is expected to be unobservably small.

c. UIr

UIr at ambient pressure is an Ising-like FM with $T_C \approx 46$ K. High-quality samples with a RRR ≈ 250 have been investigated under hydrostatic pressure (Akazawa *et al.*, 2004; Kobayashi *et al.*, 2006, 2007). The overall phase diagram is similar to that of UGe_2, but the details are different. With increasing pressure there are three distinct FM phases labeled FM1, FM2, and FM3 (Kobayashi *et al.*, 2006), and strain and resistivity measurements suggest that they have slightly different crystal structures (Kotegawa *et al.*, 2011).

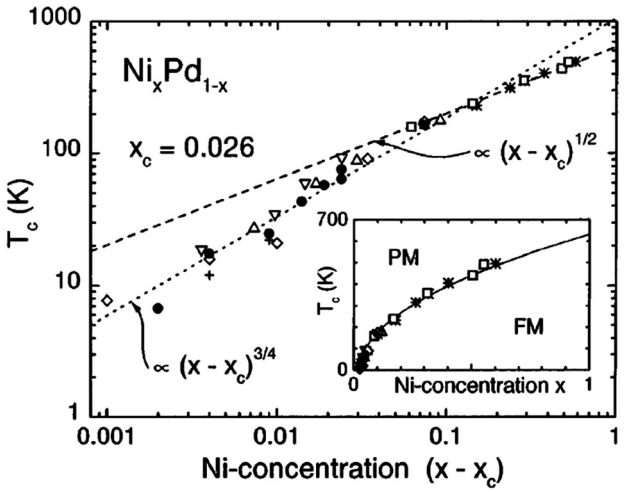

FIG. 14. Observed phase diagram of Ni_xPd_{1-x}. Solid dots are data taken by Nicklas *et al.* (1999), and the other symbols represent earlier data. From Nicklas *et al.*, 1999.

FM1 has an ordered moment of $0.5\mu_B/U$. There is a first-order metamagnetic transition between FM1 and FM2 at $p \approx 1.7$ GPa (at $T = 0$). The ordered moment in FM2 and FM3 is less than $0.5\mu_B/U$. T_C goes to zero, and FM3 gives way to paramagnetism, at a critical pressure $p_c \approx 2.8$ GPa. Near p_c in the FM3 phase, superconductivity is observed at $T < 140$ mK (Akazawa *et al.*, 2004). The absence of metamagnetic behavior in the PM phase is indicative of the FM3-PM transition remaining second order to the lowest observed $T_C \approx 0.8$ K.

d. $UNiSi_2$

$UNiSi_2$ is a collinear ferromagnet with $T_C \approx 95$ K and U moments of $1.2\mu_B$ directed along the crystallographic c axis of the orthorhombic structure (Geibel *et al.*, 1990; Kaczorowski, 1996; Taniguchi *et al.*, 1998; Das *et al.*, 2000; Pikul, 2012). Although the amount of magnetic entropy below T_C, $\Delta S \approx 11.3$ J/mol K, suggests that the uranium moments are mostly localized, this value is lower than the value $\Delta S = R\ln(10) = 19.1$ J/mol K expected for fully localized U^{3+} moments (Sidorov, Tobash *et al.*, 2011).[14] This is possibly due to the crystalline electric field and the Kondo effect, which is seen in the $\rho \propto -\ln T$ behavior of the resistivity above T_C (Kaczorowski, 1996; Sidorov, Tobash *et al.*, 2011). In polycrystalline samples as well as in single crystals of good quality (RRR ≈ 7) the FM phase transition in zero field is second order, characterized by a λ-like peak in $C(T)/T$ (Pikul, 2012). Partial substitution of Th for U suppresses T_C and leads to pronounced disorder effects; this system is discussed in Sec. II.E.2.a. Sidorov, Tobash *et al.* (2011) investigated single crystals of $UNiSi_2$ under hydrostatic pressure, up to about 6 GPa. With increasing pressure T_C decreases, moderately for pressures up to about 4 GPa, and then more sharply, vanishing above 5.5 GPa; see Fig. 16. The FM phase transition remains second order (from ac-calorimetry measurements) in the pressure range $0 \le p \le 5.1$ GPa where the transition could be detected. In the pressure range near the QPT, between 5.1 and 5.5 GPa, another phase appears (small shaded region in Fig. 16), which is characterized by weak FM. This feature, which is reminiscent of the distinct FM phases in UIr (see Sec. II.C.1.c), is indicated by an upturn in the ac susceptibility and signatures in the resistivity and the specific heat (Sidorov, Tobash *et al.*, 2011). The magnetic entropy is strongly reduced under pressure. This and the enhanced Sommerfeld coefficient and resistivity at 5.5 GPa led Sidorov, Tobash *et al.* (2011) to suggest a delocalization of the f electrons at the QPT.

e. $(Cr_{1-x}Fe_x)_2B$

Ferromagnetism can be induced in the paramagnetic compound Cr_2B by doping with Fe. The resulting system $(Cr_{1-x}Fe_x)_2B$ undergoes a QPT near $x_c = 0.02$ (Schoop *et al.*, 2014). Doping introduces a substantial amount of disorder resulting in a residual resistivity near x_c of $\rho_0 \approx 35\ \mu\Omega$ cm. The exponent n in Eq. (2.1) falls from its Fermi-liquid value $n = 2$ at $x = 0$ to $n = 1$ at x_c, and remains there for larger values of x. The prefactor A peaks around x_c. However, the absolute change of ρ with temperature in the linear-in-T range is extremely small. For instance, for $x = 0.025$ between 8 and 20 K $\Delta\rho = \rho - \rho_0 \approx 0.2\ \mu\Omega$ cm, which is very small compared to the rather large value of $\rho_0 = 40\ \mu\Omega$ cm. This results in a small value of $A \approx 18$ nΩ cm/K; for other values of x it is even smaller. A magnetic field of 14 T restores the Fermi-liquid value $n = 2$. The specific heat shows a $T\ln T$ term similar to that observed in $Ni_{1-x}Pd_x$, with a prefactor that is largest around x_c, but again the maximal change is very small, $\Delta C/T \approx 2$ mJ/K^2 mol. These observations are in principle consistent with the existence of a QCP at x_c, but the NFL properties characteristic of critical behavior are extremely weak. Given the disorder strength, the theory reviewed in Sec. III.B predicts a continuous transition.

f. $Zr_{1-x}Nb_xZn_2$

Itinerant ferromagnetism in $ZrZn_2$ ($T_C = 28.5$ K) (Matthias and Bozorth, 1958; Pickart *et al.*, 1964) can be tuned to zero by substituting Nb for Zr. Sokolov *et al.* (2006) investigated the magnetization of several polycrystalline samples of the series $Zr_{1-x}Nb_xZn_2$ with $0 \le x \le 0.14$ down to 1.8 K. From an Arrott-plot analysis they found that T_C is suppressed to zero at $x_c \approx 0.08$. The x dependence of T_C is well described by $T_C \propto (x - x_c)^{3/4}$, and the spontaneous moment vanishes linearly with T_C. Furthermore, the inverse magnetic susceptibility could be fitted to $\chi^{-1} = aT^{4/3} + b(x - x_c)$, with a and b constants. All of this is consistent with the results of Hertz-Millis-Moriya theory; see Sec. III.C.2.b. There were no indications of a first-order transition or metamagnetism.

These results are reminiscent of those for $Ni_{1-x}Pd_x$ (cf. Sec. II.C.1.a). However, in the present case little is known about the disorder present in the samples. X-ray diffraction experiments revealed single-phase specimens with Laves phase C15 structure, but no resistivity data are available (Sokolov, 2015).

[14] Pikul (2012) found an even lower value, $\Delta S \approx 8$ J/mol K.

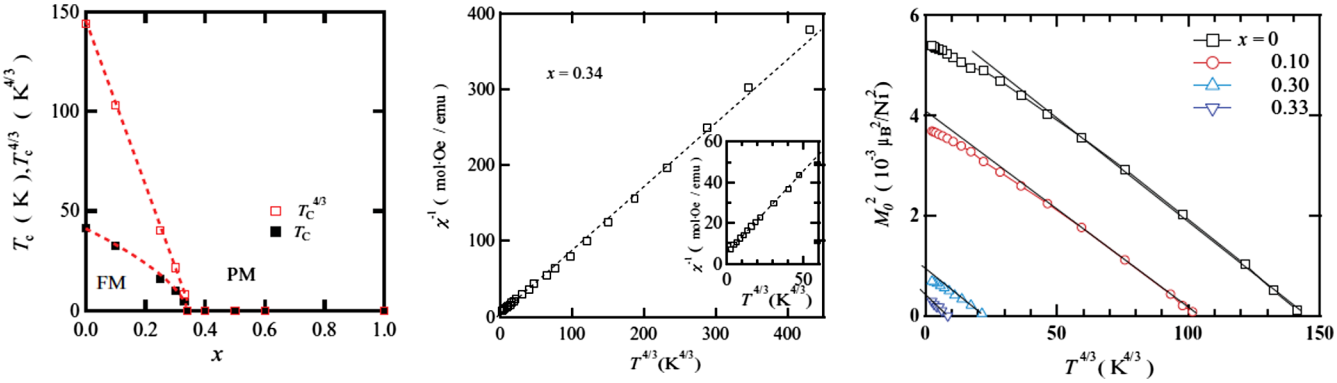

FIG. 15. Hertz-type scaling behavior as observed in $Ni_3Al_{1-x}Ga_x$. From left to right: T_C vs x phase diagram, inverse magnetic susceptibility vs $T^{4/3}$ for $x = x_c$, and magnetization squared vs $T^{4/3}$ for various x. From Yang *et al.*, 2011.

g. $Sr_{1-x}Ca_xRuO_3$ *(bulk powder samples)*

Early studies of polycrystalline $Sr_{1-x}Ca_xRuO_3$ samples showed that T_C goes to zero linearly as x approaches $x_c \approx 0.7$ (Kanbayasi, 1978; Kiyama *et al.*, 1999), which led to the proposal of a QCP in this material. Itoh, Mizoguchi, and Yoshimura (2008) studied powder samples and concluded from magnetization measurements that there is indeed a QCP. From Arrott plots for x near x_c they inferred a field dependence of the magnetization $M \propto H^{2/3}$, i.e., a critical exponent $\delta = 3/2$. This agrees with the prediction of the generalized Landau theory for disordered systems described in Sec. III.B.3. No information is available about the disorder strength in these samples. Huang *et al.* (2015) studied the dynamical scaling of the magnetization and specific heat and found $\delta = 1.6$ in agreement with Itoh, Mizoguchi, and Yoshimura (2008). Their scaling analysis yields a very unusual temperature dependence of the specific-heat coefficient $\gamma \propto \text{const} - T^{0.7}$. The behavior is markedly different from that of ceramic samples (see Sec. II.B.4.a) and epitaxial thin films (see Sec. II.E.3).

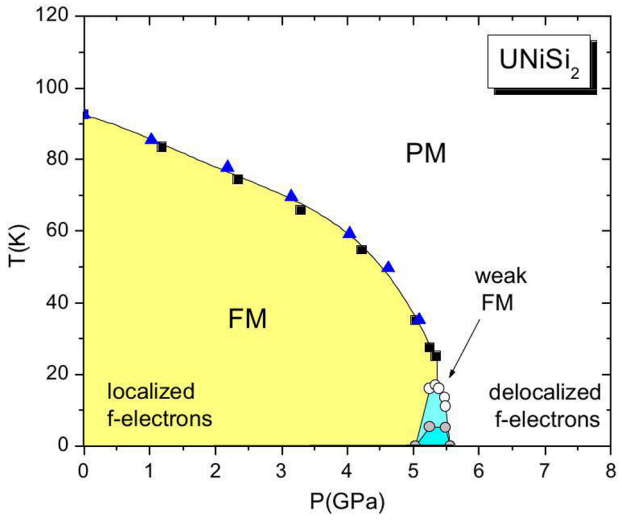

FIG. 16. Temperature-pressure (T-P) phase diagram of $UNiSi_2$ from resistivity, ac susceptibility, and specific-heat measurements. The small, shaded (turquoise) region represents a separate phase characterized by weak FM and a large Sommerfeld coefficient. In the PM phase the Sommerfeld coefficient remains large as does the resistivity. From Sidorov, Tobash *et al.*, 2011.

h. $SrCo_2(Ge_{1-x}P_x)_2$

For the ferromagnetism that develops in $SrCo_2(Ge_{1-x}P_x)_2$ at $x \approx 0.325$, Jia *et al.* (2011) proposed a new tuning mechanism: the breaking of bonds in Ge-Ge dimers, in which they argue is more important than the simple change in carrier concentration with x. $SrCo_2Ge_2$ forms in the $ThCr_2Si_2$ structure, with Co_2Ge_2 layers separated by a Ge-Ge interlayer bond, i.e., a dimer. This causes the layers to be pulled t ogether and to form a collapsed tetragonal cell with a three-dimensional electronic structure. $SrCo_2Ge_2$ is a simple Pauli paramagnet. The lack of such a dimer in $SrCo_2P_2$ causes the same structure to be uncollapsed and, therefore, to have a more two-dimensional electronic structure and a shorter Co-Co separation within the layers, which increases the Co-Co interaction. From measurements of the magnetization, the susceptibility, and the specific heat of polycrystalline samples Jia *et al.* (2011) concluded that at $x \approx 0.325$ the system develops bulk ferromagnetism via a QCP. The Curie temperature increases with increasing x, reaches a maximum of $T_C \approx 35$ K at $x \approx 0.55$, and then decreases. For $x \gtrsim 0.75$ Jia *et al.* (2011) found that the ground state is a Stoner-enhanced paramagnet rather than a ferromagnet. The ferromagnetism is of the itinerant type, characterized by a Curie-Weiss behavior with an effective moment much larger than the saturation moment. This is in agreement with band-structure calculations, which show a maximum in the density of states at $x \approx 0.5$, where T_C reaches its maximal value (Cuervo-Reyes and Nesper, 2014). T_C increases linearly from $x = 0.3$ to 0.5 having a value of about 5 K for $x = 0.35$. No sign of a first-order transition or spin-glass behavior was detected. For a sample with $x = 0.325$ and no T_C the susceptibility was found to behave as $\chi \propto T^{-4/3}$ (down to 2 K) and the specific heat $C/T \propto -\ln T$ (down to 0.4 K), in agreement with Hertz-Millis-Moriya theory (cf. Sec. III.C.2). No resistivity measurements have been reported, and the role of disorder in this material is unknown.

i. $CeSi_x$

$CeSi_x$ can be considered a FM dense Kondo system (Yashima *et al.*, 1982; Sato *et al.*, 1988). It crystallizes in

the α-$ThSi_2$ structure with a broad homogeneity range $1.7 \leq x \leq 2$ (Ruggiero and Olcese, 1964; Yashima *et al.*, 1982; Yashima and Satoh, 1982). It shows a paramagnetic ground state for $x \geq 1.85$, while a magnetically ordered state was found for $x \leq 1.8$ with a transition temperature around 10 K. The nature of the magnetic order is not clear (Drotziger *et al.*, 2006). Susceptibility measurements suggest that the magnetic structure depends on the Si vacancy distribution (Shaheen and Mendoza, 1999), and magnetization measurements indicate that the ground state may not be pure FM, but rather a ferrimagnet or canted ferromagnet resulting from the Ruderman-Kittel-Kasuya-Yosida (RKKY) interaction between the Ce $4f$ local moments on two different lattice sites (Drotziger *et al.*, 2006).

Drotziger *et al.* (2006) studied the magnetization of a single crystal of $CeSi_{1.81}$ as a function of temperature and hydrostatic pressure. Pressure was found to suppress T_C monotonically from its ambient-pressure value of 9.5 K. T_C vanishes at a critical pressure $p_c \approx 13.1$ kbar, with a concomitant continuous suppression of the magnetic moment from $0.2\mu_B$/Ce to zero. The transition at T_C was found to be of second order down to the lowest observed value of $T_C \approx 3$ K. The electrical resistivity of the $x = 1.81$ sample is not known, but for $x = 1.86$ a residual resistivity of 12 $\mu\Omega$ cm (with current along the a axis) and 30 $\mu\Omega$ cm (with current along the c axis) has been reported (Sato *et al.*, 1988). If these values are representative for the $x = 1.81$ critical sample as well, they put the system $CeSi_x$ in a moderately disordered regime where a continuous transition is expected theoretically; see Sec. III.B.3. However, questions about both the nature of the ordered phase and the nature of the transition at low T remain (Drotziger *et al.*, 2006).

j. $CePd_{1-x}Ni_x$

The FM T_C of CePd ($T_C = 6.5$ K) initially increases upon alloying with nickel, then decreases for $x \gtrsim 0.8$, and vanishes at a Ni concentration $x_c \approx 0.95$ (Kappler *et al.*, 1997). Measurements of the specific heat, magnetization, and resistivity have shown NFL behavior of the resistivity for $3 < T < 30$ K, and logarithmic behavior of the specific-heat coefficient in a temperature window between about 1 and 10 K.

k. $(Sc_{1-x}Lu_x)_{3.1}In$

Upon doping of the nonstoichiometric FM compound $Sc_{3.1}In$ with lutetium, evidence for a QCP with unusual values of the critical exponents in $(Sc_{1-x}Lu_x)_{3.1}In$ has been found near a critical concentration $x_c \approx 0.035$ (Svanidze *et al.*, 2015). NFL behavior has been observed in both the FM and PM phases, in addition to the vicinity of the QCP. This material may be characterized by a reduced dimensionality due to the one-dimensional nature of the Sc-In chains (Jeong and Kwon, 2007; Svanidze *et al.*, 2015).

l. $U_4Ru_7Ge_6$ *and* $U_4(Ru_{1-x}Os_x)_7Ge_6$

$U_4Ru_7Ge_6$ is ferromagnetic below $T_C \approx 12$ K; it is a metal with Kondo-like and heavy-fermion features, while $U_4Os_7Ge_6$ is a paramagnet. The system $U_4(Ru_{1-x}Os_x)_7Ge_6$ has been investigated by Colineau *et al.* (2001), who found that T_C is suppressed to zero for $x \approx 0.3$.

Hydrostatic pressure applied to $U_4Ru_7Ge_6$ also suppresses T_C, with a FM-PM QPT at $p \approx 2.6$ GPa. Resistivity measurements on polycrystalline samples by Hidaka *et al.* (2011) suggest the existence of a QCP with Hertz-type behavior. The residual resistivity at $p = 2.36$ GPa was about 58 $\mu\Omega$ cm. The resistivity of the $U_4(Ru_{1-x}Os_x)_7Ge_6$ samples is not known, but is presumably higher. This places this system in the disorder regime II (intermediate disorder) discussed in Sec. III.B.3, which is consistent with the observations.

2. Strongly disordered systems

a. $LaV_xCr_{1-x}Ge_3$

Upon substitution of vanadium for chromium in $LaCrGe_3$, the FM T_C drops from 88 to 36 K for $x = 0.21$ (Lin *et al.*, 2013). Pressure applied to a sample with $x = 0.16$ leads to a further decrease of T_C, with a QPT at $p \approx 3$ GPa. The lowest T_C achieved was about 20 K; the order of the QPT is not known.

b. $URu_{2-x}Re_xSi_2$

The parent compound of $URu_{2-x}Re_xSi_2$, URu_2Si_2, is a heavy-fermion superconductor (superconducting $T_c \approx 1.5$ K) that has an ordered phase of unknown nature, usually referred to as the "hidden-order" phase, below about 17 K; see Mydosh and Oppeneer (2011) for a recent overview. Substitution of Re, Tc, or Mn leads to the destruction of the hidden-order phase and the emergence of ferromagnetism past a certain dopant concentration (Dalichaouch *et al.*, 1990). Only $URu_{2-x}Re_xSi_2$ has been studied in detail. In this system, the hidden-order phase disappears for $x \approx 0.1$ and the system develops a FM ground state for $x \gtrsim 0.15$ (Butch and Maple, 2010). T_C increases monotonically with increasing x and reaches a maximum of almost 40 K at $x \approx 0.8$, above which the material does not remain in a single phase. The existence of FM long-range order has been ascertained by neutron scattering for $x = 0.8$ (Torikachvili *et al.*, 1992) and by ^{29}Si NMR for $x \geq 0.4$ (Kohori *et al.*, 1993). Pronounced NFL behavior has been observed in the specific heat and the electrical resistivity for a large concentration range $0.15 \lesssim x \lesssim 0.8$ (Bauer *et al.*, 2005), and the dynamical magnetic susceptibility shows unusual behavior for $0.2 < x < 0.6$ (Krishnamurthy *et al.*, 2008). The system is highly disordered as judged from the residual resistivity, which is on the order of 100 $\mu\Omega$ cm (Butch and Maple, 2010), and the magnetic moment appears to go to zero continuously. Attempts to determine critical exponents have been hampered by difficulties in precisely determining the critical concentration (Bauer *et al.*, 2005; Butch and Maple, 2009, 2010). Results from scaling plots yield exponents δ and γ that vary continuously with x and approach 1 and 0, respectively, for x approaching the critical value $x_c \approx 0.15$, while $\beta \approx 0.8$ is independent of x (Butch and Maple, 2009, 2010). These results are hard to understand within any phase-transition scenario, even if one interprets the exponents as effective ones in a preasymptotic region. $\gamma = 0$, in particular, contradicts the very notion of a FM order parameter. There currently is no resolution of this problem. The uncertainty about x_c may be to

blame, and the strong disorder may lead to unusual effects. For instance, it is conceivable that there is a Re concentration region that represents a quantum Griffiths phase (see Secs. II.E and III.D.1) rather than true long-range FM order. It has also been speculated that an interplay between remnants of the hidden order and ferromagnetism leads to unusual behavior near the onset of ferromagnetism (Butch and Maple, 2010).

c. $URh_{1-x}Ru_xGe$

Doping URhGe with Ru decreases T_C after a small initial increase and suppresses it to zero at a Ru concentration close to $x = 0.38$ (Huy, Gasparini, Klaasse *et al.*, 2007; Sakarya *et al.*, 2008); see Fig. 8. Huy, Gasparini, Klaasse *et al.* (2007) found the QPT to be second order with a pronounced $T \ln T$ contribution to the specific heat at the critical concentration. The T dependence of the electrical resistivity shows a non-Fermi-liquid T^n behavior, with $n < 2$ over a wide range of concentrations, with a minimum of $n = 1.2$ at the critical concentration. Such NFL behavior has been interpreted as indicative of the existence of a QPT. The continuous nature of the transition is consistent with theoretical expectations, assuming that the large critical Ru concentration leads to a substantial amount of disorder. The strength of the microscopic disorder is hard to determine experimentally, since cracks in the brittle system lead to an artificially high residual resistivity of 200–300 $\mu\Omega$ cm. The Grüneisen parameter Γ is observed to stay finite at the transition, in disagreement with a theoretical result that predicts a diverging Γ (Zhu *et al.*, 2003).

Si doping up to $x \approx 0.2$ has little effect on the T_C of $URhGe_{1-x}Si_x$ (Fig. 8), and no quantum phase transition has been observed in this material (Sakarya *et al.*, 2008).

d. $UCo_{1-x}Fe_xGe$

Doping of the weak FM UCoGe (see Sec. II.B.2.c) with Fe initially increases T_C to a maximum of $T_C \approx 8.5$ K around $x = 0.075$. With further increasing x, T_C decreases and vanishes at an extrapolated $x_c \approx 0.22$ (Huang *et al.*, 2013). The QPT is believed to be second order, and there is some evidence for quantum-critical behavior in the transport and specific-heat data. Since the transition in UCoGe is first order this implies the existence of a tricritical point in the phase diagram, but this has not been investigated. The origin of the very large residual resistivity is not clear.

e. $Th_{1-x}U_xCu_2Si_2$

UCu_2Si_2 orders ferromagnetically below $T_C \approx 101$ K, and $ThCu_2Si_2$ is paramagnetic. In $Th_{1-x}U_xCu_2Si_2$, Lenkewitz *et al.* (1997) found a QPT for $x \approx 0.15$, with a logarithmic T dependence of the specific-heat coefficient. The large residual resistivity ($\rho_0 > 200$ $\mu\Omega$ cm) is due to microcracks in the samples and not a measure of intrinsic disorder.

3. Quasi-one-dimensional systems

a. $YbNi_4P_2$

$YbNi_4P_2$ is the stoichiometric metallic ferromagnet with the lowest T_C observed to date, $T_C = 0.15$ K (Steppke *et al.*, 2013). In this compound Ni is not magnetic (Députier *et al.*, 1997; Krellner *et al.*, 2011). The Yb atoms are arranged in chains along the c direction and are located between Ni tetrahedra, forming a $ZrFe_4Si_2$ structure type with a lattice-constant ratio $c/a \approx 0.5$. Band-structure calculations show quasi-1D Fermi surfaces (Krellner *et al.*, 2011), which are believed to be responsible for the observed anisotropy of the resistivity, $\rho_a/\rho_c \approx 5$ at 1.8 K (Krellner and Geibel, 2012).

The Yb^{3+} ion is located in an orthorhombic crystalline electric field (CEF) which splits the $J = 7/2$ energy levels, leaving a Kramers doublet as the ground state (Huesges *et al.*, 2013), and causes the crystalline c axis to be the magnetic easy axis (Krellner and Geibel, 2012). This can be seen in Fig. 17, which shows the ac susceptibility $\chi'(T)$ in a small field H parallel and perpendicular, respectively, to the c axis. Although $YbNi_4P_2$ is a heavy-fermion system with a Kondo temperature of 8 K, a small unscreened moment of about $0.05\mu_B$/Yb orders ferromagnetically at 0.15 K (Krellner *et al.*, 2011; Spehling *et al.*, 2012; Steppke *et al.*, 2013; Gegenwart *et al.*, 2015). In addition, despite the strong CEF anisotropy the moments align within the *ab* plane, i.e., the magnetically hard direction (see Fig. 17). $YbNi_4P_2$ shares this uncommon behavior with just a few other FM Kondo-lattice systems, such as CeRuPO (Sec. II.D.2.a), $CeAgSb_2$ (Sec. II.D.3.a), YbNiSn (Bonville *et al.*, 1992), and $Yb(Rh_{0.73}Co_{0.27})_2Si_2$ (Sec. II.D.3.c). An explanation within a local-moment Heisenberg model with competing exchange interactions (Andrade *et al.*, 2014) does not work for $YbNi_4P_2$ where quantum effects are strong. For instance, $\chi'(T)$ in classical Ising or Heisenberg systems is characterized by a power-law behavior at the transition with well-known universal exponents, while the divergence of $\chi' \perp c$ in Fig. 17 just above T_C is much stronger than a power law. It is even stronger than what is expected for a pure

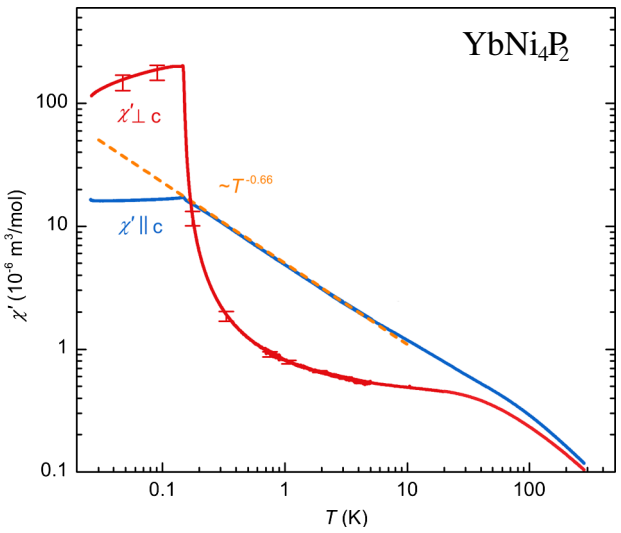

FIG. 17. Temperature dependence of the ac susceptibility $\chi'(T)$ measured with a modulation-field amplitude $\mu_0 H = 15$ μT parallel and perpendicular, respectively, to the c axis. The large value $\chi'(T_C) \approx 200 \times 10^{-6}$ m^3/ mol indicates a FM phase transition. The dashed line indicates that $\chi'_{\parallel}(T) \propto T^{-2/3}$ above T_C. From Steppke *et al.*, 2013.

one-dimensional Ising ferromagnet, where $\chi'(T) \propto T^{-1}\exp(2J/k_BT)$, with J the coupling constant (Ising, 1925). Another proposed explanation is strong transverse spin fluctuations which at sufficiently low temperature dominate the magnetic anisotropy (Krüger, Pedder, and Green, 2014). This model, however, implies a first-order phase transition at T_C, which is not observed in $YbNi_4P_2$ (Steppke *et al.*, 2013).

$YbNi_4P_2$ also has a number of other unconventional properties. For instance, polycrystals in a broad T region above T_C show strong NFL behavior in the resistivity $\rho(T) \propto T$, the specific heat $C/T \propto T^{-0.42}$, and the NMR relaxation rate $1/T_1T \propto T^{-3/4}$ (Krellner *et al.*, 2011; Sarkar *et al.*, 2012).

b. $YbNi_4(P_{1-x}As_x)_2$

The results reviewed in Sec. II.C.3.a motivated the growth of single crystals with phosphorus substituted by arsenic (which amounts to negative chemical pressure) in order to reduce T_C and look for FM quantum criticality. Four single crystals of the series $YbNi_4(P_{1-x}As_x)_2$ were grown with a minimum value of $\rho_0 = 5.5\ \mu\Omega$ cm for the stochiometric $YbNi_4P_2$. Steppke *et al.* (2013) investigated the magnetic and thermodynamic properties down to 20 mK and, in particular, measured the Grüneisen ratio $\Gamma(T) = \beta(T)/C(T)$, where $\beta(T)$ is the volume thermal expansion coefficient. According to Zhu *et al.* (2003), this quantity should diverge as $\Gamma(T) \propto T^{-\lambda}$ at any QCP, where $\lambda = 1/\nu z$ is given in terms of the correlation-length exponent ν and the dynamical exponent z (cf. Sec. III). Steppke *et al.* (2013) found that the FM phase transition is suppressed at $x_c \approx 0.1$ [Fig. 18(a)] and that it remains second order even in the sample with $x = 0.08$ with a T_C of about 25 mK. Both $C(T)/T$ and $\beta(T)/T$ diverge [see Fig. 18(b)] with exponents that are approximately independent of the As concentration, which rules out a possible quantum Griffiths phase (cf. Sec. III.D.1). Most importantly, $\Gamma(T) \propto T^{-0.22}$ in the sample with $x = 0.08$ which is located almost at x_c [see Fig. 18(b)]. This provides evidence that in $YbNi_4(P_{1-x}As_x)_2$ a FM QCP exists. The nature of this QCP is still unclear. The exponent $\lambda = 0.22$ yields a value of $\nu z \approx 5$, which is rather large. For instance, within Hertz-Millis-Moriya theory one has $\nu = 1/2$, $z = 3$ (cf. Sec. III.C.2.b). This is not surprising, as no existing theory is expected to apply to this material. Any theoretical framework will have to take into account the local nature of the Yb $4f$ states with spin-orbit coupling, a strong Kondo effect, and the quasi-1D electronic structure. The absence of a first-order transition is likely due to the latter; see the following discussion.

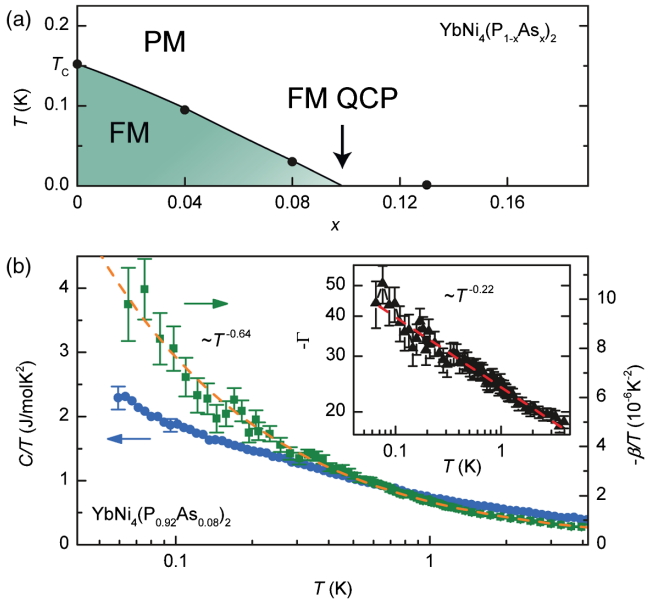

FIG. 18. (a) Phase diagram of $YbNi_4(P_{1-x}As_x)_2$. (b) Specific-heat (blue, left axis) and volume thermal expansion coefficient (green, right axis) for the sample with $T_C \approx 25$ mK ($x = 0.08$). Inset: T dependence of the Grüneisen ratio $\Gamma(T) = \beta(T)/C(T) \propto T^{-0.22}$. From Steppke *et al.*, 2013.

4. Discussion, and comparison with theory

The materials in which a continuous transition is observed to the lowest temperatures achieved have been grouped into three distinct classes; see Tables III, IV, and V: weakly disordered, strongly disordered, and quasi-one-dimensional. For the last group, the conduction-electron system is expected to be a Fermi liquid (FL) at asymptotically low temperatures, but it will cross over to a Luttinger liquid at a temperature that depends on the electronic anisotropy. A determination of the temperature range where the theories discussed in Sec. III, which all depend on an underlying Fermi liquid, still apply requires detailed theoretical considerations that are currently not available. For the strongly disordered bulk systems, the theory discussed in Sec. III.C.3 predicts a continuous transition, and Griffiths effects may also be present; see Sec. III.D.1. Of the two systems in this category, $URu_{2-x}Re_xSi_2$ is the more thoroughly studied one. As discussed in Sec. II.C.2.b, the current experimental results cannot be easily interpreted with any existing theory. A major obstacle is the uncertainty about the critical concentration x_c, and additional studies about the onset of long-range FM order are desirable.

In the weakly disordered group, $CeSi_x$ and Ni_xPd_{1-x} come with open questions regarding the nature of the transition, or the presence of phases other than the FM one, at low temperatures. Given the residual resistivities of these materials, theoretically one would expect a continuous transition in $CeSi_x$, and a first-order one in Ni_xPd_{1-x}, provided the transition is not preempted by a different phase. In $(Cr_{1-x}Fe_x)_2B$ one expects a second-order transition, and the observed mean-field critical behavior is consistent with theoretical expectations; see Sec. III.B.3. For the remaining systems no information about the disorder strength is available, which makes a comparison with theoretical predictions difficult.

These somewhat inconclusive results may well have to be revisited if cleaner samples and/or measurements at lower temperatures should become available in the future. The history of $ZrZn_2$, Sec. II.B.1.b, shows that improving sample quality can change the conclusion about the order of the transition. One also needs to keep in mind that the tricritical temperatures listed in Tables I and II span a substantial range,

TABLE VI. Systems showing change into a spin-density-wave (SDW) or antiferromagnetic (AFM) order. T_C = Curie temperature, T_N = Néel temperature, ρ_0 = residual resistivity, QC = quantum critical, and n.a. = not available.

System	Order of transition[a]	T_C/K	T_N/K	Magnetic moment/μ_B[b]	Tuning parameter	Disorder ($\rho_0/\mu\Omega$ cm)[c]	Comments
$Nb_{1-y}Fe_{2+y}$	1st (?)[d,1]	$72-6$[e]	$32-2.8$[f]	≈ 0.02[2]	Composition[3] pressure[5]	5.5–17[3,4]	SDW phase, Lifshitz point
PrPtAl	1st[g,6]	4.7[6]	5.85, 5.5[h,6]	≈ 1[6]	None	n.a.	Spiral phase, two SDW phases
CeRuPO	1st[i,7]	$15-11$[j,7,8]	$10-1$[j,7,8]	1.2[8]	Pressure[7,8]	≈ 30[7,k]	AFM phase
$CeFeAs_{1-x}P_xO$	n.a.	$\approx 10-6$[l,9,10]	≈ 3[m,11]	$0.95-0$[9]	Composition[9,10]	n.a.	Conflicting results
$CeRu_{1-x}Fe_xPO$	n.a.	$15-0.3$[12]	$\approx 0.5-0$[12]	1.2[13]	Composition[12]	n.a.	QC flucts., possible AFM phase
$CeAgSb_2$	1st[14]	$9.6-2$[14]	$\approx 6-4$[14]	0.41[15]	Pressure[14,16] $\perp$ field[16]	0.2[14]	AFM phase not always observed
$CeRu_2(Ge_{1-x}Si_x)_2$	n.a.	$8-2.5$[17]	$10-1$[17]	n.a.	Comp./press.[1,18]	0.3[18]	Hybridization suppresses FM
$Yb(Rh_{1-x}Co_x)_2Si_2$	n.a.	1.3[n,19]	$1.2-0.07$[o,20]	$0.1-0.002$[p,22,19]	Composition[20] pressure[23,24]	0.5–10[20,21]	Field-induced AFM QPT

[a]For the FM-to-AFM or SDW transition at the lowest temperature achieved.
[b]Per formula unit unless otherwise noted.
[c]For the highest-quality samples.
[d]For the FM-SDW transition. The FM-PM transition on the Nb-rich side is second order to the lowest T_C measured (≈ 2 K).
[e]For $0.04 > y > 0.007$ (Brando *et al.*, 2008; Moroni-Klementowicz *et al.*, 2009).
[f]For $0.015 > y > -0.01$ (Brando *et al.*, 2008; Moroni-Klementowicz *et al.*, 2009).
[g]For the FM-SDW2 and SDW2-SDW1 transitions. The SDW1-PM is 2nd order (Abdul-Jabbar *et al.*, 2015).
[h]For the SDW1-PM and SDW2-SDW1 transitions, respectively (Abdul-Jabbar *et al.*, 2015).
[i]For the FM-AFM transition at $T \gtrsim 9$ K. The order of the transition at low T is not known.
[j]FM for $0 \leq p \lesssim 0.7$ GPa and AFM for $0.7 \lesssim p \leq 2.8$ GPa (Kotegawa *et al.*, 2013; Lengyel *et al.*, 2015).
[k]Near the FM-AFM transition.
[l]For $x = 0.4$–0.8 (Luo *et al.*, 2010; Jesche *et al.*, 2012).
[m]For $x = 0.9$ (Jesche, 2011).
[n]For $Yb(Rh_{0.73}Co_{0.27})_2Si_2$ (Lausberg *et al.*, 2013).
[o]For $x = 0.27 - 0$ (Klingner *et al.*, 2011).
[p]0.002 μ_B for $YbRh_2Si_2$ (Ishida *et al.*, 2003); 0.1 μ_B for $Yb(Rh_{0.73}Co_{0.27})_2Si_2$ (Lausberg *et al.*, 2013).
[1]Friedemann (2015). [2]Brando *et al.* (2008). [3]Moroni-Klementowicz *et al.* (2009). [4]Friedemann *et al.* (2013).
[5]Duncan *et al.* (2010). [6]Abdul-Jabbar *et al.* (2015). [7]Kotegawa *et al.* (2013). [8]Lengyel *et al.* (2015). [9]Luo *et al.* (2010).
[10]Jesche *et al.* (2012). [11]Jesche (2011). [12]Kitagawa *et al.* (2012). [13]Krellner *et al.* (2007). [14]Sidorov *et al.* (2003).
[15]Araki *et al.* (2003). [16]Logg *et al.* (2013). [17]Süllow *et al.* (1999). [18]Wilhelm and Jaccard (1998). [19]Lausberg *et al.* (2013).
[20]Klingner *et al.* (2011). [21]Krellner *et al.* (2009). [22]Ishida *et al.* (2003). [23]Mederle *et al.* (2001). [24]Knebel *et al.* (2006).

and the T_{tc} in, for instance, URhGe is barely higher than the lowest temperature at which UIr has been measured.

D. Systems changing to spin-density-wave or antiferromagnetic order

In some systems the FM phase undergoes a transition to a spatially modulated magnetic phase as T_C decreases; see the schematic phase diagram in Fig. 2(c).[15] This produces a Lifshitz point, where the FM, modulated, and PM phases meet, as well as two QPTs, one from the FM phase to the modulated one, and one from the modulated phase to the PM. They are discussed later, and their properties are summarized in Table VI. In some of these materials the evidence for a modulated phase is stronger than in others, and in some cases there are conflicting experimental results. The classification of some of these systems within our scheme should thus be considered tentative.

1. Simple ferromagnets

a. An itinerant magnet: $Nb_{1-y}Fe_{2+y}$

The Laves phase compound $NbFe_2$ shows itinerant antiferromagnetism on the border of a FM phase. First indications of a low-T AFM ordered state with $T_N \simeq 10$ K were found in magnetization and NMR experiments on polycrystals (Shiga and Nakamura, 1987; Yamada and Sakata, 1988; Crook and Cywinski, 1995). This was recently confirmed by a microscopic study with electron spin resonance, muon-spin relaxation, and Mössbauer spectroscopy on single crystals (Rauch *et al.*, 2015). However, this state is characterized by an unusually high magnetic susceptibility, $\chi \approx 0.02$ in SI units, which corresponds to a large Stoner enhancement factor of the order of 180 (Brando *et al.*, 2008). They speculated that the magnetic order in $NbFe_2$ is a long-wavelength modulated state with a small ordering wave number $Q \approx 0.05$ Å^{-1}. This

[15]There also are cases of transitions from a metallic AFM state to a metallic FM state, with the FM being the ground state; see Sec. IV.B, point 3. We do not discuss these materials.

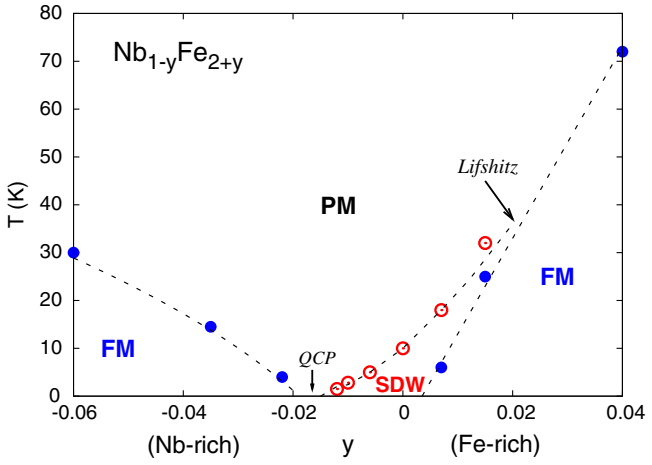

FIG. 19. Phase diagram of $Nb_{1-y}Fe_{2+y}$. From Moroni-Klementowicz *et al.*, 2009.

was corroborated by recent neutron scattering experiments (Niklowitz, 2015).

The Wilson ratio (i.e., the low-T susceptibility divided by the specific-heat coefficient) is about 60, which indicates that the susceptibility is much more enhanced than the effective electron mass. This suggests that stoichiometric $NbFe_2$ is very close to the border of ferromagnetism. Indeed, a FM ground state is found in iron-rich samples (Yamada and Sakata, 1988; Crook and Cywinski, 1995; Moroni-Klementowicz *et al.*, 2009). By varying the iron content in $Nb_{1-y}Fe_{2+y}$ within a narrow homogeneity range, $NbFe_2$ can be tuned from ferromagnetism for $y \gtrsim 0.01$ via an intermediate SDW modulated state around $y \simeq 0$ to a QCP at $y \approx -0.015$. For $y < -0.015$ the ground state becomes FM again (Fig. 19). The fact that both iron and niobium-rich samples are FM at low temperature has been linked to the peculiar electronic structure of this material (Subedi and Singh, 2010; Tompsett *et al.*, 2010; Alam and Johnson, 2011; Neal, Ylvisaker, and Pickett, 2011). Part of the phase diagram can also be reproduced by applying hydrostatic pressure (Duncan *et al.*, 2010): Starting with a FM sample with $y = 0.015$, increasing pressure is equivalent to moving the system to the left in the phase diagram of Fig. 19. A pressure of 2.5 GPa roughly corresponds to a shift in composition from $y = 0.015$ to 0.007. For $y \gtrsim -0.015$, $Nb_{1-y}Fe_{2+y}$ is thus an itinerant system in which a SDW state with a small wave vector connects continuously to the FM state at a Lifshitz point; cf. Fig. 19. Signatures of quantum-critical behavior have been observed near the QPT where the SDW order disappears: the electrical resistivity displays a $T^{3/2}$ power-law behavior, and the specific-heat coefficient γ shows a logarithmic temperature dependence down to 0.1 K (Brando *et al.*, 2008). The latter is consistent with Hertz-Millis-Moriya theory for a clean FM,[16] but the former disagrees with the $T^{5/3}$ behavior expected for this case; see Eqs. (3.62) and (3.64). A $T^{3/2}$ behavior of the resistivity has also been observed in other systems, e.g., in MnSi and $ZrZn_2$, even far from the QPT, which suggests a more general phenomenon that remains incompletely understood; see Sec. IV.A. In the current case, the proximity to both FM and SDW order may result in fluctuations with different wave vectors that have different effects on the transport and thermodynamic properties, respectively. This might explain the apparent inconsistency between the behavior of the specific heat and the resistivity (see footnote [16]).

The existence of a QCP indicates that the PM-to-SDW transition is second order, at least at low temperature. There are indications that the FM-to-SDW transition at $y = 0.015$ is first order (Friedemann, 2015). On the Nb-rich side of the phase diagram, the transition was found to be second order for all samples investigated by Moroni-Klementowicz *et al.* (2009).

b. An induced-moment magnet: PrPtAl

Another example of a modulated magnetic state in a narrow temperature range above the FM phase is given by PrPtAl. Since the orthorhombic TiNiSi-type structure of PrPtAl is inversion symmetric, the modulated order cannot be due to a Dzyaloshinski-Moriya interaction. Neutron scattering data in conjunction with a theoretical analysis have been interpreted as indicating that it is a result of quantum-critical fluctuations, in accord with the mechanism reviewed in Sec. III.E (Abdul-Jabbar *et al.*, 2015).

Initial experiments on polycrystals identified a second-order phase transition into a FM state at $T_C = 5.8$ K with an ordered saturation moment of $1\mu_B/\mathrm{Pr}$ (Hulliger, 1993; Kitazawa *et al.*, 1998). As in other rare-earth systems, the origin of magnetism in PrPtAl is subtle. Although the ground state of the Pr^{3+} ion is a nonmagnetic singlet, magnetic moments are induced by an interplay between the exchange interaction and the CEF. This causes strong short-range correlations, which are responsible for the small entropy release (only about 15% of $R \ln 2$) below T_C and significant magnetic anisotropy (Kitazawa *et al.*, 1998).

Neutron scattering experiments on single crystals have revealed two SDW phases just above T_C: Below $T_1 = 5.85$ K Abdul-Jabbar *et al.* (2015) found a doubly modulated incommensurate SDW (SDW1), followed by a single incommensurate modulation (SDW2) at a different ordering vector below $T_2 = 5.5$ K, and eventually the transition into the FM state at $T_C = 4.7$ K. Both SDW phases are suppressed by a weak magnetic field; this may be the reason why these phases were not seen before. The magnetic structure in the SDW2 phase is an elliptical spiral. Spiral order preceding a FM transition is not uncommon in rare-earth magnets such as, for instance, Tb and Dy, and is usually attributed to a complex interplay between the anisotropy energy and the exchange interaction (Miwa and Yosida, 1961). However, in PrPtAl Abdul-Jabbar *et al.* (2015) pointed at the lack of apparent nesting vectors which would favor spiral order, the temperature dependence of the ordering wave vector in the spiral phase SDW2, the low critical magnetic fields required to tune between the SDW2 phase and FM, and the second-order nature of the transition at T_1, which contrasts with the first-order nature at T_2 and T_C. They argued that the mechanism behind the spiral formation in SDW2 must involve the strong magnetic fluctuations in the competing ordered states. Starting from the model proposed by Karahasanovic, Krüger, and

[16] As explained in Sec. III.C.2, in the FM case this does not represent true critical behavior, but it may be observable in a sizable preasymptotic region.

Green (2012) and adding local moments, the strong anisotropy, and weak disorder, they derived a theory that can describe key experimental results observed by neutron scattering and measurements of the magnetoresistivity and the specific heat. Although the full phase diagram has not been accessed experimentally, the proposed phase diagram is similar to that in Fig. 39 without the nematic phase. This material may thus represent a case in which the mechanism discussed in Sec. III.E is realized.

2. Ferromagnetic Kondo-lattice systems: CeTPO

Quantum criticality in FM Kondo-lattice systems has received little attention compared to their AFM counterparts (Gegenwart, Si, and Steglich, 2008 and references therein.) Often these materials possess peculiar crystal structures, such as the quasi-1D heavy-fermion material $YbNi_4P_2$ (Sec. II.C.3), or the quasi-2D cerium transition-metal (T) phosphide oxides CePTO, which are the topic of this section. For other Kondo-lattice systems, see Sec. II.D.3.

The quasi-2D tetragonal ZrCuSiAs-type of the CePTO systems is familiar from some of the iron-based superconductors, such as LaFePO (Kamihara *et al.*, 2006). It consists of alternating layers of TP_4 and OCe_4 along the crystallographic c axis (Zimmer *et al.*, 1995). The Ce-Ce interatomic distance is in the range where the RKKY interaction is ferromagnetic (Sereni, 1991; Chevalier and Malaman, 2004). However, not all CeTPO systems are FM, for instance, CeOsPO is an AFM (Krellner *et al.*, 2007). Two compounds that have been studied with respect to FM quantum criticality are CeRuPO and CeFePO. CeRuPO is a ferromagnet with $T_C = 15$ K (Krellner *et al.*, 2007), and CeFePO is a paramagnet with strong in-plane FM fluctuations (Brüning *et al.*, 2008). In what follows we review studies of CeRuPO under hydrostatic pressure, and of $CeRu_{1-x}Fe_xPO$ and $CeFeAs_{1-x}P_xO$. The special case of stoichiometric CeFePO is discussed in Sec. II.E.4.

a. CeRuPO

The low-T properties of CeRuPO polycrystalline samples (RRR = 50) were first investigated by Krellner *et al.* (2007). They found a Curie-Weiss behavior of the susceptibility at high T (Ce is trivalent in this compound and Fe is nonmagnetic) with a positive Weiss temperature $\Theta_W = 8$ K and FM order below $T_C = 15$ K. The transition at T_C is second order, indicated by the λ-like shape of the specific heat. The resistivity shows a distinctive drop below about 50 K which is a signature of coherent Kondo scattering. The Kondo temperature $T_K \approx 10$ K, estimated from an analysis of the entropy, is comparable with T_C.

Using a Sn-flux method, Krellner *et al.* (2007) grew high-quality single crystals with $\rho_0 = 5\ \mu\Omega\,\mathrm{cm}$ (RRR = 30) (Krellner and Geibel, 2008), and studied the magnetic anisotropy. At high T the susceptibility measured with $H\|c$ and $H\perp c$ shows a Curie-Weiss behavior, but with very different Weiss temperatures for the two cases: $\Theta_W^{ab} \approx 4$ K and $\Theta_W^{c} = -250$ K. This temperature difference can be expressed in terms of the first CEF parameter, which is a measure of the strength of the magnetocrystalline anisotropy (Bowden, Bunbury, and McCausland, 1971). It indicates that the CEF anisotropy favors the moments to be aligned within the ab plane. However, the magnetic moments below T_C align along the c axis. This is shown in Fig. 20, which displays the magnetization isotherms at 2 K. Ordering of the moments along the magnetic hard direction is also found in YbNiSn (Bonville *et al.*, 1992), $Yb(Rh_{0.73}Co_{0.27})_2Si_2$ (Lausberg *et al.*, 2013), $YbNi_4P_2$ (Steppke *et al.*, 2013), and $CeAgSb_2$ (Araki *et al.*, 2003).

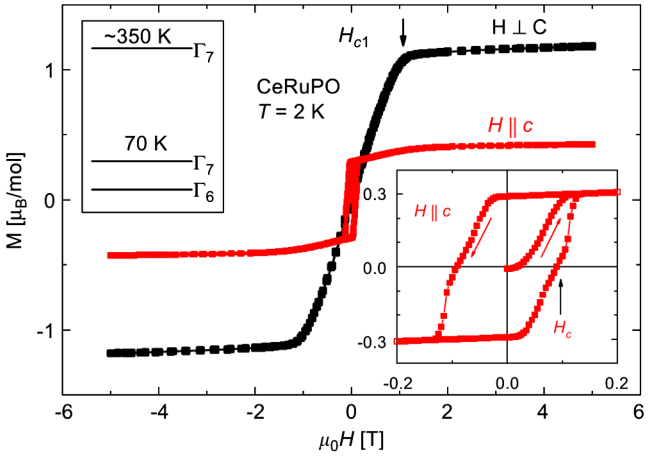

FIG. 20. Magnetization isotherms at 2 K with $H\|c$ and $H\perp c$. From Krellner and Geibel, 2008.

Quantum criticality in CeRuPO has been looked for by means of resistivity measurements under pressure, with the current in the ab plane. Pressure was found to decrease T_C, to 5.9 K at 2.1 GPa, which by extrapolation suggested a QCP at about 3.2 GPa (Macovei *et al.*, 2009). Lengyel *et al.* (2015) investigated the ac susceptibility under pressure and performed resistivity experiments at pressures up to 7.5 GPa. These experiments found that the FM ground state changed into an AFM one (with unknown structure) at a pressure of about 0.87 GPa. At $p \geq 3$ GPa the resistivity no longer shows a phase transition, and the observations suggested a first-order QPT at a critical pressure $p_c \approx 3$ GPa, with no QCP. Above p_c the ground state was proposed to be a Fermi liquid, due to a T^2 behavior of the resistivity. The coefficient of the T^2 term in the resistivity shows a maximum at about 4 GPa, well inside the FL paramagnetic state.

The T-p-H phase diagram of CeRuPO, up to $p = 3.5$ GPa, was investigated by Kotegawa *et al.* (2013); see Fig. 21. The observed sensitivity of the magnetic order to a magnetic field ascertained that the FM state changes into an AFM one above $p \approx 0.7$ GPa, and the magnetic order was found to be completely suppressed at $p_c = 2.8$ GPa. CeRuPO is thus another case where an anticipated FM QPT is not realized because a modulated phase intervenes. Although the authors could not determine the order of the transition at p_c the coefficient of the T^2 term in the resistivity shows a maximum around p_c, which suggests the presence of an AFM QCP. This is in disagreement with Lengyel *et al.* (2015). ^{31}P-NMR experiments revealed the fact that the magnetic correlations are 3D over the entire pressure range investigated (Kitagawa *et al.*, 2014), in contrast to what was found in $Ce(Rh_{1-x}Fe_x)PO$; see Sec. II.D.2.c. The FM-AFM transition was found to be first order at the two points denoted by open circles in Fig. 21; the order of the transition at lower

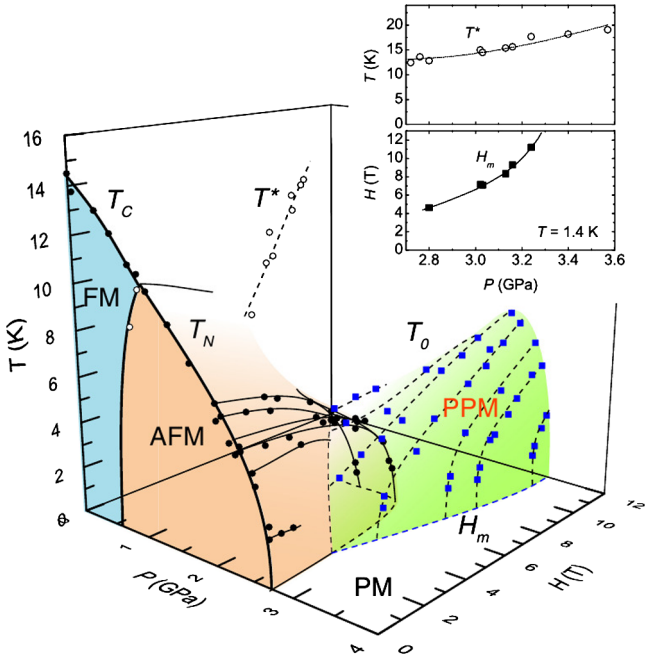

FIG. 21. Pressure-temperature-magnetic field phase diagram of CeRuPO derived from resistivity measurements. At ambient pressure and $H = 0$ the ground state is FM, but changes into an AFM one at about 0.7 GPa. Magnetism is suppressed at $p_c \approx 2.8$ GPa. The AFM state is identified by the transition temperature decreasing with increasing field (solid black lines). At even larger fields (H_m) a metamagnetic crossover occurs from a PM state to a polarized PM (PPM) state. T^* indicated the Kondo coherence temperature which increases with increasing pressure. From Kotegawa *et al.*, 2013.

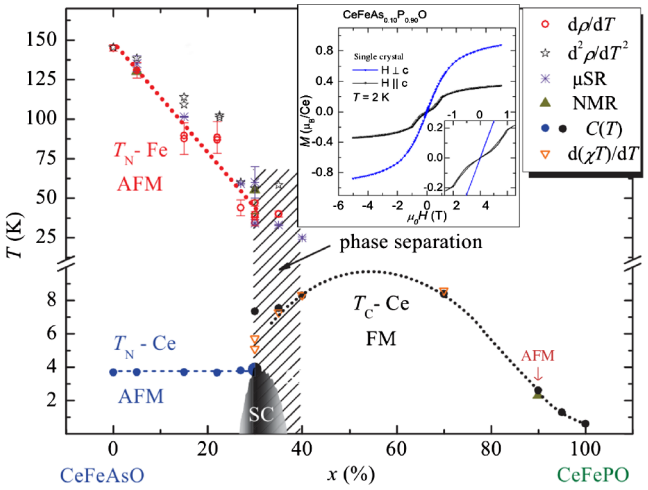

FIG. 22. T-x phase diagram of $CeFeAs_{1-x}P_xO$ obtained by a variety of techniques (list in the right inset) for single and polycrystalline samples. Red and blue dotted lines indicate the AFM ordering temperature of the Fe and Ce sublattices, respectively. Superconductivity (SC) is found near $x = 0.3$. The dotted black line is the Curie temperature for the FM order of the Ce atoms. From Jesche, 2011, and Jesche *et al.*, 2012.

temperatures is not known. We note that the AFM-to-FM transition in $Yb(Rh_{1-x}Co_x)_2Si_2$ with $x = 0.215$ (see Fig. 27) has also been reported to be first order (Klingner *et al.*, 2011; Hamann, 2015), as has the SDW-to-FM transition in $Nb_{1-y}Fe_{2+y}$ (see Fig. 19) (Friedemann, 2015).

At pressures close to p_c, Kotegawa *et al.* (2013) observed another resistivity feature at a magnetic field H_m and a temperature T_0, which increases with increasing field (see Fig. 21). They ascribed this to a metamagnetic crossover from a PM state to a polarized PM (PPM) state. This is similar to what was observed in doped $CeRu_2Si_2$ (Flouquet *et al.*, 2002, 2010; Shimizu *et al.*, 2012).

b. $CeFeAs_{1-x}P_xO$

CeFePO is a PM very close to a FM instability (Brüning *et al.*, 2008), which motivated searches for an FM phase nearby. The substitution of As at the P site acts as negative chemical pressure and favors magnetic order in Ce-based systems. It also permits one to study the evolution of Fe and Ce magnetism from the AFM CeFeAsO (Zhao *et al.*, 2008) to CeFePO. This was done independently by two groups (Luo *et al.*, 2010; Jesche *et al.*, 2012).

Luo *et al.* (2010) measured the phase diagram of polycrystalline samples of $CeFeAs_{1-x}P_xO$ and confirmed that the commensurate AFM order of the Fe sublattice below $T_N^{Fe} \approx 140$ K in CeFeAsO is suppressed by P substitution. With increasing x the unit cell shrinks along the c axis substantially faster than along the a axis, which is important for the evolution of the f-d hybridization strength. The AFM order disappears at $x \approx 0.4$, and an AFM QCP was suspected (Luo *et al.*, 2010; de la Cruz *et al.*, 2010). Moreover, Luo *et al.* (2010) found that the Ce sublattice also orders antiferromagnetically at $T_N^{Ce} = 4.16$ K, which is very weakly x dependent for small x. At $x \approx 0.37$ the ground state of the Ce sublattice changes from AFM to FM, and FM order was found to persist up to $x \approx 0.9$. In a small concentration region at $x \lesssim 1$ the system was found to be a HF paramagnet with strong FM fluctuations, in agreement with Brüning *et al.* (2008), and a second QCP, for the FM-HF transition, was suggested.

Later studies by Jesche (2011, 2012) found additional features in the phase diagram (see Fig. 22) and disagree in some respects with Luo *et al.* (2010). Instead of an AFM QCP they found that the AFM order terminates at a nonzero $T_N^{Fe} \approx 30$ K and is followed by a region of phase separation, indicating a possible tricritical point. They also found superconductivity, possibly coexisting with Ce ferromagnetism, in a small dome around $x = 0.3$ at temperatures up to 4 K. On the large-x side of the phase diagram Jesche (2011) and Krellner and Jesche (2014) found that a single-crystal sample with $x = 0.9$ had an AFM ground state rather than a FM one. This evidence is shown in the inset of Fig. 22, which shows the isothermal magnetization at $T = 2$ K, i.e., below the transition temperature of about 2.7 K for this concentration. There is no remanent magnetization at $B = 0$ in both field directions, and a metamagnetic transition at $B = 1$ T implies that the ground state is indeed AFM. This indicates that $CeFeAs_{1-x}P_xO$ belongs to the class of systems where the order changes from FM to AFM as T_C decreases, as is the case in CeRuPO under pressure (Sec. II.D.2.a), and $CeRu_{1-x}Fe_xPO$ (Sec. II.D.2.c). This implies that there must be a Lifshitz point on the phase boundary shown in Fig. 22, and a QPT from the FM phase to

the AFM phase, followed by an AFM QPT. These issues have not been investigated.

c. $CeRu_{1-x}Fe_xPO$

CeRuPO is a low-temperature FM (see Sec. II.D.2.a), while CeFePO is a PM with strong FM fluctuations (see Sec. II.D.2.b); this motivated the study of the series $CeRu_{1-x}Fe_xPO$. The substitution of Fe for Ru is isoelectronic and affects just the Fe(Ru)P layers without causing much disorder in the CeO layers responsible for the magnetism. Kitagawa *et al.* (2012) investigated polycrystalline (oriented powder) samples by ^{31}P NMR. They measured the Knight shift K, which is proportional to the uniform magnetization, and the spin-lattice relaxation rate $(1/T_1)$, which is a measure of the fluctuations perpendicular to the applied field direction, for fields parallel ($\|$) and perpendicular ($\perp$) to the c axis of the tetragonal crystallographic structure. Because of the XY-type anisotropy, the largest signal is found for $K_\perp$ and $(1/T_1)_\|$, which both show a strong T dependence.

The FM transition temperature was determined by the large increase of $K(T)$ at T_C and the peak in $(1/T_1)_\|$ as shown in Fig. 23 for $\mu_0 H = 0.5$ T; the resulting phase diagram is shown in Fig. 24. With increasing Fe content, both T_C and the ordered moment, as determined from the Knight shift (not shown), are continuously suppressed until both vanish at $x_c \approx 0.86$. The phase transition is clearly second order at $x = 0$ and remains second order for all concentrations, although a significant broadening of the relaxation rate and of the Knight-shift increase is seen at $x = 0.85$. This might indicate a spin-glass-like or short-range ordered state, as was observed in pure CeFePO (Lausberg *et al.*, 2012), see Sec. II.E.4, but this is not quite clear. It is possible that short-range order, if it is present, is suppressed by the applied field (about 0.5 T is needed for most NMR measurements); in CeFePO the short-range ordered state is suppressed at this field strength. One thus must keep in mind that Fig. 24 does not show a zero-field phase diagram, and this is more relevant for $x \approx x_c$ than for small x.

The strong fluctuations observed near x_c are a clear sign of a QCP, the nature of which is not purely ferromagnetic. The NMR data in a field $\mu_0 H = 0.07$ T for a sample with $x = 0.85$ showed that, in addition to the homogeneous FM ($q = 0$) component of the fluctuations that levels off below $T = 3$ K, there are AFM ($q \neq 0$) components that continue to increase as the temperature is lowered toward $T_C \approx 300$ mK (Kitagawa *et al.*, 2012). Similar behavior was found in $YbRh_2Si_2$ near an AFM QCP (Ishida *et al.*, 2003). The behavior near the QCP was further investigated by Kitagawa *et al.* (2013), who concluded that the suppression of ferromagnetism is due to a change of the effective dimensionality of the FM fluctuations from 3D to 2D near x_c. This is in contrast to what was observed in stoichiometric CeRuPO under hydrostatic pressure, where the magnetic correlations remain 3D at all values of the pressure, including p_c (Kitagawa *et al.*, 2014). Another interesting effect is a metamagnetic crossover (not a first-order transition) at a field H_M perpendicular to the c axis (Kitagawa *et al.*, 2011, 2012). The tips of these "crossover wings" coincide with the QCP and the wings grow with increasing field; their shape is thus very different from that of the tricritical wings discussed in Sec. II.B. A possibly related observation is that pure CeFePO at $\mu_0 H \approx 4$ T shows NFL behavior commonly associated with a QCP (Kitagawa *et al.*, 2011). They suggested that H_M represents the field that breaks the local Kondo singlet,

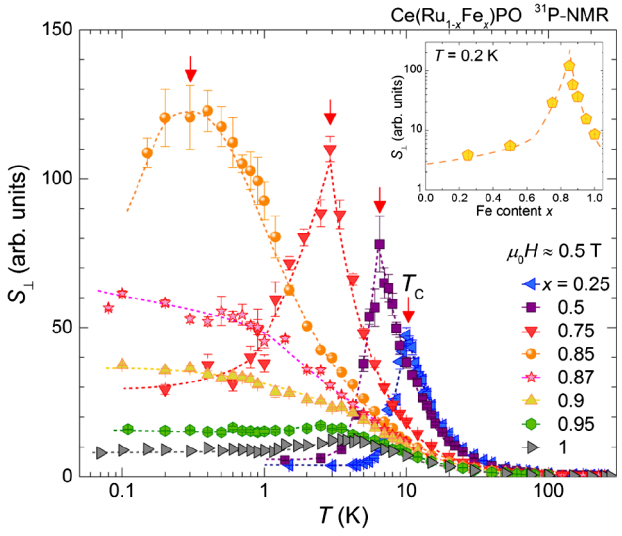

FIG. 23. Temperature dependence of the in-plane spin fluctuations $S_\perp = (1/2T_1)_{H\|c}$ at $\mu_0 H = 0.5$ T for various values of x. The peak indicates the FM transition temperature T_C, which is visible only for $x \leq 0.85$. For $x > 0.85$, $S_\perp$ is constant at low T. The inset shows the x dependence of $S_\perp$ at a temperature of 200 mK. $S_\perp$ peaks at x_c indicating the presence of a QCP. From Kitagawa *et al.*, 2012.

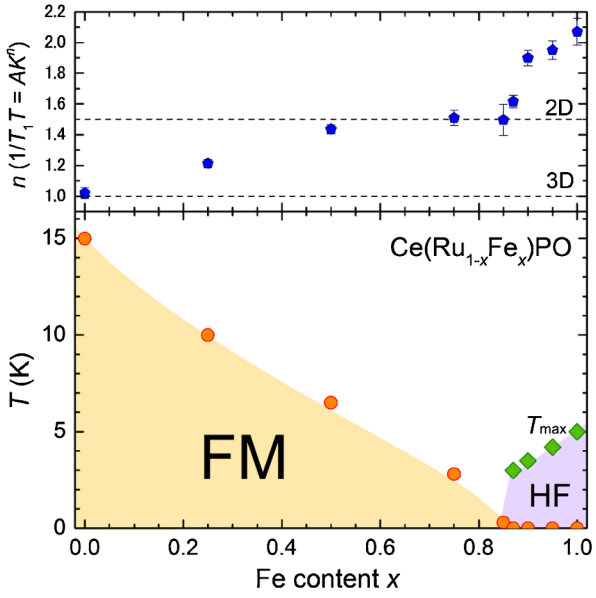

FIG. 24. Lower panel: x-T phase diagram of $CeRu_{1-x}Fe_xPO$ derived from NMR studies. Strong fluctuations are indicative of a QCP at $x_c \approx 0.86$. At larger x the ground state is a heavy-fermion (HF) paramagnet, bounded by the temperature T_{max} where the Knight shift shows a peak. Upper panel: The exponent n is indicative of the effective dimensionality of magnetic correlations, with $n = 1.5$ corresponding to 2D correlations. From Kitagawa *et al.*, 2013.

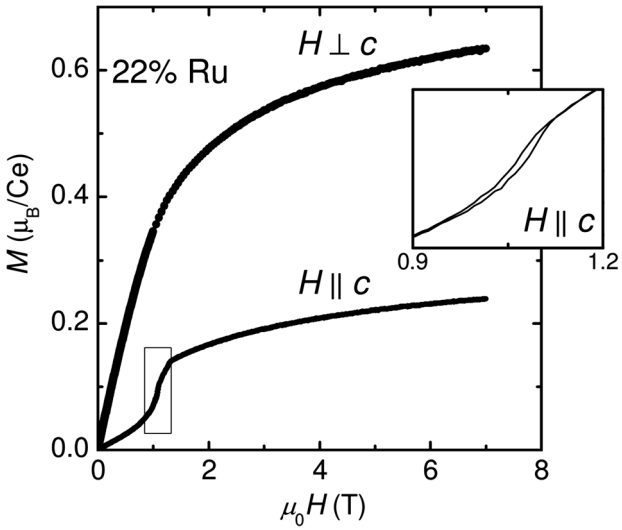

FIG. 25. Isothermal magnetization of a single crystal of $CeRu_{0.22}Fe_{0.78}PO$ for $H\|c$ and $H\perp c$ at $T \approx 1.8$ K. Note the absence of a remanent magnetization at $H = 0$. The inset shows a weak hysteresis loop near $\mu_0 H = 1.1$ T for $H\|c$. From Jesche *et al.*, 2016.

and that the critical behavior is driven by the Kondo breakdown accompanied by a Fermi-surface instability.

These NMR results paint a picture that is rather different from that of CeRuPO under pressure, where a phase of an AFM character intervenes before the FM QCP is reached; see Sec. II.D.2.a. However, Jesche *et al.*, 2016 found an AFM ground state between the FM and PM phases in single crystals with a Ru content close to 20%, just as in CeRuPO under pressure. An example is shown in Fig. 25 that displays the field dependence of the magnetization for a sample with 22% of Ru content at $T \approx 1.8$ K, below the transition temperature of 2.5 K for this concentration. There is no remanent magnetization at zero field in either field direction. In addition, for $H\|c$ a metamagnetic increase of the magnetization with a small hysteresis loop is found for $\mu_0 H \approx 1.1$ T (see the inset in Fig. 25) indicating a first-order metamagnetic transition. This is reminiscent of the situation in $CeFeAs_{1-x}P_xO$ (cf. the inset in Fig. 22) and $NbFe_2$ (Moroni-Klementowicz *et al.*, 2009).

3. Other Kondo-lattice systems

a. $CeAgSb_2$

Neutron scattering experiments on the Kondo-lattice system $CeAgSb_2$ found an ordered moment of $0.41\mu_B$/Ce that aligns uniaxially along the tetragonal c axis, whereas magnetization measurements indicate a strong magnetocrystalline anisotropy with the basal plane as the magnetic easy plane (Araki *et al.*, 2003; Takeuchi *et al.*, 2003). For other examples of such alignment along the hard direction see Sec. II.D.2.a. For this reason, quantum criticality in $CeAgSb_2$ has been studied by transversal-field tuning with $H\perp c$. The critical field is $H_c \approx 2.8$ T (Strydom, Mhlungu, and Thamizhavel, 2008; Logg *et al.*, 2013; Zou *et al.*, 2013). The transition is suspected to remain second order to the lowest T_C measured, about 2 K.

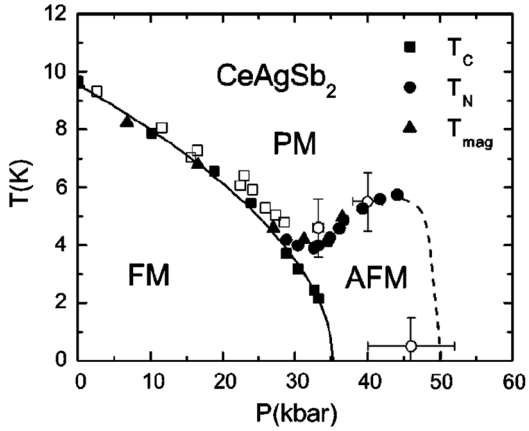

FIG. 26. Pressure-temperature phase diagram of $CeAgSb_2$. T_C and T_N were determined from $d\rho/dT$ while T_{mag} is from ac-calorimetry measurements. From Sidorov *et al.*, 2003.

The FM order in $CeAgSb_2$ can also be suppressed by hydrostatic pressure. Sidorov *et al.* (2003) measured the resistivity and the ac heat capacity of very pure single crystals (RRR $\approx$ 285–480) at pressures $p \lesssim 50$ kbar. They found that the FM state changes into a presumably AFM state above 27 kbar, with the new phase persisting to about 46 kbar (see Fig. 26). The thermal FM phase transition is second order for $p < 27$ kbar and the entropy below T_C indicates that the Kondo temperature in this material is well below T_C (Sidorov *et al.*, 2003; Zou *et al.*, 2013). For $27 < p < 33$ kbar the resistivity signature (specifically in $d\rho/dT$) at the FM transition sharpens considerably with increasing p, indicating that the FM-to-AFM transition is first order. This is reminiscent of the situation observed in other ferromagnets which show a change to AFM order, such as $Yb(Rh_{1-x}Co_x)_2Si_2$, CeRuPO, or $Nb_{1-y}Fe_{2+y}$ (cf. Table VI). However, subsequent experiments by other groups, measuring the resistivity and magnetization under pressure, could not detect the AFM phase, possibly because of lower sample quality (RRR $\approx$ 110) or the limited resolution of the measurements (Kobayashi *et al.*, 2007; Logg *et al.*, 2013).

b. $CeRu_2Ge_2$ *and* $CeRu_2(Ge_{1-x}Si_x)_2$

$CeRu_2Ge_2$ is a FM Kondo-lattice system with $T_C \approx 8$ K, a spontaneous magnetization of $1.96\mu_B$ along the tetragonal c axis (Böhm *et al.*, 1988; Besnus *et al.*, 1991), a Kondo temperature $T_K \approx 2$ K, and a rather small Sommerfeld coefficient of 20 mJ/K^2 mol. In some crystalline samples specific-heat and magnetization measurements exhibit two transitions, a hump at $T_N \approx 8.2$ K and a sharp transition at $T_C \approx 7.7$ K (Fontes *et al.*, 1996; Raymond, Raoelison *et al.*, 1999). Between T_C and T_N, long-range order was identified to be AFM with an incommensurate wave vector $\boldsymbol{q} = (0.31, 0, 0)$. Studies under hydrostatic pressure (Kobayashi *et al.*, 1998; Wilhelm and Jaccard, 1998; Süllow *et al.*, 1999) revealed a rich p-T phase diagram that is well reproduced by Si substitution for Ge (Haen, Bioud, and Fukuhara, 1999). Both local-moment FM and AFM phases exist at low pressures. Above 20 kbar the FM phase changes into a second low-T AFM phase. The magnetic order is then rapidly suppressed near $p_c \approx 67$ kbar, accompanied by NFL behavior

with a linear-in-T resistivity. For $p > p_c$ the ground state is a Fermi liquid with an enhanced quasiparticle mass that decreases toward higher pressures (Süllow *et al.*, 1999). A similar phase diagram was obtained by substituting Ru by Fe (Raymond, Raoelison *et al.*, 1999).

Although the p-T phase diagram of $CeRu_2Ge_2$ and its Si-doped variety has the general shape shown in Fig. 2(c), the underlying physics may be different from other systems. This is because the change in the ground state from FM to AFM occurs when the Kondo temperature is much smaller than the transition temperatures (Süllow *et al.*, 1999). The modification of the ordered state is therefore likely due to a pressure dependence of the exchange interaction and is not driven by the mechanism discussed in Sec. III.E.

c. $YbRh_2Si_2$ and $Yb(Rh_{1-x}Co_x)_2Si_2$

The heavy-fermion metal $YbRh_2Si_2$ (Trovarelli *et al.*, 2000) is a prototypical example of a quantum-critical system (Gegenwart *et al.*, 2002; Custers *et al.*, 2003); for reviews, see Gegenwart, Si, and Steglich (2008) and Si and Steglich (2010). Here we focus only on properties that are related to ferromagnetism.

$YbRh_2Si_2$ crystallizes in the body-centered tetragonal $ThCr_2Si_2$ structure. The Yb ions are in the trivalent state as indicated by the high-T Curie-Weiss behavior of the susceptibility $\chi(T)$ with an effective magnetic moment of $4.4\mu_B$, i.e., close to what is expected for a free Yb^{3+} ion. The Weiss temperatures $\Theta_W(B\|c) = -180$ K and $\Theta_W(B\perp c) = -9$ K indicate a strong magnetocrystalline anisotropy (Trovarelli *et al.*, 2000). The CEF splits the $J = 7/2$ levels into four Kramers doublets, leaving the ground state separated from the three excited doublets by approximately 17, 25, and 43 meV, respectively (Stockert *et al.*, 2006). $YbRh_2Si_2$ has a high Kondo temperature $T_K \approx 25$ K (Köhler *et al.*, 2008), but a small unscreened magnetic moment of about $10^{-3}\mu_B$/Yb (Ishida *et al.*, 2003) orders antiferromagnetically below $T_N \approx 0.07$ K (Trovarelli *et al.*, 2000). The exact magnetic structure is still unknown. T_N can be suppressed by a magnetic field $B \approx 0.06$ T perpendicular to the magnetically hard c axis (Gegenwart *et al.*, 2002), or by negative chemical pressure ($p \approx -0.25$ GPa) (Mederle *et al.*, 2001; Macovei *et al.*, 2008), which tunes the system to QCPs.

$YbRh_2Si_2$ shows pronounced NFL behavior in transport and thermodynamic quantities, indicating the presence of strong spin fluctuations. For instance, the resistivity $\rho(T) \propto T$ below 10 K and the Sommerfeld coefficient diverges as a power law $C/T \propto T^{-0.34}$ for $T \lesssim 0.3$ K, similar to what is observed in the low-T FM $YbNi_4P_2$ (Krellner *et al.*, 2009). The latter behavior has been interpreted in terms of a breakup of the heavy quasiparticles at the QCP (Custers *et al.*, 2003). At low temperature the susceptibility $\chi_{\perp c}$ is very large for an AFM ($\approx 8.5 \times 10^{-6}$ m^3/mol ≈ 0.18 SI) and about 20 times larger than $\chi_{\|c}$. This and the value of the Sommerfeld-Wilson ratio of about 30 indicate the presence of strong FM fluctuations (Gegenwart *et al.*, 2005), consistent with NMR (Ishida *et al.*, 2003) and neutron scattering data (Stock *et al.*, 2012). In an intermediate temperature range, for $0.3 \lesssim T \lesssim 4$ K, $C(T)/T \propto \ln(T_0/T)$, with $T_0 \approx 25$ K the characteristic spin-fluctuation temperature according to Moriya (1985). Pressure stabilizes the magnetic order, increasing both T_N and the ordered moment (Mederle *et al.*, 2001; Knebel *et al.*, 2006). At small pressures an additional transition is observed at a lower temperature T_L, which moves toward T_N with increasing pressure. At about 5 GPa, $T_L \approx T_N$ and Knebel *et al.* (2006) proposed a FM ground state above 5 GPa in $YbRh_2Si_2$.

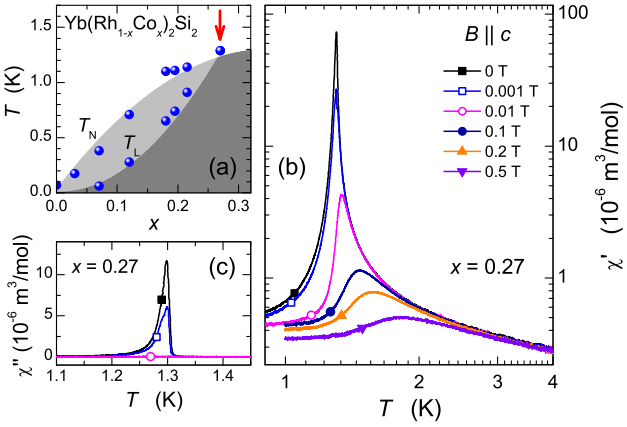

FIG. 27. (a) T-x phase diagram of $Yb(Rh_{1-x}Co_x)_2Si_2$ as measured by Klingner *et al.* (2011) showing the transition temperatures T_L and T_N. The red arrow marks the sample with $x = 0.27$ which is FM. (b) Real part $\chi'(T)$ of the susceptibility for $Yb(Rh_{0.73}Co_{0.27})_2Si_2$ in different magnetic fields with $B\|c$. The sharp peak at $T_C = 1.30$ K and $B = 0$ is suppressed and shifted toward higher T with increasing field. (c) Temperature dependence of the imaginary part $\chi''(T)$ of the susceptibility. From Lausberg *et al.*, 2013.

Isoelectronic substitution of Rh by Co in $Yb(Rh_{1-x}Co_x)_2Si_2$ leads to a similar effect as pressure; the correspondence is excellent for $p \leq 2.5$ GPa (Klingner *et al.*, 2011). The phase diagram for $x < 0.3$ is shown in Fig. 27. At $x = 0.27$, which corresponds to about 4.5 GPa, $T_L = T_N = 1.3$ K. In this sample FM order was indeed found by Lausberg *et al.* (2013). The moments order along the magnetically hard c axis, similar to $YbNi_4P_2$ (Steppke *et al.*, 2013) and CeRuPO (Krellner *et al.*, 2007), and despite the large magnetocrystalline anisotropy [which is about 6 in $Yb(Rh_{0.73}Co_{0.27})_2Si_2$]. A plot of the real and imaginary parts of the susceptibility with $B\|c$ is shown in Figs. 27(b) and 27(c), respectively. A pronounced peak is seen in both quantities, with large absolute values. In $Yb(Rh_{0.73}Co_{0.27})_2Si_2$ this anomalous behavior can be well explained in terms of a Heisenberg model with competing FM and AFM exchange interactions (Andrade *et al.*, 2014). This model also explains the observation that the transition from the AFM to the FM at, e.g., $x = 0.21$, is first order, as it is in $Nb_{1-y}Fe_{2+y}$; see Sec. II.D.1.a.

The discovery of FM in $Yb(Rh_{0.73}Co_{0.27})_2Si_2$ suggests that the state below T_L [the dark gray area in Fig. 27(a)] is also FM with a field-induced FM QCP. However, recent investigations by Hamann (2015) indicate a much richer phase diagram with additional AFM phases. $Yb(Rh_{1-x}Co_x)_2Si_2$ thus appears to be one of the systems whose ground state changes from FM into AFM while approaching the putative FM QCP [cf. Fig. 2(c)].

As in $CeRu_2Si_2$, the physics of $Yb(Rh_{1-x}Co_x)_2Si_2$ is controlled by the evolution of the Kondo temperature, the magnetic anisotropy, and the exchange interactions, and not simply by the mechanism discussed in Sec. III.E that could be valid for a simpler system such as $Nb_{1-y}Fe_{2+y}$.

4. Discussion, and comparison with theory

All of the phase diagrams discussed in this section have the same overall structure: As the Curie temperature decreases, the ground state changes from a homogeneous FM to some modulated magnetic state that is often summarily referred to as AFM, even if its detailed structure is not known.[17] This is an important distinction from a theoretical point of view, as classic AFM involves structure on an atomic scale, whereas other modulated states, such as the SDW in $Nb_{1-y}Fe_{2+y}$, Sec. II.D.1.a, or the helimagnetism in MnSi, Sec. II.B.1.a, are long-wavelength phenomena. The general structure of these phase diagrams is shown schematically in Fig. 2(c). It contains two QPTs (between the FM and modulated states, and between the modulated and nonmagnetic states, respectively), and a multicritical point where the three phases meet.

The issues related to the nature and properties of AFM QCPs are very different from those of FM QCPs. Most of the theoretical concepts discussed in Sec. III, with the exception of Sec. III.E, apply to FM QCPs only, and questions related to the first-order versus second-order nature of any AFM QPT must not be confused with the corresponding questions for FM QPTs. Moreover, in some systems, especially Kondo-lattice systems, such a change from FM to AFM order can occur as the result of competing interactions, i.e., frustration, as a result of pressure or chemical substitution. These mechanisms are very different from the one discussed in Sec. III.E.

An interesting topic is the order of the QPT from the FM to the modulated phase. FM-to-AFM transitions are common even at high temperatures and are often accompanied by a structural phase transition, which makes them first order. The nature of the FM-to-AFM and SDW transitions discussed in this section is probably different, as indicated by the small wave number that characterizes the modulated phase. They likely belong to the class of Lifshitz transitions, which separate a homogeneous phase from a phase with a modulated order parameter [see Hornreich, Luban, and Shtrikman (1975) and references therein, and Chaikin and Lubensky (1995)], and have been considered in many contexts. On the basis of the mechanism discussed in Sec. III there are theoretical reasons to believe that a QPT from a metallic FM to a modulated magnet is generically of first order, although a detailed theory remains to be worked out; see Sec. IV.B. Classically, this transition can be either first or second order (Chaikin and Lubensky, 1995). A generalization of the theory reviewed in Sec. III.B that allows for a modulated order parameter has been developed by Karahasanovic, Krüger, and Green (2012) [see Fig. 39 (the nematic phase may or may not be present) and the discussion in Sec. III.E]. The structure of the resulting phase diagram agrees with what is observed in, e.g., $Nb_{1-y}Fe_{2+y}$; see Fig. 19. However, the theory predicts a first-order transition from the AFM or spiral phase to the PM, whereas the SDW-PM transition in $Nb_{1-y}Fe_{2+y}$ is observed to be continuous.

FM Kondo-lattice systems have been studied theoretically by Perkins *et al.* (2007) by means of a mean-field theory, and by Yamamoto and Si (2010) by means of a RG treatment. Both found a second-order QPT, i.e., the RG treatment found that the earlier generalized Stoner theory is exact with respect to the order of the transition. Technically, this is because the calculation by Yamamoto and Si (2010) does not yield the nonanalytic wave-number dependence of the spin propagator found in a related model (Chubukov, Pépin, and Rech, 2004), which destroys the FM QCP and leads to a first-order transition as described in Sec. III.B.2. While it is conceivable that the two models are different in this respect, this seems unlikely. There is reason to believe that the theory reviewed in Sec. III, if applied to Kondo-lattice systems, will yield a first-order transition. However, this has not been worked out in detail and more work on this topic is needed. In any case, these theories consider a QPT from a FM metal to a PM metal, which so far has not been observed in Kondo-lattice systems (although in some materials the experimental situation is not quite clear yet, see, e.g., $CeRu_{1-x}Fe_xPO$ in Sec. II.D.2.c).

E. System showing glasslike behavior, short-range order, or other strong-disorder effects

This section (with the exception of Sec. II.E.5) describes FM metallic systems that display effects believed to be characteristic of strong disorder in the region where the FM order is destroyed, and for many of them the nature and precise location of the FM QPT is not clear. Some materials display effects that have been interpreted as evidence for a quantum Griffiths region on the PM side of the QCP, with or without glassy freezing of the rare regions or clusters that characterize the Griffiths region. A special case is CeFePO, which displays short-range magnetic order in the absence of strong quenched disorder. The systems discussed here are listed in Table VII.[18] They are arranged with respect to their phenomenology and/or its interpretation.

The behavior characteristic of these materials can often be obtained by substituting a magnetic element by a nonmagnetic one of the same series, e.g., uranium by thorium in $U_{1-x}Th_xNiSi_2$, or nickel by vanadium in $Ni_{1-x}V_x$. This usually introduces substantial amounts of quenched disorder. The x-T phase diagram is often characterized by a pronounced tail [cf. Fig. 2(d)], and the region immediately above the tail is generally characterized by NFL behavior. The tail has been interpreted in terms of locally ordered clusters, and the NFL behavior in terms of quantum Griffiths singularities, a topic reviewed in Sec. III.D. This is, however, not the only possible explanation for a tail in the phase diagram; see the discussion in Sec. III.B.3. Some of the theoretical and experimental results pertinent to this section have been summarized by

[17]The evidence for an AFM phase is stronger in some materials than in others, and additional experimental work is needed in many cases; see the earlier discussions of the individual systems.

[18]We do not include diluted magnetic semiconductors, such as $Fe_{1-x}Co_xS_2$. For an example, see Guo *et al.* (2008).

TABLE VII. Systems showing short-range order or spin-glass (SG) freezing. T_C = Curie temperature, T_g = freezing temperature, ρ_0 = residual resistivity, QC = quantum critical, QGP = quantum Griffiths phase, N/A = not applicable, and n.a. = not available.

System	Order of transition[a]	T_C/K	T_g/K	Magnetic moment/μ_B[b]	Tuning parameter	Disorder ($\rho_0/\mu\Omega$ cm)[c]	Comments
$CePd_{1-x}Rh_x$	n.a.	$6.6-3$[d]	$3-0$[e]	n.a.	Composition[1,2]	n.a.	Kondo cluster glass
$CePt_{1-x}Rh_x$	n.a.	$6-2$[f]	$3-2$[g]	n.a.	Composition[3]	n.a.	Cluster glass (?)[h]
$Ni_{1-x}V_x$	n.a.	$633-\approx 30$[i,4]	$\approx 30-0.2$[j,4]	$0.6-0$	Composition[4]	n.a.	cluster glass (?)[h]
$UNi_{1-x}Co_xSi_2$	n.a.	$95-8.6$[k,5]	6 (?)[l,5]	n.a.	Composition[5]	15 $\mu\Omega$ cm[m,6]	Glassy phase?
$U_{1-x}Th_xNiSi_2$	n.a.	$95-29$[n,7]	$29-\approx 4$[o,7]	n.a.	Composition[7]	n.a.	Possible QGP
$CeTi_{1-x}V_xGe_3$	2nd[8,9]	$14-2.8$[8,9]	n.a.	1.5[9]	Composition[9]	22[p,9]	QGP?
$Sr_{1-x}Ca_xRuO_3$	n.a.	$\approx 100-40$[q,10]	$\approx 40-\approx 5$[r,10]	$1-0$	Composition[10]	8[s]	Thin films
CeFePO	N/A	N/A	0.9[11]	n.a.	None	800[t,12]	Low intrinsic disorder

[a]For the disappearance of homogeneous FM order.
[b]Per formula unit unless otherwise noted.
[c]For the highest-quality samples.
[d]For $x = 1-0.6$ (Sereni *et al.*, 2007)
[e]For $x = 0.6$–0.9 (Sereni *et al.*, 2007; Westerkamp *et al.*, 2009).
[f]For $x = 0$–0.7
[g]For $x = 0.5$ and 0.6.
[h]See footnote [19].
[i]For $x = 0$–0.105 (Ubaid-Kassis, Vojta, and Schroeder, 2010).
[j]For $x = 0.11-0.1225$ (Ubaid-Kassis, Vojta, and Schroeder, 2010).
[k]For $x = 0$–0.96 (Pikul and Kaczorowski, 2012).
[l]For $x = 0.98$ (Pikul and Kaczorowski, 2012).
[m]For UNiCoSi.
[n]For $x = 0$–0.7 (Pikul, 2012).
[o]For $x = 0.7$–0.9 (Pikul, 2012).
[p]For $CeTiGe_3$.
[q]For $x = 0.15$–0.38 (Demko *et al.*, 2012).
[r]For $x = 0.38$–0.52 (Demko *et al.*, 2012).
[s]For $x = 0$ (Schneider, Moshnyaga, and Gegenwart, 2010). RRR values varied from a high of 28.9 for $x = 0$ to a low of 2.9 for $x = 0.5$.
[t]High ρ_0 not intrinsic, but due to granularity of the polycrystalline sample.
[1]Sereni *et al.* (2007). [2]Westerkamp *et al.* (2009). [3]Kawasaki *et al.* (2008, 2009). [4]Ubaid-Kassis, Vojta, and Schroeder (2010). [5]Pikul and Kaczorowski (2012). [6]Kaczorowski (1996). [7]Pikul (2012). [8]Manfrinetti *et al.* (2005). [9]Kittler *et al.* (2013). [10]Demko *et al.* (2012). [11]Lausberg *et al.* (2012). [12]Brüning *et al.* (2008).

Vojta (2010). As in the case of Sec. II.D, different experiments and their interpretations are not consistent for some materials, and it is possible that some of the systems discussed later will eventually be classified with those in Sec. II.C. Conversely, some materials discussed in Sec. II.C may eventually be found to belong in the current section, especially $URu_{2-x}Re_xSi_2$, Sec. II.C.2.b, and possibly Ni_xPd_{1-x}, Sec. II.C.1.a, while CeFePO may belong into Sec. II.B according to some experimental results; see Sec. II.E.4.

1. Systems with glasslike features

Systems with strong-disorder effects include $CePd_{1-x}Rh_x$, $Ni_{1-x}V_x$, and $UNi_{1-x}Co_xSi_2$. Their behavior has been interpreted in terms of a Griffiths region in the PM phase, with symptoms of glassy freezing at the lowest temperatures.

a. $CePd_{1-x}Rh_x$

This series crystallizes in the orthorhombic CrB structure and evolves from a FM ground state in CePd with $T_C = 6.6$ K to a nonmagnetic intermediate-valence state in CeRh (Kappler *et al.*, 1991; Sereni, Beaurepaire, and Kappler, 1993). The chemical substitution of the Ce-ligand Pd with Rh induces not just a volume effect (positive chemical pressure), but also increases the local hybridization strength of the cerium $4f$ electrons with the conduction electrons, leading to a strong enhancement of the Kondo temperature T_K (Sereni *et al.*, 2007). In addition, the Rh substitution introduces disorder.

Evidence for the FM nature of the ordered state comes from the T dependence of the ac susceptibility $\chi'(T)$, which shows large and sharp maxima for all samples ranging from $x = 0.6$ to 0.87 (Sereni *et al.*, 2007). No maximum was observed down to 20 mK in a sample with $x = 0.9$; this indicates a critical concentration for the loss of ferromagnetism very close to $x_c = 0.87$ (Westerkamp *et al.*, 2009). The phase diagram in Fig. 28 shows the transition temperature deduced from measurements of various observables as a function of x. Westerkamp *et al.* (2009) attributed the continuous decrease of T_C with increasing x on the competition between FM order and growing Kondo screening. The curvature of T_C changes from negative to positive at $x \approx 0.6$, displaying a long tail toward higher Rh contents. In this concentration range, the Kondo temperature $T_K \approx 2|\theta_P|$, with θ_P the paramagnetic Weiss temperature obtained from fits of the dc susceptibility at high temperatures, strongly increases with x. The main

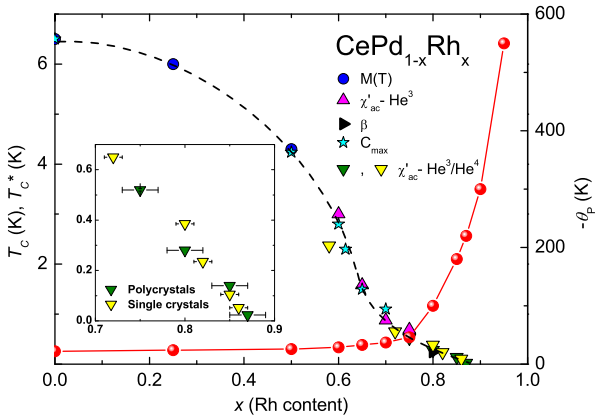

FIG. 28. Magnetic phase diagram of $CePd_{1-x}Rh_x$. Left scale: Composition dependence of the ordering (freezing) temperature T_C (T_C^*) deduced from various measurement techniques: magnetization (M), ac susceptibility (χ'_{ac}), thermal expansion (β) and specific heat (C). The inset shows T_C (x) values observed in $\chi'_{ac}(T)$ for $x > 0.7$ in polycrystals and single crystals. Right scale: The Weiss temperature θ_P. From Sereni *et al.*, 2007 and Westerkamp *et al.*, 2009.

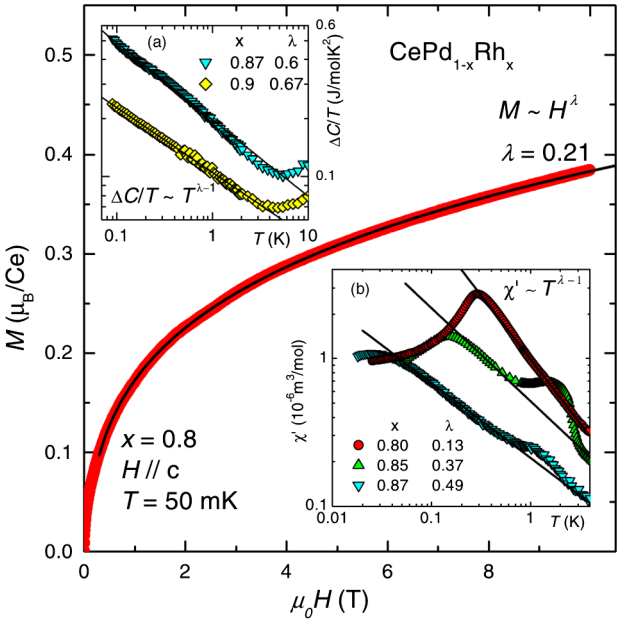

FIG. 29. Comparison of thermodynamic data for $CePd_{1-x}Rh_x$ with the quantum-Griffiths-phase scenario (cf. Sec. III.D). Main figure: Field dependence of the magnetization M for a single crystal with $x = 0.8$ at 50 mK. The data follow a power law $M \propto H^\lambda$ with $\lambda = 0.21$. Inset (a): $4f$ Sommerfeld coefficient for polycrystals with $x = 0.87$ and 0.9 (Pikul *et al.*, 2006) plotted on a double-logarithmic scale. Solid lines indicate a $T^{\lambda-1}$ power-law behavior. Inset (b): T dependence of the ac susceptibility $\chi'(T)$ of three polycrystals with $x = 0.8$, 0.85, and 0.87. The lines are fits to a $T^{\lambda-1}$ power law. From Westerkamp *et al.*, 2009.

mechanism governing T_K is the hybridization of the Ce $4f$ electrons with the valence electrons of the surrounding ligands. In Ce-based compounds, Rh ligands are known to lead to much larger T_K than Pd ligands (Koelling, Dunlap, and Crabtree, 1985). Thus, in $CePd_{1-x}Rh_x$ the effect of the Rh ligands is much stronger than the effect of the Pd ligands once the Rh content reaches a critical value close to 0.7. The random distribution of Rh and Pd ligands likely creates regions with different local values of T_K. An analysis of the entropy and the slope of $\chi'(T)$ at 2 K revealed some fraction of unscreened magnetic moments, even at large x, where the average T_K is already above 50 K. The pronounced maxima in $\chi'(T)$ of samples with concentrations $x \geq 0.6$ exhibit a frequency dependence similar to that observed in spin glasses (Westerkamp *et al.*, 2009). The relative temperature shift of about 3% to 10% per frequency decade is considerably larger than that in canonical metallic spin glasses (where typical values are 1% to 2%), but well below the value of about 28% observed in superparamagnets (Mydosh, 1993). This behavior and zero-field-cooled and field-cooled magnetization measurements have been interpreted as evidence for the existence of clusters of magnetic moments in the system below a certain temperature $T_{cluster}$ (Westerkamp *et al.*, 2009). Since the broad distribution of local Kondo temperatures is thought to be responsible for the cluster formation, Westerkamp *et al.* (2009) called the low-T state in $CePd_{1-x}Rh_x$ a "Kondo-cluster glass." [19] The observation of reentrant depolarization in recent neutron-depolarization imaging experiments (Schmakat *et al.*, 2015) on the same samples investigated by Westerkamp *et al.* (2009) seems to confirm the presence of such a state. The general behavior of $CePd_{1-x}Rh_x$ is quite different from that observed in many other disordered NFL systems, such as $CeNi_{1-x}Cu_x$, where the Ce valence remains nearly trivalent and where a percolative cluster scenario was proposed (Marcano *et al.*, 2007).

Specific-heat measurements have shown the existence of NFL behavior for concentrations $0.85 \leq x \leq 0.9$ (Deppe *et al.*, 2006; Pikul *et al.*, 2006). Samples in this concentration range show a power-law dependence $C(T)/T \sim T^{\lambda-1}$, with exponents $\lambda = 0.6$ and 0.67 for $x = 0.87$ and 0.9, respectively (see inset *a* of Fig. 29). Power-law behavior has also been found for the T-dependent ac susceptibility; see inset *b* of Fig. 29. These findings suggest that there are strong fluctuations in an entire range of Rh concentrations, which raises the question whether T_C going to zero near $x = 0.87$ represents a FM QCP or not.

A clear answer was given by Westerkamp *et al.* (2009) who measured the Grüneisen ratio, defined as $\Gamma \propto \beta/C$, with β the volume thermal expansion coefficient and C the specific heat. Γ must diverge as a power law as T goes to zero at any QCP (Zhu *et al.*, 2003); this was confirmed experimentally for several Kondo-lattice systems exhibiting an AFM QCP (Küchler *et al.*, 2003). Close to the critical concentration, where the anomaly in $\chi'(T)$ disappears, $\Gamma(T) \propto \ln T$ was found, contrary to the power-law divergence expected at a FM QCP. This shows that there is no FM QCP in $CePd_{1-x}Rh_x$ at this concentration. Rather, in the region $0.7 < x < 0.9$ and in the temperature range $T_C \leq T \leq T_{cluster}$ the observations are consistent with the quantum-Griffiths-phase scenario that

[19] The term "cluster glass" is frequently used in a spin-glass context [see, e.g., Itoh *et al.* (1994)], and different authors use it for various phenomena and concepts whose underlying physics may be quite different.

predicts $\chi'(T) \propto C(T)/T \propto T^{\lambda-1}$ and $M \propto H^{\lambda}$, with $0 \leq \lambda \leq 1$ and x-dependent exponents (Castro Neto, Castilla, and Jones, 1998; Dobrosavljević and Miranda, 2005), and $\Gamma(T) \propto \log(T)$ (Vojta, 2009); see Sec. III.D. This is demonstrated in Fig. 29. However, the exponents λ obtained from the specific heat and the susceptibility are not the same, contrary to the theoretical prediction.

The field-dependent magnetization at 50 mK also follows a power law (Westerkamp *et al.*, 2009; Brando *et al.*, 2010). $CePd_{1-x}Rh_x$ has a very small magnetic anisotropy at $x \approx 0.8$ (Deppe *et al.*, 2006), suggesting Heisenberg symmetry which is needed for the realization of the quantum-Griffiths-phase scenario (Vojta and Schmalian, 2005). According to this interpretation, the observations for $0.7 \lesssim x \lesssim 0.9$ represent quantum Griffiths behavior in the PM phase, and the true QCP, which one expects for $x \approx 0.7$, so far has not been observed.

b. $CePt_{1-x}Rh_x$

Kawasaki *et al.* (2008, 2009) found that $CePt_{1-x}Rh_x$ behaves similarly to $CePd_{1-x}Rh_x$ and successfully fitted the freezing temperature, identified as the temperature where the ac susceptibility shows a pronounced peak, to a Vogel-Fulcher law.

c. $Ni_{1-x}V_x$

A small amount of vanadium (about 12%) suppresses T_C to zero from $T_C \approx 630$ K in pure nickel (Bölling, 1968). $Ni_{1-x}V_x$ is attractive for studying quantum Griffiths effects for several reasons: (i) it is simpler than Kondo-lattice ferromagnets and has Heisenberg symmetry, (ii) the high T_C of nickel allows the effects to be observable in a larger temperature range than in other systems, and (iii) a vanadium impurity causes a strong reduction (about 90%) of the magnetic moment of the neighboring Ni atoms, which creates significant disorder. This is in contrast to $Ni_{1-x}Pd_x$, where isoelectronic Pd substitution does not introduce much disorder, and a large amount of Pd (about 97.5%) is needed to suppress T_C to zero; see Sec. II.C.1.a.

Ubaid-Kassis, Vojta, and Schroeder (2010) measured the magnetization M and the ac susceptibility χ of several samples with $0 \leq x \leq 0.15$. The x-T phase diagram is shown in Fig. 30 (note the log-linear plot). For $x \leq 0.11$ T_C was estimated from standard Arrott plots $H/M = a + bM^2$. For larger x the determination of T_C was model dependent; for $x \geq 0.11$ and fields $H > 0.5$ T a modified Arrott plot $M^{1/\beta} = M_0^{1/\beta}(T) + c(H/M)^{1/\gamma}$ was used. Recent μSR data confirmed that the long-range FM order is lost for x close to 0.11 (Schroeder *et al.*, 2014). In addition to the Arrott plots, the temperature T_{max} of the maximum in the ac susceptibility was determined as in the case of $CePd_{1-x}Rh_x$. The field and frequency dependence of T_{max} for $x \approx 0.12$ was found to be consistent with what is expected for a cluster glass (see Sec. III.D.3). The dashed line in Fig. 30 is a linear extrapolation of $\ln T_C$ vs x, which represents a shape of the phase diagram similar to that in Fig. 2(d).

In the PM region of the phase diagram with $0.114 \leq x \leq 0.15$ the T dependence of the susceptibility $\chi_m = M/H - \chi_{orb}$ (with a small orbital contribution $\chi_{orb} = 6 \times 10^{-5}$ emu/mol) can be fitted to a power law $T^{-\gamma}$ for $10 \leq T \leq 300$ K; see

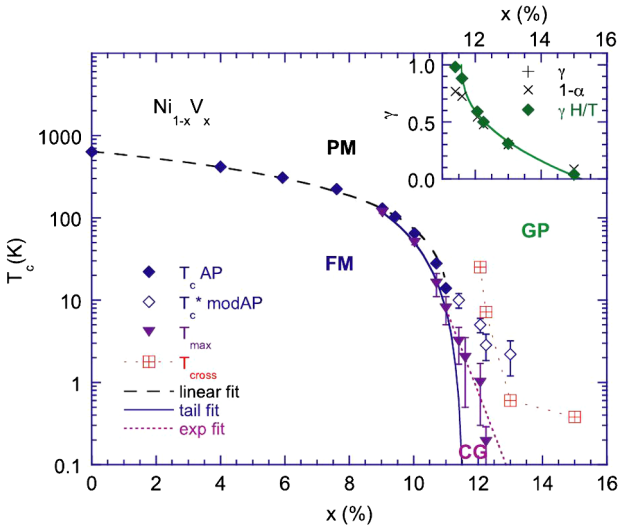

FIG. 30. x-T phase diagram of $Ni_{1-x}V_x$. T_{max}, where the ac susceptibility peaks, marks the freezing into the cluster-glass (CG) state. For $0.114 \leq x \leq 0.15$ effects consistent with a quantum Griffiths phase (GP) were observed in the susceptibility ($\chi \propto T^{-\gamma}$) and magnetization ($M \propto H^{\alpha}$), see Fig. 31. The orange squares mark the crossover from the GP to the CG phase. The inset shows the x dependence of the exponents. From Schroeder, Ubaid-Kassis, and Vojta, 2011.

Fig. 31. The magnetization $M_m = M - \chi_{orb}H$ also shows a power-law behavior, H^{α} at 2 K, for $3000 \leq H \leq 50\,000$ G; both are characteristic of a quantum Griffiths phase. Deviations from this behavior at low T have been ascribed to the formation of a cluster-glass phase (Ubaid-Kassis, Vojta, and Schroeder, 2010); the crossover between the two is marked by orange squares in Fig. 30. It is not known whether the specific heat of these samples also follows a power law.

d. $UNi_{1-x}Co_xSi_2$

$UNiSi_2$ is a ferromagnet (see Sec. II.C.1.d) and $UCoSi_2$ is a paramagnet with strong spin fluctuations (Kaczorowski, 1996). The series $UNi_{1-x}Co_xSi_2$ was investigated by Pikul

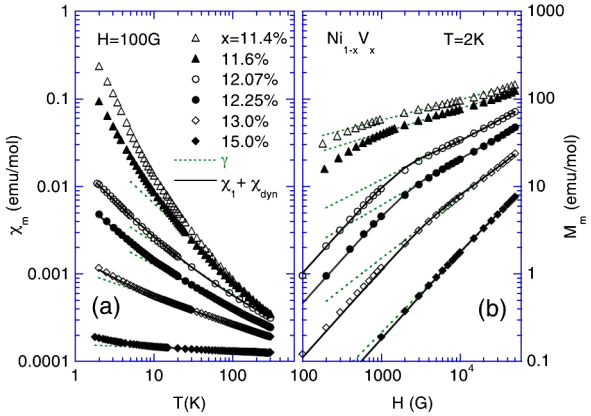

FIG. 31. The low-field susceptibility $\chi_m = M/H - \chi_{orb}$ vs T, and the magnetization $M_m = M - \chi_{orb}H$ at 2 K vs H for samples with $0.114 \leq x \leq 0.15$. χ_{orb} is the orbital contribution to χ. The dashed lines indicate power-law behaviors $\chi_m \propto T^{-\gamma}$ and $M_m \propto H^{\alpha}$. From Ubaid-Kassis, Vojta, and Schroeder, 2010.

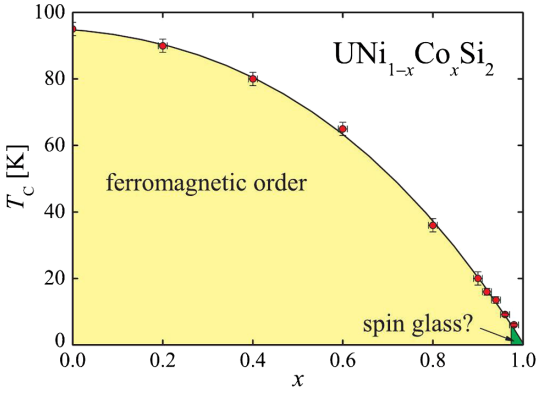

FIG. 32. x-T phase diagram of $UNi_{1-x}Co_xSi_2$. From Pikul and Kaczorowski, 2012.

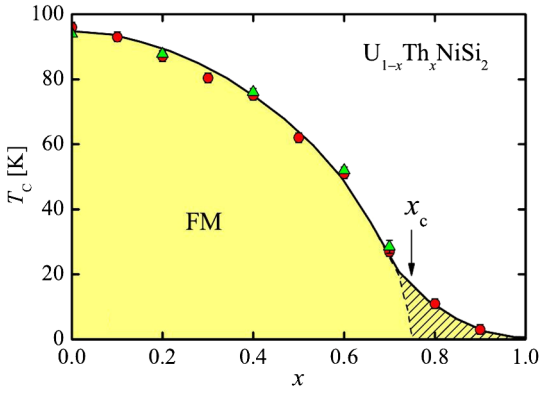

FIG. 33. T-x phase diagram of $U_{1-x}Th_xNiSi_2$ derived from magnetization $M(T)$ and specific-heat $C(T)$ measurements. The circles correspond to the maxima in $\chi(T) = M(T)/B$ or minima in $\partial M(T)/\partial T$, and the triangles correspond to the minima in $\partial[C(T)/T]/\partial T$. The arrow ($x_c$) indicates the position of the putative FM QCP obtained from extrapolating the low-x curvature of the phase separation line. From Pikul, 2012.

and Kaczorowski (2012). Cobalt substitution leaves both the uranium lattice and the orthorhombic crystal structure intact, while reducing the unit cell volume by about 1.2%. Since the b axis stretches with increasing x, while the a and c axes shrink, Co substitution is not equivalent to hydrostatic pressure. The main effect of the doping seems to be the modification of the intersite coupling between the U magnetic moments: A Curie-Weiss analysis of the susceptibility shows that the effective moment is almost unaffected by the Co substitution, whereas the Curie-Weiss temperature θ_{CW} varies from 95 K in $UNiSi_2$ to −70 K in $UCoSi_2$. T_C as well as the remanent magnetization decreases continuously with increasing x. The clear onset of the magnetization observed at T_C for $0 \leq x \leq 0.96$ evolves for $x = 0.98$ into a small anomaly at $T \approx 6$ K, which is also seen in $C(T)/T$ as a broad hump. For $x = 1$ the anomaly is absent. The ground state of the $x = 0.98$ sample is unknown; Pikul and Kaczorowski (2012) suggested that it is a spin-glass-like state with competing FM and AFM interactions (see Fig. 32). The FM transition at nonzero temperature appears to be second order for all samples where it is clearly present; the order of the transition from the FM state to the glassy state, if it exists, is not known. $UCoSi_2$ shows a logarithmic enhancement of the Sommerfeld coefficient $C(T)/T \propto -\ln T$ down to the lowest temperature measured $T = 2$ K, which Pikul and Kaczorowski (2012) interpreted as indicating vicinity to a QCP.

2. Other systems showing effects of strong disorder

a. $U_{1-x}Th_xNiSi_2$

The system $U_{1-x}Th_xNiSi_2$ was investigated by Pikul (2012). Alloying with nonmagnetic Th causes the unit cell volume to expand without changing the crystal structure. This shifts the FM phase transition to lower temperatures as shown in Fig. 33; see also Fig. 4 in Pikul (2012). The feature in the specific heat that signals the phase transition broadens with increasing x. At $x = 0.8$ the transition is no longer clearly visible in $C(T)/T$, while it can still be seen in $\partial M(T)/\partial T$. At $x_c \approx 0.75$ the long-range FM order seen for $0 \leq x \leq 0.7$ changes smoothly into short-range or spin-glass-like order. x_c indicates the position of the putative FM QCP; around this concentration the phase boundary changes its curvature and develops a marked tail [cf. Figs. 2(d) and 33]. For the sample with $x = 0.8$, $C(T)/T$ does not show a maximum, as one would expect in a spin glass (Mydosh, 1993), and it does not level off either as in a Fermi liquid, but keeps increasing with decreasing T. This anomalous behavior was also observed in other doped FM systems, for instance, $CePd_{1-x}Rh_x$, where the thermodynamics in the "tail" region of the phase diagram are believed to be dominated by quantum Griffiths effects [see Westerkamp *et al.* (2009) and Sec. II.E.1.a].

b. $CeTi_{1-x}V_xGe_3$

$CeTiGe_3$ is a FM Kondo-lattice system with $T_C = 14$ K and a hexagonal perovskite $BaNiO_3$-type structure (Manfrinetti *et al.*, 2005). The system $CeTi_{1-x}V_xGe_3$ was studied by Kittler *et al.* (2013). So far only polycrystalline samples with a relatively large residual resistivity $\rho_0 \approx 22\ \mu\Omega\,\mathrm{cm}$ (for $CeTiGe_3$) have been investigated. At high temperature the susceptibility was reported to follow a Curie-Weiss behavior with a negative Weiss temperature $\theta_W = -36.5$ K, indicating predominantly AFM interactions. The effective moment is $2.64\mu_B$, close to the value of $2.54\mu_B$ for trivalent free $^{+3}$Ce ions. The resistivity increases with decreasing temperature, displaying a maximum at about 35 K which indicates the onset of Kondo coherence. The Ce ground state is a Kramers doublet, but the entropy just above T_C is larger than the $R\ln 2$ expected for a doublet ground state, suggesting that the CEF splitting is small and that the Kondo temperature cannot easily be determined from the entropy. The ordered moment measured by neutron powder diffraction within the FM phase is $1.5\mu_B$/Ce, and the ordering is collinear, with moments pointing along the crystallographic c axis (Kittler *et al.*, 2013). The specific heat below T_C suggests the presence of a spin gap $\Delta/k_B \approx 0.8\ T_C$ in the magnetic excitation spectrum, which indicates a strong magnetic anisotropy.

Nonisoelectronic vanadium substitution for titanium in $CeTi_{1-x}V_xGe_3$ permits one to reduce T_C and completely suppress it at $x_c \approx 0.35$, while Ce retains its +3 valence in all samples (Kittler *et al.*, 2013). $CeVGe_3$ shows AFM order

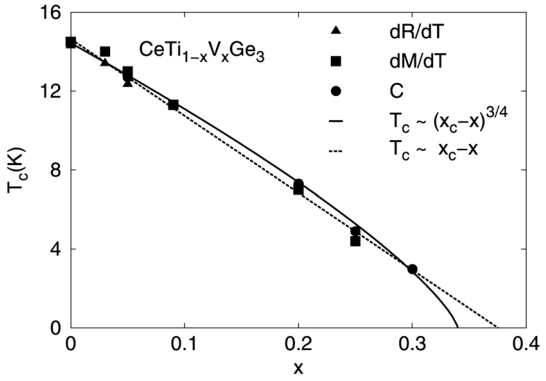

FIG. 34. x-T phase diagram of $CeTi_{1-x}V_xGe_3$. T_C decreases approximately linearly with increasing x, as indicated by the dotted line. Also shown is a fit by $T_C \propto (x_c - x)^{3/4}$ (solid line), which is expected within the Herz-Millis-Moriya theory (cf. Sec. III.C.2). From Kittler *et al.*, 2013.

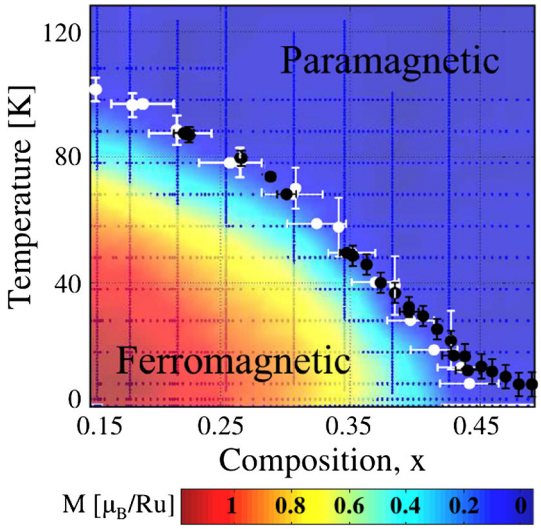

FIG. 35. Contour plot of the remanent magnetization in the T-x plane for an epitaxial film of $Sr_{1-x}Ca_xRuO_3$. Black and white symbols indicate the transition temperature determined from susceptibility and magnetization measurements, respectively. From Demko *et al.*, 2012.

below 4 K (Bie and Mar, 2009). Magnetization measurements demonstrate that the ordered moment is also reduced with increasing x. The phase transition is second order down to about 3 K, as indicated by the mean-field-like feature in the specific heat, and remains second order and ferromagnetic even at higher V concentrations, but it broadens strongly for x close to x_c. This is an indication of strong-disorder effects. The logarithmic increase of C_{4f}/T toward low temperatures for the $x = 0.3$ sample indicates the presence of spin fluctuations, which might arise from the presence of a QCP at x_c or, more probably, from quantum Griffiths effects, similarly to what was observed in $CePd_{1-x}Rh_x$ and $Ni_{1-x}V_x$. The experimental phase diagram of $CeTi_{1-x}V_xGe_3$ is shown in Fig. 34. The dotted line denotes a linear decrease of T_C with x, and the solid line is a fit to the behavior expected from Hertz-Millis-Moriya theory, $T_C \sim (x_c - x)^{3/4}$; see Sec. III.C.2. The lowest temperature achieved was 2 K. Low-T data in the region at $x \approx x_c$ are required to determine whether or not a Griffiths region as discussed in Sec. III.D is indeed present in this system.

3. A thin-film system: $Sr_{1-x}Ca_xRuO_3$ (thin-film samples)

Bulk (ceramic and powder) samples of $Sr_{1-x}Ca_xRuO_3$ were discussed in Secs. II.B.4 and II.C.1, respectively. Thin films have been grown epitaxially by Schneider, Moshnyaga, and Gegenwart (2010), Wissinger *et al.* (2011), and Demko *et al.* (2012). Schneider *et al.* found that T_C decreases roughly linearly with x, with an extrapolated critical value $x_c \approx 0.7$, in agreement with results on powder, polycrystalline, and ceramic samples. However, Wissinger *et al.* (2011) found significant differences between film and bulk samples, including a higher value of x_c for films. Demko *et al.* (2012) measured the magnetization and susceptibility using a magneto-optical technique on a composition-spread epitaxial film of 200 nm thickness. They found a phase diagram that differs markedly from previous results, including those by Schneider, Moshnyaga, and Gegenwart (2010), namely, a pronounced tail with an onset around $x = 0.4$; see Fig. 35. They interpreted their results as the FM-to-PM quantum phase transition being destroyed by the disorder. This is consistent with a microscopic model which considers spatial disorder correlations at smeared phase transitions (Vojta, 2003) with a behavior different from that at critical points (Demko *et al.*, 2012; Svoboda *et al.*, 2012).

4. A system showing short-range order: CeFePO

CeFePO, a homologue of the quaternary pnictides, is a stoichiometric Kondo-lattice system that is very close to a FM instability (Brüning *et al.*, 2008). However, its ground state is neither FM nor PM, but a short-range ordered state (Lausberg *et al.*, 2012), which is very unusual for a clean system. The first comprehensive low-T study of CeFePO was performed by Brüning *et al.* (2008), who investigated polycrystals by measurements of the uniform susceptibility, resistivity, NMR (oriented powder) down to 2 K, and specific heat down to 0.4 K. They found that CeFePO is a heavy-fermion system (iron is not magnetic in this compound) with a Kondo temperature $T_K \approx 10$ K, a Sommerfeld coefficient $\gamma = 0.7\,\mathrm{J/K^2\,mol}$, which corresponds to a mass enhancement of 50, a Sommerfeld-Wilson ratio of 5.5, and a Korringa ratio $S_0/T_1TK^2 \approx 0.065$, indicating the presence of FM correlations. Below 10 K the broadening of the line shape of the NMR spectra for small fields $H \perp c$, but not for $H \| c$, suggests that in this temperature regime short-range FM correlations that cannot be ascribed to disorder start to be relevant. Thus, only the basal-plane component of the cerium $4f$ moment is FM correlated. This strong anisotropy reflects the quasi-2D crystal structure. Later, μSR experiments were performed on polycrystals and single crystals, together with ac susceptibility and specific-heat measurements down to 0.02 K (Lausberg *et al.*, 2012). The ac susceptibility shows a frequency-dependent peak at $T_g \approx 0.9$ K, whose dependence on the modulation frequency is larger than that found in canonical spin glasses and smaller than that of superparamagnets. The entropy measured below the freezing maximum is just 1% of

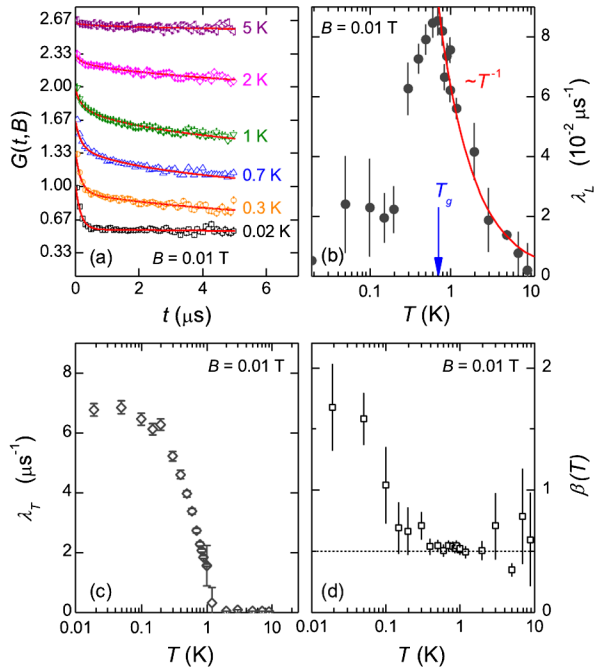

FIG. 36. Normalized muon-spin asymmetry function $G(t, B)$ in CeFePO at different temperatures. The lines are fits to $G(t, B) = G_1 e^{-(\lambda_T t)} + G_2 e^{-(\lambda_L t)^\beta}$. The peak in $\lambda_L(T)$ and the strong increase of $\lambda_L(T)$ mark the spin-freezing temperature T_g. From Lausberg *et al.*, 2012.

$R \ln 2$. A summary of the μSR results in zero and small longitudinal field is shown in Fig. 36. In conclusion, there is no FM QCP in CeFePO but rather some short-range order with a particular texture whose nature is unknown. The fact that in CeFePO strong FM fluctuations are present, and that AFM phases were observed in samples slightly doped with Ru or As (see Secs. II.D.2.c and II.D.2.b), suggests a delicate interplay between FM and AFM correlations in this system. This might cause frustration and favor exotic states. There are theoretical predictions of textured states in itinerant systems close to a FM instability; see Sec. III.E. An interesting proposal was put forward by Thomson, Krüger, and Green (2013), who suggested a helical glass state as the result of weak disorder which destabilizes the FM state and leads to incommensurate spiral magnetic order. Even the best samples of CeFePO have a relatively small RRR of approximately 5, but this may be attributed to the presence of strong FM fluctuations rather than quenched disorder. Since the amount of disorder necessary to generate the spiral state is rather small, the mechanism proposed by Thomson, Krüger, and Green (2013) is a viable candidate for explaining the observations.

5. Discussion and comparison with theory

The properties of $CePd_{1-x}Rh_x$ and $Ni_{1-x}V_x$ have been interpreted in terms of the theoretical ideas discussed in Secs. III.D.1 and III.D.3, namely, a quantum Griffiths phase and interactions between rare regions that lead to glassy properties. While some aspects of the theory agree very well with the experimental results (see, e.g., the fits in Fig. 29), there also are discrepancies. For instance, the theory predicts that the field dependence of the magnetization and the temperature dependence of the specific-heat coefficient are governed by the same exponent λ, whereas the data yield different values; see Fig. 29. For Kondo systems there are other scenarios that so far have not been explored in the context of these experiments; see Sec. III.D.2. The evidence for a glassy phase in $UNi_{1-x}Co_xSi_2$ (Sec. II.E.1.d) is much weaker, and the lowest T_C where a clear FM transition has been observed is $T_C = 8.6$ K. Experiments at lower temperatures in the region close to $x = 1$ are needed to determine the nature of the FM QCP in this system.

The evidence for strong-disorder effects in the systems discussed in Sec. II.E.2 is weaker and largely based on the shape of the phase diagram. As discussed in Sec. III.B.3 there are other possible explanations for a tail in the phase diagram (see Fig. 38) and further investigations are needed to ascertain whether quantum Griffiths or related effects are indeed present in these materials.

III. THEORETICAL RESULTS

A. Soft modes in metals

In Sec. I.B we discussed why, in the absence of soft modes other than the order-parameter fluctuations, the quantum FM transition in clean systems is expected to be generically continuous with mean-field static exponents and a dynamical exponent $z = 3$. We also mentioned that this expectation breaks down in general, and in Sec. II we discussed many experiments that show a first-order transition rather than a continuous one. Indeed, Tables I, II, III, IV, and V show that most of the observed low-temperature transitions into a homogeneous FM phase are first order unless the system is either disordered or quasi-1D. We argue next that the systems in Table III can be understood in terms of a crossover from an asymptotic first-order transition to a preasymptotic regime that is described by Hertz theory. Underlying the breakdown of the original expectation for metallic magnets are soft two-particle excitations that couple to the magnetization. These excitations are the result of two characteristic properties of metals, viz., (1) a sharp Fermi surface, and (2) a nonzero density of states at the Fermi level. As we will see, they can be understood as representing a Goldstone mode that results from a spontaneously broken gauge symmetry. In disordered systems, soft critical order-parameter fluctuations exist in addition to this fermionic soft mode and govern the critical behavior. Finally, the rare-region effects mentioned in Sec. I.B can also be understood as a certain class of soft excitations. In this section we explain the importance of soft modes, give a classification, and discuss in more detail the fermionic Goldstone mode that is of particular importance for quantum FMs.

1. Why we should care about soft modes

The only way in which observables, be it thermodynamic quantities or time-correlation functions, can display nonanalytic behavior as a function of temperature, frequency, wave number, or an external field is via the existence of soft modes, i.e., correlation functions that diverge as the frequency and the wave number go to zero. It is useful in this context to consider soft modes as leading to a distribution of

relaxation times. Consider, for example, a diffusive process [see, e.g., Forster (1975)], i.e., a correlation function that behaves for small wave vectors $\boldsymbol{k}$ and long times t as

$$C(\boldsymbol{k},t) \propto e^{-\nu k^2 t}, \tag{3.1a}$$

with ν some kinetic coefficient. This corresponds to a $\boldsymbol{k}$-dependent relaxation time

$$\tau(\boldsymbol{k}) = 1/\nu\boldsymbol{k}^2. \tag{3.1b}$$

For a fixed wave vector the decay is exponential, but the relaxation time diverges as $\boldsymbol{k} \to 0$. As a result, the local time-correlation function in d dimensions

$$C(\boldsymbol{x}=0,t) = \frac{1}{V}\sum_{\boldsymbol{k}} C(\boldsymbol{k},t) \propto 1/t^{d/2} \tag{3.2}$$

decays algebraically with time. We write the local time-correlation function as an integral,

$$C(\boldsymbol{x}=0,t) = \int_{\tau_0}^{\infty} d\tau P(\tau) e^{-t/\tau}. \tag{3.3a}$$

Here τ is a relaxation time $\tau_0 = 1/\nu k_0^2$ with k_0 the upper cutoff on the momentum integral in Eq. (3.2), and $P(\tau)$ is a relaxation-time distribution function. Comparing Eqs. (3.2) and (3.3a) we see that

$$P(\tau) \propto 1/\tau^{(d+2)/2}. \tag{3.3b}$$

The algebraic decay, or long-time tail, of the time-correlation function is thus a result of the power-law decay of the distribution function $P(\tau)$. The Laplace transform $C(z)$ of $C(\boldsymbol{x}=0,t)$ is a nonanalytic function of the complex frequency z at $z=0$; for $\mathrm{Im}z > 0$ and $(d-2)/2$ not integer the leading low-frequency behavior is

$$\begin{aligned} C(z) &= i\int_0^{\infty} dt e^{izt} C(\boldsymbol{x}=0,t) \\ &\propto z^{(d-2)/2} + (\text{terms analytic in } z). \end{aligned} \tag{3.4}$$

Observables that couple to such diffusive modes will be given in terms of integrals whose integrands contain diffusive correlation functions. This results in a nonanalytic dependence on, e.g., the temperature or the frequency.

Such nonanalytic behavior can be generic, i.e., exist in an entire phase, or it can occur only at special points in the phase diagram. An example of the former is Goldstone modes, which arise from the spontaneous breaking of a global continuous symmetry (Forster, 1975; Zinn-Justin, 1996). Prime examples of the latter are critical fluctuations, which are soft only at a critical point (Ma, 1976). Other mechanisms for producing generic soft modes include conservation laws and gauge invariance (Belitz, Kirkpatrick, and Vojta, 2005). For the purposes of this review, we are interested in four classes of soft modes in metals. The first class consists of

(i) Single-particle excitations: These are represented by the soft single-particle Green's function. They exist because of the sharpness of the Fermi surface and the existence of a nonvanishing quasiparticle weight. They are responsible for the leading behavior of observables in a Fermi liquid, e.g., the linear T dependence of the specific heat.

An example of the effects of soft single-particle excitations is the paramagnon propagator in a metallic magnet. As a function of the wave vector $\boldsymbol{k}$ and the imaginary Matsubara frequency $i\Omega$ it has the form (Doniach and Engelsberg, 1966; Hertz, 1976)

$$P(\boldsymbol{k}, i\Omega) = \frac{1}{t + a\boldsymbol{k}^2 + b|\Omega|/|\boldsymbol{k}|^n}. \tag{3.5a}$$

Here t is the distance from the magnetic transition, and a and b are constants. n is an integer that depends on the physical situation. For clean and disordered metallic FMs, $n=1$ and 2, respectively. For AFMs, $n=0$. The spectrum or dissipative part of the corresponding causal function $P''(\boldsymbol{k},\omega) = \mathrm{Im}P(\boldsymbol{k}, i\Omega \to \omega + i0)$ reads

$$P''(\boldsymbol{k},\omega) = \frac{\omega/|\boldsymbol{k}|^n}{(t+a\boldsymbol{k}^2)^2 + \omega^2/|\boldsymbol{k}|^{2n}}. \tag{3.5b}$$

We see that the paramagnon excitation is damped with a damping coefficient given by $\omega/|\boldsymbol{k}|^n$. Physically, this reflects the coupling of the magnetic collective mode to the soft single-particle excitations in the itinerant electron system. It is usually referred to as Landau damping, in analogy to the corresponding effect in a collisionless classical plasma (Lifshitz and Pitaevskii, 1981). The same damping mechanism is applicable to the plasmon mode in a charged Fermi liquid, and the zero-sound mode in a neutral one (Pines and Nozières, 1989). We also note that the $|\Omega|$ singularity on the imaginary-frequency axis in Eq. (3.5) implies, for fixed $\boldsymbol{k}$, a $1/\tau^2$ long-time tail for P as a function of the imaginary time τ [see, e.g., Belitz, Kirkpatrick, and Vojta (2005)]. We will encounter the FM paramagnon propagator again later in this section [see Eqs. (3.44) and (3.75)], and the $1/\tau^2$ long-time tail will be important for the discussion in Sec. III.D.3.

The second class consists of

(ii) Two-particle excitations that are the Goldstone modes of a broken gauge symmetry with the density of states at the Fermi level as the order parameter. They were first identified as Goldstone modes by Wegner (1979) in the context of disordered electron system; we will discuss them in Sec. III.A.2.

The third class is

(iii) Griffiths or rare-region effects in disordered systems (Griffiths, 1969; McCoy, 1969).

These are normally not thought of as soft modes. To see the connection, consider a classical Ising system with randomly missing bonds in its disordered phase. In an infinite system, below the transition temperature of the clean system, but above the one of the actual bond-disordered one, one can find arbitrarily large regions with linear dimension L

that happen to contain no missing bonds. In such a region, the spins are ordered, but the probability of finding such a region will decrease exponentially with its volume L^d. In order to destroy such a rare region, a surface free energy must be overcome. The relaxation time for a cluster of linear size L will therefore be (Randeria, Sethna, and Palmer, 1985; Bray, 1988)

$$\tau(L) = \tau_0 e^{\sigma L^{d-1}}, \tag{3.6}$$

with τ_0 a microscopic time scale and σ a surface tension. This time scale diverges as $L \to \infty$, just as the diffusive relaxation time in Eq. (3.1b) diverges as $\boldsymbol{k} \to 0$, only here the divergence is exponential. In order to estimate time-correlation functions $C(t)$ we need to weigh a factor $\exp[-t/\tau(L)]$ with the probability $P(L) \propto \exp(-cL^d)$ of finding a rare region in the first place and integrate over all sizes L. We thus expect

$$C(t) \propto \int_0^\infty dL \exp\left[-cL^d - (t/\tau_0)e^{-\sigma L^{d-1}}\right], \tag{3.7a}$$

where c is a constant. For large times t the integral can be evaluated by the method of steepest descent. The typical length scale L is $L_{\text{typ}} \propto [\ln(T/\tau_0)]^{1/(d-1)}$, and the leading contribution to $C(t)$ is (Randeria, Sethna, and Palmer, 1985)

$$C(t \to \infty) \propto \exp\{-b[\ln(t/\tau_0)]^{d/(d-1)}\}, \tag{3.7b}$$

with $b = c/\sigma^{d/(d-1)}$ another constant. We see that the time-correlation function again decays slower than exponentially, albeit faster than any power. We again define a distribution function for relaxation times by writing

$$C(t) = \int_{\tau_0}^\infty d\tau P(\tau) e^{-t/\tau}. \tag{3.8a}$$

The leading behavior for large τ is

$$P(\tau \to \infty) \propto \exp\{-b[\ln(\tau/\tau_0)]^{d/(d-1)}\}. \tag{3.8b}$$

The analogy to diffusive soft modes, Eqs. (3.1)–(3.3), is now obvious.

For later reference we mention that Eq. (3.6) holds for classical Ising magnets only; for other systems the exponent may be different. We will discuss Griffiths effects in more detail in Sec. III.D.

All of these are generic soft modes. In addition, we will encounter

(iv) Critical fluctuations at the QCP in disordered FMs. These are analogous to the critical fluctuations at classical transitions (Ma, 1976). However, as seen in Sec. III.C.2 their effects at the quantum ferromagnetic transition are rather weak.

Another class of generic soft modes is represented by phonons or elastic deformations in a continuum model. Their coupling to the magnetization has been studied extensively for classical magnets [see Bergman and Halperin (1976), and references therein]. For quantum magnets no convincing treatment exists; see Sec. III.F.

2. Goldstone modes in metals

We now illustrate the nature of the listed second class of soft modes, which are of crucial importance for the breakdown of Hertz theory. We first show that spinless noninteracting electrons, at $T = 0$, possess Goldstone modes resulting from a spontaneously broken gauge symmetry. We then generalize these arguments to the case of interacting electrons with spin.

a. Goldstone modes in a Fermi gas

Consider free electrons with mass m_e and chemical potential μ described by fermionic (i.e., Grassmann-valued) fields $\bar{\psi}_n(\boldsymbol{k})$ and $\psi_n(\boldsymbol{k})$ that depend on a wave vector $\boldsymbol{k}$ and a fermionic Matsubara frequency $\omega_n = 2\pi T(n+1/2)$ ($n = 0, \pm 1, \pm 2, \ldots$). These fields are temporal Fourier transforms of fields $\bar{\psi}(\boldsymbol{k}, \tau)$ and $\psi(\boldsymbol{k}, \tau)$ that depend on the imaginary-time variable τ. In terms of these fields, the free-fermion action reads (Negele and Orland, 1988)

$$S_0[\bar{\psi}, \psi] = \sum_{\boldsymbol{k}} \sum_n \bar{\psi}_n(\boldsymbol{k})[i\omega_n - \boldsymbol{k}^2/2m_e + \mu]\psi_n(\boldsymbol{k}). \tag{3.9}$$

Single-particle excitations are described by the Green's function

$$G_n(\boldsymbol{k}) = \langle \psi_n(\boldsymbol{k})\bar{\psi}_n(\boldsymbol{k})\rangle = 1/(i\omega_n - \xi_{\boldsymbol{k}}) \tag{3.10}$$

with $\xi_{\boldsymbol{k}} = \boldsymbol{k}^2/2m_e - \mu$. These are soft in the sense that $G_n(\boldsymbol{k})$ diverges for wave vectors on the Fermi surface $\xi_{\boldsymbol{k}} = 0$ as the frequency approaches zero. Of greater interest in the current context are two-particle excitations. Consider the correlation function

$$\begin{aligned} D_{nm}(\boldsymbol{k}, \boldsymbol{q}) &\equiv \langle \bar{\psi}_n(\boldsymbol{k}_+)\psi_m(\boldsymbol{k}_-)\bar{\psi}_m(\boldsymbol{k}_-)\psi_n(\boldsymbol{k}_+)\rangle \\ &= \delta_{nm}\delta_{\boldsymbol{q},0}[G_n(\boldsymbol{k})]^2 - G_n(\boldsymbol{k}_+)G_m(\boldsymbol{k}_-), \end{aligned} \tag{3.11a}$$

where $\boldsymbol{k}_\pm = \boldsymbol{k} \pm \boldsymbol{q}/2$, and the second line follows from Wick's theorem. Multiplying Eq. (3.11a) with the inverse of $G_n(\boldsymbol{k}_+)$ and $G_m(\boldsymbol{k}_-)$, respectively, and subtracting the resulting two equations, we find

$$(i\Omega_{n-m} - \boldsymbol{k}\cdot\boldsymbol{q}/m_e)D_{nm}(\boldsymbol{k}, \boldsymbol{q}) = G_n(\boldsymbol{k}_+) - G_m(\boldsymbol{k}_-). \tag{3.11b}$$

Now analytically continue to real frequencies according to $i\omega_n \to \Omega + i0$, $i\omega_m \to -\Omega - i0$, and consider the limit $\boldsymbol{q} \to 0$, $\Omega \to 0$. Equation (3.11b) then becomes

$$D^{+-}(\boldsymbol{k}, \boldsymbol{q} \to 0; \Omega \to 0) = \frac{iG''(\boldsymbol{k}, \Omega = 0)}{\Omega - \boldsymbol{k}\cdot\boldsymbol{q}/m_e}. \tag{3.12}$$

Here $D^{+-}(\Omega)$ is the analytic continuation of D_{nm}, and G'' denotes the spectrum of the Green's function. D^{+-} diverges in the limit of zero wave vector $\boldsymbol{q}$ and zero frequency Ω, provided the spectrum of the Green's function is nonzero. For free electrons this is the case for all values of $\boldsymbol{k}$; if we replace the free electrons by band electrons $\xi_{\boldsymbol{k}} = \epsilon_{\boldsymbol{k}} - \mu$, where $\epsilon_{\boldsymbol{k}}$ is determined by the lattice structure, it remains true everywhere within the band. Equivalently, it is true whenever the density

of states is nonzero. We have thus identified the correlation function $D_{nm}(\boldsymbol{k},\boldsymbol{q})$, Eq. (3.11a), as a soft mode of noninteracting electrons. The nature of this soft mode is ballistic, i.e., the frequency Ω scales linearly with the wave number.

This simple result is more general and significant than one might expect, as can be seen from the following analogy. Consider a classical XY ferromagnet with magnetization $\boldsymbol{m}$ in the presence of a small magnetic field $\boldsymbol{h}$. Let the magnitudes of $\boldsymbol{m}$ and $\boldsymbol{h}$ be m and h, respectively. In the PM phase, $\boldsymbol{m}$ is proportional to $\boldsymbol{h}$, and $m(h)$ is an analytic function of h; in particular, $m(h=0)=0$. However, in the FM phase this is not true. $\boldsymbol{m}$ still points in the same direction as $\boldsymbol{h}$, but m is not an analytic function of h at $h=0$: $m(h=\pm 0)=\pm m_0$, with m_0 the spontaneous magnetization. Now let the system be in the FM phase and consider an infinitesimal rotation of the field $\boldsymbol{h}\to\boldsymbol{h}+\delta\boldsymbol{h}$ that leaves h unchanged. Then the magnetization simply follows the field, with m also unchanged. Hence $|\delta\boldsymbol{m}|/m=|\delta\boldsymbol{h}|/h$. But $|\delta\boldsymbol{m}|/|\delta\boldsymbol{h}|$ is the homogeneous transverse susceptibility $\chi_\perp$, and hence

$$h\chi_\perp = m. \tag{3.13}$$

This simple argument (Ma, 1976) shows that the transverse susceptibility diverges in the limit of zero field everywhere in the ordered phase where $m(h\to 0)\neq 0$. It can be made technically more elaborate by proving a Ward identity that takes the form of Eq. (3.13) (Zinn-Justin, 1996), but the simple argument contains all physically relevant points: The soft mode (that is, the magnon or transverse magnetization fluctuation) is a Goldstone mode that results from a spontaneously broken continuous symmetry (Goldstone, 1961; Forster, 1975; Zinn-Justin, 1996); in this case, the rotational symmetry in spin space leads to a nonzero order parameter m.

Now return to free fermions. Consider a local (in imaginary time) gauge transformation

$$\bar\psi(\boldsymbol{k},\tau)\to e^{-i\alpha\tau}\bar\psi(\boldsymbol{k},\tau),\quad \psi(\boldsymbol{k},\tau)\to e^{i\alpha\tau}\psi(\boldsymbol{k},\tau) \tag{3.14a}$$

with α real, or, equivalently,

$$\bar\psi_n(\boldsymbol{k})\to\bar\psi_{n-\alpha}(\boldsymbol{k}),\qquad \psi_n(\boldsymbol{k})\to\psi_{n-\alpha}(\boldsymbol{k}). \tag{3.14b}$$

The second and third terms in Eq. (3.9) are invariant under this transformation, but the frequency term is not; it acts analogously to a magnetic field in the classical XY model. Explicitly, we have

$$S_0[\bar\psi,\psi]\to\sum_{\boldsymbol{k}}\sum_n\bar\psi_n(\boldsymbol{k})[i\omega_n-\boldsymbol{k}^2/2m_{\rm e}+\mu+i\alpha]\psi_n(\boldsymbol{k}). \tag{3.15}$$

If we now let $\alpha\to 0$ and consider the expectation value $\langle\psi_n(\boldsymbol{k})\bar\psi_n(\boldsymbol{k})\rangle$ we see that, upon analytic continuation to real frequencies, $\alpha>0$ vs $\alpha<0$ makes the difference between a retarded and an advanced Green's function. The latter are not the same anywhere within the band, and the U(1) gauge symmetry expressed by Eqs. (3.14) is thus *spontaneously* broken. Equation (3.12) can now be interpreted in analogy to Eq. (3.13): The spectrum of the Green's function is the order parameter of a spontaneously broken continuous symmetry, the frequency acts as the field conjugate to the order parameter, and the soft correlation function D^{+-} is the Goldstone mode associated with the broken symmetry. This remarkable analogy was first found by Wegner (1979) [see also Schäfer and Wegner (1980) and McKane and Stone (1981)] in the context of disordered electrons, where the soft modes are diffusive and commonly referred to as "diffusons" (Akkermans and Montambaux, 2011). The same argument holds for clean electrons, with the diffusive soft modes replaced by ballistic ones (Belitz and Kirkpatrick, 1997, 2012). In these papers the symmetry considered was an SO(2) rotation in frequency space that is isomorphic to the U(1) gauge transformation above. We stress that the broken symmetry discussed previously, and the resulting existence of the soft modes, has nothing to do with the conservation law for the particle number.

b. Goldstone modes in a Fermi liquid

We now take into account electron-electron interactions and spin. Interactions have two effects. One is the appearance of an inelastic scattering rate, both in the Green's function and in the propagator D^{+-}. However, this rate vanishes at $T=0$. The second change is the appearance of an additional term on the right-hand side of Eq. (3.11b), which is related to a three-particle correlation function. This term has a different functional dependence on the interaction than the difference of the Green's functions in Eq. (3.11b) and therefore cannot change the fact that D^{+-} diverges in the limit of vanishing frequency and wave number (Belitz and Kirkpatrick, 2012). This is consistent with Fermi-liquid theory, which posits that there is a one-to-one correspondence between free-electron states and states in a Fermi liquid (Lifshitz and Pitaevskii, 1991). Basic properties such as the soft-mode spectrum will thus not be changed by interactions, and only the coefficients in the soft propagator will acquire interaction dependences.

Spin provides another complication, which is conveniently dealt with by means of introducing bosonic matrix variables Q:

$$Q_{nm}(\boldsymbol{x},\boldsymbol{y})\cong\frac{i}{2}\begin{pmatrix}
-\psi_{n\uparrow}(\boldsymbol{x})\bar\psi_{m\uparrow}(\boldsymbol{y}) & -\psi_{n\uparrow}(\boldsymbol{x})\bar\psi_{m\downarrow}(\boldsymbol{y}) & -\psi_{n\uparrow}(\boldsymbol{x})\psi_{m\downarrow}(\boldsymbol{y}) & \psi_{n\uparrow}(\boldsymbol{x})\psi_{m\uparrow}(\boldsymbol{y})\\
-\psi_{n\downarrow}(\boldsymbol{x})\bar\psi_{m\uparrow}(\boldsymbol{y}) & -\psi_{n\downarrow}(\boldsymbol{x})\bar\psi_{m\downarrow}(\boldsymbol{y}) & -\psi_{n\downarrow}(\boldsymbol{x})\psi_{m\downarrow}(\boldsymbol{y}) & \psi_{n\downarrow}(\boldsymbol{x})\psi_{m\uparrow}(\boldsymbol{y})\\
\bar\psi_{n\downarrow}(\boldsymbol{x})\bar\psi_{m\uparrow}(\boldsymbol{y}) & \bar\psi_{n\downarrow}(\boldsymbol{x})\bar\psi_{m\downarrow}(\boldsymbol{y}) & \bar\psi_{n\downarrow}(\boldsymbol{x})\psi_{m\downarrow}(\boldsymbol{y}) & -\bar\psi_{n\downarrow}(\boldsymbol{x})\psi_{m\uparrow}(\boldsymbol{y})\\
-\bar\psi_{n\uparrow}(\boldsymbol{x})\bar\psi_{m\uparrow}(\boldsymbol{y}) & -\bar\psi_{n\uparrow}(\boldsymbol{x})\bar\psi_{m\downarrow}(\boldsymbol{y}) & -\bar\psi_{n\uparrow}(\boldsymbol{x})\psi_{m\downarrow}(\boldsymbol{y}) & \bar\psi_{n\uparrow}(\boldsymbol{x})\psi_{m\uparrow}(\boldsymbol{y})
\end{pmatrix}. \tag{3.16}$$

Here $\cong$ means that Q is isomorphic to $\bar{\psi}\psi$. We also define the Fourier transforms

$$Q_{nm}(\boldsymbol{k},\boldsymbol{p}) = \frac{1}{V}\int d\boldsymbol{x}d\boldsymbol{y}e^{-i\boldsymbol{k}\cdot\boldsymbol{x}+i\boldsymbol{p}\cdot\boldsymbol{y}}Q_{nm}(\boldsymbol{x},\boldsymbol{y}) \tag{3.17a}$$

and

$$Q_{nm}(\boldsymbol{k};\boldsymbol{q}) = Q_{nm}(\boldsymbol{k}+\boldsymbol{q}/2,\boldsymbol{k}-\boldsymbol{q}/2). \tag{3.17b}$$

The 4×4 matrix Q_{nm} can be expanded in a spin-quaternion basis

$$Q_{nm}(\boldsymbol{x},\boldsymbol{y}) = \sum_{r,i=0}^{3}(\tau_r \otimes s_i)^i_r Q_{nm}(\boldsymbol{x},\boldsymbol{y}), \tag{3.18}$$

where $\tau_0 = s_0 = \mathbb{1}_2$ is the unit 2×2 matrix, and $\tau_{1,2,3} = -s_{1,2,3} = -i\sigma^{1,2,3}$ with $\sigma^{1,2,3}$ the Pauli matrices. Inspection shows that $i = 0$ and $i = 1, 2, 3$ represent the spin-singlet and triplet channels, respectively. Similarly, $r = 0, 3$ represents the particle-hole channel, i.e., products of the form $\bar{\psi}\psi$, whereas $r = 1, 2$ represents the particle-particle channel, i.e., products of the form $\bar{\psi}\,\bar{\psi}$ or $\psi\psi$. We need only the particle-hole degrees of freedom. All of the Q_{nm} are not independent; a convenient choice of the independent elements are those with $n \geq m$.

These considerations show that the matrix elements ${}^0_0Q_{nm}$ with $n \geq 0$ and $m < 0$ are soft modes. It is easy to see, by using discrete symmetries that connect the various channels, that in the absence of external fields all of the ${}^i_rQ_{nm}$ with $n \geq 0$, $m < 0$ are soft (Belitz and Kirkpatrick, 1997, 2012). Symmetry-breaking fields change this. For instance, an external magnetic field gives a mass to the particle-particle channel, and also to two of the particle-hole spin-triplet channels ($i = 1$, 2 for a magnetic field in the z direction). A nonzero magnetization with a homogeneous component in a magnetically ordered phase has the same effect.

To summarize, of the two-particle degrees of freedom ${}^i_rQ_{nm}(\boldsymbol{k};\boldsymbol{q})$ defined by Eqs. (3.16)–(3.18), those with $n \geq 0$ and $m < 0$ are soft modes in the sense that their two-point correlation functions diverge in the limit of vanishing wave vector $\boldsymbol{q}$ and vanishing frequency $i\Omega_{n-m} \to \Omega + i0$. They represent the Goldstone mode of a spontaneously broken continuous symmetry expressed by the gauge transformation in Eqs. (3.14). Physically, the broken symmetry reflects the difference between retarded and advanced degrees of freedom, and the spectrum of the single-particle Green's function is the corresponding order parameter. Note that the ${}^i_rQ_{nm}(\boldsymbol{k};\boldsymbol{q})$ are soft for any value of $\boldsymbol{k}$ for which the spectrum of the Green's function is nonzero. Thus there are an infinite number of soft two-particle modes in a Fermi liquid. This is qualitatively different from the case of electrons in the presence of quenched disorder, for which only the zeroth moment $\sum_{\boldsymbol{k}}{}^i_rQ_{nm}(\boldsymbol{k};\boldsymbol{q})$ is soft.

c. Goldstone modes in a disordered Fermi liquid: Diffusons

Historically, the notion of a spontaneously broken continuous symmetry, and the resulting Goldstone modes, in many-fermion systems was first developed for noninteracting electrons in the presence of quenched disorder (Wegner, 1979; Schäfer and Wegner, 1980; McKane and Stone, 1981; Pruisken and Schäfer, 1982), and it was instrumental for Wegner's matrix nonlinear sigma model describing the Anderson metal-insulator transition (Wegner, 1979). The derivation of Schäfer and Wegner (1980) was later generalized to the case of interacting electrons in the presence of disorder (Belitz and Kirkpatrick, 1997). In the notation of Eq. (3.11b), the two crucial differences in the disordered case are (1) Only the zeroth moment with respect to $\boldsymbol{k}$ of the disorder average of D_{nm}, $\sum_{\boldsymbol{k}}D_{nm}(\boldsymbol{k},\boldsymbol{q})$, is soft if n and m have different signs, and (2) the resulting soft modes have a diffusive character, $\Omega \sim \boldsymbol{q}^2$, as opposed to the ballistic modes in the clean case. Denoting the soft modes analogous to Eq. (3.12) by $D^{+-}(\boldsymbol{q},\Omega)$, one has

$$D^{+-}(\boldsymbol{q}\to 0,\Omega\to 0) = \frac{\pi N(\epsilon_{\mathrm{F}})}{\Omega + D\boldsymbol{q}^2}, \tag{3.19}$$

with $N(\epsilon_{\mathrm{F}})$ the density of states at the Fermi level, and D a diffusion coefficient. These diffusive soft modes are often referred to as diffusons in the literature, and their counterparts in the particle-particle channel as Cooperons. In the language of the Q matrices, Eqs. (3.16)–(3.18), the diffusons and Cooperons are given by the correlation functions of the $\sum_{\boldsymbol{k}}{}^i_rQ_{nm}(\boldsymbol{k};\boldsymbol{q})$. Note that there are many more soft modes in a clean system than in a disordered one, which makes the soft-mode analysis in clean systems more complicated.

B. Effects of fermionic soft modes: Simple physical arguments

We now give simple arguments for why fermionic fluctuations cause the FM QPT in clean 2D or 3D metals to always be discontinuous. We then discuss how the presence of quenched disorder modifies this conclusion.

1. Renormalized Landau theory

We need a theory that describes the magnetization or order-parameter (OP) field $\boldsymbol{m}$, the fermionic degrees of freedom or conduction electrons described by the Grassmann fields of Sec. III.A, and the coupling between them. Accordingly, the action consist of three parts,

$$S[\boldsymbol{m};\bar{\psi},\psi] = -\mathcal{A}_{\mathrm{OP}}[\boldsymbol{m}] + S_{\mathrm{F}}[\bar{\psi},\psi] + S_{\mathrm{c}}[\boldsymbol{m};\bar{\psi},\psi]. \tag{3.20}$$

They denote a purely bosonic part of the action that governs the OP, a purely fermionic one that describes the conduction electrons, and a coupling between the two.[20] The partition function is given by

$$Z = \int D[\boldsymbol{m}]D[\bar{\psi},\psi]e^{S[\boldsymbol{m};\bar{\psi},\psi]}. \tag{3.21}$$

[20]We denote actions that depend on bosonic (number-valued) fields only by $\mathcal{A}$, actions that depend on fermionic (Grassmann-valued) fields, or a mix of bosonic and fermionic fields, by S, and use a sign convention such that S and $\mathcal{A}$ enter the exponential with a plus and minus sign, respectively.

Note that we do not specify the origin of the magnetization; in general it can be due to the conduction electrons, or due to localized electrons in a different band, or a combination of the two. If one formally integrates out the conduction electrons one obtains an effective LGW action in terms of the OP only,

$$Z = \int D[\boldsymbol{m}] e^{-\mathcal{A}_{\rm eff}[\boldsymbol{m}]}, \tag{3.22a}$$

where

$$\mathcal{A}_{\rm eff}[\boldsymbol{m}] = \mathcal{A}_{\rm OP}[\boldsymbol{m}] - \ln \int D[\bar{\psi},\psi] e^{S_{\rm F}[\bar{\psi},\psi]+S_{\rm c}[\boldsymbol{m};\bar{\psi},\psi]}. \tag{3.22b}$$

In general, the magnetization will couple both to the orbital angular momentum and to the spin of the electrons. The former poses interesting questions that have received little attention to date, and we do not discuss it here. The latter coupling is via a Zeeman-like term

$$S_{\rm c}[\boldsymbol{m};\bar{\psi},\psi] = c \int dx \boldsymbol{m}(x) \cdot \boldsymbol{n}_{\rm s}(x). \tag{3.23}$$

Here c is a coupling constant and $\boldsymbol{n}_{\rm s}$ is the electronic spin density,

$$\boldsymbol{n}_{\rm s}(x) = \sum_{a,b} \bar{\psi}_a(x) \boldsymbol{\sigma}_{ab} \psi_b(x), \tag{3.24}$$

with $\boldsymbol{\sigma} = (\sigma^1, \sigma^2, \sigma^3)$ the Pauli matrices. $a, b = (\uparrow, \downarrow)$ are spin indices, $x \equiv (\boldsymbol{x}, \tau)$ comprises both the real-space position $\boldsymbol{x}$ and the imaginary-time variable τ, and $\int dx \equiv \int_V d\boldsymbol{x} \int_0^{1/T} d\tau$, with V the system volume.

For simplicity we now treat the OP in a mean-field approximation, i.e., we replace the fluctuating magnetization $\boldsymbol{m}(x)$ by an x-independent magnetization m that we take to point in the 3-direction. We will discuss the validity of this approximation in Sec. III.C. Denoting the 3-component of $\boldsymbol{n}_{\rm s}$ by $n_{\rm s}$, the second term in Eq. (3.22b), which describes the effect of the coupling between the fermions and the OP, can be written

$$\begin{aligned}\delta\mathcal{A}[m] &= -\ln \int D[\bar{\psi},\psi] e^{S_{\rm F}[\bar{\psi},\psi]+cm\int dx n_{\rm s}(x)} \\ &= -\ln \langle e^{cm\int dx n_{\rm s}(x)} \rangle_{\rm F},\end{aligned} \tag{3.25}$$

where in the second line we dropped a constant contribution to the action, and $\langle \cdots \rangle_{\rm F}$ denotes an average with the action $S_{\rm F}$.

Now consider the longitudinal spin susceptibility $\chi(h)$ of fermions governed by the action $S_{\rm F}$ and subject to a magnetic field h. It is given by the correlation function

$$\chi(h) = \frac{T}{V} \int dx dy \langle \delta n_{\rm s}(x) \delta n_{\rm s}(y) \rangle_{S_{\rm h}}, \tag{3.26}$$

where $S_{\rm h} = S_{\rm F} + h \int dx n_{\rm s}(x)$, and $\delta n_{\rm s}(x) = n_{\rm s}(x) - \langle n_{\rm s}(x) \rangle_{S_{\rm m}}$. By differentiating Eq. (3.25) twice with respect to m it is easy to show that

$$\frac{d^2\delta\mathcal{A}}{dm^2} = -\frac{V}{T} c^2 \chi(cm). \tag{3.27}$$

Since $\delta\mathcal{A}[m=0] = d\delta\mathcal{A}/dm|_{m=0} = 0$, we now have

$$\delta\mathcal{A}[m] = \frac{-V}{T} c^2 \int_0^m dm_1 \int_0^{m_1} dm_2 \chi(cm_2). \tag{3.28}$$

$S_{\rm OP}$ will have the usual Landau form of a power series in powers of m^2, and the complete renormalized Landau free-energy density $f_{\rm eft} = -(T/V)\mathcal{A}_{\rm eft}$ thus is

$$f_{\rm eff}[m] = tm^2 + \delta f[m] + um^4 + O(m^6). \tag{3.29a}$$

Here t and u are Landau parameters, and

$$\delta f[m] = -c^2 \int_0^m dm_1 \int_0^{m_1} dm_2 \chi(cm_2). \tag{3.29b}$$

This result expresses the correction to the usual Landau action in terms of the spin susceptibility of nonmagnetic fermions in the presence of an effective homogeneous magnetic field given by cm. It is a "renormalized Landau theory" in the sense that it includes the effects of fluctuations extraneous to the OP fluctuations. The remaining question is the behavior of the susceptibility χ that represents these fluctuations for small m. As we will see, χ is not an analytic function of m at $m = 0$.

2. Clean systems

Various observables in a Fermi liquid are nonanalytic functions of the temperature. For instance, the specific-heat coefficient has a $T^2 \ln T$ term (Baym and Pethick, 1991). The spin susceptibility in a 3D system has no such nonanalytic behavior (Carneiro and Pethick, 1977). However, this absence of a nonanalyticity was later shown to be accidental, and to pertain only to the T dependence in $d = 3$. In dimensions $d \neq 3$ there is a T^{d-1} nonanalyticity, and even in $d = 3$ at $T = 0$ the inhomogeneous spin susceptibility has a $k^2 \ln k$ wave-number dependence (Belitz, Kirkpatrick, and Vojta, 1997; Chitov and Millis, 2001; Galitski, Chubukov, and Das Sarma, 2005). This nonanalyticity is a direct consequence of the soft modes discussed in Sec. III.A. From scaling arguments one expects a corresponding nonanalyticity for the homogeneous susceptibility at $T = 0$ as a function of a magnetic field h, namely, $\chi(h) \propto \text{const} + h^{d-1}$ in generic dimensions, and $\chi(h) \propto \text{const} - h^2 \ln h$ in $d = 3$. These scaling arguments have been shown to be exact, as far as the exponent is concerned, by a RG treatment (Belitz and Kirkpatrick, 2014), and they are consistent with explicit perturbative calculations (Misawa, 1971; Barnea and Edwards, 1977; Betouras, Efremov, and Chubukov, 2005). The sign of the effect is universal and can be established as follows. Fluctuations suppress the tendency of a Fermi liquid to order ferromagnetically, and therefore the fluctuation correction to the bare zero-field susceptibility is negative, $\delta\chi(0) < 0$. A magnetic field suppresses the fluctuations, and therefore $\delta\chi(h) - \delta\chi(0) > 0$. This implies that the nonanalyticity in $\chi(h \to 0)$ has a positive sign:

$$\chi(h \to 0) = \chi(0) + \begin{cases} a_d h^{d-1}, & \text{for } 1 < d < 3, \\ a_3 h^2 \ln(1/h), & \text{for } d = 3, \end{cases} \tag{3.30}$$

where $a_d > 0$. For the renormalized Landau free-energy density, Eq. (3.29a), we thus obtain

$$f_{\text{eff}}[m] = -hm + tm^2 + um^4 - v_d \times \begin{cases} m^{d+1} + um^4 & (1 < d < 3), \\ m^4 \ln(1/m) & (d = 3). \end{cases} \tag{3.31}$$

Here $v_d \propto c^{d+1} > 0$, and we have added an external magnetic field h. For $d = 3$ this result was first derived by Belitz, Kirkpatrick, and Vojta (1999). The negative term in the free energy, which dominates the quartic term for all $d \leq 3$, necessarily leads to a first-order ferromagnetic transition. We stress that while this is a fluctuation-induced first-order quantum phase transition, the relevant fluctuations are not the OP fluctuations, but are fermionic in nature. For purposes of an analogy with the well-known classical fluctuation-induced first-order transitions (Halperin, Lubensky, and Ma, 1974), the latter play a role that is analogous to that of the vector potential in superconductors, or the director fluctuations at the nematic-smectic-*A* transition. An important difference, however, is that in these classical systems the OP fluctuations are below their upper critical dimension, which makes them strong enough to make the first-order transition weak and hard to observe at best, and destroy it altogether at worst (Anisimov *et al.*, 1990). In contrast, in the case of a quantum FM the OP fluctuations are *above* their upper critical dimension, so the first-order transition predicted by the renormalized Landau theory will be much more robust.

A nonzero temperature cuts off the magnetic field singularity (Betouras, Efremov, and Chubukov, 2005), and with increasing temperature the fluctuation-induced term in the free energy becomes less and less negative. Suppose the Landau parameter t at $T = 0$ is a monotonically increasing function of, say, hydrostatic pressure p, and let $t(p = 0, T = 0) < 0$. Then there will be a QPT at some nonzero pressure p_c. As the transition temperature is increased from zero by lowering p, one expects a tricritical point in the phase diagram. Below the tricritical temperature the transition will be discontinuous due to the mechanism described earlier, while at higher temperatures it will be continuous. In the presence of an external magnetic field there appear surfaces of first-order transitions, or tricritical wings (Belitz, Kirkpatrick, and Rollbühler, 2005), and the phase diagram has the schematic structure shown in the rightmost panel in Fig. 37.[21] The third law of thermodynamics, in conjunction with various Clapeyron-Clausius relations, puts constraints on the shape of the wings at low temperatures (Kirkpatrick and Belitz, 2015b). Most importantly, the wings must be perpendicular to the $T = 0$ plane, and they cannot be perpendicular to the zero-field plane. These constraints, as well as the overall wing structure, are in excellent agreement with experimentally observed phase diagrams; see, for instance, Figs. 1, 3, 6, and 10.

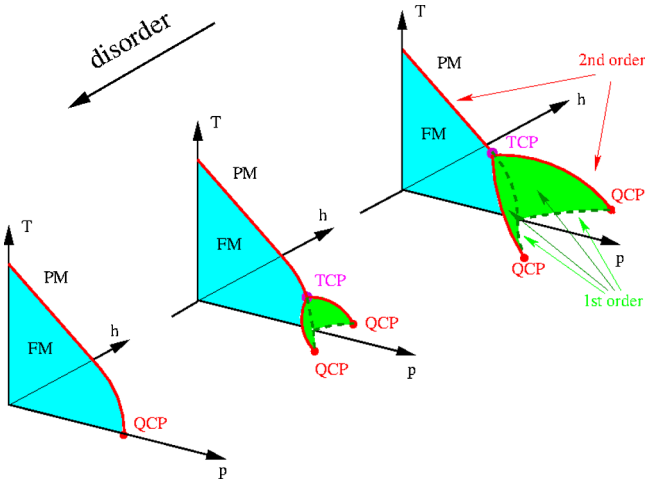

FIG. 37. Schematic phase diagram in the space spanned by temperature (T), hydrostatic pressure (p), and magnetic field (h). Shown are the FM and PM phases, the tricritical point (TCP), and various QCPs. Solid and dashed lines denote second- and first-order transitions, respectively. The tricritical wings emerging from the TCP are surfaces of first-order transitions. The three panels show the predicted change with increasing disorder. From Sang, Belitz, and Kirkpatrick, 2014.

The theory also predicts a correlation between the tricritical temperature T_{tc} and the magnetic moment m_1 just on the FM side of the first-order transition. In terms of the parameters in Eq. (3.31) one finds $T_{tc} = T_0 e^{-u/v_3}$ and $m_1 = m_0 e^{-1/2} e^{-u/v_3}$, where T_0 and m_0 are microscopic temperature and magnetization scales, respectively (Belitz, Kirkpatrick, and Rollbühler, 2005). For given scales T_0 and m_0, which one expects to vary little within members of a given class of materials, the theory thus predicts that T_{tc} is proportional to m_1. As pointed out in Sec. II.B.5, this is in good agreement with experiments.

3. Disordered systems

In the presence of quenched disorder the logic of these arguments remains intact, but important aspects change. First, the fermionic soft modes are diffusive in nature, rather than ballistic; see Sec. III.A.2.c. This slowing down of the electrons favors the tendency toward ferromagnetism, and the combined disorder and interaction fluctuations increase the bare susceptibility $\delta\chi(0) > 0$.[22] A small magnetic field again suppresses the effect of the fluctuations, and the nonanalytic contribution to $\chi(h)$ therefore has a negative sign. Second, the changed nature of the fermionic soft modes leads to a different exponent, namely,

[21] The presence of tricritical wings is characteristic of any phase diagram that contains a tricritical point (Griffiths, 1970, 1973), it is not restricted to the ferromagnetic quantum phase transition.

[22] The notion that quenched disorder *favors* ferromagnetic order is somewhat counterintuitive, given that in classical systems, long-range order is negatively affected by it (Cardy, 1996). Indeed, the ferromagnetic T_c usually decreases with increasing disorder; see Sec. II. However, at sufficiently low temperature the diffusive motion of the electrons leads to an increase in the effective exchange interaction. The interplay between these two effects is discussed at the end of this section.

$$\chi(h \to 0) = \chi(0) - \tilde{a}_d h^{(d-2)/2}, \quad \text{for } d > 2, \tag{3.32}$$

with $\tilde{a}_d > 0$. This expectation is borne out by explicit perturbative calculations (Altshuler, Aronov, and Zyuzin, 1983). Third, the notion of a disordered Fermi liquid breaks down for $d \leq 2$ due to localization effects (Lee and Ramakrishnan, 1985; Belitz and Kirkpatrick, 1994), so the only physical dimension where the current discussion applies is $d = 3$.

The renormalized Landau free-energy density in $d = 3$ now becomes (Belitz and Kirkpatrick, 1996; Kirkpatrick and Belitz, 1996)

$$f_{\text{eff}}[m] = -hm + tm^2 + vm^{5/2} + um^4, \tag{3.33}$$

with $v > 0$. We see that, for very general reasons, quenched disorder leads to a second-order or continuous transition, but the Landau theory for this transition is not standard because of the $m^{5/2}$ term which leads to unusual critical exponents. In particular, the exponents β and δ for the OP, and γ for the OP susceptibility, are

$$\beta = 2, \qquad \delta = 3/2, \qquad \gamma = 1. \tag{3.34}$$

Other critical exponents are discussed in Sec. III.C.

Equations (3.31) and (3.33) are valid for the extreme cases of ultraclean and strongly disordered systems, respectively. An equation of state that interpolates between the two was constructed by Sang, Belitz, and Kirkpatrick (2014); the schematic evolution of the phase diagram with increasing disorder is shown in Fig. 37. The theory allows one to distinguish between three distinct disorder regimes, characterized by the residual resistivity ρ_0:

Regime I (clean): $\rho_0 \lesssim \rho_0^{(1)}$. The transition at low temperature is first order, and there is a tricritical point in the phase diagram. The tricritical temperature decreases with increasing disorder.

Regime II (intermediate): $\rho_0^{(1)} \lesssim \rho_0 \lesssim \rho_0^{(2)}$. The transition is second order down to $T = 0$. The critical behavior is mean field like, as predicted by Hertz theory, except extremely close to the critical point, where it crosses over to the exponents given by Eq. (3.34).

Regime III (disordered): $\rho_0 \gtrsim \rho_0^{(2)}$. The transition is second order, and the critical exponents are given by Eq. (3.34). In this regime the quantum Griffiths effects discussed in Sec. III.D are expected to be present and to compete with the critical behavior.

A rough estimate (see footnote [10]) for the boundaries between the three regimes yields $\rho_0^{(1)} \approx 1$ to several $\mu\Omega\,\text{cm}$, and $\rho_0^{(2)} \approx 100$ to several hundred $\mu\Omega\,\text{cm}$.

We now discuss the expected qualitative shape of the phase diagram. Let x be a dimensionless measure of the disorder, $x \propto 1/\tau$ with τ the elastic mean-free time. As mentioned previously (see footnote [22]), there are two competing influences of x on the critical temperature. One is a classical dilution effect that suppresses T_c to zero at sufficiently large values of x (Cardy, 1996). For simplicity, let us assume that this leads to $T_c(x) = 1 - x^2$, with T_c measured in units of $T_c(x = 0)$. (Adding a term linear in x does not change the qualitative discussion that follows.) The other is an increase in

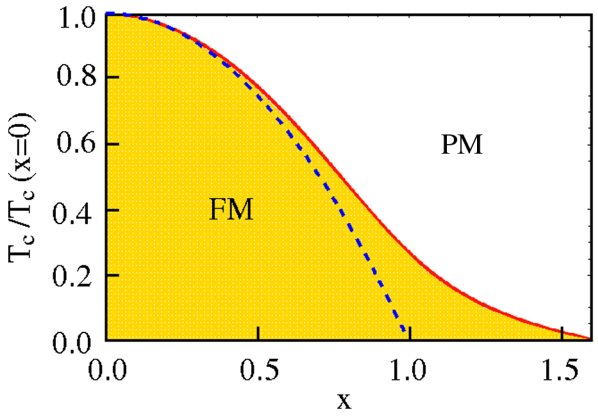

FIG. 38. Phase diagram in the temperature-disorder plane as given by Eq. (3.35). The dashed line reflects the classical dilution effect of the disorder only [$a = 0$ in Eq. (3.35)]; the solid (red) line also reflects the quantum effects, with $a = 1$, $b = 10$, due to the diffusive dynamics of the electrons.

T_c due to the diffusive nature of the electron dynamics, which increases the effective spin-triplet interaction (Altshuler, Aronov, and Zyuzin, 1983). Indeed, the increase in the zero-field susceptibility mentioned before Eq. (3.32) is proportional to this increase in the interaction amplitude. For small disorder, this effect is linear in the disorder at $T = 0$, and it is cut off by the temperature itself, i.e., it is strongest for small values of T_c. A simple schematic way to represent these two effects is

$$T_c(x) = 1 - x^2 + \frac{ax}{1 + bT_c(x)/x}. \tag{3.35}$$

The resulting qualitative shape of the phase diagram is shown in Fig. 38. The two competing disorder effects can lead to an inflection point in T_c vs x that is often seen in experiments; see Figs. 28 and 33. Another possible interpretation of this shape of the phase diagram is a smeared transition due to quantum Griffiths effects that have been ignored in these arguments; this is discussed in Sec. III.D. In addition to the inflection point in the phase diagram, the unusually large value of the exponent β, Eq. (3.34), can also mimic a smeared transition.

We finally recall a very general result for systems with quenched disorder due to Harris (1974) and Chayes *et al.* (1986). Harris investigated a necessary condition for the critical behavior of a clean system to remain unchanged by a small amount of quenched disorder. In order for the transition to stay sharp, the disorder-induced fluctuations of the location of the critical point in parameter space must be small compared to the distance from the critical point. This implies that the correlation length must diverge sufficiently fast as the critical point is approached, which leads to a requirement for the correlation-length exponent ν,

$$\nu \geq 2/d. \tag{3.36}$$

This is often referred to as the Harris criterion. In Harris's original argument this was a constraint on the exponent ν of the *clean* system which, if hyperscaling holds, is equivalent to the condition $\alpha < 0$ for the specific-heat exponent α. It does not apply to the quantum FM transition, since the latter is not

continuous in clean systems. However, Chayes *et al.* (1986) showed rigorously that, for a large class of disordered systems that undergoes a continuous phase transition, Eq. (3.36) must hold for the exponent ν that characterizes the *disordered* fixed point. The value of ν corresponding to the exponents given in Eq. (3.34), viz., $\nu = 1$ in $d = 3$ (Kirkpatrick and Belitz, 1996), satisfies this constraint, while the mean-field value $\nu = 1/2$ of Hertz theory does not. We come back to this point in Sec. III.C.2.

C. Effects of order-parameter fluctuations, and comparison with experiment

In Sec. III.B.3 we treated the OP in a mean-field approximation and integrated out all fermionic degrees of freedom. The fermionic soft modes then led to a Landau free energy that is not an analytic function of the magnetization. We now discuss the order-parameter fluctuations that were neglected in this procedure and also consider the behavior not asymptotically close to the quantum phase transition. All of these issues are important for the relation of the theory to the experimental results discussed in Sec. II.

1. Coupled field theory for soft modes

We return to the coupled field theory in Eq. (3.20). For the purposes of discussing fluctuation effects, integrating out the fermions, as in Eq. (3.22), is not desirable, as it results in a nonlocal field theory for the order-parameter fluctuations.[23] A better strategy is to separate the fermionic degrees of freedom into soft and massive modes and integrate out only the latter to arrive at an effective theory that treats all of the soft modes on equal footing. This is possible using the identification of fermionic soft modes explained in Sec. III.A. The resulting effective action can then be analyzed by means of RG methods.

In Sec. III.A we have seen that the soft fermionic degrees of freedom are given by those matrix elements Q_{nm}, Eq. (3.16), for which the two Matsubara frequencies have different signs. Denoting these by q_{nm} [with $n > 0$, $m < 0$ implied, see the remark after Eq. (3.10)], and the massive modes by P_{nm}, we first rewrite the action from Eq. (3.20) in terms of the q and P[24]:

$$\begin{aligned}\mathcal{A}[\boldsymbol{m}; q, P] &\equiv -S[\boldsymbol{m}; \bar{\psi}, \psi] \\ &= \mathcal{A}_{\mathrm{OP}}[\boldsymbol{m}] + \mathcal{A}_{\mathrm{F}}[q, P] + \mathcal{A}_{\mathrm{c}}[\boldsymbol{m}; q, P]. \end{aligned} \tag{3.37}$$

If we now integrate out the massive modes P, we can formally write the partition function

$$Z = \int D[\boldsymbol{m}] D[q] e^{-\mathcal{A}_{\mathrm{eff}}[\boldsymbol{m}, q]}, \tag{3.38a}$$

in terms of an effective action

$$\begin{aligned}\mathcal{A}_{\mathrm{eff}}[\boldsymbol{m}, q] &= \mathcal{A}_{\mathrm{OP}}[\boldsymbol{m}] - \ln \int D[P] e^{-\mathcal{A}_{\mathrm{F}}[q,P] - \mathcal{A}_{\mathrm{c}}[\boldsymbol{m}; q, P]} \\ &\equiv \mathcal{A}_{\mathrm{OP}}[\boldsymbol{m}] + \mathcal{A}_{\mathrm{F}}[q] + \mathcal{A}_{\mathrm{c}}[\boldsymbol{m}, q]. \end{aligned} \tag{3.38b}$$

Integrating out the P cannot be done exactly, but any approximation that respects the symmetries of the action suffices.

Before we discuss the various terms in this effective action in more detail, we make a few general remarks. $\mathcal{A}_{\mathrm{OP}}$ is a standard LGW action, supplemented by a random-mass term in the disordered case; see Eq. (3.74) below. $\mathcal{A}_{\mathrm{F}}$ has a Gaussian contribution that reflects the soft modes identified in Sec. III.A.2, as well as higher-order terms to all orders in q. The soft modes are diffusive in disordered systems, and ballistic in clean ones, but apart from this and the random-mass term in $\mathcal{A}_{\mathrm{OP}}$ there are no structural differences between clean and disordered systems as far as these two terms in the action are concerned. The coupling $\mathcal{A}_{\mathrm{c}}$ has a contribution that is bilinear in $\boldsymbol{m}$ and q, and in addition terms of order $\boldsymbol{m}q^n$, where n can be any integer. The bilinear term leads to the characteristic Landau damping in the paramagnon propagator (Doniach and Engelsberg, 1966; Hertz, 1976), i.e., to a frequency dependence of the form $|\Omega|/|\boldsymbol{k}|$ in clean systems, and $|\Omega|/\boldsymbol{k}^2$ in disordered ones. At the level of terms bilinear in $\boldsymbol{m}$ and q there is again no other structural difference between the clean and disordered cases. However, the terms of order $\boldsymbol{m}q^2$ generate, in a renormalization procedure, a nonanalytic wave-number dependence of the paramagnon propagator that has the form $|\boldsymbol{k}|^{d-1}$ in clean systems, and $|\boldsymbol{k}|^{d-2}$ in disordered ones. The sign of this term is different in the two cases. If one replaces the fluctuating order parameter by its expectation value, this term leads to the renormalized Landau theory described in Sec. III.B.1.

2. Clean systems

In clean systems, the transition at $T = 0$ in zero field is first order if OP fluctuations are neglected; see Sec. III.B.2. OP fluctuations are thus cut off before the system reaches a critical point, remain finite, and do not change the nature of the transition.[25] However, if the transition is weakly first order there will be a sizable region in parameter space where the

[23] Historically, this was the route taken by Hertz (1976), who integrated out the fermions in a tree approximation. For disordered systems, it was later refined by Kirkpatrick and Belitz (1996), who showed that fermionic loops destabilize Hertz's critical fixed point. While this method works for power-counting purposes, the coupled local field theory developed later for disordered (Belitz *et al.*, 2001a, 2001b) and clean (Kirkpatrick and Belitz, 2012b) systems is more versatile and easier to handle, and we use it here. For clean systems, the fermionic fluctuations destroy the critical fixed point and change the order of the transition, as discussed in Sec. III.B.2. However, the preasymptotic behavior, which is governed by a critical fixed point that ultimately is unstable, can still be important and is discussed in Sec. III.C.2.

[24] Technically, this can be achieved by constraining all terms in the action that contain the Grassmann fields to higher than bilinear order to the matrix field Q from Eq. (3.16) by means of a Lagrange multiplier field and integrating out the Grassmann fields; see Belitz and Kirkpatrick (1997, 2012). For simplicity we suppress the dependence of the action on the Lagrange multiplier field in our notation.

[25] This needs to be interpreted with care in light of footnote [8]. The first-order transition is described by a strong-coupling fixed point (Nienhuis and Nauenberg, 1975; Fisher and Berker, 1982), and the relevant fluctuations are effectively already included in the generalized Landau theory represented by Eq. (3.31)

physical behavior is controlled by the unstable fixed point that is described by Hertz theory, and only asymptotically close to the transition will the RG flow turn away toward the strong-coupling fixed point that describes the first-order transition. It is therefore important to fully understand the results of Hertz theory and its predecessors, even if they ultimately do not describe the nature of the transition correctly. Also, OP fluctuations affect the various lines of second-order transitions in the phase diagram shown schematically in Fig. 37.

a. Hertz's action, and relation to spin-fluctuation theory

In clean systems, the relevant fermionic soft modes are the Fermi-liquid Goldstone modes discussed in Sec. III.A.2. The soft-mode action has not been derived in a closed form, but can be obtained to any desired order in the soft degrees of freedom q. To Gaussian order it reads (Belitz and Kirkpatrick, 2012)

$$\mathcal{A}_{\mathrm{F}}[q] = -8\sum_{r=0,3}\sum_{i=0}^{3}\sum_{\substack{1,2\\3,4}}\frac{1}{V}\sum_{\boldsymbol{k}}{}_r^i q_{12}(\boldsymbol{k})\,{}_r^i q_{34}(-\boldsymbol{k}) \times\left(\delta_{13}\delta_{24}\frac{1}{\varphi_{12}(\boldsymbol{k})}-\delta_{1-2,3-4}2T\gamma_i\right)+O(q^3). \quad (3.39)$$

Here γ_0 and $\gamma_{1,2,3}$ are the spin-singlet and spin-triplet interaction amplitudes, respectively, $1\equiv n_1$ etc. is a shorthand for Matsubara frequencies, and the function φ is given by

$$\varphi_{12}(\boldsymbol{k}) = N_{\mathrm{F}}\frac{2\pi G}{k}\varphi_d(Gi\Omega_{1-2}/k), \quad (3.40)$$

where G is a coupling constant whose bare value is the inverse Fermi velocity $1/v_{\mathrm{F}}$. φ_d can be expressed in terms of Gauss's hypergeometric function. For $d=1$, 2, and 3 it reduces to the familiar expressions for the hydrodynamic part of the Lindhard function in these dimensions:

$$\varphi_{d=1}(z) = -iz/(1-z^2), \quad (3.41a)$$

$$\varphi_{d=2}(z) = i/\sqrt{z+1}\sqrt{z-1}, \quad (3.41b)$$

$$\varphi_{d=3}(z) = \frac{-i}{2}\ln\left(\frac{1-z}{-1-z}\right). \quad (3.41c)$$

Note that the vertex $1/\varphi$ scales as a function that is linear in either the frequency or the wave number (except in $d=1$), and that this is true also for the interaction term in Eq. (3.39) due to the structure of the frequency constraint. This feature reflects the Goldstone modes.

The order-parameter field $\boldsymbol{m}$ couples linearly to the electron spin density with a dimensionless coupling constant $c=O(1)$. To linear order in the soft component q the coupling reads

$$\mathcal{A}_{\mathrm{c}}[\boldsymbol{m},q] = 8c\sqrt{T}\sum_{\boldsymbol{k}}\sum_{12}\sum_{r,i}{}_r^i q_{12}(\boldsymbol{k})\,{}_r^i b_{12}(-\boldsymbol{k})+O(mq^2), \quad (3.42a)$$

where

$${}_r^i b_{12}(\boldsymbol{k}) = (-)^{r/2}\sum_n \delta_{n,n_1-n_2}[m_n^i(\boldsymbol{k})+(-)^{r+1}m_{-n}^i(\boldsymbol{k})] \quad (3.42b)$$

is a symmetrized version of the order-parameter field $\boldsymbol{m}_n(\boldsymbol{k})$ with components $m_n^{1,2,3}$.

Finally, the order-parameter action is an ordinary quantum ϕ^4 theory,[26]

$$\mathcal{A}_{\mathrm{OP}}[\boldsymbol{m}] = -\sum_{\boldsymbol{k},n}\boldsymbol{m}_n(\boldsymbol{k})[t+a\boldsymbol{k}^2+b(\Omega_n)^2]\cdot\boldsymbol{m}_{-n}(-\boldsymbol{k}) + u\int d\boldsymbol{x}T\sum_{n_1,n_2,n_3}[\boldsymbol{m}_{n_1}(\boldsymbol{x})\cdot\boldsymbol{m}_{n_1}(\boldsymbol{x})] \times[\boldsymbol{m}_{n_3}(\boldsymbol{x})\cdot\boldsymbol{m}_{-n_1-n_2-n_3}(\boldsymbol{x})], \quad (3.43)$$

with t, a, b, and u the coupling constants of this LGW action.

We now have specified all parts of the effective action, Eq. (3.38b), to bilinear order in $\boldsymbol{m}$ and q. This is not a fixed-point action corresponding to a critical fixed point. The terms of $O(mq^2)$ that are not shown explicitly in Eq. (3.42) are relevant with respect to the fixed point represented by this action and lead to the first-order transition described in Sec. III.B.2. However, depending on the strength of the first-order transition, there will be a sizable regime where the RG flow is dominated by the unstable fixed point. The physical behavior in this regime will thus be given by the action as written earlier, before it crosses over to the first-order transition. To study this preasymptotic behavior it is convenient to integrate out the fermion fields q, which yields the action derived by Hertz (1976). In particular, the Gaussian OP or paramagnon propagator reads

$$\langle m_n^i(\boldsymbol{k})m_m^j(\boldsymbol{p})\rangle = \delta_{\boldsymbol{k},-\boldsymbol{p}}\delta_{n,-m}\delta_{ij}\frac{1}{2} \times\frac{1}{t+a\boldsymbol{k}^2+b(\Omega_n)^2+Gc|\Omega_n|/|\boldsymbol{k}|}. \quad (3.44)$$

Here we replaced the vertex $1/\varphi_{12}(\boldsymbol{k})$ in Eq. (3.39) with a schematic one that is linear in Ω and k for simplicity. We see that the coupling to the electronic Goldstone modes generates the characteristic Landau-damping term proportional to $|\Omega_n|/|\boldsymbol{k}|$ in the paramagnon propagator. The term quadratic in the frequency in Eq. (3.43) is therefore not the leading frequency dependence and can be dropped. The approximate effective action becomes

[26]This action is missing a term of order $\Omega\boldsymbol{m}^3$ that describes the Bloch spin precession of the OP in the field of all the other magnetic moments. This term is absent in the case of an Ising OP, but in all other cases it is important for producing the correct dynamics of the spin waves. In a field-theoretic context, it is sometimes referred to as a Wess-Zumino or Chern-Simons term, and its topological aspects are stressed (Fradkin, 1991). For the purposes of our discussion it is RG irrelevant, and we drop it.

$$\mathcal{A}_{\text{Hertz}} = -\sum_{\boldsymbol{k},n} \boldsymbol{m}_n(\boldsymbol{k})[t + a\boldsymbol{k}^2 + Gc|\Omega_n|/|\boldsymbol{k}|] \cdot \boldsymbol{m}_{-n}(\boldsymbol{k}) + u \int d\boldsymbol{x} T \sum_{n_1,n_2,n_3} [\boldsymbol{m}_{n_1}(\boldsymbol{x}) \cdot \boldsymbol{m}_{n_2}(\boldsymbol{x})] \times [\boldsymbol{m}_{n_3}(\boldsymbol{x}) \cdot \boldsymbol{m}_{-n_1-n_2-n_3}(\boldsymbol{x})]. \quad (3.45)$$

This action was derived and studied by Hertz (1976), and its finite-temperature properties were analyzed by Millis (1993). Many of the explicit results were derived earlier by means of a theory of spin fluctuations that one would now classify as a self-consistent one-loop theory; see Moriya (1985), Lonzarich and Taillefer (1985), and Lonzarich (1997). This development was analogous to that in the area of classical critical dynamics, where mode-coupling theories (Fixman, 1962; Kawasaki, 1967, 1970, 1976; Kadanoff and Swift, 1968) were followed by RG treatments (Hohenberg and Halperin, 1977). In what follows, we will derive these results by means of scaling arguments, which is analogous to a third angle of attack on the classical dynamical scaling problem (Ferrell *et al.*, 1967; Halperin and Hohenberg, 1967; Ferrell *et al.*, 1968).

b. Scaling analysis of the preasymptotic regime

From the action, Eq. (3.45), we see that the frequency scales as $\Omega \sim k^3$. That is, the dynamical exponent is

$$z = 3, \quad (3.46)$$

independent of the dimensionality. The theory thus is above its upper critical dimension for all $d > 4 - z = 1$. Let t be the distance[27] from criticality at $T = 0$ and define static exponents by the dependence of the observables on t in the usual way; see Appendix B. The static exponents ν, β, η, γ, and δ then all have their usual mean-field values for all $d > 1$:

$$\nu = \beta = 1/2, \qquad \eta = 0, \qquad \gamma = 1, \qquad \delta = 3. \quad (3.47)$$

The quartic coefficient u with scale dimension $[u] = -(d + z - 4) = -(d - 1)$ is a dangerous irrelevant variable (DIV) with respect to the order parameter, which is why β and δ deviate from the naive scaling results. [For a general discussion of the DIV concept, see, Ma (1976) and Fisher (1983).]

The coefficient u also plays an important role for the temperature dependence of many observables, which is not simply determined by z due to the dangerous irrelevancy of u. We now show how the relevant results can be obtained from scaling arguments. Scaling functions will be denoted by F with a subscript indicating the observable in question.

(i) Correlation length: Let $\delta(t, T)$ be the T-dependent distance from the QCP, such that $\delta(t, 0) = t$. Then the homogeneity law for δ is

$$\delta(t, T) = b^{-\gamma/\nu} F_\delta(tb^{1/\nu}, Tb^z, ub^{-(d-1)}) = b^{-2} F_\delta(tb^2, Tb^3, ub^{-(d-1)}). \quad (3.48)$$

The temperature dependence of δ results from a one-loop contribution that is proportional to u. Therefore,

$$F_\delta(0, 1, y \to 0) \propto y. \quad (3.49a)$$

This is in agreement with the perturbative result for $d = 3$ obtained by Moriya and Kawabata (1973),

$$\delta = t + \text{const} \times uT^{4/3}. \quad (3.49b)$$

u is thus dangerously irrelevant with respect to the T dependence of δ. In contrast, $F_\delta(1, 0, y \to 0) \propto \text{const}$, and also $\partial F_\delta(x, 1, y \to 0)/\partial x|_{x=0} = \text{const}$. Choosing $b = T^{-1/3}$ we can therefore Taylor expand in the first argument of F_δ. Specializing to $d = 3$ we have, for $t/T^{2/3} \ll 1$,

$$\delta(t, T) = T^{2/3} F_\delta(t/T^{2/3}, 1, uT^{2/3}) \propto T^{2/3}[uT^{2/3} + \text{const} \times t/T^{2/3} + \cdots]. \quad (3.50)$$

For T_c, defined by $\delta(t, T_c) = 0$, this gives $t \propto T_c^{2/3} \times uT_c^{2/3} \propto T_c^{4/3}$, or (Moriya and Kawabata, 1973)

$$T_c \propto (-t)^{3/4}. \quad (3.51)$$

This result is due to the dangerous irrelevancy of u; in its absence one would have $T_c \propto (-t)^{3/2}$. This result was confirmed by Millis (1993), who showed how to obtain it from an RG analysis of Hertz's action. The importance of the DIV was stressed by him and also by Sachdev (1997).

These results also determine the behavior of the correlation length $\xi \propto 1/\sqrt{|\delta|}$: At $T = 0$ we have $\xi(t \to 0, T = 0) \propto |t|^{-1/2}$, in agreement with the value of ν in Eq. (3.47), whereas at $t = 0$ we have $\xi(t = 0, T \to 0) \propto T^{-\nu_T}$, with (Millis, 1993)

$$\nu_T = 2/3. \quad (3.52)$$

For general d, $\nu_T = (d + 1)/6$.

(ii) Magnetic susceptibility: Now consider the magnetization susceptibility χ. The scaling law is

$$\chi(t, T) = b^{\gamma/\nu} F_\chi(tb^{1/\nu}, Tb^z, ub^{-(d-1)}) = b^2 F_\chi(tb^2, Tb^3, ub^{-(d-1)}). \quad (3.53)$$

Since we are dealing with a Gaussian theory $\delta(t, T) \sim 1/\chi(t, T)$, and we know from the behavior of $\delta(t, T)$ that u is dangerously irrelevant, viz.

$$F_\chi(0, 1, y \to 0) \propto 1/y. \quad (3.54)$$

At $t = 0$ in $d = 3$ we thus have $\chi(t = 0, T \to 0) \propto T^{-\gamma_T}$ with

$$\gamma_T = 4/3, \quad (3.55)$$

and more generally $\gamma_T = (d + 1)/3$. At $T = 0$, on the other hand, we have $F_\chi(1, 0, y \to 0) = \text{const}$, and hence $\chi(t \to 0, T = 0) \propto |t|^{-1}$ in agreement with the value of γ in Eq. (3.47).

[27] t in Eqs. (3.43)–(3.45) denotes the bare distance from criticality; here and in what follows we use the same symbol for its renormalized or physical counterpart.

(iii) Magnetization: The magnetization m obeys a scaling law

$$m(t,T) = b^{-(d+z-2+\eta)/2} F_m(tb^{1/\nu}, Tb^z, ub^{-(d-1)}) = b^{-(d+1)/2} F_m(tb^2, Tb^3, ub^{-(d-1)}). \quad (3.56)$$

In general, m is affected by the DIV u, just as χ is. However, at $t=0$ this is not the case: Since $m \propto \sqrt{-\delta/u}$, and $\delta(t=0) \propto u$, see Eq. (3.49b), u drops out and hyperscaling works. We thus have

$$m(t=0,T) = b^{-(d+1)/2} F_m(0, Tb^3, 0), \quad (3.57)$$

or $m(t=0,T) \propto T^{\beta_T}$ with $\beta_T = (d+1)/6$ in general, or

$$\beta_T = 2/3 \quad (3.58)$$

for $d=3$. In interpreting this exponent one needs to keep in mind that the magnetization is nonzero only for $-t > uT^{4/3}$ (putting a constant equal to unity); see Eq. (3.50). For $-t \gg uT^{4/3}$ one observes static scaling with small temperature corrections, and for $-t < uT^{4/3}$ the scaling function vanishes identically. The exponent β_T therefore cannot be observed via the T dependence of m at $r=0$. It does, however, determine the more general scaling form of m as a function of t and T; see Kirkpatrick and Belitz (2015a).

We also note that combining $m \propto \sqrt{-\delta}$ with $\delta \propto T^{4/3} - T_c^{4/3}$, which follows from Eq. (3.49b), yields (Moriya, 1985)

$$m^2 \propto T_c^{4/3} - T^{4/3}. \quad (3.59)$$

(iv) Specific heat: The free-energy density f obeys a homogeneity law

$$f(t,T) = b^{-(d+z)} F_f(tb^{1/\nu}, Tb^z). \quad (3.60)$$

For the specific-heat coefficient $\gamma = -\partial^2 f/\partial T^2$ this implies

$$\gamma(t,T) = b^{3-d} F_\gamma(tb^2, Tb^3). \quad (3.61)$$

For $d=3$ scaling thus yields $\gamma = \text{const}$. An explicit calculation of the Gaussian fluctuation contribution to the free energy (Brinkman and Engelsberg, 1968; Makoshi and Moriya, 1975; Millis, 1993; Lonzarich, 1997) yields

$$\gamma(t,T=0) \propto \ln t, \qquad \gamma(t=0,T) \propto \ln T. \quad (3.62)$$

For general $d>1$, the exponents $\bar{\alpha}$ and $\bar{\alpha}_T$ (for a definition, see Appendix B) are $\bar{\alpha} = (3-d)/2$ and $\bar{\alpha}_T = (3-d)/3$.[28]

(v) Electrical resistivity: In order to discuss relaxation rates, we start with the single-particle rate $1/\tau_{sp}$. This is dimensionally an energy, and hence has a scale dimension $[1/\tau_{sp}] = z = 3$. The relevant homogeneity law is

$$1/\tau_{sp}(t,T) = b^{-z} F_\tau(tb^{1/\nu}, Tb^z) = TF_\tau(1, T/t^{3/2}). \quad (3.63)$$

At $t=0$ we have $1/\tau_{sp}(t=0, T\to 0) \propto T$. For $t \neq 0$ we must recover the Fermi-liquid result $1/\tau_{sp} \propto T^2$, which implies $F_\tau(1, x\to 0) \propto x$, or $1/\tau_{sp} \propto T^2/t^{3/2}$.

The transport rate $1/\tau_{tr}$, which determines the electrical resistivity, is also dimensionally an energy, but its scale dimension is not equal to z. The reason is the backscattering factor in the Boltzmann equation, which provides an extra factor of $k^2 \sim b^{-2}$, with k the hydrodynamic wave number.[29] We thus have $[1/\tau_{tr}] = z+2$, and the homogeneity law for the resistivity ρ is

$$\rho(t,T) = b^{-(z+2)} F_\rho(tb^{1/\nu}, Tb^z) = T^{5/3} F_\rho(1, T/t^{3/2}). \quad (3.64)$$

At $t=0$ we recover the result of Mathon (1968): $\rho(t=0, T\to 0) \propto T^{5/3}$. For $t \neq 0$ we can again invoke the Fermi-liquid T^2 behavior to conclude $\rho \propto T^2/t^{1/2}$.

Note that ρ does not obey naive scaling. While this is true for many of the observables discussed, in this case the reason is not a DIV. Rather, the underlying relaxation rate does not have its naive scale dimension. As in the case of a DIV, this must be established by explicit calculations; it cannot be deduced from general scaling arguments. In the disordered case, this particular complication does not occur; see Sec. III.C.3.e, point (iii).

To summarize, the critical exponents at Hertz's fixed point, which determine the preasymptotic behavior in a clean system before the first-order nature of the transition becomes manifest, are given for all $d > 1$[30] by

$$\begin{aligned} z &= 3, \\ \nu &= 1/2, & \nu_T &= (d+1)/6, \\ \beta &= 1/2, & \beta_T &= (d+1)/6, \\ \delta &= 3, \\ \gamma &= 1, & \gamma_T &= (d+1)/3, \\ \eta &= 0, \\ \bar{\alpha} &= (3-d)/2, & \bar{\alpha}_T &= (3-d)/3. \end{aligned} \quad (3.65)$$

c. First- and second-order transitions, tricritical behavior, and quantum-critical points

OP fluctuations affect the second-order transition above the tricritical temperature (the line of second-order transitions about TCP in Fig. 37), where the critical behavior is in the appropriate classical universality class: Heisenberg, XY, or Ising, depending on the nature of the magnet. Along the wing-critical lines (between TCP and QCP in Fig. 37) the critical behavior is always in the classical Ising universality class, since the presence of a magnetic field effectively makes the OP one dimensional. The tricritical behavior is described by the mean-field theory with logarithmic corrections, as the upper critical dimension for a classical tricritical point is $d_c^+ = 3$ (Wegner and Riedel, 1973).

[28] These exponents describe the leading fluctuation contribution to the specific-heat coefficient. For $d>3$ the latter is subleading compared to a constant nonscaling contribution.

[29] This is true for scattering by long-wavelength magnetic excitations. In a Fermi liquid, both $1/\tau_{sp}$ and $1/\tau_{tr}$ scale as T^2.

[30] See footnote [28] for the interpretation of $\bar{\alpha}$ and $\bar{\alpha}_T$ for $d>3$.

d. Quantum-critical points at the wing tips

A magnetic field restores the QCP that is suppressed in zero field: The tricritical wings end in a pair of QCPs (see Fig. 37) in the $T = 0$ plane at a point (t_c, h_c), with t_c and h_c the critical values of the control parameter and the magnetic field, respectively. The magnetization is nonzero at this point and has a value m_c. This QCP has the remarkable property that the quantum-critical behavior can be determined exactly. The reason is that the nonzero field and magnetization give the fermionic Goldstone modes a mass, and the field conjugate to the OP therefore does not change the soft-mode structure of the system. Under these conditions, Hertz theory is expected to be valid (Belitz, Kirkpatrick, and Vojta, 2002). In the present case, an expansion in powers of $\delta m = m - m_c$ about the QCP shows that the quantity $\mathfrak{h} = 2m_c\delta t - \delta h$, with $\delta t = t - t_c$ and $\delta h = h - h_c$ plays the role of the conjugate field. Switching on an external magnetic field from $h = 0$ gives certain soft modes a mass, but changing h from $h_c \neq 0$ does not lead to further changes in the soft-mode spectrum, and neither does changing the value of t. Hertz theory thus gives the exact static quantum-critical behavior, i.e.,

$$\beta = \nu = 1/2, \qquad \gamma = 1, \qquad \eta = 0, \qquad \delta = 3. \quad (3.66)$$

The dynamical behavior can be determined as follows. The magnetization at criticality as a function of the conjugate field obeys the homogeneity law (which has the effects of the DIV u built in)

$$\delta m(\mathfrak{h}) = b^{-\beta/\nu} F_{\delta m}(\mathfrak{h} b^{\beta\delta/\nu}). \quad (3.67)$$

With mean-field values for the exponents this yields $\delta m \propto \mathfrak{h}^{1/3}$. But δt, and therefore $\mathfrak{h}$, within Hertz theory scales as $T^{(d+1)/3}$; see Eq. (3.49b) and its generalization to a general d. We thus find that, at the QCP as a function of T, the magnetization decreases as

$$\delta m(T) = m(T) - m(T = 0) \propto -\mathfrak{h}^{1/3} \propto -T^{(d+1)/9}, \quad (3.68)$$

or $T^{4/9}$ in $d = 3$. This is the result obtained by Belitz, Kirkpatrick, and Rollbühler (2005) using different arguments. This reasoning has the advantage that it also immediately yields the behavior of the magnetic susceptibility χ, which is easier to measure. It obeys

$$\chi(\mathfrak{h}) = b^{\gamma/\nu} F_\chi(\mathfrak{h} b^{\delta\beta/\nu}), \quad (3.69)$$

which yields for the T dependence of χ at the QCP

$$\chi(T) \propto T^{-2(d+1)/9}, \quad (3.70)$$

or $T^{-8/9}$ in $d = 3$. We stress again that this is the exact quantum-critical behavior.

We also mention that in the presence of weak quenched disorder, weak enough for the tricritical wings to still be present (see Fig. 37 and the related discussion), the asymptotic critical behavior is unknown. In a transient preasymptotic region the behavior is governed by Hertz's fixed point for disordered systems; for a discussion of preasymptotic behavior, see Kirkpatrick and Belitz (2015a). However, this fixed point is ultimately unstable since it violates the Harris criterion and the true critical fixed point may be of a strong-disorder type.

e. Comparison with experiment

In order to compare these theoretical predictions with experiments, we recall that the theory states that if there is a QPT to a homogeneous FM state in a clean bulk system, then the transition is first order. This qualification is important for several reasons: (1) The transition at low temperatures may be to a different state; see Secs. II.D, II.E, and III.E. (2) The presence of quenched disorder has a qualitative effect on the transition, and sufficiently strong disorder will always render the transition second order; see Secs. III.B.3 and III.C.2. (3) The fermionic soft modes that drive the transition first order exist only in 2D and 3D systems; the theory therefore does not apply to quasi-1D materials.

With these caveats taken into account, we consider the systems listed in Tables I and II. With one exception, these are all rather clean systems that show a first-order transition, as expected. The only questionable case is $YbCu_2Si_2$, which is strongly disordered; however, the nature of the magnetic order is not clear. In the rather clean system URhAl a tricritical point is suspected but so far has not been conclusively observed (Combier, 2013).

The materials in Table III comprise systems that are rather clean, with residual resistivities comparable to those in Tables I and II, yet show a second-order transition. The behavior observed in these systems is consistent with the preasymptotic critical behavior governed by Hertz's fixed point discussed in Sec. III.C.2.b. In particular, the characteristic $(-t)^{3/4}$ behavior of the Curie temperature, Eq. (3.51), was observed as early as 1975 by Sato (1975) in $(Ni_{1-x}Pd_x)_3Al$, and the behavior of the specific-heat coefficient is consistent with Eq. (3.62). For a more recent observation of the scaling of T_C, see Fig. 14. The most obvious interpretation of these observations is that these experiments indeed probe the preasymptotic region, and following T_c to lower values would reveal a tricritical point and a first-order transition at the lowest temperatures. This expectation is supported by the fact that the lowest T_c observed so far in these systems is relatively high, and by the observation that T_c at intermediate temperatures also follows the $(-t)^{3/4}$ law in systems where the transition at asymptotically low temperatures is known to be first order, for instance, in MnSi (Pfleiderer *et al.*, 1997). An experimental confirmation or otherwise of this expectation would be important. Another experimental check of the theory would be the critical behavior at the wing tips, Eqs. (3.66), (3.68), and (3.70), which has not been studied so far.

3. Disordered systems

For disordered systems, the situation is qualitatively different since the transition is continuous at the mean-field level. While the development of the effective action proceeds in exact analogy to Sec. III.C.2, the final result is a stable critical fixed point where the asymptotic critical behavior is not given

by power laws due to the existence of marginal operators (Belitz *et al.*, 2001a, 2001b).

a. Effective soft-mode action

In a disordered system, the relevant fermionic soft modes are the diffusons discussed in Sec. III.A.2. Their effective action can be written in a closed form, namely, the matrix nonlinear sigma model developed by Finkelstein (1983) for studying the Anderson-Mott metal-insulator transition problem [for reviews, see Belitz and Kirkpatrick (1994) and Finkelstein (2010)]. The quenched disorder is handled technically by means of the replica trick (Edwards and Anderson, 1975; Grinstein, 1985). If one denotes the soft modes by ${}^{i}_{r}q^{\alpha\beta}_{nm}(\boldsymbol{q}) = \Theta(-nm)\sum_{\boldsymbol{k}}{}^{i}_{r}Q^{\alpha\beta}_{nm}(\boldsymbol{k};\boldsymbol{q})$, with Q_{nm} from Eqs. (3.16) and α, β replica indices, it can be written

$$\begin{aligned}\mathcal{A}_{\mathrm{F}}[q] &= \mathcal{A}_{\mathrm{NL}\sigma\mathrm{M}}[q] \\ &= \frac{-1}{2G}\int d\mathbf{x}\,\mathrm{tr}[\nabla\hat{Q}(\mathbf{x})]^2 + 2H\int d\mathbf{x}\,\mathrm{tr}[\Omega\hat{Q}(\mathbf{x})] \\ &\quad + \mathcal{A}^{(s)}_{\mathrm{int}}[\pi N_{\mathrm{F}}\hat{Q}/2] + \mathcal{A}^{(t)}_{\mathrm{int}}[\pi N_{\mathrm{F}}\hat{Q}/2], \end{aligned} \tag{3.71a}$$

where

$$\hat{Q} = \begin{pmatrix} \sqrt{1-qq^\dagger} & q \\ q^\dagger & -\sqrt{1-q^\dagger q} \end{pmatrix} \tag{3.71b}$$

is a nonlinear function of q, and Ω is a frequency matrix with elements

$$\Omega_{12} = (\tau_0 \otimes s_0)\delta_{12}\omega_{n_1}. \tag{3.71c}$$

Here $1 \equiv (n_1, \alpha_1)$, etc., and tr denotes a trace over all discrete degrees of freedom (frequency, spin, particle-hole, and replica). The coupling constant G is proportional to the bare (i.e., Boltzmann) resistivity, and thus is a measure of the disorder strength. H is proportional to the specific-heat coefficient. The first two terms in Eq. (3.71a) describe noninteracting electrons. They are the fermionic version (Efetov, Larkin, and Khmelnitskii, 1980) of Wegner's nonlinear sigma model for the Anderson localization problem (Wegner, 1979). Note the diffusive structure of these two terms once they are expanded to $O(q^2)$, with the gradient-squared scaling as a frequency. The last two terms reflect the electron-electron interactions in the spin-singlet and spin-triplet channels, respectively. They are quadratic in $\hat{Q}$ with coupling constants K_s and K_t, respectively, and are effectively linear in the frequency (Finkelstein, 1983). They therefore do not spoil the soft-mode structure of the nonlinear sigma model but just renormalize the prefactor of the frequency in the diffusion pole.

The magnetization again couples linearly to the electron spin density, the soft part of which is linear in $\hat{Q}$. The coupling term reads

$$\begin{aligned}\mathcal{A}_{\mathrm{c}} &= \sqrt{\pi T c}\int d\mathbf{x}\sum_{\alpha}\sum_{n}\sum_{i=1}^{3} m^{i,\alpha}_{n}(\mathbf{x})\sum_{r=0,3}(\sqrt{-1})^r \\ &\quad\times\sum_{m}\mathrm{tr}[(\tau_r\otimes s_i)\hat{Q}^{\alpha\alpha}_{m,m+n}(\mathbf{x})], \end{aligned} \tag{3.72}$$

with c a coupling constant. m^i ($i = 1, 2, 3$) denotes again the three components of the order-parameter field $\boldsymbol{m}$, which now also carries a replica index α. It determines the physical magnetization m via

$$m = \mu_{\mathrm{B}}\sqrt{\pi N_{\mathrm{F}}^2 T/K_t}\langle m^{i,\alpha}_{n=0}(\boldsymbol{x})\rangle. \tag{3.73}$$

The order-parameter action is similar to the one in the clean case, Eq. (3.43), but there is an additional quartic term that arises from the quenched disorder,

$$\begin{aligned}\mathcal{A}_{\mathrm{OP}} &= -\sum_{\mathbf{k},n}\sum_{\alpha}\boldsymbol{m}^{\alpha}_{n}(\mathbf{k})[t + a\mathbf{k}^2 + b(\Omega_n)^2]\cdot\boldsymbol{m}^{\alpha}_{-n}(-\mathbf{k}) \\ &\quad + u\int d\mathbf{x}T\sum_{n_1,n_2,n_3}\sum_{\alpha}[\mathbf{m}^{\alpha}_{n_1}(\mathbf{x})\cdot\mathbf{m}^{\alpha}_{n_2}(\mathbf{x})] \\ &\quad\times[\mathbf{m}^{\alpha}_{n_3}(\mathbf{x})\cdot\mathbf{m}^{\alpha}_{-n_1-n_2-n_3}(\mathbf{x})] \\ &\quad + v\int d\mathbf{x}\sum_{n_1,n_2}\sum_{\alpha,\beta}|\mathbf{m}^{\alpha}_{n_1}(\mathbf{x})|^2|\mathbf{m}^{\beta}_{n_2}(\mathbf{x})|^2. \end{aligned} \tag{3.74}$$

The last term, with coupling constant v, is a random-mass or random-temperature term that arises from the disorder dependence of the bare distance from criticality whose disorder average is given by t. There also is a term cubic in m, which carries at least one gradient or frequency and is less relevant for the critical behavior than the terms shown.

The soft-mode action given by Eqs. (3.71)–(3.74) was motivated and derived by Belitz *et al.* (2001a) from an underlying microscopic fermionic action.[31] However, such a derivation is not necessary. All parts of the effective action can be obtained from more general considerations, namely, (1) the existence of an effective soft-mode theory for disordered interacting electrons, (2) symmetry considerations for a quantum ϕ^4 theory with a vector OP, and (3) the Zeeman coupling between the OP and the electron spin density. In particular, the OP part of the action can be either written down based on symmetry considerations or derived by means of a Hubbard-Stratonovich decoupling of the particle-hole spin-triplet interaction term in the underlying fermionic action. In the latter case, a spin-triplet interaction will be generated again by renormalization in the fermionic sector as long as a spin-singlet interaction is present. The presence of the last term in Eq. (3.71a) therefore does not constitute any double counting.

b. Hertz's action

As in the clean case, if we keep only the term of $O(Mq)$ in Eq. (3.72) and integrate out the fermions, we recover Hertz's action (Hertz, 1976) (plus the random-mass term, which was not considered by Hertz). The Landau-damping term now has the form $|\Omega|/\boldsymbol{k}^2$ due to the diffusive nature of the fermionic soft modes. The paramagnon propagator thus reads

[31]The term $b(\Omega_n)^2$ in Eq. (3.74) was erroneously written as $b|\Omega_n|$ in Belitz *et al.* (2001a). This is of no consequence, as the term in question is RG irrelevant in either case.

$$\langle {}^{i}M_n^{\alpha}(\boldsymbol{k})\,{}^{j}M_m^{\beta}(\boldsymbol{p})\rangle = \delta_{\boldsymbol{k},-\boldsymbol{p}}\delta_{n,-m}\delta_{ij}\delta_{\alpha\beta}\frac{1}{2} \times \frac{1}{t + a\boldsymbol{k}^2 + b(\Omega_n)^2 + Gc|\Omega_n|/(\boldsymbol{k}^2 + GH|\Omega_n|)}. \tag{3.75}$$

Dropping the random-mass terms, the action becomes

$$\begin{aligned}\mathcal{A}_{\text{Hertz}} = &-\sum_{\mathbf{k},n}\sum_{\alpha}\boldsymbol{m}_n^{\alpha}(\mathbf{k})[t + a\mathbf{k}^2 + Gc|\Omega_n|/\boldsymbol{k}^2] \\ &\times \boldsymbol{m}_{-n}^{\alpha}(-\mathbf{k}) \\ &+ u_4\int d\mathbf{x}T\sum_{n_1,n_2,n_3}\sum_{\alpha}[\mathbf{m}_{n_1}^{\alpha}(\mathbf{x})\cdot\mathbf{m}_{n_2}^{\alpha}(\mathbf{x})] \\ &\times [\mathbf{m}_{n_3}^{\alpha}(\boldsymbol{x})\cdot\boldsymbol{m}_{-n_1-n_2-n_3}^{\alpha}(\boldsymbol{x})].\end{aligned} \tag{3.76}$$

Power counting again suggests a continuous phase transition with mean-field static critical exponents, only now the upper critical dimension is $d_c^+ = 0$, and the dynamical critical exponent is $z = 4$. This fixed point is ultimately unstable, since the same physics that leads to the Landau-damping term also leads to the terms of higher order in q in Eq. (3.72). Nevertheless, as in the clean case (see Sec. III.C.2) it is important to study this fixed point since it is experimentally relevant in a preasymptotic crossover region (Kirkpatrick and Belitz, 2014). In the disordered case this is true *a fortiori* since the effects that destabilize Hertz's fixed point still result in a continuous transition, albeit with different exponents.

The homogeneity relations and exponents for Hertz's action are obtained by a straightforward modification of the development in Sec. III.C.2.b. The dynamical critical exponent is now

$$z = 4, \tag{3.77a}$$

which yields an upper critical dimensionality $d_c^+ = 0$, and the DIV u has a scale dimension $[u] = -d$. For all $d > 0$ the exponents are [cf. Eqs. (3.65) for the clean case]

$$\begin{aligned}&\nu = 1/2, && \nu_T = (d+2)/8, \\ &\beta = 1/2, && \beta_T = (d+2)/8, \\ &\delta = 3, \\ &\gamma = 1, && \gamma_T = (d+2)/4, \\ &\eta = 0, \\ &\bar{\alpha} = (4-d)/2, && \bar{\alpha}_T = (4-d)/4.\end{aligned} \tag{3.77b}$$

For $d > 4$, $\bar{\alpha}$ and $\bar{\alpha}_T$ describe the leading fluctuation contribution to the specific-heat coefficient; see footnote [28] for the analogous statement in the clean case.

As mentioned, these exponents do not describe the physical asymptotic critical behavior. Another indication of this is the value of the correlation-length exponent $\nu = 1/2$, which violates the requirement $\nu \geq 2/d$, Eq. (3.36), for all $d < 4$. For finding the true asymptotic critical behavior it is preferable to not integrate out the fermions, but rather deal with the coupled soft-mode field theory for analyzing the fixed-point structure.

c. Fixed-point action

The lowest-order term that was neglected in Eq. (3.76) is the term of $O(mq^2)$ in Eq. (3.72). It is easy to see that this generates a renormalization of the 2-point m vertex that is proportional to $|\boldsymbol{k}|^{d-2}$. For dimensions $d < 4$, the gradient-squared term in Eq. (3.74) is therefore not the leading wave-number dependence, and it is convenient to add the generated term to the bare action. In a schematic form that suppresses everything not necessary for power counting, the effective action then reads (Belitz *et al.*, 2001a)

$$\begin{aligned}\mathcal{A}_{\text{eff}}[m,q] = &-\int d\boldsymbol{x}m[t + a_{d-2}\partial_{\boldsymbol{x}}^{d-2} + a_2\partial_{\boldsymbol{x}}^2]m + O(\partial_{\boldsymbol{x}}^4 m^2, m^4) \\ &-\frac{1}{G}\int d\boldsymbol{x}(\partial_{\boldsymbol{x}}q)^2 + H\int d\boldsymbol{x}\Omega q^2 + (K_s + K_t)T\int d\boldsymbol{x}q^2 \\ &-\frac{1}{G_4}\int d\boldsymbol{x}\partial_{\boldsymbol{x}}^2 q^4 + H_4\int d\boldsymbol{x}\Omega q^4 + O(Tq^3, \partial_{\boldsymbol{x}}^2 q^6, \Omega q^6) \\ &+\sqrt{T}c_1\int d\boldsymbol{x}mq + \sqrt{T}c_2\int d\boldsymbol{x}mq^2 + O(\sqrt{T}mq^4).\end{aligned} \tag{3.78}$$

Here the fields are understood to be functions of position and frequency, and only quantities that carry a scale dimension are shown. The bare values of G_4 and H_4 are proportional to those of G and H. K_s and K_t are the coupling constants of the terms of $O(q^2)$ in the interacting parts of $\mathcal{A}_{\text{NL}\sigma\text{M}}$. A term of order Tq^3 that arises from the same part of the action is not important for the problem of magnetic criticality. It therefore is not shown although its coupling constant squared has the same scale dimension as $1/G_4$ and H_4. c_1 and c_2 are the coupling constants of the terms that result from expanding $\mathcal{A}_c$ in powers of q. Their bare values are proportional to c.

d. Fixed points, and their stability

The action shown schematically in Eq. (3.78) can be analyzed for critical fixed points by means of standard RG techniques (Ma, 1976). We assign a scale dimension $[L] = -1$ to a length L, and $[\tau] = -z$ to the imaginary time τ (with z to be determined). Under renormalization with a length rescaling factor b, all scaling quantities A transform according to $A \to Ab^{[A]}$. In particular, temperature T and frequency Ω have scale dimensions $[T] = [\Omega] = z$.

It is illustrative to again look for a fixed point that describes the mean-field critical behavior of Hertz theory. To this end, let us look for a fixed point where the coupling constants a_2 and c_1 are marginal. This results in standard mean-field static critical behavior, and a dynamical exponent $z = 4$, all of which is consistent with the action given in Eq. (3.76) and with the paramagnon propagator, Eq. (3.75). The requirement that the action be dimensionless leads to $[m] = (d-2)/2$, which makes t relevant with $[t] = 2$. The critical exponents η and ν are thus $\eta = 0$, and $\nu = 1/2$. This fixed point is unstable for $d < 4$, since $[a_{d-2}] = 4 - d$, and a_{d-2} is thus relevant for all $d < 4$. This is obvious if one adds the term with coupling constant a_{d-2} to the bare action, as we have done above, but less so if one chooses the bare value of a_{d-2} to be zero and

have the physics related to a_{d-2} be generated by the term with coupling constant c_2. In that case, a careful analysis of the time scales involved leads to the same conclusion (Belitz *et al.*, 2001a). All of this is consistent with the fact that the mean-field value $\nu = 1/2$ violates the Harris criterion discussed in Sec. III.B.3, see Eq. (3.27), and therefore cannot represent the correct critical behavior in a disordered system.

The previous discussion suggests that one should look for a fixed point where only c_1 is required to be marginal, which implies $[m] = 1 + (d - z)/2$. The diffusons will be unaffected by the magnetic transition, and hence the scale dimension of the soft fermion field q is $[q] = (d - 2)/2$. This also implies that there is a diffusive time scale characterized by a dynamical exponent

$$z_{\text{diff}} = 2 \tag{3.79}$$

in addition to the critical dynamical time scale whose exponent we denote by z_c. This presence of more than one time scale complicates the power-counting arguments, as the scale dimensions of various coupling constants can depend on the context they appear in. That is, the scale dimension z of the various factors of temperature or frequency in the effective action can be equal to z_{diff} or z_c, depending on the context. In particular, a_{d-2} can be irrelevant if the paramagnon propagator appears as an internal propagator in the loop expansion, while it will be marginal in the critical paramagnon propagator, which implies $[m] = 1$. This leads to $z_c = d$ and $\eta = 4 - d$. This makes a_2 irrelevant, while t is relevant with $[t] = d - 2$. The three independent critical exponents thus are

$$\nu = \frac{1}{d-2}, \qquad \eta = 4 - d, \qquad z_c = d. \tag{3.80a}$$

For this fixed point, ν satisfies the Harris criterion. The remaining static exponents are given by d-dependent generalizations of Eq. (3.25) (Belitz *et al.*, 2001b):

$$\beta = \frac{2}{d-2}, \qquad \gamma = 1, \qquad \delta = d/2. \tag{3.80b}$$

Equation (3.80b) is valid for $2 < d < 6$. For $d \geq 6$, β and δ lock into their mean-field values; for ν and η this happens for $d \geq 4$. The T dependence of the observables at criticality $t = 0$ is determined by (Belitz *et al.*, 2001b)

$$\beta_T = \beta/2\nu, \qquad \gamma_T = \gamma/2\nu. \tag{3.80c}$$

To discuss the stability of this fixed point we now consider the remaining coupling constants in the effective action, Eq. (3.78). c_2 has a scale dimension $[c_2] = 1 - z/2$, and thus is irrelevant if $z = z_c$, but marginal if $z = z_{\text{diff}}$. Moreover, due to the existence of two different time scales even some operators that are irrelevant by power counting may effectively act as marginal operators (Belitz *et al.*, 2001b). The reason is that naive power counting is based on a length scale argument, which can be modified if the scale factor b represents a frequency rather than a length. Since the difference between the two dynamical exponents z_{diff} and z_c is equal to $d - 2$, this implies that coupling constants with a naive scale dimension given by $-(d - 2)$ can act as marginal operators under certain conditions. As a consequence all terms that are shown explicitly in Eq. (3.78) are important for determining the leading critical behavior and constitute the fixed-point action.

e. Asymptotic critical behavior

The conclusion so far is that the fixed-point action represented by Eq. (3.78) contains marginal operators that result, order by order in a loop expansion, in logarithmic corrections to the fixed point with critical exponents given by Eqs. (3.80). The remaining question is what is the result if the loop expansion is summed to all orders?

(i) Integral equations for the diffusion coefficients: This question can be answered exactly without resorting to a small parameter (such as an expansion in $\epsilon = d - 4$) (Kirkpatrick and Belitz, 1996; Belitz *et al.*, 2001a, 2001b). This hinges on various properties of the loop expansion: First, at the fixed point of interest the fermionic dynamics remain diffusive. The coupling constants K_s and K_t do not change this and therefore can be ignored. Second, G and c_2 are not singularly renormalized. Third, the renormalized versions of G_4 and H_4 are proportional to those of G and H, as are their bare values. Finally, c_1 is held fixed by definition of the fixed point. This leaves the renormalizations of H and the two-point order-parameter vertex $u_2 = t + a_{d-2}|\boldsymbol{k}|^{d-2} + a_2\boldsymbol{k}^2$ to be determined. The resummation of the loop expansion to all orders can be expressed in terms of two coupled integral equations for H and u_2 or, equivalently, for the thermal diffusion coefficient $D(\Omega) = 1/GH(\Omega)$ and the spin diffusion coefficient $D_s(\boldsymbol{k}, \Omega) = 16\pi u_2(\boldsymbol{k}, \Omega)/Gc_1^2$, both of which acquire a frequency dependence under renormalization. D and D_s simultaneously go to zero at a critical value of G, and in the vicinity of that critical point the integral equations can be solved analytically. It turns out that the logarithmic corrections obtained in perturbation theory do not change the power laws given in Eqs. (3.80), but rather result in log-normal corrections to power-law scaling. For instance, the magnetization $m(t, T = 0)$ $d = 3$ has an asymptotic behavior (Belitz *et al.*, 2001b)

$$m(t \to 0) \propto |tg[\ln(1/|t|)]|^{\beta}, \tag{3.81a}$$

with $\beta = 2$ from Eqs. (3.80) and

$$g(x \to \infty) \propto e^{(\ln x)^2/2\ln(3/2)}. \tag{3.81b}$$

Similarly, at $t = 0$ as a function of a magnetic field h,

$$m(t = 0, h \to 0) \propto [hg(\tfrac{1}{3}\ln(1/h))]^{1/\delta}, \tag{3.81c}$$

with $\delta = 3/2$ from Eqs. (3.80). The specific heat also has a log-normal critical behavior. However, the critical exponent γ comes without logarithmic corrections; the magnetic susceptibility diverges as

$$\chi(t \to 0) \propto 1/|t|. \tag{3.81d}$$

(ii) Scaling considerations: Thermodynamic quantities. All of these results are conveniently summarized in the following

generalized homogeneity law for the free-energy density (Belitz *et al.*, 2001b):

$$f(t,T,h) = b^{-(d+z_c)} f_1(tb^{1/\nu}, Tb^{z_c}, hb^{z_c}) + b^{-(d+z_g)} f_2(tb^{1/\nu}, Tb^{z_g}, hb^{z_c}). \quad (3.82)$$

Here z_c is the critical dynamical exponent, which determines the temperature dependence of the specific heat, and z_g is the dynamical exponent due to the generic soft modes, which determines the temperature dependence of the order parameter and its susceptibility. If $z_c \geq z_g$ (this has to be the case, see Sec. III.C.4), we obtain homogeneity laws for the order parameter $\partial f/\partial h$, the order-parameter susceptibility $\chi = \partial^2 f/\partial h^2$, and the specific-heat coefficient $\gamma_C = -\partial^2 f/\partial T^2$,

$$m(t,T,h) = b^{-(d+z_g-z_c)} F_m(tb^{1/\nu}, Tb^{z_g}, hb^{z_c}), \quad (3.83a)$$

$$\chi(t,T;k) = b^{-(d+z_g-2z_c)} F_\chi(tb^{1/\nu}, Tb^{z_g}; kb), \quad (3.83b)$$

$$\gamma_C(t,T) = b^{-(d-z_c)} F_\gamma(tb^{1/\nu}, Tb^{z_c}). \quad (3.83c)$$

In Eq. (3.83b) we have added the wave-number dependence of χ. Also of interest is the scaling of the critical temperature T_c with t. T_c is the temperature where the order parameter vanishes, or the susceptibility diverges, and from Eq. (3.83a) or (3.83b) we obtain

$$T_c \propto (-t)^{\nu z_g}. \quad (3.83d)$$

All critical exponents can now be expressed in terms of z_c, z_g, and ν. We have

$$\bar{\alpha} = \nu(z_c - d), \qquad \bar{\alpha}_T = (z_c - d)/z_c, \quad (3.84a)$$

$$\beta = \nu(d + z_g - z_c), \qquad \beta_T = (d + z_g - z_c)/z_g, \quad (3.84b)$$

$$\gamma = \nu(2z_c - d - z_g), \qquad \gamma_T = (2z_c - d - z_g)/z_g, \quad (3.84c)$$

$$\delta = z_c/(d + z_g - z_c). \quad (3.84d)$$

$$\eta = d + 2 + z_g - 2z_c. \quad (3.84e)$$

Finally, ν_T follows from the requirement that $\chi(t=0, T \to 0; k)$ must be proportional to $T^{-\gamma_T}$ times a function of $k\xi$, which yields

$$\nu_T = 1/z_g. \quad (3.84f)$$

The log-normal terms multiplying the power laws can be expressed in terms of a scale dependence of the independent exponents z_c, z_g, and ν. It is convenient to write, for $2 < d < 4$,

$$z_c = d + \lambda, \qquad z_g = 2 + \lambda, \qquad 1/\nu = d - 2 + \lambda, \quad (3.85)$$

where λ is defined as

$$\lambda = \ln g(\ln b)/\ln b, \quad (3.86)$$

with $g(\ln b)$ from Eq. (3.81b).

This critical behavior is expected to be exact provided a continuous transition into a homogeneous FM phase occurs. However, rare-region effects may mask this critical behavior. Theories that deal with such effects are discussed in Secs. III.D and III.E.

(iii) Scaling considerations: Electrical resistivity. We finally mention the electrical resistivity ρ. The transport relaxation rate is dominated by the disorder, which is unaffected by the magnetic ordering. The scale dimension of ρ at a ferromagnetic QCP is therefore zero. However, ρ depends on the critical dynamics, since the paramagnon propagator enters the calculation of ρ in perturbation theory. From Eq. (3.78) we see that one-loop corrections to ρ can be constructed, for instance, from one vertex with coupling constant $1/G_4$, or from two vertices with coupling constant c_2. These terms belong to the class of least irrelevant variables with respect to the critical fixed point; their scale dimension is $-(d-2)$. Denoting the least irrelevant variables collectively by u, we have the following homogeneity law for the resistivity:

$$\rho(t,T) = F_\rho(tb^{1/\nu}, Tb^{z_c}, ub^{-(d-2)}) = \text{const} + b^{-(d-2)} \tilde{F}_\rho(tb^{1/\nu}, Tb^{z_c}), \quad (3.87)$$

where we used the fact that the leading correction to ρ is linear in u. At criticality, this yields

$$\rho(t=0,T) \propto T^{(d-2)/z_c} \quad (3.88)$$

For the t dependence at $T=0$ there are additional logarithmic complications due to a resonance between the scale dimensions of u and t; see Belitz *et al.* (2001b).

Alternatively, one can argue that ρ consists of a background contribution that does not scale, and a singular contribution $\delta\rho$ that does. Since ρ is dimensionally a length to the power $d-2$, one expects

$$\delta\rho(t,T) = b^{-(d-2)} F_{\delta\rho}(tb^{1/\nu}, Tb^{z_c}), \quad (3.89)$$

which again yields Eq. (3.88). Note that this argument builds in the DIV u, so naive scaling works.

f. Preasymptotic behavior

The logarithmic nature of the asymptotic critical behavior described previously suggests that it is valid only in an exponentially small region around the critical point. Indeed, a numerical solution of the integral equations mentioned in Sec. III.C.3.e shows that the behavior in an observable region around criticality is given by effective power laws that correspond to the quantity λ defined in Sec. III.C.3.e being $\lambda \approx 2/3$ in a large range of scales (Kirkpatrick and Belitz, 2014). For instance, the specific-heat coefficient follows effective power laws with exponents (see footnote [5])

$$\bar{\alpha}^{\text{eff}} \approx 0.4, \qquad \bar{\alpha}_T^{\text{eff}} \approx 0.18 \quad (3.90a)$$

over almost three decades. Similarly, the critical temperature dependence of the spin susceptibility and the magnetization is given by effective exponents

$$\gamma_T^{\text{eff}} \approx 0.625, \qquad \beta_T^{\text{eff}} \approx 0.75, \tag{3.90b}$$

and the corresponding effective static exponents are

$$\gamma = 1, \qquad \beta^{\text{eff}} \approx 1.2, \qquad \delta^{\text{eff}} \approx 1.83. \tag{3.90c}$$

For the exponent that determines the shape of the phase diagram in the T-t plane, Eq. (3.83d), we have

$$(\nu z_g)^{\text{eff}} \approx 1.6. \tag{3.90d}$$

Only the value of γ is the same in the preasymptotic and asymptotic regions, respectively. This is important for the interpretation of experiments.

g. Summary of critical exponents in the disordered case

In summary, the critical exponents for the disordered case in $2 < d < 4$ dimensions in both the asymptotic and preasymptotic regions are given by Eqs. (3.84) and (3.85). In the asymptotic regime they do not represent pure power-law behavior since λ is the scale-dependent object given in Eq. (3.86). In the preasymptotic regime $\lambda \approx 2/3$, and the exponents represent effective power laws.

h. Relation to experiment

The interpretation of experiments on strongly disordered systems is difficult for various reasons. First, the control parameter tends to be the chemical composition, which necessitates the preparation of a separate sample for each data point. This makes the precise determination of the critical point difficult, and neither the precision nor the absolute values of the distance from criticality are anywhere near the values that in classical systems are known to be necessary for a reliable determination of critical exponents. Second, the Griffiths-region effects discussed in Sec. III.D are expected to be pronounced in strongly disordered systems and coexist with critical phenomena.

A well-studied strongly disordered system is $URu_{2-x}Re_xSi_2$; see Sec. II.C.2. Bauer *et al.* (2005) found a QCP at $x \approx 0.3$; scaling plots yielded exponent values $\delta = 1.56$ and $\beta_T = 0.9$. γ_T was inferred from the Widom relation [which holds in this context, see Kirkpatrick and Belitz (2015a)], $\gamma_T = \beta_T(\delta - 1) = 0.5$. The specific-heat coefficient showed a $\ln T$ behavior over a wide range of x values. A later analysis (Butch and Maple, 2009) put the critical concentration at $x \approx 0.15$ and found continuously varying exponents in the range $0.6 \geq x \geq 0.2$, with $\delta \to 1$, $\gamma_T \to 0$, and $\beta_T \approx 0.8$ roughly constant. If the data represent critical phenomena, then continuously varying exponents are hard to understand. Also, an exponent $\gamma_T = 0$, which must signal a divergence of the OP susceptibility that is only logarithmic, would be very unusual.

In $Ni_{1-x}V_x$ (Sec. II.E.1.c), Ubaid-Kassis and Schroeder (2008) found a critical point at $x_c \approx 0.11$ with $\gamma_T = 0.37 \pm 0.07$, $\beta_T \approx 0.5$, and $\delta = 1.8 \pm 0.2$. The value of δ agrees very well with Eqs. (3.90); the agreement for γ_T and β_T is less satisfactory. These data were reinterpreted by Ubaid-Kassis, Vojta, and Schroeder (2010) in terms of a Griffiths phase for $x < x_c$.

Finally, the exponent that governs the scaling of T_c with the control parameter is equal to 2 asymptotically, and about 1.6 in the preasymptotic region; see Eqs. (3.83d) and (3.90d). This is in contrast to the result from Hertz theory in the clean case, where the corresponding value is 3/4; see Eq. (3.51). An exponent much greater than 1 is qualitatively consistent with the tail in the phase diagram observed in many disordered systems (see Figs. 33 and 35), and also with the schematic phase diagram shown in Fig. 38. As discussed in Sec. II.E, these tails are often interpreted as signalizing quantum Griffiths effects. These two interpretations are not mutually contradictory; more detailed experimental investigations are needed to distinguish between them.

4. Exponent relations

At a classical critical point, only two static critical exponents are independent. This implies that there must exist relations between various exponents.[32] These relations have a complicated history, and some of them were initially found empirically (Stanley, 1971). Several of them take the form of a rigorous inequality that turns into an equality if certain conditions are fulfilled. Well-known examples are Widom's equality $\gamma = \beta(\delta - 1)$ (Widom, 1964) and Fisher's equality $\gamma = (2 - \eta)\nu$ (Fisher, 1964). Relations between the exponents at a QCP defined in Appendix B have been derived and discussed by Kirkpatrick and Belitz (2015a).

D. Rare-region effects in disordered systems

1. Quantum Griffiths effects

The notion of a Griffiths phase is well established in both classical and quantum disordered systems (Griffiths, 1969; McCoy, 1969; Randeria, Sethna, and Palmer, 1985; Bray, 1987; Millis, Morr, and Schmalian, 2002; Vojta, 2010). The basic idea can be illustrated by considering a classical randomly diluted Ising FM in d dimensions.[33] In this model some of the FM bonds are missing with a probability p. As a result, the critical temperature T_c in the random system is lower than the corresponding critical temperature in the pure or nonrandom system. In random systems, the latter is often denoted by T_G and referred to as the Griffiths temperature. In general, interesting effects occur both in the "paramagnetic" phase $T > T_G$ and in the "Griffiths phase" $T_c < T < T_G$. Here we focus on the latter.

[32]These exponent relations are also often referred to as "scaling relations" or "scaling laws," the latter not to be confused with the homogeneity laws that are often referred to by the same term.

[33]The relevant concepts were put forth simultaneously by Griffiths (1969) and McCoy (1969). McCoy considered a strip-random two-dimensional classical model (McCoy and Wu, 1968) that is closely related to the quantum-mechanical problem of a random transverse-field Ising spin chain (Fisher, 1995). This observation and phenomena deriving from it are often referred to as (quantum) Griffiths-phase effects.

Griffiths argued that in such a system there always exist regions of linear size L that happen to contain no missing bonds, and thus behave as a region of the same size in the corresponding pure system. This is true even for arbitrarily large L, but the probability of finding a large region devoid of missing bonds is exponentially small,

$$P(L) \propto \exp(-cL^d). \tag{3.91}$$

Here d is the spatial dimensionality of the system, and c is a constant. If the size of these rare regions is large compared to the local correlation length, then it is meaningful to speak of them as being magnetically ordered. At criticality in a mean-field theory, the correlation length ξ as a function of an applied magnetic field h scales as $\xi \sim 1/h^{1/3}$. This in turn suggests that in the entire Griffiths phase there is a contribution δF_G to the free energy that reflects both the exponentially small probability of rare regions and the scaling of the correlation length with the magnetic field (Dotsenko, 2006):

$$\delta F_G \propto \exp[-c' h^{-d/3}], \tag{3.92}$$

with c' another constant. That is, in the entire Griffiths phase the free energy is a nonanalytic function of the field h at $h = 0$. However, the singularity is only a very weak essential one.

The weak singularities in the thermodynamic properties in the classical Griffiths phase are difficult to detect experimentally. However, the existence of ordered rare regions has a qualitative effect on the dynamics of the equilibrium time-correlation functions. This is physically obvious since overturning large clusters of ordered spins takes a time that grows exponentially with the size of the cluster, and time-correlation functions in the Griffiths phase will depend on such dynamical processes. We have given the qualitative argument in Sec. III.A.1. The result, Eq. (3.7b), was that time-correlation functions are expected to decay slower than any exponential.

The conclusion is that the static effects in the classical Griffiths phase are very weak, but dynamic Griffiths effects are quite profound, changing exponential decay of time-correlation functions into nonexponential decay. As stressed in Sec. I, in quantum statistical mechanics the statics and the dynamics are coupled. This implies that Griffith-phase effects are expected to be important for both the statics and the dynamics near QPTs in disordered systems in general, and in disordered quantum FMs, in particular. In fact, it turns out that in the quantum case the dynamical singularities are even stronger than suggested by the classical arguments.

In the context of quantum mechanics, this goes back to the model proposed and studied by McCoy and Wu (1968) (McCoy, 1969; McCoy and Wu, 1969), which is closely related to a 1D quantum problem. This model was later generalized (McCoy, 1970; Shankar and Murthy, 1987), and its quantum-mechanical interpretation was studied in detail by Fisher (1992, 1995) and others (Rieger and Young, 1996; Young, 1997; Pich *et al.*, 1998). The crucial point is that the slow dynamics associated with the Griffiths phase greatly affects the zero-temperature behavior. To see this, consider a local magnetized rare region of linear size L, separated by a domain wall from the rest of the system as in the classical case.[34] Its imaginary-time local dynamic susceptibility will decay exponentially by a quantum tunneling process. For long imaginary times we have

$$\chi_{\rm loc}(\tau \to \infty) \propto \exp[-\tau/\bar{\tau}(L)], \tag{3.93}$$

where $\bar{\tau}(L)$ is the characteristic relaxation time for the tunneling process. To estimate $\bar{\tau}(L)$ we imagine a domain wall in imaginary-time space for a cluster of size L^d in real space. This was considered for Ising systems (Thill and Huse, 1995;Guo, Bhatt, and Huse, 1996; Rieger and Young, 1996; Pich *et al.*, 1998; Motrunich *et al.*, 2000; Millis, Morr, and Schmalian, 2002) and for Heisenberg magnets (Vojta and Schmalian, 2005); for a review, see Vojta (2010).[35] Most of the work on this topic was done for AFMs, i.e., the case of a nonconserved OP. One finds

$$\bar{\tau}(L) \sim \tau_0 \exp(\bar{\sigma} L^d). \tag{3.94}$$

Here τ_0 is a microscopic time scale, $\bar{\sigma}$ is a constant, and the overbars distinguish $\bar{\tau}$ and $\bar{\sigma}$ from the corresponding quantities in the classical case, Eq. (3.6). Effectively, in the quantum case the volume of the region is L^{d+z}, with z the dynamical exponent, and the domain wall is a hypersurface with area $L^{d+z-z} = L^d$. Physically, the decay of the rare region in the quantum case is much slower than its classical counterpart, Eq. (3.6), since at $T > 0$ the cluster can flip via thermal activation in addition to quantum tunneling. Equations (3.91), (3.93), and (3.94) imply for the average local dynamic susceptibility

$$\chi^{\rm av}_{\rm loc}(\tau) = \int_0^\infty dL \exp[-cL^d - (\tau/\tau_0) e^{-\bar{\sigma} L^d}]. \tag{3.95a}$$

In this case the typical length scale is $L_{\rm typ} \propto [\ln(\tau/\tau_0)]^{1/d}$, and in the limit of large imaginary time the method of steepest descent yields

$$\chi^{\rm av}_{\rm loc}(\tau \to \infty) \propto (\tau/\tau_0)^{-c/\bar{\sigma}}. \tag{3.95b}$$

We see that quantum mechanics leads to a power-law decay. This is in contrast to the classical case; see Sec. III.A.1. The T dependence of the static susceptibility is

[34] Griffiths effects also exist in the ordered phase. However, they are weaker than the corresponding effects in the disordered phase except in certain special models (Senthil and Sachdev, 1996; Motrunich *et al.*, 2000). Here we focus on the disordered phase.

[35] Strictly speaking the considerations presented here are valid only for non-Ising metallic magnets, i.e., systems with an order-parameter dimensionality $n > 1$. The reason is that the $|\Omega_n|$ term in the Gaussian order-parameter action corresponds, at $T = 0$, to a long-ranged $1/\tau^2$ decay in imaginary-time space. Because a one-dimensional Ising model ($n = 1$) can have a phase transition with such an interaction, this implies that there might be a freezing phase transition in imaginary-time space that is not included in the simple Griffiths arguments given here. One-dimensional models with $n > 1$ do not have such a phase transition because they are below their lower critical dimension even with this long-ranged interaction.

$$\chi^{\rm av}_{\rm loc}(T\to 0)=\int_0^{1/T} d\tau \chi^{\rm av}_{\rm loc}(\tau)\sim T^{c/\bar{\sigma}-1}. \tag{3.96}$$

The conclusion is that Griffiths-phase dynamical singularities lead to low-T singularities in static quantities. Similarly, the contribution to the specific heat is $C^{\rm av}_{\rm loc}(T)\sim T^{c/\bar{\sigma}}$. If $c/\bar{\sigma}<1$, then these local rare-region contributions dominate the usual Fermi-liquid ones.

The conserved disordered FM case is even more dramatic. Physically this is because a conservation law is equivalent to a long-ranged interaction (Hoyos and Vojta, 2007), and hence slows down relaxation even more. Nozadze and Vojta (2012) argued that in this case the relaxation time in $d=3$ scales as

$$\bar{\tau}(L)\propto \exp[\bar{\sigma}L^{3+n}], \tag{3.97}$$

where $n=1$ if the itinerant electrons are ballistic, and $n=2$ if they are diffusive. Technically, the extra factor of L^n compared to the AFM (nonconserved) case is a result of the $1/|\boldsymbol{k}|^n$ in the paramagnon propagator, Eq. (3.5a). Following the same steps as before, one can determine the physical observables. The local susceptibility behaves as

$$\chi^{\rm av}_{\rm loc}(T\to 0)\propto \frac{1}{T}\exp[-A\{\ln(T_0/T)\}^{3/(3+n)}]. \tag{3.98}$$

Here A is a constant and T_0 is a microscopic temperature scale. The specific heat is proportional to

$$C^{\rm av}_{\rm loc}(T\to 0)\propto \exp[-A\{\ln(T_0/T)\}^{3/(3+n)}]. \tag{3.99}$$

Finally, the magnetization m at zero temperature as a function of an applied field H is

$$m(H\to 0)\propto \exp[-A\{\ln(H_0/H)\}^{3/(3+n)}], \tag{3.100}$$

where H_0 is a microscopic magnetic field scale. Note that these exponentials go to zero slower than any power law.

2. Disordered local moments

A related concept in the presence of quenched disorder is that of local magnetic moments (Milovanovich, Sachdev, and Bhatt, 1989; Bhatt and Fisher, 1992). This topic was reviewed by Belitz and Kirkpatrick (1994). An important conclusion is that the interactions between the local moments, or rare regions, are very important.

3. Interacting rare regions

One conclusion of the previous section is that long-ranged RKKY interactions between local moments, in conjunction with rare-region effects, can have qualitative effects. This suggests that similar interactions between rare regions in a quantum Griffith phase might also be important. This question was studied by Dobrosavljević and Miranda (2005) and Case and Dobrosavljević (2007) for the case of a Heisenberg AFM. The applicability of these ideas, with suitable modifications, to FMs remains to be studied.

Dobrosavljević and Miranda (2005) considered rare regions centered at points $\boldsymbol{R}_i$ ($i=1,2,3,\ldots$) that are characterized by local N-component ($N>1$) OPs $\boldsymbol{\phi}_i(\tau)$, with τ the imaginary-time variable. The Gaussian part of the action has the form

$$S^{(2)}=S_0^{(2)}+S_{\rm int}^{(2)}. \tag{3.101}$$

Here $S_0^{(2)}$ is the noninteracting part,

$$\begin{aligned} S_0^{(2)}&=\sum_i\int_0^\beta d\tau d\tau' \boldsymbol{\phi}_i(\tau)\Gamma_0(\tau-\tau')\cdot\boldsymbol{\phi}_i(\tau')\\ &=\sum_{n,i}\boldsymbol{\phi}_i(\Omega_n)\Gamma_0(\Omega_n)\cdot\boldsymbol{\phi}_i(-\Omega_n) \end{aligned} \tag{3.102}$$

with Ω_n a bosonic Matsubara frequency. Let us assume for simplicity that the OP is not conserved, so that the noninteracting vertex is given by

$$\Gamma_0(\Omega_n)=\Gamma_0(0)+|\Omega_n|. \tag{3.103}$$

The $|\Omega_n|$ nonanalyticity is the Landau-damping mechanism due to the coupling of the magnetic OP to the conduction electrons that was discussed in Sec. III.A.1. In imaginary-time space, it corresponds to a power-law decay $\Gamma_0(\tau\to\infty)\propto 1/\tau^2$. This puts the rare region or droplet, now considered a 1D classical system in τ space with a $1/\tau^2$ interaction, at its lower critical dimension (Joyce, 1969). This means that the noninteracting rare regions cannot develop long-range order.

The interacting part of the Gaussian action is given by

$$S_{\rm int}^{(2)}=\frac{1}{2}\sum_{i\neq j}\int_0^\beta d\tau d\tau' \boldsymbol{\phi}_i(\tau)V(R_{ij},\tau-\tau')\cdot\boldsymbol{\phi}_j(\tau'). \tag{3.104}$$

The interaction between two rare regions is assumed to be a static RKKY interaction given by

$$V(R_{ij},\tau)=\frac{J_{ij}}{(R_{ij})^d}\delta(\tau). \tag{3.105}$$

J_{ij} is assumed to be a random amplitude of zero mean and variance $\langle J_{ij}^2\rangle=J^2$. Using replica methods, Dobrosavljević and Miranda (2005) concluded that the effective contribution to the total action from rare-region interactions is

$$\begin{aligned} \delta S=&-\frac{1}{2}\sum_{i,j}(1-\delta_{ij})\sum_{\alpha\beta}\frac{J^2}{(R_{ij})^{2d}}\\ &\times\int d\tau d\tau'[\boldsymbol{\phi}_i^\alpha(\tau)\cdot\boldsymbol{\phi}_j^\alpha(\tau)][\boldsymbol{\phi}_i^\beta(\tau')\cdot\boldsymbol{\phi}_j^\beta(\tau')]. \end{aligned} \tag{3.106}$$

Here $(\alpha,\beta)=1,2,\ldots,n$ are replica labels, and the replica limit $n\to 0$ is implied. Treating this interaction in a standard mean-field approximation gives

$$\delta S=-\sum_{\alpha\beta}\sum_{n,i}\boldsymbol{\phi}_i^\alpha(\Omega_n)\Delta_i^{\alpha\beta}(\Omega_n)\cdot\boldsymbol{\phi}_i^\beta(-\Omega_n), \tag{3.107}$$

where $\Delta_i^{\alpha\beta}(\Omega_n)$ is proportional to a weighted spatial average of a local rare-region susceptibility,

$$\Delta_i^{\alpha\beta}(\Omega_n) = \frac{1}{N}\sum_{j\neq i}\frac{J^2}{(R_{ij})^{2d}}\langle \boldsymbol{\phi}_j^{\alpha}(\Omega_n)\cdot\boldsymbol{\phi}_j^{\beta}(-\Omega_n)\rangle. \quad (3.108)$$

Within a self-consistent mean-field theory, the average in Eq. (3.108) is to be taken with respect to the complete action, including the rare-region interaction term.

Comparing Eqs. (3.102) and (3.107) we see that the rare-region interactions have renormalized the Gaussian part of the noninteracting action S_0. This is analogous to the effects of the fermionic soft modes discussed in Secs. III.B and III.C. The importance of this term depends on its behavior for long times or low frequencies. Dobrosavljević and Miranda (2005) concluded that effectively the noninteracting vertex Γ_0, Eq. (3.103), gets augmented by an additive term of the form

$$\delta\Gamma(\Omega_n) \propto \text{const} + |\Omega_n|^{\alpha-1}. \quad (3.109)$$

Here $\alpha = c/\bar{\sigma}$ is the same exponent that appears in Eqs. (3.95b) and (3.96). It is nonuniversal and is expected to decrease as the magnetically ordered phase is approached. Once $\alpha < 2$, the nonanalyticity coming from the rare-region interaction is stronger than the one due to Landau damping in the bare action, Eq. (3.103). The OP correlation function then falls off more slowly than $1/\tau^2$ for large imaginary times. The rare region thus is above its lower critical dimension and can develop long-range order. This in turn implies that sufficiently large droplets will freeze and form a cluster-glass phase (see footnote [19]). This concept was used to analyze and interpret experiments on $CePd_{1-x}Rh_x$; see the discussion in Sec. II.E.1.a.

Based on these considerations, which suggest that the Griffiths phase is unstable, Dobrosavljević and Miranda (2005) proposed a phase diagram where a cluster-glass phase appears between the PM phase and the magnetically ordered phase. This was further discussed by Case and Dobrosavljević (2007), who argued that the transition from the PM to the cluster glass is a fluctuation-induced first-order transition at low T and continuous at higher T, with a tricritical point in between. This mechanism is analogous to the one described in Sec. III.B for clean FMs with the ordinary FM OP replaced by the droplet OP, and the fermionic soft modes replaced by the Griffiths fluctuations that were discussed in Sec. III.A.1.

4. The size of Griffiths effects

The arguments for Griffiths-phase effects are all asymptotic in nature, a characteristic they share with other rare-region effects, e.g., Lifshitz tails in the density of states of disordered solid (Lifshitz, 1964). A question for all of these phenomena is the range of their validity. For instance, we need to ask how far from its initial value a time-correlation function has to decay before the asymptotic behavior becomes realized, or how low a temperature one has to consider in order for the effects described in Sec. III.D.1 to become observable. These and related questions have a long history. They were initially investigated for classical systems, where the predicted effects were not always observed. However, for quantum systems more recent numerical evidence indicates substantial effects (Guo, Bhatt, and Huse, 1996; Rieger and Young, 1996; Pich *et al.*, 1998; Vojta, 2010), and experimental observations in many strongly disordered systems have been interpreted as due to quantum Griffiths effects; see Secs. II.C and II.E.

For classical systems, several rigorous results are available. One example is the problem of a random walk with a random distribution of static traps that immobilize the diffusing particle if it hits one. It has been rigorously shown (Donsker and Varadhan, 1975, 1979) that the survival probability $P(c,t)$, with c the concentration of traps, decays for asymptotically long times as

$$\ln P(c, t\to\infty) \propto -\lambda^{2/(d+2)}t^{d/(d+2)} \quad (3.110)$$

with $\lambda = -\ln(1-c)$. The same result was obtained by means of Griffiths-Lifshitz arguments by Grassberger and Procaccia (1982) and Kayser and Hubbard (1983), who showed that the asymptotic long-time behavior is dominated by the existence of arbitrarily large, but exponentially rare, trap-free regions. This work left open the size of the asymptotic region. After many earlier studies, Barkema, Biswas, and van Beijeren (2001) showed conclusively by means of Monte Carlo studies that the asymptotic result is valid only when $P(c,t)$ is exceedingly small. For instance, in $d=3$ the asymptotic behavior sets in only when $P(c,t)\approx 10^{-30}$ and 10^{-80} for $c =$ 0.1 and 0.01, respectively. For shorter times, $P(c,t)$ decays exponentially.

The Griffiths phase of the classical bond-diluted Ising model mentioned in Sec. III.D.1 was also studied. The time-dependent local spin-spin correlation function $C(t)$ is predicted to decay as (Bray, 1988, 1989)

$$C(t\to\infty) \sim \exp[-\text{const}\times(\ln t)^{d/(d-1)}]. \quad (3.111)$$

Monte Carlo simulations for $d=3$ (Colborne and Bray, 1989) showed poor agreement with Eq. (3.111). Plotting $\ln C(t)$ against $(\ln t)^{3/2}$ yielded substantial curvature. A better fit was obtained by plotting $\ln C(t)$ against $[\ln(t/\tau)]^{3/2}$, with $\tau(T)$ an adjustable parameter. A still better fit was found using a stretched exponential or Kohlrausch form $C(t)\sim \exp[-(t/\tau)^{\beta}]$, with β an increasing function of temperature that is on the order of 0.4. Various others (Colborne and Bray, 1989; Jain, 1995; Cao *et al.*, 2006) found that $C(t)$ must be less than 10^{-4} of its initial value before the asymptotic behavior sets in.

The situation is different for classical n-dimensional spins with $n \geq 2$. In this case, the Griffiths arguments predict (Bray, 1987, 1988, 1989)

$$C(t\to\infty) \sim \exp[-\text{const}\times t^{1/2}]. \quad (3.112)$$

Monte Carlo data are entirely consistent with this prediction for all but short times (Colborne and Bray, 1989).

For quantum systems, the increasing power of numerical methods has yielded interesting results. For a transverse-field Ising spin glass, Monte Carlo simulations on 2D and 3D systems by Guo, Bhatt, and Huse (1996) and Rieger and Young (1996) found clear evidence of Griffiths-phase effects. The size of the effects decreased by about a factor of 4 from $d=2$ to 3. The strength of the effects, compared with classical systems, is sometimes attributed to the fact that in the quantum case the Griffiths clusters occur as line defects, as

opposed to point defects in classical models. Perhaps more importantly, because quantum tunneling of a rare region is a slower process [$\tau \propto \exp(L^d)$] than thermally activated dynamics ($\tau \leq \exp L^{(d-1)}$) of the same rare region, the Griffiths singularities in the quantum case lead to power-law decays in time, or power-law singularities at low T. These power-law effects in temperature can dominate the usual Fermi-liquid power laws in metals. Various susceptibilities may even diverge as $T \to 0$.

Collectively, these results imply that the importance of the Griffiths effects is not *a priori* clear and may strongly depend on the nature of the system. For instance, in the classical case there is a qualitative difference between Ising and XY or Heisenberg models; see Eqs. (3.111) and (3.112). The quantum FM case, for both Ising and Heisenberg symmetry, is similar to the classical Ising model in the sense that there is an activation barrier to transport, unlike the classical Heisenberg case. On the other hand, there is numerical evidence for quantum mechanics enhancing the Griffiths effects.

E. Textured phases as a way to avoid a quantum-critical point

Various others realized that the instability of Hertz theory can signalize either a first-order transition, or a transition into a nonhomogeneous phase (Belitz, Kirkpatrick, and Vojta, 1997; Chubukov, Pépin, and Rech, 2004; Rech, Pépin, and Chubukov, 2006). The respective conditions were investigated by several others (Maslov, Chubukov, and Saha, 2006; Efremov, Betouras, and Chubukov, 2008). Maslov and Chubukov (2009) concluded that in a model with a long-ranged exchange interaction the first-order transition always preempts the formation of a spiral phase.

Conduit, Green, and Simons (2009) used a self-consistent many-body approach supplemented by a numerical evaluation of fluctuation corrections to the free energy to argue that a spiral state can preempt the first-order transition as the FM state is approached from the PM phase. This textured magnetic phase is analogous to the Fulde-Ferrell-Larkin-Ovchinnikov state in superconductors (Fulde and Ferrell, 1964; Larkin and Ovchinnikov, 1964). Karahasanovic, Krüger, and Green (2012) expanded this to a purely analytical theory that allows for instabilities toward spin-nematic phases in addition to a spiral one. They proposed a phase diagram, Fig. 39, where upon approaching from the PM at low T one first encounters a spin-nematic phase, followed by a spiral phase, and finally a uniform FM. The possibility of a Pomeranchuk instability toward a non-s-wave ferromagnet or magnetic nematic had also been discussed earlier by Chubukov and Maslov (2009). Later work concluded that an infinite resummation of fluctuation contributions to the free energy results in the spiral phase occupying a substantially smaller part of the phase diagram (within about 1% of the transition point at $T = 0$) than the original theory predicted (Pedder, Krüger, and Green, 2013), but the topology of the phase diagram remained the same. Such a narrow slice of spiral order would be easy to overlook experimentally and has so far not been observed. In 2D the theory predicts a much larger spiral phase. One must keep in mind, however, that no true long-range FM order is possible in $d = 2$ at $T > 0$.

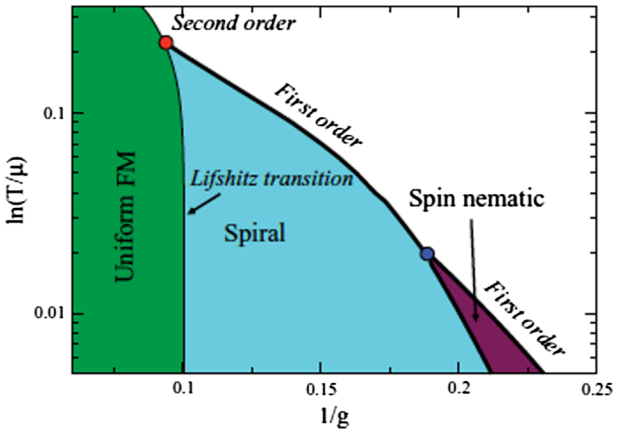

FIG. 39. Proposed phase diagram for a model allowing for spiral and spin-nematic order. μ is the chemical potential, and g is the exchange coupling. From Karahasanovic, Krüger, and Green, 2012.

F. Other mechanisms for a first-order transition

The mechanism for a first-order transition in clean quantum FMs that was discussed in Sec. III.B.2 is remarkable because of its universality. However, in any given material a less universal mechanism may be present that by itself would suffice to drive the transition first order. Here we briefly discuss two such mechanisms.

1. Band-structure effects

The coefficients in the Landau free energy

$$f_{\mathrm{L}}[m] = tm^2 + u_4 m^4 + u_6 m^6 + O(m^8) \tag{3.113}$$

depend in complicated ways on the microscopic details of the system, and, in particular, on band structure. In any given material it is possible that band-structure effects lead to a negative value of u_4. If $u_6 > 0$, this leads to a first-order transition at some positive value of t, which preempts the second-order transition at $t = 0$. Under certain conditions, correlations can have the same effect (Yamada, 1993). However, this cannot explain the universality of the observed effect in clean low-T FMs that is displayed by Tables I and II.

It is interesting that UGe_2, in addition to the pressure-induced first-order PM-to-FM transition at $p \approx 16$ kbar, shows a metamagnetic transition at a lower pressure that is also of first order. This transition, as well as the superconductivity that coexists with the ferromagnetism at low T and intermediate pressures, has been attributed to a special feature in the density of states of UGe_2 (Pfleiderer and Huxley, 2002; Sandeman, Lonzarich, and Schofield, 2003; Shick *et al.*, 2004a, 2004b).

2. Magnetoelastic effects

Phonons are generic soft modes in the sense of Sec. III.A.1 that couple to the magnetization. This can lead to a weakly first-order transition in classical magnets (Rice, 1954; Bean and Rodbell, 1962; Larkin and Pikin, 1969; Sak, 1974; Wegner, 1974; Bergman and Halperin, 1976; de Moura *et al.*, 1976). We briefly review the conclusions

for classical magnets and then the relevance of these results for quantum FMs.

a. Classical magnets

Consider an LGW theory for a FM with OP $\boldsymbol{M}$ that couples to harmonic elastic degrees of freedom. In the simplest case of an isotropic 3D system in the continuum limit the action reads (Aharony, 1976)

$$S = \int d\boldsymbol{x}\left[t\boldsymbol{M}^2 + (\nabla \boldsymbol{M})^2 + u_4\boldsymbol{M}^4 + \left(\frac{K}{2} - \frac{\mu}{3}\right)\left(\sum_{\alpha=1}^{3} u_{\alpha\alpha}\right)^2 + \mu\sum_{\alpha,\beta} u_{\alpha\beta}^2 + g\boldsymbol{M}^2\sum_{\alpha} u_{\alpha\alpha}\right]. \tag{3.114}$$

Here K and μ are elastic coefficients, and

$$u_{\alpha\beta} = \frac{1}{2}\left(\partial_\beta u_\alpha + \partial_\alpha u_\beta + \sum_\gamma \partial_\alpha u_\gamma \partial_\beta u_\gamma\right) \tag{3.115}$$

is the strain tensor in terms of derivatives of the displacement vector $\boldsymbol{u}(\boldsymbol{x})$. g is the magnetoelastic coupling constant. In systems on a lattice there are additional terms (Bergman and Halperin, 1976; de Moura *et al.*, 1976), but the general structure of the action is the same. At constant pressure, additional terms coupling the pressure to the strain tensor need to be added (Imry, 1974).

There are several important features of this action. First, the coupling is to the square of the OP. Second, the coupling is to the divergence of the soft mode, i.e., the displacement vector. This is in contrast to the case of the smectic OP coupling to the nematic Goldstone modes at a nematic-to-smectic-A transition, or the superconducting OP coupling to the electromagnetic vector potential (Halperin, Lubensky, and Ma, 1974). In both of these cases, the coupling is directly to a soft mode, which leads to a nonanalytic dependence of the free energy on the OP in a renormalized Landau theory. Here, by contrast, the coupling is much weaker due to the additional gradient, and the net effects of the elastic modes are additional terms of quartic order in the OP. Schematically, one can see this by replacing the strain tensor $u_{\alpha\beta}$ by a scalar ϵ and considering a Landau free energy

$$f[m,\epsilon] = tm^2 + u_4 m^4 + K\epsilon^2 + gm^2\epsilon. \tag{3.116}$$

Decoupling m and ϵ shows that the transition in mean-field approximation is first order if $g^2 > 4Ku_4$. The nature of the phase transition as described by the LGW action (3.114) and its generalizations was studied by de Moura *et al.* (1976), who integrated out the elastic degrees of freedom, and by Bergman and Halperin (1976), who performed an RG analysis of the full coupled theory. The conclusion is consistent with the simple argument given above: For a sufficiently large magnetoelastic coupling the transition may become first order, but whether or not this occurs depends on the bare values of the parameters in the LGW theory, i.e., on microscopic details, as well as on the dimensionality of the OP (Nattermann, 1977). Magnetoelastic effects are a route to a first-order transition but not a universal route.

b. Quantum magnets

Gehring (2008) [see also Gehring and Ahmed (2010)] and Mineev (2011) proposed to apply these results for classical magnets to the quantum FM transition in pressure-driven systems by generalizing the Landau free energy (3.116) to

$$f[m,\epsilon] = t(\epsilon)m^2 + u_4 m^4 + K\epsilon^2, \tag{3.117}$$

with $t(\epsilon) = T - T_c(\epsilon)$ representing the dependence of T_c on the strain (or, equivalently, on the pressure p). Expanding $T_c(\epsilon)$ for small ϵ leads to the coupling given in Eq. (3.116) with $g \propto dT_c/dp$. Since experimentally one finds $dT_c/dp \to \infty$ as $T_c \to 0$, they argued that effectively the magnetoelastic coupling g increases without bounds as T_c decreases, necessarily leading to a first-order transition at sufficiently low T_c. This line of reasoning is problematic. First, a singular dependence of a coefficient on a field must not be built into a Landau theory if the theory is to have any predictive value. Such a singular dependence may result from integrating out soft modes, such as in the treatment of classical liquid crystals or superconductors by Halperin, Lubensky, and Ma (1974), or in the renormalized Landau theory reviewed in Sec. III.B. In the case of compressible magnets such a result is implausible. The coupling between the magnetic OP and the elastic deformations is weak even in the classical case, see above, and in the quantum case it will be even weaker due to an additional frequency integral. Second, a diverging effective magnetoelastic coupling results in a diverging volume change (Bean and Rodbell, 1962). Therefore, even if one accepts the substitution of the observed $T_c(p)$ into the Landau theory, it predicts that a structural phase transition must necessarily accompany the first-order magnetic transition. There is no experimental evidence for this. We conclude that currently no convincing theory for magnetoelastic effects in the quantum regime exists.

IV. SUMMARY, DISCUSSION, AND OUTLOOK

A. Summary and discussion

We have given an overview of the quantum phase-transition problem in metallic ferromagnets. Experimentally, a variety of phase diagrams are observed; see Fig. 2. Apart from discontinuous (first-order) and continuous (second-order) QPTs FM to a PM, a QPT from a FM state to an AFM or spin-wave state is observed in some systems, while in others the low-T phase near the onset of FM is some sort of a magnetic glass. In many systems with quenched disorder there is evidence for quantum Griffiths effects on the PM side of the transition. The experimental results are described in Sec. II, organized with respect to the structure of the phase diagram.

Theoretically, the transition from a PM quantum FM is expected to be discontinuous in clean systems and continuous in disordered ones. In either case the behavior at the QPT is very different from the one expected from Hertz theory. This is because of a coupling between the magnetization and soft fermionic excitations in metals that was included in Hertz theory in too simple an approximation and treated more thoroughly in the theory originally developed by two of us and T. Vojta that is reviewed in Sec. III. The results obtained

by Moriya, Hertz, and Millis are still expected to be observable in certain preasymptotic regimes. The agreement between these theoretical predictions and experimental results is generally very good for clean systems. Strongly disordered systems are much more complicated. Although the critical singularities at the continuous quantum FM transition have been calculated exactly, Griffiths-phase effects coexist with the critical singularities and complicate the experimental analysis.

We now add some remarks to the discussion in the main text and mention some related topics that we did not cover. The references in this section are intended to be illustrative, rather than exhaustive.

(1) Nematic phases and transitions in a Fermi liquid have been investigated theoretically by Oganesyan, Kivelson, and Fradkin (2001). They used a Hertz-type theory, which yields a continuous transition with mean-field critical behavior in spatial dimensions $d = 2$, 3 for all types of nematics considered. The case of a metallic spin nematic, or non-s-wave FM, is theoretically closely related to the FM one. For such systems in the absence of quenched disorder it was later shown that the same mechanism operative in FMs generically causes the spin-nematic transition to be of first order (Kirkpatrick and Belitz, 2011).

For charge nematics the mechanism leading to a first-order transition does not apply (Belitz, Kirkpatrick, and Vojta, 2002). Still, later work showed that the Hertz approach breaks down even in this case, but the breakdown is less dramatic than in the spin channel and the transition is believed to remain continuous (Dell'Anna and Metzner, 2006; Lee, 2009; Metliski and Sachdev, 2010).

There is experimental evidence of charge Ising-nematic order in systems including the pnictides (Chuang *et al.*, 2010), $Sr_3Ru_2O_7$ (Borzi *et al.*, 2007), and the normal state of the cuprates, in particular, $YBa_2Cu_3O_y$ (Daou *et al.*, 2010). For a review, see Fradkin *et al.* (2010).

(2) Another point is related to the models used to theoretically study the FM QPT. Hertz (1976) considered a continuum model of free electrons that interacts via a pointlike spin-triplet interaction. There are good reasons to believe that such a model does not actually have a FM phase; see Sec. IV.B.4. However, the point of an effective field theory such as Hertz's is not to establish whether or not there is a phase transition in this, or any, model; it is to describe the properties of the transition, provided one actually occurs. The complicated band structure and other microscopic details that may well be necessary to produce a transition in the first place do not affect the universal properties at the transition and therefore can safely be omitted from the effective theory.

More recent theories [see, e.g., Kirkpatrick and Belitz (2012a)] considered an effective OP theory that has the existence of a magnetic transition encoded in the parameters of the effective LGW functional. All details of the solid-state structure that are necessary for FM to occur are thus hidden in these parameters. The OP is then coupled to fermions, and for capturing the qualitative effects of the latter on the FM transition again a simple continuum model suffices.

(3) The near-universal observation of a first-order QPT in clean FMs is surprising even given the robustness of the effect discussed in Sec. III.B.2, since the term in the renormalized Landau theory that is responsible for it is logarithmic, which results in an exponential dependence of observables on parameters. It is possible that, perhaps as a result of strong electron correlations, an analog of van der Waals's law of corresponding states for classical liquids holds for strongly correlated Fermi liquids, making the relevant parameters, measured in natural units, roughly the same in different materials. This notion is consistent with the discussion in Sec. II.B.5, and especially with the fact that the tricritical temperature scales roughly with the magnetic moment.

(4) In Secs. II and III we emphasized the fact that experimental observations of continuous FM QPTs in strongly disordered systems are often difficult to interpret, and the critical exponents that characterize these transitions are hard to measure. However, qualitative features of both theoretical results and experimental observations indicate that several exponents are drastically different from both the mean-field exponents expected in a preasymptotic regime in weakly disordered systems and classical exponents in common universality classes.

For instance, the OP exponent β is predicted to be larger than unity (about 1.2) in the preasymptotic regime where an effective power-law behavior is expected, whereas the exponent δ is unusually small (about 1.8); see Eq. (3.90c). In contrast, the mean-field values are $\beta = 1/2$ and $\delta = 3$, and the corresponding classical values for 3D Heisenberg FMs are about 0.37 and 4.8, respectively. Experiments do indeed tend to find values of β and δ that are larger and smaller, respectively, than their respective mean-field values; see Secs. II.C.2 and III.C.3.h. A related issue is the shape of the phase boundary near the QPT, with both theory and experiments finding a tail in the phase diagram; see the discussion in Sec. III.C.3.h. Griffiths effects may also contribute to the observed properties in this region, which makes more detailed investigations desirable.

This superposition of critical phenomena and additional disorder effects notwithstanding, the results reviewed in Sec. III.C.3.e for the critical behavior of an FM OP coupled to diffusive fermions are believed to be exact. This type of problem also appears elsewhere. For instance, Savary, Moon, and Balents (2014) considered a model for pyrochlore iridates that couples a quantum φ^4 theory to (in this case exotic) fermions, which results in a phase transition with similarly unusual critical properties.

(5) Even far away from any QPT FM metals at low T have interesting properties. This is not as well appreciated as the problems posed by AFMs, or by FMs near a QPT. For instance, in many clean FMs a *generic*

(i.e., existing in an entire phase) non-Fermi-liquid $T^{3/2}$ resistivity is observed over a large low-T range in both the FM and PM phases (Sato, 1975; Pfleiderer *et al.*, 2001; Niklowitz *et al.*, 2005; Takashima *et al.*, 2007; Brando *et al.*, 2008). This is not well understood; see Sec. IV.B.

In disordered systems, Griffith effects lead to generic NFL behavior on the PM side of the phase boundary as was discussed in Sec. III.D. In either phase, weak-localization (Lee and Ramakrishnan, 1985) and Altshuler-Aronov (Altshuler and Aronov, 1984), effects are expected in disordered systems. The resulting superimposed temperature dependences of observables can be quite intricate (Butenko, Bol'shutkin, and Percherskaya, 1990) but in general little attention has been paid to them.

(6) There has been interesting work on FM transitions in metals under nonequilibrium conditions (Mitra *et al.*, 2006; Mitra and Millis, 2008), where correlations are generally greatly enhanced compared to systems in equilibrium (Belitz, Kirkpatrick, and Vojta, 2005). In these systems the fermionic soft modes discussed in Sec. III are suppressed by boundary effects. As a consequence a Hertz-type nonequilibrium transition has been predicted.

(7) Unusual phases are expected in systems where both electronic correlations and a strong spin-orbit interaction are present (Wan *et al.*, 2011). In particular, topological semimetal phases can occur which may be realized in $Y_2Ir_2O_7$ (Wan *et al.*, 2011), Bi_2Se_3 (Zhang *et al.*, 2009), and $HgCr_2Se_4$ (Xu *et al.*, 2011), or in heterostructures of topological and normal insulators (Burkov and Balents, 2011). This semimetal state is a 3D analog of graphene and provides a condensed-matter realization of Weyl fermions. Calculations based on the LSDA + U + SO method (local spin-density approximation plus correlations plus spin-orbit coupling) have suggested a rich phase diagram with a QPT between a FM metal and a Weyl semimetal (Wan *et al.*, 2011). The nature of this transition has not been investigated.

Weyl semimetals also have interesting properties apart from any QPT. Ideas associated with them have been used to understand the intrinsic anomalous Hall effect in metallic FMs (Chen, Bergman, and Burkov, 2013). They argued that even Weyl nodes that do not coincide with the Fermi energy, as is believed to be the case in $SrRuO_3$, contribute to the intrinsic anomalous Hall conductivity in FM metals. This in turn implies that this conductivity in FMs is not purely a Fermi-surface property, which contradicts earlier conclusions (Haldane, 2004).

(8) FM transitions have been observed in a variety of quantum Hall systems. For instance, in a GaAs system in a perpendicular magnetic field, Piazza *et al.* (1999) observed a first-order transition in the $\nu = 2$ and 4 quantum Hall states. They suggested that the source of the observed hysteresis effects was not exotic, but was due to the expected domain structure in an easy-axis FM. Similar behavior was observed by De Poortere, Tutuc, and Shayegan (2003) in AlAs quantum wells. Drichko *et al.* (2012) measured magnetoresistance properties in two p-Si/SiGe/Si quantum-well samples in a tilted magnetic field. In a sample with $p = 2 \times 10^{11}$ cm^{-2} they observed phase coexistence and concluded that there was a first-order FM-PM transition. However, in the second sample with $p = 7.2 \times 10^{10}$ cm^{-2} no transition was observed. Stoner or RPA-like theories have been used to discuss FM transitions in quantum Hall systems (Burkov and MacDonald, 2002; Lopatnikova, Simon, and Demler, 2004), and for the pseudospin FM realized in bilayer quantum Hall systems there is evidence for a first-order transition (Schliemann, Girvin, and MacDonald, 2001; Zou *et al.*, 2010; Lee *et al.*, 2014).

B. Open problems

We finally mention some open problems.

(1) Additional work is needed to disentangle Griffiths singularities and critical singularities near the FM QPT in disordered metals. Since Griffiths singularities generically are stronger on the PM side of the transition (Motrunich *et al.*, 2000), the QPT is best studied from the FM side. Although Griffiths singularities exist in weaker forms also on the FM side, the existence of a zero-field magnetization uniquely implies long-ranged FM order, so the singular behavior of the zero-field magnetization itself can distinguish between Griffiths singularities and critical singularities. The relation between Griffiths physics and the Harris criterion was discussed by Vojta and Hoyos (2014) and Vojta, Igo, and Hoyos (2014).

The NFL behavior observed in many clean materials in large parts of the phase diagram was reviewed by Stewart (2001) and remains incompletely understood. One manifestation is the $T^{3/2}$ behavior of the resistivity that was mentioned in Sec. IV.A. An explanation in terms of columnar fluctuations, which is applicable to MnSi, was proposed by Kirkpatrick and Belitz (2010). However, because of the large variety of materials where a $T^{3/2}$ resistivity is observed, it is likely that more than one mechanism can lead to this behavior. For a related discussion of $ZrZn_2$, see Smith *et al.* (2008).

Similarly, weak-localization and Altshuler-Aronov effects in weakly disordered FMs deserve more attention. The T dependence of the resistivity can be complicated, with many contributions from very different sources (Mizutani *et al.*, 1988; Butenko, Bol'shutkin, and Percherskaya, 1990; Yildiz *et al.*, 2009).

(2) In the presence of magnetic impurities, or impurities with a large spin-orbit coupling, the soft fermionic modes in the disordered case will be suppressed (Lee and Ramakrishnan, 1985; Belitz and Kirkpatrick, 1994), and the nature of the FM QPT is unclear. It is possible that, once the generic soft modes have been eliminated, the transition will resemble the one in disordered AFM metals, but not much is known about this case.

(3) There are materials in which no FM transition has been observed, but that nonetheless display very interesting properties. One of these is YFe_2Al_{10}. It crystallizes in the eponymous orthorhombic structure with a single Fe site (Kerkau *et al.*, 2012). Initial experiments identified correlated FM behavior (Strydom and Peratheepan, 2010). Further detailed studies on single crystals found anomalies in the magnetic susceptibility and the specific heat which obey a peculiar NFL field-temperature scaling (Park *et al.*, 2011; Wu *et al.*, 2014). In addition, FM correlations have been found in NMR experiments (Khuntia *et al.*, 2012). These observations have been interpreted as indicating that the material is close to a FM QPT. However, no FM transition has been detected so far at temperatures down to 50 mK, even upon doping with a small surplus of Fe (Strydom *et al.*, 2013). On the contrary, Fe excess or deficiency drive YFe_2Al_{10} away from the critical behavior. The low-T resistivity shows a Kondo-like logarithmic increase below 30 K with a high $\rho_0 \approx 75\ \mu\Omega\,\mathrm{cm}$ (RRR ≈ 2), which puts YFe_2Al_{10} in the group of strongly disordered systems (cf. Sec. II.C.2). However, single-crystal structure refinement did not find any deviation from the ideal composition (Kerkau *et al.*, 2012), so the origin of the large resistivity is not clear. The observed scaling behavior and the lack of a magnetically ordered phase in YFe_2Al_{10} need further investigation. We also mention that in the closely related system $YbFe_2Al_{10}$ strong FM correlations have been observed at low T (Khuntia *et al.*, 2014). In this material, the Yb-derived electrons at low T form a nonmagnetic intermediate-valent state and therefore the Fe atoms alone are responsible for the FM correlations, as is the case in YFe_2Al_{10}.

(4) There are materials that display a transition from a metallic AFM state to a FM at low T. Two examples are $CeRu_2Ge_2$ (Raymond, Haen *et al.*, 1999) and $CeRu_2Al_2B$ (Baumbach *et al.*, 2012). In both cases, the AFM-FM transition is first order, whereas the transition from a PM to an AFM at a higher Néel temperature is second order. It is plausible that the QPT from a metallic AFM to a FM in clean systems is first order for the same reasons as that from a metallic PM to a FM, but no theory is available for this case.

A related issue is the detailed structure of the phase diagrams discussed in Sec. II.D. These systems all must display a Lifshitz point and at least two QPTs. In clean systems, the QPT from the FM phase to the modulated phase is expected to be first order, but this needs experimental confirmation. In disordered systems, it may well be a novel type of QCP. Similarly, the Lifshitz point may be a multicritical point with very interesting properties.

(5) An old question is what ingredients in a model are necessary for producing itinerant FM [see, e.g., Varma (2010) and Shimizu (1964), and references therein]. It has long been suspected that in simple electron-fluid models there is no FM phase (Ceperley and Alder, 1980; Chang, Zhang, and Ceperley, 2010), although some recent quantum Monte Carlo studies suggest otherwise (Pilati *et al.*, 2010; Pilati, Zitchenko, and Troyer, 2014). This topic has received much attention recently in the context of optical lattices, especially an experiment that reported itinerant FM in a Fermi gas of ultracold atoms (Jo *et al.*, 2009). However, subsequent experiments by the same group cast doubt on the original interpretation of the data (Sanner *et al.*, 2012). FM solid-state systems typically have a complicated band structure. Whether or not FM can occur in optical lattices is an open question. If it does, the transition is expected to be first order for the same reasons as in clean solid-state systems (Duine and MacDonald, 2005), and a quantum Monte Carlo study of a 2D Stoner Hamiltonian suggests that the strength of the first-order transition depends on the range of the interaction (Conduit, 2013).

(6) Quenches, i.e., rapid changes of external parameter values, at $T = 0$ in both clean and disordered metallic FMs are interesting. Belitz, Kirkpatrick, and Saha (2007) showed that the coupling of the OP to the fermionic soft modes leads to qualitatively new effects for the late-stage coarsening. Gagel, Orth, and Schmalian (2014) showed that there is universal preasymptotic behavior in general quantum quench problems due to long-range boundary effects. In FM metals this effect is expected to be even more interesting because of the coupling to the fermionic soft modes.

(7) The experimental coexistence curve appears to be extremely steep in many FM systems [see, e.g., Figs. 5 and 10, and the phase diagrams for $ZrZn_2$ measured by Uhlarz, Pfleiderer, and Hayden (2004) and Takashima *et al.* (2007)], but determining the coexistence curve from different observables can lead to different detailed shapes (Kabeya *et al.*, 2010). Studies of the detailed shape, by pressure cycling in the p-T plane, or field cycling in the p-H plane, would be interesting. Theoretically, the shape of the coexistence curve can be determined from the Clapeyron-Clausius equation, which has been discussed for quantum Hall systems by Zou *et al.* (2010) and for QPTs in general and FMs, in particular, by Kirkpatrick and Belitz (2015b).

(8) Without trying to be exhaustive, we mention a few other FM materials that may be candidates for suppressing T_C via pressure or chemical substitution: $NpNiSi_2$, a Kondo-lattice system with $T_C = 51.5$ K (Colineau *et al.*, 2008); $Sr_4Ru_3O_{10}$, a layered FM with $T_C = 148$ K (Cao *et al.*, 1997; Crawford *et al.*, 2002) (see also Sec. II.B.4); the enhanced PM $TiBe_2$ which shows metamagnetism at 5 T (Wohlfarth, 1980); and $TiBe_{2-x}Cu_x$ which shows a transition to a FM ordered state (Giorgi *et al.*, 1979; Acker *et al.*, 1981). The latter system was intensively investigated in the early 1980s, but a detailed and conclusive phase diagram does not exist. Since recent band-structure calculations (Jeong, Kyker, and Pickett, 2006) suggest that $TiBe_2$ is close to an AFM instability, it would be interesting to revisit the phase diagram of $TiBe_{2-x}Cu_x$.

ACKNOWLEDGMENTS

We have benefited from collaborations, discussions, and correspondence with many colleagues, including Dai Aoki, Megan Aronson, Michael Baenitz, Eric Bauer, Ryan Baumbach, Nick Butch, Roberto Caciuffo, Bob Cava, Andrey Chubukov, Piers Coleman, Tristan Combier, Gareth Conduit, Ramzy Daou, William Duncan, David Edwards, Tobias Förster, Sven Friedemann, Veronika Fritsch, Markus Garst, Philipp Gegenwart, Christoph Geibel, Andrew Green, Sandra Hamann, Clifford Hicks, Andrew Huxley, Donjing Jang, Marc Janoschek, Anton Jesche, Georg Knebel, Guido Kreiner, Cornelius Krellner, Frank Krüger, Robert Küchler, Stefan Lausberg, Gilbert Lonzarich, Jeff Lynn, Andy MacKenzie, Dmitrii Maslov, Maria Teresa Mercaldo, Andy Millis, Satoru Nakatsuji, Andreas Neubauer, Michael Nicklas, Luis Pedrero, Heike Pfau, Christian Pfleiderer, Adam Pikul, Jörg Rollbühler, Achim Rosch, Burkhard Schmidt, Andy Schofield, Julian Sereni, Sharon Sessions, Qimiao Si, Jörg Sichelschmidt, Dmitry Sokolov, Frank Steglich, Alexander Steppke, Greg Stewart, Andre Strydom, Stefan Süllow, Tomo Uemura, Chandra Varma, Matthias Vojta, Thomas Vojta, and Tanja Westerkamp. This work was supported by the National Science Foundation under Grants No. NSF DMR-09-01952, No. DMR-09-01907, No. DMR-1401410, and No. DMR-1401449, by the EPSRC of the UK under Grant No. EP/K012894, and by the Deutsche Forschungsgemeinschaft under Grant No. FOR-960. Part of this work was supported by the National Science Foundation under Grant. No. PHYS-1066293. We acknowledge the Aspen Center for Physics for their hospitality.

APPENDIX A: LIST OF ACRONYMS

AFM	Antiferromagnet, or antiferromagnetism, or antiferromagnetic
CDW	Charge-density wave
CEF	Crystalline electric field
CEP	Critical end point
DIV	Dangerous irrelevant variable
FM	Ferromagnet, or ferromagnetism, ferromagnetic
LGW	Landau-Ginzburg-Wilson
NFL	Non-Fermi liquid
PM	Paramagnet, or paramagnetic
RG	Renormalization group
QCP	Quantum critical point
QCEP	Quantum critical end point
QPT	Quantum phase transition
RG	Renormalization group
RRR	Residual resistance ratio

APPENDIX B: DEFINITIONS OF CRITICAL EXPONENTS

Let T be the temperature, t the dimensionless distance from criticality at $T=0$, and h the magnetic field. Consider the correlation length ξ, the magnetization m, the magnetic susceptibility χ, and the specific-heat coefficient $\gamma = C/T$ as functions of t, T, and h, and the susceptibility also as a function of the wave number k. We define critical exponents as follows.

Correlation length:

$$\xi(t \to 0, T = 0) \propto |t|^{-\nu},$$
$$\xi(t = 0, T \to 0) \propto T^{-\nu_T}. \tag{B1}$$

Order parameter:

$$m(t \to 0, T = 0, h = 0) \propto (-t)^{\beta},$$
$$m(t = 0, T \to 0, h = 0) \propto T^{\beta_T},$$
$$m(t = 0, T = 0, h \to 0) \propto h^{1/\delta}. \tag{B2}$$

Order-parameter susceptibility:

$$\chi(t \to 0, T = 0; k = 0) \propto |t|^{-\gamma},$$
$$\chi(t = 0, T \to 0; k = 0) \propto T^{-\gamma_T},$$
$$\chi(t = 0, T = 0, k \to 0) \propto 1/k^{2-\eta}. \tag{B3}$$

Specific-heat coefficient:

$$\gamma(t \to 0, T = 0) \propto |t|^{-\bar{\alpha}},$$
$$\gamma(t = 0, T \to 0) \propto T^{-\bar{\alpha}_T}. \tag{B4}$$

ν, β, γ, δ, and η are defined in analogy to the corresponding exponents at a classical phase transition. The definition of $\bar{\alpha}$ deviates from the one of the classical exponent customarily denoted by α, which is defined in terms of the specific heat rather than the specific-heat coefficient. At a classical phase transition, $\bar{\alpha}$ coincides with α, $\bar{\alpha}_T$, ν_T, β_T, and γ_T reflect the fact that a QPT can be approached either in the $T=0$ plane, or from $T>0$. The definition of β_T in Eq. (B2) is purely formal; see Kirkpatrick and Belitz (2015a) and the discussion after Eq. (3.58).

REFERENCES

Abdul-Jabbar, G., *et al.*, 2015, Nat. Phys. **11**, 321.
Acker, F., Z. Fisk, J. Smith, and C. Huang, 1981, J. Magn. Magn. Mater. **22**, 250.
Adachi, K., and K. Ohkohchi, 1980, J. Phys. Soc. Jpn. **49**, 154.
Adachi, K., K. Sato, and M. Takeda, 1969, J. Phys. Soc. Jpn. **26**, 631.
Aharony, A., 1976, in *Phase Transitions and Critical Phenomena*, Vol. 6, edited by C. Domb, and M. S. Green (Academic, New York), p. 358.
Akazawa, T., H. Hidaka, T. Fujiwara, T. C. Kobayashi, E. Yamamoto, Y. Haga, R. Settai, and Y. Ōnuki, 2004, J. Phys. Condens. Matter **16**, L29.
Akkermans, E., and G. Montambaux, 2011, *Mesoscopic Physics of Electrons and Photons* (Cambridge University Press, Cambridge, England).
Alam, A., and D. D. Johnson, 2011, Phys. Rev. Lett. **107**, 206401.
Alami-Yadri, K., and D. Jaccard, 1996, Solid State Commun. **100**, 385.

Alami-Yadri, K., H. Wilhelm, and D. Jaccard, 1998, Eur. Phys. J. B **6**, 5.

Altshuler, B. L., and A. G. Aronov, 1984, *Electron-Electron Interactions in Disordered Systems*, edited by M. Pollak, and A. L. Efros (North-Holland, Amsterdam).

Altshuler, B. L., A. G. Aronov, and A. Y. Zyuzin, 1983, Zh. Eksp. Teor. Fiz. **84**, 1525 [Sov. Phys. JETP **57**, 889 (1983)].

Anderson, P. W., 1958, Phys. Rev. **109**, 1492.

Andrade, E. C., M. Brando, C. Geibel, and M. Vojta, 2014, Phys. Rev. B **90**, 075138.

Andreev, A. V., R. Z. Levitin, Y. F. Popov, and R. Y. Yumaguzhin, 1985, Sov. Phys. Solid State **27**, 1145.

Anisimov, M. A., P. E. Cladis, E. E. Gorodetskii, D. A. Huse, V. E. Podneks, V. G. Taratuta, W. van Saarloos, and V. P. Voronov, 1990, Phys. Rev. A **41**, 6749.

Aoki, D., T. Combier, V. Taufour, T. D. Matsuda, G. Knebel, H. Kotegawa, and J. Flouquet, 2011, J. Phys. Soc. Jpn. **80**, 094711.

Aoki, D., and J. Flouquet, 2012, J. Phys. Soc. Jpn. **81**, 011003.

Aoki, D., and J. Flouquet, 2014, J. Phys. Soc. Jpn. **83**, 061011.

Aoki, D., F. Hardy, A. Miyake, V. Taufour, T. D. Matsuda, and J. Flouquet, 2011, C.R. Phys. **12**, 573.

Aoki, D., A. Huxley, E. Ressouche, D. Braithwaite, J. Floquet, J.-P. Brison, E. Lhotel, and C. Paulsen, 2001, Nature (London) **413**, 613.

Araki, S., N. Metoki, A. Galatanu, E. Yamamoto, A. Thamizhavel, and Y. Ōnuki, 2003, Phys. Rev. B **68**, 024408.

Araki, S., *et al.*, 2015, J. Phys. Soc. Jpn. **84**, 024705.

Bak, P., and M. H. Jensen, 1980, J. Phys. C **13**, L881.

Balents, L., 2010, Nature (London) **464**, 199.

Barakat, S., D. Braithwaite, P. Alireza, K. Grube, M. Uhlarz, J. Wilson, C. Pfleiderer, J. Flouquet, and G. Lonzarich, 2005, Physica B (Amsterdam) **359–361**, 1216.

Barkema, G. T., P. Biswas, and H. van Beijeren, 2001, Phys. Rev. Lett. **87**, 170601.

Barnea, G., and D. M. Edwards, 1977, J. Phys. F **7**, 1323.

Bauer, E. D., V. S. Zapf, P.-C. Ho, N. P. Butch, E. J. Freeman, C. Sirvent, and M. B. Maple, 2005, Phys. Rev. Lett. **94**, 046401.

Baumbach, R. E., H. Chudo, H. Yasuoka, F. Ronning, E. D. Bauer, and J. D. Thompson, 2012, Phys. Rev. B **85**, 094422.

Baym, G., and C. Pethick, 1991, *Landau Fermi-Liquid Theory* (Wiley, New York).

Bean, C. P., and D. S. Rodbell, 1962, Phys. Rev. **126**, 104.

Belitz, D., and T. R. Kirkpatrick, 1994, Rev. Mod. Phys. **66**, 261.

Belitz, D., and T. R. Kirkpatrick, 1996, Europhys. Lett. **35**, 201.

Belitz, D., and T. R. Kirkpatrick, 1997, Phys. Rev. B **56**, 6513.

Belitz, D., and T. R. Kirkpatrick, 2012, Phys. Rev. B **85**, 125126.

Belitz, D., and T. R. Kirkpatrick, 2014, Phys. Rev. B **89**, 035130.

Belitz, D., T. R. Kirkpatrick, M. T. Mercaldo, and S. Sessions, 2001a, Phys. Rev. B **63**, 174427.

Belitz, D., T. R. Kirkpatrick, M. T. Mercaldo, and S. Sessions, 2001b, Phys. Rev. B **63**, 174428.

Belitz, D., T. R. Kirkpatrick, and J. Rollbühler, 2005, Phys. Rev. Lett. **94**, 247205.

Belitz, D., T. R. Kirkpatrick, and R. Saha, 2007, Phys. Rev. B **75**, 144418.

Belitz, D., T. R. Kirkpatrick, and T. Vojta, 1997, Phys. Rev. B **55**, 9452.

Belitz, D., T. R. Kirkpatrick, and T. Vojta, 1999, Phys. Rev. Lett. **82**, 4707.

Belitz, D., T. R. Kirkpatrick, and T. Vojta, 2002, Phys. Rev. B **65**, 165112.

Belitz, D., T. R. Kirkpatrick, and T. Vojta, 2005, Rev. Mod. Phys. **77**, 579.

Bergman, D. J., and B. I. Halperin, 1976, Phys. Rev. B **13**, 2145.

Bernhoeft, N. R., G. G. Lonzarich, P. W. Mitchell, and D. M. Paul, 1983, Phys. Rev. B **28**, 422.

Berridge, A. M., A. G. Green, S. A. Grigera, and B. D. Simons, 2009, Phys. Rev. Lett. **102**, 136404.

Berridge, A. M., S. A. Grigera, B. D. Simons, and A. G. Green, 2010, Phys. Rev. B **81**, 054429.

Besnus, M., A. Essaihi, N. Hamdaoui, G. Fischer, J. Kappler, A. Meyer, J. Pierre, P. Haen, and P. Lejay, 1991, Physica (Amsterdam) **171B**, 350.

Betouras, J., D. Efremov, and A. Chubukov, 2005, Phys. Rev. B **72**, 115112.

Bhatt, R. N., and D. S. Fisher, 1992, Phys. Rev. Lett. **68**, 3072.

Bie, H., and A. Mar, 2009, J. Mater. Chem. **19**, 6225.

Böhm, A., R. Caspary, U. Habel, L. Pawlak, A. Zuber, F. Steglich, and A. Loidl, 1988, J. Magn. Magn. Mater. **76–77**, 150.

Bölling, F., 1968, Phys. kondens. Materie. **7**, 162.

Bonville, P., *et al.*, 1992, Physica (Amsterdam) **182B**, 105.

Borzi, R. A., S. A. Grigera, J. Farrell, R. S. Perry, S. J. S. Lister, S. L. Lee, D. A. Tennant, Y. Maeno, and A. P. Mackenzie, 2007, Science **315**, 214.

Bowden, G. J., D. S. P. Bunbury, and M. A. H. McCausland, 1971, J. Phys. C **4**, 1840.

Brando, M., W. J. Duncan, D. Moroni-Klementowicz, C. Albrecht, D. Gruner, R. Ballou, and F. M. Grosche, 2008, Phys. Rev. Lett. **101**, 026401.

Brando, M., T. Westerkamp, M. Deppe, P. Gegenwart, C. Geibel, and F. Steglich, 2010, J. Phys. Conf. Ser. **200**, 012016.

Bray, A. J., 1987, Phys. Rev. Lett. **59**, 586.

Bray, A. J., 1988, Phys. Rev. Lett. **60**, 720.

Bray, A. J., 1989, J. Phys. A **22**, L81.

Brazovskiĭ, S. A., 1975, Zh. Eksp. Teor. Fiz. **68**, 175 [Sov. Phys. JETP **41**, 85 (1975)].

Brinkman, W. F., and S. Engelsberg, 1968, Phys. Rev. **169**, 417.

Brüning, E. M., C. Krellner, M. Baenitz, A. Jesche, F. Steglich, and C. Geibel, 2008, Phys. Rev. Lett. **101**, 117206.

Burkov, A. A., and L. Balents, 2011, Phys. Rev. Lett. **107**, 127205.

Burkov, A. A., and A. H. MacDonald, 2002, Phys. Rev. B **66**, 115323.

Burlet, P., J. Rossat-Mignod, R. Troć, and Z. Henkie, 1981, Solid State Commun. **39**, 745.

Butch, N. P., and M. B. Maple, 2009, Phys. Rev. Lett. **103**, 076404.

Butch, N. P., and M. B. Maple, 2010, J. Phys. Condens. Matter **22**, 164204.

Butenko, A. V., D. N. Bol'shutkin, and V. I. Percherskaya, 1990, Zh. Eksp. Teor. Fiz. **98**, 1752 [Sov. Phys. JETP **71**, 983 (1990)].

Canepa, F., P. Manfrinetti, M. Pani, and A. Palenzona, 1996, J. Alloys Compd. **234**, 225.

Cao, G., S. K. McCall, J. E. Crow, and R. P. Guertin, 1997, Phys. Rev. B **56**, R5740.

Cao, H., S.-L. Yuan, J.-L. Shang, X.-L. Jiang, P. Li, Y.-Q. Wang, and L. Liu, 2006, Chin. Phys. Lett. **23**, 1176.

Cardy, J., 1996, *Scaling and Renormalization in Statistical Physics* (Cambridge University Press, Cambridge, England).

Carneiro, G. M., and C. J. Pethick, 1977, Phys. Rev. B **16**, 1933.

Case, M. J., and V. Dobrosavljević, 2007, Phys. Rev. Lett. **99**, 147204.

Casher, A., D. Lurié, and M. Revzen, 1968, J. Math. Phys. (N.Y.) **9**, 1312.

Castro Neto, A. H., G. Castilla, and B. A. Jones, 1998, Phys. Rev. Lett. **81**, 3531.

Ceperley, D. M., and B. J. Alder, 1980, Phys. Rev. Lett. **45**, 566.

Chaikin, P., and T. C. Lubensky, 1995, *Principles of Condensed Matter Physics* (Cambridge University, Cambridge, England).

Chakravarty, S., B. I. Halperin, and D. R. Nelson, 1989, Phys. Rev. B **39**, 2344.
Chang, C.-C., S. Zhang, and D. M. Ceperley, 2010, Phys. Rev. A **82**, 061603(R).
Chayes, J. T., L. Chayes, D. S. Fisher, and T. Spencer, 1986, Phys. Rev. Lett. **57**, 2999.
Chen, J. H., T. C. Lubensky, and D. R. Nelson, 1978, Phys. Rev. B **17**, 4274.
Chen, Y., D. L. Bergman, and A. A. Burkov, 2013, Phys. Rev. B **88**, 125110.
Chevalier, B., and B. Malaman, 2004, Solid State Commun. **130**, 711.
Chiao, M., C. Pfleiderer, S. R. Julian, G. G. Lonzarich, R. S. Perry, A. P. Mackenzie, and Y. Maeno, 2002, Physica B (Amsterdam) **312–313**, 698.
Chitov, G. Y., and A. J. Millis, 2001, Phys. Rev. B **64**, 054414.
Chuang, T. M., M. P. Allan, J. Lee, Y. Xie, N. Ni, S. L. Bud'ko, G. S. Boebinger, P. C. Canfield, and J. C. Davis, 2010, Science **327**, 181.
Chubukov, A., J. J. Betouras, and D. V. Efremov, 2014, Phys. Rev. Lett. **112**, 037202.
Chubukov, A., and D. Maslov, 2009, Phys. Rev. Lett. **103**, 216401.
Chubukov, A. V., C. Pépin, and J. Rech, 2004, Phys. Rev. Lett. **92**, 147003.
Colborne, S. G. W., and A. J. Bray, 1989, J. Phys. A **22**, 2505.
Colineau, E., F. Wastin, E. J. Higgins, and J. Rebizant, 2001, J. Alloys Compd. **317–318**, 336.
Colineau, E., F. Wastin, J. P. Sanchez, and J. Rebizant, 2008, J. Phys. Condens. Matter **20**, 075207.
Colombier, E., D. Braithwaite, G. Lapertot, B. Salce, and G. Knebel, 2009, Phys. Rev. B **79**, 245113.
Combier, T., 2013, "Ferromagnetic quantum criticality in the uranium-based ternary compounds URhSi, URhAl, and UCoAl," Ph.D. thesis (École doctorale de Physique Grenoble, France).
Combier, T., D. Aoki, G. Knebel, and J. Flouquet, 2013, J. Phys. Soc. Jpn. **82**, 104705.
Conduit, G. J., 2013, Phys. Rev. B **87**, 184414.
Conduit, G. J., A. G. Green, and B. D. Simons, 2009, Phys. Rev. Lett. **103**, 207201.
Crawford, M. K., R. L. Harlow, W. Marshall, Z. Li, G. Cao, R. L. Lindstrom, Q. Huang, and J. W. Lynn, 2002, Phys. Rev. B **65**, 214412.
Crook, M., and R. Cywinski, 1995, J. Magn. Magn. Mater. **140–144**, 71.
Cuervo-Reyes, E., and R. Nesper, 2014, Phys. Rev. B **90**, 064416.
Custers, J., P. Gegenwart, H. Wilhelm, K. Neumaier, Y. Tokiwa, O. Trovarelli, C. Geibel, F. Steglich, C. Pépin, and P. Coleman, 2003, Nature (London) **424**, 524.
Dalichaouch, Y., M. B. Maple, R. P. Guertin, M. V. Kuric, M. S. Torikachvili, and A. L. Giorgi, 1990, Physica (Amsterdam) **163B**, 113.
Daou, R., *et al.*, 2010, Nature (London) **463**, 519.
Das, A., S. Paranjpe, P. Raj, A. Satyamoorthy, K. Shashikala, and S. Malik, 2000, Solid State Commun. **114**, 87.
de Boer, F. R., C. J. Schinkel, J. Biesterbos, and S. Proost, 1969, J. Appl. Phys. **40**, 1049.
DeGennes, P. G., 1963, Solid State Commun. **1**, 132.
de la Cruz, C., *et al.*, 2010, Phys. Rev. Lett. **104**, 017204.
Dell'Anna, L., and W. Metzner, 2006, Phys. Rev. B **73**, 045127.
Demko, L., *et al.*, 2012, Phys. Rev. Lett. **108**, 185701.
de Moura, M. A., T. C. Lubensky, Y. Imry, and A. Aharony, 1976, Phys. Rev. B **13**, 2176.
De Poortere, E. P., E. Tutuc, and M. Shayegan, 2003, Phys. Rev. Lett. **91**, 216802.
Deppe, M., P. Pedrazzini, N. Caroca-Canales, C. Geibel, and J. G. Sereni, 2006, Physica B (Amsterdam) **378–380**, 96.
Députier, S., O. Peña, T. L. Bihan, J. Pivan, and R. Guérin, 1997, Physica (Amsterdam) **233B**, 26.
Dobrosavljević, V., and E. Miranda, 2005, Phys. Rev. Lett. **94**, 187203.
Doniach, S., and S. Engelsberg, 1966, Phys. Rev. Lett. **17**, 750.
Donsker, M., and S. R. S. Varadhan, 1975, Commun. Pure Appl. Math. **28**, 525.
Donsker, M., and S. R. S. Varadhan, 1979, Commun. Pure Appl. Math. **32**, 721.
Dotsenko, V., 2006, J. Stat. Phys. **122**, 197.
Drichko, I. L., I. Y. Smirnov, A. V. Suslov, O. A. Mironov, and D. R. Leadley, 2012, J. Phys. Conf. Ser. **400**, 042005.
Drotziger, S., C. Pfleiderer, M. Uhlarz, H. v. Löhneysen, D. Souptel, W. Löset, and G. Behr, 2006, Phys. Rev. B **73**, 214413.
Duine, R. A., and A. H. MacDonald, 2005, Phys. Rev. Lett. **95**, 230403.
Duncan, W. J., *et al.*, 2010, Phys. Status Solidi (b) **247**, 544.
Edwards, D. M., and E. P. Wohlfarth, 1968, Proc. R. Soc. A **303**, 127.
Edwards, S. F., and P. W. Anderson, 1975, J. Phys. F **5**, 965.
Efetov, K. B., A. I. Larkin, and D. E. Khmelnitskii, 1980, Zh. Eksp. Teor. Fiz. **79**, 1120 [Sov. Phys. JETP **52**, 568 (1980)].
Efremov, D. V., J. J. Betouras, and A. Chubukov, 2008, Phys. Rev. B **77**, 220401.
Eisert, J., M. Cramer, and M. B. Plenio, 2010, Rev. Mod. Phys. **82**, 277.
Eriksson, O., B. Johansson, and M. S. S. Brooks, 1989, J. Phys. Condens. Matter **1**, 4005.
Evers, F., and A. D. Mirlin, 2008, Rev. Mod. Phys. **80**, 1355.
Fernandez-Pañella, A., D. Braithwaite, B. Salce, G. Lapertot, and J. Flouquet, 2011, Phys. Rev. B **84**, 134416.
Ferrell, R. A., N. Menyhard, H. Schmidt, F. Schwabl, and P. Szepfalusy, 1967, Phys. Rev. Lett. **18**, 891.
Ferrell, R. A., N. Menyhard, H. Schmidt, F. Schwabl, and P. Szepfalusy, 1968, Ann. Phys. (N.Y.) **47**, 565.
Finkelstein, A. M., 1983, Zh. Eksp. Teor. Fiz. **84**, 168 [Sov. Phys. JETP **57**, 97 (1983)].
Finkelstein, A. M., 1984, Zh. Eksp. Teor. Fiz. **86**, 367 [Sov. Phys. JETP **59**, 212 (1984)].
Finkelstein, A. M., 2010, in *50 Year of Anderson Localization*, edited by E. Abrahams (World Scientific, Singapore), p. 385.
Fisher, D. S., 1992, Phys. Rev. Lett. **69**, 534.
Fisher, D. S., 1995, Phys. Rev. B **51**, 6411.
Fisher, M. E., 1964, J. Math. Phys. (N.Y.) **5**, 944.
Fisher, M. E., 1983, in *Advanced Course on Critical Phenomena*, edited by F. W. Hahne (Springer, Berlin), p. 1.
Fisher, M. E., and A. N. Berker, 1982, Phys. Rev. B **26**, 2507.
Fixman, M., 1962, J. Chem. Phys. **36**, 310.
Flouquet, J., D. Aoki, W. Knafo, G. Knebel, T. D. Matsuda, S. Raymond, C. Proust, C. Paulsen, and P. Haen, 2010, J. Low Temp. Phys. **161**, 83.
Flouquet, J., P. Haen, S. Raymond, D. Aoki, and G. Knebel, 2002, Physica (Amsterdam) **319B**, 251.
Fluitman, J. H. J., R. Boom, P. F. De Chatel, C. J. Schinkel, J. L. L. Tilanus, and B. R. de Vries, 1973, J. Phys. F **3**, 109.
Fontes, M., M. Continentino, S. Bud'ko, M. El-Massalami, L. Sampaio, A. Guimarães, E. Baggio-Saitovitch, M. Hundley, and A. Lacerda, 1996, Phys. Rev. B **53**, 11678.
Forster, D., 1975, *Hydrodynamic Fluctuations, Broken Symmetry, and Correlation Functions* (Benjamin, Reading, MA).
Fradkin, E., 1991, *Field Theories of Condensed Matter Systems* (Addison Wesley, New York).

Fradkin, E., S. A. Kivelson, M. J. Lawler, J. P. Eisenstein, and A. P. Mackenzie, 2010, Annu. Rev. Condens. Matter Phys. **1**, 153.
Franz, C., C. Pfleiderer, A. Neubauer, M. Schulz, B. Pedersen, and P. Böni, 2010, J. Phys. Conf. Ser. **200**, 012036.
Friedemann, S., 2015 (private communication).
Friedemann, S., M. Brando, W. J. Duncan, A. Neubauer, C. Pfleiderer, and F. M. Grosche, 2013, Phys. Rev. B **87**, 024410.
Fujimori, S., *et al.*, 2012, J. Phys. Soc. Jpn. **81**, 014703.
Fulde, P., and R. A. Ferrell, 1964, Phys. Rev. **135**, A550.
Gagel, P., P. P. Orth, and J. Schmalian, 2014, Phys. Rev. Lett. **113**, 220401.
Galitski, V. M., A. V. Chubukov, and S. Das Sarma, 2005, Phys. Rev. B **71**, 201302.
Gegenwart, P., J. Custers, C. Geibel, K. Neumaier, T. Tayama, K. Tenya, O. Trovarelli, and F. Steglich, 2002, Phys. Rev. Lett. **89**, 056402.
Gegenwart, P., J. Custers, Y. Tokiwa, C. Geibel, and F. Steglich, 2005, Phys. Rev. Lett. **94**, 076402.
Gegenwart, P., Q. Si, and F. Steglich, 2008, Nat. Phys. **4**, 186.
Gegenwart, P., F. Steglich, C. Geibel, and M. Brando, 2015, Eur. Phys. J. Spec. Top. **224**, 975.
Gehring, G. A., 2008, Europhys. Lett. **82**, 60004.
Gehring, G. A., and M. R. Ahmed, 2010, J. Appl. Phys. **107**, 09E125.
Geibel, C., C. Kämmerer, E. Göring, R. Moog, G. Sparn, R. Henseleit, G. Cordier, S. Horn, and F. Steglich, 1990, J. Magn. Magn. Mater. **90–91**, 435.
Giorgi, A. L., B. T. Matthias, G. R. Stewart, F. Acker, and J. L. Smith, 1979, Solid State Commun. **32**, 455.
Goldstone, J., 1961, Nuovo Cimento **19**, 154.
Goto, T., K. Fukamichi, and H. Yamada, 2001, Physica (Amsterdam) **300B**, 167.
Goto, T., Y. Shindo, H. Takahashi, and S. Ogawa, 1997, Phys. Rev. B **56**, 14019.
Grange, W., M. Finazzi, J. P. Kappler, A. Delobbe, G. Krill, P. Sainctavit, J. P. Sanchez, A. Rogalev, and J. Goulon, 1998, J. Alloys Compd. **275–277**, 583.
Grassberger, P., and I. Procaccia, 1982, J. Chem. Phys. **77**, 6281.
Green, A. G., S. A. Grigera, R. A. Borzi, A. P. Mackenzie, R. S. Perry, and B. D. Simons, 2005, Phys. Rev. Lett. **95**, 086402.
Griffiths, R. B., 1969, Phys. Rev. Lett. **23**, 17.
Griffiths, R. B., 1970, Phys. Rev. Lett. **24**, 715.
Griffiths, R. B., 1973, Phys. Rev. B **7**, 545.
Grigera, S. A., R. A. Borzi, A. P. Mackenzie, S. R. Julian, R. S. Perry, and Y. Maeno, 2003, Phys. Rev. B **67**, 214427.
Grigera, S. A., R. S. Perry, A. J. Schofield, M. Chiao, S. R. Julian, G. G. Lonzarich, S. I. Ikeda, Y. Maeno, A. J. Millis, and A. P. Mackenzie, 2001, Science **294**, 329.
Grigera, S. A., *et al.*, 2004, Science **306**, 1154.
Grinstein, G., 1985, in *Fundamental Problems in Statistical Mechanics VI*, edited by E. G. D. Cohen (Elsevier, New York), p. 147.
Grosche, F., S. Julian, N. Mathur, and G. Lonzarich, 1996, Physica B (Amsterdam) **223–224**, 50.
Grosche, M., C. Pfleiderer, G. J. McMullan, G. G. Lonzarich, and N. R. Bernhoeft, 1995, Physica B (Amsterdam) **206–207**, 20.
Guo, M., R. N. Bhatt, and D. A. Huse, 1996, Phys. Rev. B **54**, 3336.
Guo, S., D. P. Young, R. T. Macaluso, D. A. Browne, N. L. Henderson, J. Y. Chan, L. L. Henry, and J. F. DiTusa, 2008, Phys. Rev. Lett. **100**, 017209.
Haen, P., H. Bioud, and T. Fukuhara, 1999, Physica B (Amsterdam) **259–261**, 85.
Haldane, F. D. M., 2004, Phys. Rev. Lett. **93**, 206602.
Halperin, B. I., and P. C. Hohenberg, 1967, Phys. Rev. Lett. **19**, 700.
Halperin, B. I., and P. C. Hohenberg, 1969, Phys. Rev. **177**, 952.
Halperin, B. I., T. C. Lubensky, and S.-K. Ma, 1974, Phys. Rev. Lett. **32**, 292.
Hamann, S., 2015 (private communication).
Harris, A. B., 1974, J. Phys. C **7**, 1671.
Hasan, M. Z., and C. L. Kane, 2010, Rev. Mod. Phys. **82**, 3045.
Hassinger, E., D. Aoki, G. Knebel, and J. Flouquet, 2008, J. Phys. Soc. Jpn. **77**, 073703.
Hattori, T., K. Ishida, Y. Nakai, T. Ohta, K. Deguchi, N. K. Sato, and I. Satoh, 2010, Physica (Amsterdam) **470C**, S561.
Havela, L., A. Andreev, V. Sechovský, I. Kozlovskaya, K. Prokeš, P. Javorský, M. Bartashevich, T. Goto, and K. Kamishima, 1997, Physica B (Amsterdam) **230–232**, 98.
Hayden, S. M., G. G. Lonzarich, and H. L. Skriver, 1986, Phys. Rev. B **33**, 4977.
Heimbrecht, M., M. Zumbusch, and W. Biltz, 1941, Z. Anorg. Allg. Chem. **245**, 391.
Hertz, J., 1976, Phys. Rev. B **14**, 1165.
Hidaka, H., S. Takahashi, Y. Shimizu, T. Yanagisawa, and H. Amitsuka, 2011, J. Phys. Soc. Jpn. **80**, SA102.
Hiess, A., L. Havela, K. Prokes, R. S. Eccleston, and G. H. Lander, 1997, Physica B (Amsterdam) **230–232**, 89.
Hill, H. H., 1970, *Plutonium and Other Actinides* (McGraw-Hill, New York).
Hiraka, H., and Y. Endoh, 1996, J. Phys. Soc. Jpn. **65**, 3740.
Hohenberg, P. C., and B. I. Halperin, 1977, Rev. Mod. Phys. **49**, 435.
Holt, B., J. Ramsden, H. Sample, and J. Huber, 1981, Physica (Amsterdam) **107B+C**, 255.
Hornreich, R. M., M. Luban, and S. Shtrikman, 1975, Phys. Rev. Lett. **35**, 1678.
Hossain, Z., C. Geibel, F. Weickert, T. Radu, Y. Tokiwa, H. Jeevan, P. Gegenwart, and F. Steglich, 2005, Phys. Rev. B **72**, 094411.
Hoyos, J. A., and T. Vojta, 2007, Phys. Rev. B **75**, 104418.
Huang, C. L., D. Fuchs, M. Wissinger, R. Schneider, M. C. Ling, M. S. Scheurer, J. Schmalian, and H. v. Löhneysen, 2015, Nat. Commun. **6**, 8188.
Huang, K., J. J. Hamlin, R. E. Baumbach, M. Janoschek, N. Kanchanavatee, D. A. Zocco, F. Ronning, and M. B. Maple, 2013, Phys. Rev. B **87**, 054513.
Huber, J. G., M. B. Maple, and D. Wohlleben, 1975, Solid State Commun. **16**, 211.
Huesges, Z., O. Stockert, M. M. Koza, C. Krellner, C. Geibel, and F. Steglich, 2013, Phys. Status Solidi (b) **250**, 522.
Hulliger, F., 1993, J. Alloys Compd. **196**, 225.
Huxley, A., I. Sheikin, and D. Braithwaite, 2000, Physica B (Amsterdam) **284–288**, 1277.
Huxley, A., I. Sheikin, E. Ressouche, N. Kernavanois, D. Braithwaite, R. Calemczuk, and J. Flouquet, 2001, Phys. Rev. B **63**, 144519.
Huxley, A., S. J. C. Yates, F. Lévy, and I. Sheikin, 2007, J. Phys. Soc. Jpn. **76**, 051011.
Huy, N. T., A. Gasparini, D. E. de Nijs, Y. Huang, J. C. P. Klaasse, T. Gortenmulder, A. de Visser, A. Hamann, T. Görlach, and H. v. Löhneysen, 2007, Phys. Rev. Lett. **99**, 067006.
Huy, N. T., A. Gasparini, J. C. P. Klaasse, A. de Visser, S. Sakarya, and N. H. van Dijk, 2007, Phys. Rev. B **75**, 212405.
Ikeda, K., 1987, J. Appl. Phys. **62**, 4499.
Ikeda, S.-I., Y. Maeno, S. Nakatsuji, M. Kosaka, and Y. Uwatoko, 2000, Phys. Rev. B **62**, R6089.
Ikeda, S.-I., N. Shirakawa, S. Koiwai, A. Uchida, M. Kosaka, and Y. Uwatoko, 2001, Physica C (Amsterdam) **364–365**, 376.
Ikeda, S.-I., N. Shirakawa, T. Yanagisawa, Y. Yoshida, S. Koikegami, S. Koike, M. Kosaka, and Y. Uwatoko, 2004, J. Phys. Soc. Jpn. **73**, 1322.

Imry, Y., 1974, Phys. Rev. Lett. **33**, 1304.
Ishida, K., *et al.*, 2003, Phys. Rev. B **68**, 184401.
Ishii, Y., M. Kosaka, Y. Uwatoko, A. Andreev, and V. Sechovský, 2003, Physica (Amsterdam) **334B**, 160.
Ishikawa, Y., Y. Noda, C. Fincher, and G. Shirane, 1982, Phys. Rev. B **25**, 254.
Ishikawa, Y., Y. Noda, Y. J. Uemura, C. F. Majkrzak, and G. Shirane, 1985, Phys. Rev. B **31**, 5884.
Ishikawa, Y., K. Tajima, D. Bloch, and M. Roth, 1976, Solid State Commun. **19**, 525.
Ising, E., 1925, Z. Phys. **31**, 253.
Itoh, M., I. Natori, S. Kubota, and K. Motoya, 1994, J. Phys. Soc. Jpn. **63**, 1486.
Itoh, Y., T. Mizoguchi, and K. Yoshimura, 2008, J. Phys. Soc. Jpn. **77**, 123702.
Jain, S., 1995, Physica (Amsterdam) **218A**, 279.
Janoschek, M., M. Garst, A. Bauer, P. Krautscheid, R. Georgii, P. Böni, and C. Pfleiderer, 2013, Phys. Rev. B **87**, 134407.
Jarrett, H. S., W. H. Cloud, R. J. Bouchard, S. R. Butler, C. G. Frederick, and J. L. Gillson, 1968, Phys. Rev. Lett. **21**, 617.
Javorský, P., V. Sechovský, J. Schweizer, F. Bourdarot, E. Lelièvre-Berna, A. V. Andreev, and Y. Shiokawa, 2001, Phys. Rev. B **63**, 064423.
Jeong, T., and Y. Kwon, 2007, J. Korean Phys. Soc. **51**, 629.
Jeong, T., A. Kyker, and W. E. Pickett, 2006, Phys. Rev. B **73**, 115106.
Jesche, A., 2011, "3*d*- und 4*f* -Korrelationen in quaternären Eisenpniktiden: der Sonderfall $CeFeAs_{1-x}P_xO$," Ph.D. thesis (Technical University of Dresden, Germany).
Jesche, A., T. Balle, K. Kliemt, C. Geibel, M. Brando, and C. Krellner, 2016, arXiv:1605.03515.
Jesche, A., *et al.*, 2012, Phys. Rev. B **86**, 020501.
Jia, S., P. Jiramongkolchai, M. R. Suchomel, B. H. Toby, J. G. Checkelsky, N. P. Ong, and R. J. Cava, 2011, Nat. Phys. **7**, 207.
Jo, G.-B., Y.-R. Lee, J.-H. Choi, C. A. Christensen, T. H. Kim, J. H. Thywissen, D. E. Pritchard, and W. Ketterle, 2009, Science **325**, 1521.
Joyce, G. S., 1969, J. Phys. C **2**, 1531.
Jungwirth, T., J. Sinova, J. Mašek, J. Kučera, and A. H. MacDonald, 2006, Rev. Mod. Phys. **78**, 809.
Kabeya, N., R. Iijima, E. Osaki, S. Ban, K. Imura, K. Deguchi, N. Aso, Y. Homma, Y. Shiokawa, and N. K. Sato, 2010, J. Phys. Conf. Ser. **200**, 032028.
Kabeya, N., H. Maekawa, K. Deguchi, N. Kimura, H. Aoki, and N. K. Sato, 2012, J. Phys. Soc. Jpn. **81**, 073706.
Kabeya, N., H. Maekawa, K. Deguchi, N. Kimura, H. Aoki, and N. K. Sato, 2013, Phys. Status Solidi (b) **250**, 654.
Kaczorowski, D., 1996, Solid State Commun. **99**, 949.
Kadanoff, L. P., and J. Swift, 1968, Phys. Rev. **166**, 89.
Kamihara, Y., H. Hiramatsu, M. Hirano, R. Kawamura, H. Yanagi, T. Kamiya, and H. Hosono, 2006, J. Am. Chem. Soc. **128**, 10012.
Kanbayasi, A., 1978, J. Phys. Soc. Jpn. **44**, 108.
Kappler, J. P., M. J. Besnus, A. Herr, A. Meyer, and J. G. Sereni, 1991, Physica (Amsterdam) **171B**, 346.
Kappler, J.-P., M. J. Besnus, P. Haen, and J. Sereni, 1997, Physica B (Amsterdam) **230–232**, 162.
Karahasanovic, U., F. Krüger, and A. G. Green, 2012, Phys. Rev. B **85**, 165111.
Karube, K., T. Hattori, K. Ishida, and N. Kimura, 2015, Phys. Rev. B **91**, 075131.
Karube, K., T. Hattori, S. Kitagawa, K. Ishida, N. Kimura, and T. Komatsubara, 2012, Phys. Rev. B **86**, 024428.
Kawasaki, I., D. Nishikawa, H. Hidaka, T. Yanagisawa, K. Tenya, M. Yokoyama, and H. Amitsuka, 2009, Physica (Amsterdam) **404B**, 2908.
Kawasaki, I., K. Tenya, M. Yokoyama, and H. Amitsuka, 2008, Physica (Amsterdam) **403B**, 1284.
Kawasaki, K., 1967, J. Phys. Chem. Solids **28**, 1277.
Kawasaki, K., 1970, Ann. Phys. (N.Y.) **61**, 1.
Kawasaki, K., 1976, in *Phase Transitions and Critical Phenomena*, Vol. 5a, edited by C. Domb, and M. S. Green (Academic, New York), p. 165.
Kayser, R. F., and J. B. Hubbard, 1983, Phys. Rev. Lett. **51**, 79.
Kerkau, A., L. Wu, K. Park, Y. Prots, M. Brando, M. C. Aronson, and G. Kreiner, 2012, Z. Kristallogr. **227**, 289.
Khuntia, P., P. Peratheepan, A. M. Strydom, Y. Utsumi, K.-T. Ko, D.-D. Tsuei, lL. H. Tjeng, F. Steglich, and M. Baenitz, 2014, Phys. Rev. Lett. **113**, 216403.
Khuntia, P., A. M. Strydom, L. S. Wu, M. C. Aronson, F. Steglich, and M. Baenitz, 2012, Phys. Rev. B **86**, 220401.
Kim, D., B. L. Zink, F. Hellman, S. McCall, G. Cao, and J. E. Crow, 2003, Phys. Rev. B **67**, 100406.
Kimura, N., M. Endo, T. Isshiki, S. Minagawa, A. Ochiai, H. Aoki, T. Terashima, S. Uji, T. Matsumoto, and G. G. Lonzarich, 2004, Phys. Rev. Lett. **92**, 197002.
Kirkpatrick, T. R., and D. Belitz, 1996, Phys. Rev. B **53**, 14364.
Kirkpatrick, T. R., and D. Belitz, 2010, Phys. Rev. Lett. **104**, 256404.
Kirkpatrick, T. R., and D. Belitz, 2011, Phys. Rev. Lett. **106**, 105701.
Kirkpatrick, T. R., and D. Belitz, 2012a, Phys. Rev. B **85**, 134451.
Kirkpatrick, T. R., and D. Belitz, 2012b, Phys. Rev. Lett. **108**, 086404.
Kirkpatrick, T. R., and D. Belitz, 2014, Phys. Rev. Lett. **113**, 127203.
Kirkpatrick, T. R., and D. Belitz, 2015a, Phys. Rev. B **91**, 214407.
Kirkpatrick, T. R., and D. Belitz, 2015b, Phys. Rev. Lett. **115**, 020402.
Kitagawa, S., H. Ikeda, Y. Nakai, T. Hattori, K. Ishida, Y. Kamihara, M. Hirano, and H. Hosono, 2011, Phys. Rev. Lett. **107**, 277002.
Kitagawa, S., K. Ishida, T. Nakamura, M. Matoba, and Y. Kamihara, 2012, Phys. Rev. Lett. **109**, 227004.
Kitagawa, S., K. Ishida, T. Nakamura, M. Matoba, and Y. Kamihara, 2013, J. Phys. Soc. Jpn. **82**, 033704.
Kitagawa, S., H. Kotegawa, H. Tou, R. Yamauchi, E. Matsuoka, and H. Sugawara, 2014, Phys. Rev. B **90**, 134406.
Kitazawa, H., A. Dönni, L. Keller, J. Tang, F. Fauth, and G. Kido, 1998, J. Solid State Chem. **140**, 233.
Kittler, W., V. Fritsch, F. Weber, G. Fischer, D. Lamago, G. André, and H. v. Löhneysen, 2013, Phys. Rev. B **88**, 165123.
Kiyama, T., K. Yoshimura, K. Kosuge, H. Mitamura, and T. Goto, 1999, J. Phys. Soc. Jpn. **68**, 3372.
Klingner, C., *et al.*, 2011, Phys. Rev. B **83**, 144405.
Knebel, G., *et al.*, 2006, J. Phys. Soc. Jpn. **75**, 114709.
Kobayashi, T., S. Fukushima, H. Hidaka, H. Kotegawa, T. Akazawa, E. Yamamoto, Y. Haga, R. Settai, and Y. Ōnuki, 2006, Physica B (Amsterdam) **378–380**, 355.
Kobayashi, T., T. Miyazu, K. Shimizu, K. Amaya, Y. Kitaoka, Y. Ōnuki, M. Shirase, and T. Takabatake, 1998, Phys. Rev. B **57**, 5025.
Kobayashi, T. C., *et al.*, 2007, J. Phys. Condens. Matter **19**, 125205.
Koelling, D. D., B. D. Dunlap, and G. W. Crabtree, 1985, Phys. Rev. B **31**, 4966.
Köhler, U., N. Oeschler, F. Steglich, S. Maquilon, and Z. Fisk, 2008, Phys. Rev. B **77**, 104412.
Kohori, Y., Y. Noguchi, T. Kohara, Y. Dalichaouch, M. A. Lopez de la Torre, and M. B. Maple, 1993, Physica B (Amsterdam) **186–188**, 792.

Kopp, A., X. Jia, and S. Chakravarty, 2007, Ann. Phys. (N.Y.) **322**, 1466.
Kotegawa, H., V. Taufour, D. Aoki, G. Knebel, and J. Flouquet, 2011, J. Phys. Soc. Jpn. **80**, 083703.
Kotegawa, H., T. Toyama, S. Kitagawa, H. Tou, R. Yamauchi, E. Matsuoka, and H. Sugawara, 2013, J. Phys. Soc. Jpn. **82**, 123711.
Kotegawa, H., *et al.*, 2011, Phys. Rev. B **84**, 054524.
Kramer, B., and A. MacKinnon, 1993, Rep. Prog. Phys. **56**, 1469.
Krellner, C., and C. Geibel, 2008, J. Cryst. Growth **310**, 1875.
Krellner, C., and C. Geibel, 2012, J. Phys. Conf. Ser. **391**, 012032.
Krellner, C., S. Hartmann, A. Pikul, N. Oeschler, J. G. Donath, C. Geibel, F. Steglich, and J. Wosnitza, 2009, Phys. Rev. Lett. **102**, 196402.
Krellner, C., N. S. Kini, E. M. Brüning, K. Koch, H. Rosner, M. Nicklas, M. Baenitz, and C. Geibel, 2007, Phys. Rev. B **76**, 104418.
Krellner, C., S. Lausberg, A. Steppke, M. Brando, L. Pedrero, H. Pfau, S. Tencé, H. Rosner, F. Steglich, and C. Geibel, 2011, New J. Phys. **13**, 103014.
Krishnamurthy, V. V., D. T. Adroja, N. P. Butch, S. K. Sinha, M. B. Maple, R. Osborn, J. L. Robertson, S. E. Nagler, and M. C. Aronson, 2008, Phys. Rev. B **78**, 024413.
Krüger, F., C. J. Pedder, and A. G. Green, 2014, Phys. Rev. Lett. **113**, 147001.
Kučera, M., P. Beránková, M. Matyáš, I. Tichý, and A. A. Menovsky, 1998, J. Alloys Compd. **271–273**, 467.
Küchler, R., P. Gegenwart, F. Weickert, N. Oeschler, T. Cichorek, M. Nicklas, N. Carocca-Canales, C. Geibel, and F. Steglich, 2006, Physica B (Amsterdam) **378–380**, 36.
Küchler, R., *et al.*, 2003, Phys. Rev. Lett. **91**, 066405.
Kuneš, J., P. Nov'ak, M. Diviš, and P. M. Oppeneer, 2001, Phys. Rev. B **63**, 205111.
Landau, L. D., and E. M. Lifshitz, 1980, *Statistical Physics Part 1* (Butterworth Heinemann, Oxford).
Larkin, A. I., and Y. N. Ovchinnikov, 1964, Zh. Eksp. Teor. Fiz. **47**, 1136 [Sov. Phys. JETP **20**, 762 (1965)].
Larkin, A. I., and S. A. Pikin, 1969, Zh. Eksp. Teor. Fiz. **56**, 1664 [Sov. Phys. JETP **29**, 891 (1969)].
Larrea, J., M. B. Fontes, A. D. Alvarenga, and E. M. Baggio-Saitovitch, 2005, Phys. Rev. B **72**, 035129.
Lausberg, S., *et al.*, 2012, Phys. Rev. Lett. **109**, 216402.
Lausberg, S., *et al.*, 2013, Phys. Rev. Lett. **110**, 256402.
Lee, K., B. Fallahazad, J. Xue, D. C. Dillen, K. Kim, T. Taniguchi, K. Watanabe, and E. Tutuc, 2014, Science **345**, 58.
Lee, P. A., and T. V. Ramakrishnan, 1985, Rev. Mod. Phys. **57**, 287.
Lee, S.-S., 2009, Phys. Rev. B **80**, 165102.
Lengyel, E., M. E. Macovei, A. Jesche, C. Krellner, C. Geibel, and M. Nicklas, 2015, Phys. Rev. B **91**, 035130.
Lenkewitz, M., S. Corsepius, G. Blanckenhagen, and G. R. Stewart, 1997, Phys. Rev. B **55**, 6409.
Lester, C., S. Ramos, R. S. Perry, T. P. Croft, R. I. Bewley, T. Guidi, P. Manuel, D. D. Khalyavin, E. M. Forgan, and S. M. Hayden, 2015, Nat. Mater. **14**, 373.
Levy, F., L. Sheikin, B. Grenier, and A. D. Huxley, 2005, Science **309**, 1343.
Lifshitz, E. M., and L. P. Pitaevskii, 1981, *Physical Kinetics* (Butterworth-Heinemann, Oxford) Chap. 30.
Lifshitz, E. M., and L. P. Pitaevskii, 1991, *Statistical Physics, Part 2* (Pergamon, Oxford).
Lifshitz, I. M., 1964, Usp. Fiz. Nauk **83**, 617 [Sov. Phys. Usp. **7**, 549 (1965)].
Lin, X., V. Taufour, S. L. Bud'ko, and P. C. Canfield, 2013, Phys. Rev. B **88**, 094405.
Logg, P., Z. Feng, T. Ebihara, Y. Zou, S. Friedemann, P. Alireza, S. Goh, and F. M. Grosche, 2013, Phys. Status Solidi (b) **250**, 515.
Lonzarich, G. G., 1997, in *Electron*, edited by M. Springford (Cambridge University Press, Cambridge, England), p. 109.
Lonzarich, G. G., and L. Taillefer, 1985, J. Phys. C **18**, 4339.
Lopatnikova, A., S. H. Simon, and E. Demler, 2004, Phys. Rev. B **70**, 115325.
Luo, Y., Y. Li, S. Jiang, J. Dai, G. Cao, and Z.-a. Xu, 2010, Phys. Rev. B **81**, 134422.
Ma, S.-K., 1976, *Modern Theory of Critical Phenomena* (Benjamin, Reading, MA).
Mackenzie, A. P., and S. A. Grigera, 2004, J. Low Temp. Phys. **135**, 39.
Macovei, M., 2010, "Magnetism in Yb- and C-based heavy-fermion metals under pressure," Ph.D. thesis (Technical University of Dresden, Germany).
Macovei, M., M. Nicklas, C. Krellner, C. Geibel, and F. Steglich, 2009, Physica (Amsterdam) **404B**, 2934.
Macovei, M. E., M. Nicklas, C. Krellner, C. Geibel, and F. Steglich, 2008, J. Phys. Condens. Matter **20**, 505205.
Makoshi, K., and T. Moriya, 1975, J. Phys. Soc. Jpn. **38**, 10.
Manfrinetti, P., S. Dhar, R. Kulkarni, and A. Morozkin, 2005, Solid State Commun. **135**, 444.
Marcano, N., J. C. Gómez Sal, J. I. Espeso, J. M. De Teresa, P. A. Algarabel, C. Paulsen, and J. R. Iglesias, 2007, Phys. Rev. Lett. **98**, 166406.
Maslov, D., and A. V. Chubukov, 2009, Phys. Rev. B **79**, 075112.
Maslov, D., A. V. Chubukov, and R. Saha, 2006, Phys. Rev. B **74**, 220402.
Mathon, J., 1968, Proc. R. Soc. A **306**, 355.
Mathur, N. D., F. M. Grosche, S. R. Julian, I. R. Walker, D. M. Freye, R. K. W. Haselwimmer, and G. G. Lonzarich, 1998, Nature (London) **394**, 39.
Matthias, B. T., and R. M. Bozorth, 1958, Phys. Rev. **109**, 604.
Mazin, I. I., 2000, Appl. Phys. Lett. **77**, 3000.
McCoy, B., 1969, Phys. Rev. **188**, 1014.
McCoy, B., 1970, Phys. Rev. B **2**, 2795.
McCoy, B., and T. T. Wu, 1968, Phys. Rev. **176**, 631.
McCoy, B., and T. T. Wu, 1969, Phys. Rev. **188**, 982.
McKane, A. J., and M. Stone, 1981, Ann. Phys. (N.Y.) **131**, 36.
Mederle, S., R. Borth, C. Geibel, F. M. Grosche, G. Sparn, O. Trovarelli, and F. Steglich, 2001, J. Magn. Magn. Mater. **226–230**, 254.
Metliski, M., and S. Sachdev, 2010, Phys. Rev. B **82**, 075127.
Millis, A. J., 1993, Phys. Rev. B **48**, 7183.
Millis, A. J., D. K. Morr, and J. Schmalian, 2002, Phys. Rev. B **66**, 174433.
Millis, A. J., A. J. Schofield, G. G. Lonzarich, and S. A. Grigera, 2002, Phys. Rev. Lett. **88**, 217204.
Milovanovich, M., S. Sachdev, and R. N. Bhatt, 1989, Phys. Rev. Lett. **63**, 82.
Mineev, V. P., 2011, C.R. Phys. **12**, 567.
Misawa, S., 1971, Phys. Rev. Lett. **26**, 1632.
Mitra, A., and A. J. Millis, 2008, Phys. Rev. B **77**, 220404(R).
Mitra, A., S. Takei, Y. B. Kim, and A. J. Millis, 2006, Phys. Rev. Lett. **97**, 236808.
Miwa, H., and K. Yosida, 1961, Prog. Theor. Phys. **26**, 693.
Miyake, A., D. Aoki, and J. Flouquet, 2009, J. Phys. Soc. Jpn. **78**, 063703.
Mizutani, U., K. Sato, I. Sakamoto, and K. Yonemitsu, 1988, J. Phys. F **18**, 1995.
Moriya, T., 1985, *Spin Fluctuations in Itinerant Electron Magnetism* (Springer, Berlin).

Moriya, T., and A. Kawabata, 1973, J. Phys. Soc. Jpn. **34**, 639.
Moroni-Klementowicz, D., M. Brando, C. Albrecht, W. J. Duncan, F. M. Grosche, D. Grüner, and G. Kreiner, 2009, Phys. Rev. B **79**, 224410.
Motrunich, O., S.-C. Mau, D. A. Huse, and D. S. Fisher, 2000, Phys. Rev. B **61**, 1160.
Mühlbauer, S., B. Binz, F. Jonietz, C. Pfleiderer, A. Rosch, A. Neubauer, R. Georgii, and P. Böni, 2009, Science **323**, 915.
Mukherjee, K., K. K. Iyer, and E. V. Sampathkumaran, 2012, J. Phys. Condens. Matter **24**, 096006.
Murani, A. P., A. Tari, and B. R. Coles, 1974, J. Phys. F **4**, 1769.
Murata, K. K., and S. Doniach, 1972, Phys. Rev. Lett. **29**, 285.
Mushnikov, N. V., T. Goto, K. Kamishima, H. Yamada, A. V. Andreev, Y. Shiokawa, A. Iwao, and V. Sechovsky, 1999, Phys. Rev. B **59**, 6877.
Mydosh, J. A., 1993, *Spin Glasses—An Experimental Introduction* (Taylor and Francis, London).
Mydosh, J. A., and P. M. Oppeneer, 2011, Rev. Mod. Phys. **83**, 1301.
Nattermann, T., 1977, J. Phys. A **10**, 1757.
Neal, B. P., E. R. Ylvisaker, and W. E. Pickett, 2011, Phys. Rev. B **84**, 085133.
Negele, J. W., and H. Orland, 1988, *Quantum Many-Particle Systems* (Addison-Wesley, New York).
Nicklas, M., 2000, "Nicht-Fermi-Flüssigkeitsverhalten am quantenkritischen Punkt in Nickel-Palladium," Ph.D. thesis (University of Augsburg, Germany).
Nicklas, M., M. Brando, G. Knebel, F. Mayr, W. Trinkl, and A. Loidl, 1999, Phys. Rev. Lett. **82**, 4268.
Nienhuis, B., and M. Nauenberg, 1975, Phys. Rev. Lett. **35**, 477.
Niklowitz, P., 2015 (private communication).
Niklowitz, P. G., F. Beckers, G. G. Lonzarich, G. Knebel, B. Salce, J. Thomasson, N. Bernhoeft, D. Braithwaite, and J. Flouquet, 2005, Phys. Rev. B **72**, 024424.
Nozadze, D., and T. Vojta, 2012, Phys. Rev. B **85**, 174202.
Oganesyan, V., S. A. Kivelson, and E. Fradkin, 2001, Phys. Rev. B **64**, 195109.
Otero-Leal, M., F. Rivadulla, M. García-Hernández, A.Piñeiro, V. Pardo, D. Badomir, and J. Rivas, 2008, Phys. Rev. B **78**, 180415.
Otero-Leal, M., F. Rivadulla, S. S. Saxena, K. Ahilan, and J. Rivas, 2009a, Phys. Rev. B **79**, 060401.
Otero-Leal, M., F. Rivadulla, S. S. Saxena, K. Ahilan, and J. Rivas, 2009b, Phys. Rev. B **80**, 136402.
Paixao, J. A., G. H. Lander, P. J. Brown, H. Nakotte, F. R. de Boer, and E. Bruck, 1992, J. Phys. Condens. Matter **4**, 829.
Palacio-Morales, A., A. Pourret, G. Knebel, T. Combier, D. Aoki, H. Harima, and J. Flouquet, 2013, Phys. Rev. Lett. **110**, 116404.
Park, K., L. S. Wu, Y. Janssen, M. S. Kim, C. Marques, and M. C. Aronson, 2011, Phys. Rev. B **84**, 094425.
Park, T., F. Ronning, H. Q. Yuan, M. B. Salamon, R. Movshovich, J. L. Sarrao, and J. D. Thompson, 2006, Nature (London) **440**, 65.
Pedder, C. J., F. Krüger, and A. G. Green, 2013, Phys. Rev. B **88**, 165109.
Perkins, N. B., J. R. Iglesias, M. D. Núñez-Regeiro, and B. Coqblin, 2007, Europhys. Lett. **79**, 57006.
Perry, R., and Y. Maeno, 2004, J. Cryst. Growth **271**, 134.
Perry, R. S., K. Kitagawa, S. A. Grigera, R. A. Borzi, A. P. Mackenzie, K. Ishida, and Y. Maeno, 2004, Phys. Rev. Lett. **92**, 166602.
Petrova, A. E., V. N. Krasnorussky, T. A. Lograsso, and S. M. Stishov, 2009, Phys. Rev. B **79**, 100401(R).
Petrova, A. E., and S. M. Stishov, 2012, Phys. Rev. B **86**, 174407.
Pfleiderer, C., 2007, J. Low Temp. Phys. **147**, 231.
Pfleiderer, C., 2009, Rev. Mod. Phys. **81**, 1551.
Pfleiderer, C., P. Böni, T. Keller, U. K. Rößler, and A. Rosch, 2007, Science **316**, 1871.
Pfleiderer, C., and A. D. Huxley, 2002, Phys. Rev. Lett. **89**, 147005.
Pfleiderer, C., S. R. Julian, and G. G. Lonzarich, 2001, Nature (London) **414**, 427.
Pfleiderer, C., G. J. McMullan, S. R. Julian, and G. G. Lonzarich, 1997, Phys. Rev. B **55**, 8330.
Pfleiderer, C., G. McMullan, and G. Lonzarich, 1994, Physica B (Amsterdam) **199–200**, 634.
Pfleiderer, C., M. Uhlarz, S. M. Hayden, R. Vollmer, H. von Löhneysen, N. R. Bernhoeft, and G. G. Lonzarich, 2001, Nature (London) **412**, 58.
Pfleiderer, C., *et al.*, 2010, J. Low Temp. Phys. **161**, 167.
Piazza, V., V. Pellegrini, F. Betram, W. Wegscheider, T. Jungwirth, and A. H. MacDonald, 1999, Nature (London) **402**, 638.
Pich, C., A. P. Young, H. Rieger, and N. Kawashima, 1998, Phys. Rev. Lett. **81**, 5916.
Pickart, S. J., H. A. Alperin, G. Shirane, and R. Nathans, 1964, Phys. Rev. Lett. **12**, 444.
Pikul, A. P., 2012, J. Phys. Condens. Matter **24**, 276003.
Pikul, A. P., N. Caroca-Canales, M. Deppe, P. Gegenwart, J. G. Sereni, C. Geibel, and F. Steglich, 2006, J. Phys. Condens. Matter **18**, L535.
Pikul, A. P., and D. Kaczorowski, 2012, Phys. Rev. B **85**, 045113.
Pilati, S., G. Bertaina, S. Giorgini, and M. Troyer, 2010, Phys. Rev. Lett. **105**, 030405.
Pilati, S., I. Zitchenko, and M. Troyer, 2014, Phys. Rev. Lett. **112**, 015301.
Pines, D., and P. Nozières, 1989, *The Theory of Quantum Liquids* (Addison-Wesley, Redwood City, CA).
Pruisken, A. M. M., and L. Schäfer, 1982, Nucl. Phys. **B200**, 20.
Qi, X. L., and S.-C. Zhang, 2011, Rev. Mod. Phys. **83**, 1057.
Raghu, S., A. Paramekanti, E. A. Kim, R. A. Borzi, S. A. Grigera, A. P. Mackenzie, and S. A. Kivelson, 2009, Phys. Rev. B **79**, 214402.
Randeria, M., J. P. Sethna, and R. G. Palmer, 1985, Phys. Rev. Lett. **54**, 1321.
Rauch, D., *et al.*, 2015, Phys. Rev. B **91**, 174404.
Raymond, S., P. Haen, R. Calemczuk, S. Kambe, B. Fåk, P. Lejay, T. Fukuhara, and J. Flouquet, 1999, J. Phys. Condens. Matter **11**, 5547.
Raymond, S., D. Raoelison, S. Kambe, L. Regnault, B. Fåk, R. Calemczuk, J. Flouquet, P. Haen, and P. Lejay, 1999, Physica B (Amsterdam) **259–261**, 48.
Rech, J., C. Pépin, and A. V. Chubukov, 2006, Phys. Rev. B **74**, 195126.
Rice, O. K., 1954, J. Chem. Phys. **22**, 1535.
Rieger, H., and A. P. Young, 1996, Phys. Rev. B **54**, 3328.
Rojas, D. P., J. I. Espeso, and J. R. Fernández, 2013, J. Magn. Magn. Mater. **345**, 190.
Rojas, D. P., J. I. Espeso, J. R. Fernández, J. C. G. Sal, C. Rusu, D. Andreica, R. Dudric, and A. Amato, 2011, Phys. Rev. B **84**, 024403.
Rojas, D. P., J. I. Espeso, J. R. Fernández, J. C. G. Sal, J. Sanchez Marcos, and H. Müller, 2009, Phys. Rev. B **80**, 184413.
Rost, A. W., S. A. Grigera, J. A. N. Bruin, R. S. Perry, D. Tian, S. Raghu, S. A. Kivelson, and A. P. Mackenzie, 2011, Proc. Natl. Acad. Sci. U.S.A. **108**, 16549.
Ruggiero, A. F., and G. L. Olcese, 1964, Atti Accad. Naz. Lincei, Cl. Sci. Fis., Mat. Nat. Rend. **37**, 169.
Sachdev, S., 1997, Phys. Rev. B **55**, 142.
Sachdev, S., 1999, *Quantum Phase Transitions* (Cambridge University Press, Cambridge, England).

Sak, J., 1974, Phys. Rev. B **10**, 3957.
Sakarya, S., N. T. Huy, N. H. van Dijk, A. de Visser, M. Wagemaker, A. C. Moleman, T. J. Gortenmulder, J. C. P. Klaasse, M. Uhlarz, and H. v. Löhneysen, 2008, J. Alloys Compd. **457**, 51.
Sandeman, K., G. Lonzarich, and A. Schofield, 2003, Phys. Rev. Lett. **90**, 167005.
Sang, Y., D. Belitz, and T. R. Kirkpatrick, 2014, Phys. Rev. Lett. **113**, 207201.
Sanner, C., E. J. Su, W. Huang, A. Keshet, J. Gillen, and W. Ketterle, 2012, Phys. Rev. Lett. **108**, 240404.
Sarkar, R., P. Khuntia, C. Krellner, C. Geibel, F. Steglich, and M. Baenitz, 2012, Phys. Rev. B **85**, 140409.
Sato, M., 1975, J. Phys. Soc. Jpn. **39**, 98.
Sato, N., H. Mori, T. Satoh, T. Miura, and H. Takei, 1988, J. Phys. Soc. Jpn. **57**, 1384.
Savary, L., E.-G. Moon, and L. Balents, 2014, Phys. Rev. X **4**, 041027.
Saxena, S. S., *et al.*, 2000, Nature (London) **406**, 587.
Schäfer, L., and F. Wegner, 1980, Z. Phys. B **38**, 113.
Schliemann, J., S. M. Girvin, and A. H. MacDonald, 2001, Phys. Rev. Lett. **86**, 1849.
Schmakat, P., *et al.*, 2015, Eur. Phys. J. Spec. Top. **224**, 1041.
Schneider, M., V. Moshnyaga, and P. Gegenwart, 2010, Phys. Status Solidi (b) **247**, 577.
Schneider, M., *et al.*, 2014, Phys. Rev. Lett. **112**, 206403.
Schoop, L., M. Hirschberger, J. Tao, C. Felser, N. P. Ong, and R. J. Cava, 2014, Phys. Rev. B **89**, 224417.
Schroeder, A., S. Ubaid-Kassis, and T. Vojta, 2011, J. Phys. Condens. Matter **23**, 094205.
Schroeder, A., R. Wang, P. J. Baker, F. L. Pratt, S. J. Blundell, T. Lancaster, I. Franke, and J. S. Möller, 2014, J. Phys. Conf. Ser. **551**, 012003.
Sechovsky, V., and L. Havela, 1998, in *Handbook of Magnetic Materials*, Vol. 11, edited by K. H. J. Bushow, Chap. 1 (Elsevier, New York), p. 1.
Sechovsky, V., L. Havela, F. R. de Boer, J. J. M. Franse, P. A. Veenhuizen, J. Sebek, J. Stehno, and A. V. Andreev, 1986, Physica (Amsterdam) **142B+C**, 283.
Senthil, T., and S. Sachdev, 1996, Phys. Rev. Lett. **77**, 5292.
Sereni, J. G., 1991, in *Handbook for Physics and Chemistry of Rare Earths*, Vol. XV, edited by K. A. Gschneider, and L. Eyring, Chap. 98 (North-Holland, Amsterdam).
Sereni, J. G., E. Beaurepaire, and J. P. Kappler, 1993, Phys. Rev. B **48**, 3747.
Sereni, J. G., T. Westerkamp, R. Küchler, N. Caroca-Canales, P. Gegenwart, and C. Geibel, 2007, Phys. Rev. B **75**, 024432.
Shaheen, S. A., and W. A. Mendoza, 1999, Phys. Rev. B **60**, 9501.
Shankar, R., and G. Murthy, 1987, Phys. Rev. B **36**, 536.
Shick, A., V. Janiš, V. Drchal, and W. Pickett, 2004a, Mater. Res. Soc. Symp. Proc. **802**, DD6.10.1.
Shick, A., V. Janiš, V. Drchal, and W. Pickett, 2004b, Phys. Rev. B **70**, 134506.
Shiga, M., and Y. Nakamura, 1987, J. Phys. Soc. Jpn. **56**, 4040.
Shimizu, M., 1964, Proc. Phys. Soc. London **84**, 397.
Shimizu, Y., D. Braithwaite, B. Salce, T. Combier, D. Aoki, E. N. Hering, S. M. Ramos, and J. Flouquet, 2015a, J. Phys. Conf. Ser. **592**, 012088.
Shimizu, Y., D. Braithwaite, B. Salce, T. Combier, D. Aoki, E. N. Hering, S. M. Ramos, and J. Flouquet, 2015b, Phys. Rev. B **91**, 125115.
Shimizu, Y., Y. Matsumoto, K. Aoki, N. Kimura, and H. Aoki, 2012, J. Phys. Soc. Jpn. **81**, 044707.
Shimizu, Y., B. Salce, T. Combier, D. Aoki, and J. Flouquet, 2015, J. Phys. Soc. Jpn. **84**, 023704.
Si, Q., and F. Steglich, 2010, Science **329**, 1161.
Sidorov, V. A., E. D. Bauer, N. A. Frederick, J. R. Jeffries, S. Nakatsuji, N. O. Moreno, J. D. Thompson, M. B. Maple, and Z. Fisk, 2003, Phys. Rev. B **67**, 224419.
Sidorov, V. A., V. N. Krasnorussky, A. E. Petrova, A. N. Utyuzh, W. M. Yuhasz, T. A. Lograsso, J. D. Thompson, and S. M. Stishov, 2011, Phys. Rev. B **83**, 060412.
Sidorov, V. A., P. H. Tobash, C. Wang, B. L. Scott, T. Park, E. D. Bauer, F. Ronning, J. D. Thompson, and Z. Fisk, 2011, J. Phys. Conf. Ser. **273**, 012014.
Slooten, E., T. Naka, A. Gasparini, Y. K. Huang, and A. de Visser, 2009, Phys. Rev. Lett. **103**, 097003.
Smith, R. P., M. Sutherland, G. G. Lonzarich, S. S. Saxena, N. Kimura, S. Takashima, M. Nohara, and H. Takagi, 2008, Nature (London) **455**, 1220.
Smith, T. F., J. A. Mydosh, and E. P. Wohlfarth, 1971, Phys. Rev. Lett. **27**, 1732.
Sokolov, D. A., 2015 (private communication).
Sokolov, D. A., M. C. Aronson, W. Gannon, and Z. Fisk, 2006, Phys. Rev. Lett. **96**, 116404.
Spehling, J., M. Günther, C. Krellner, N. Yèche, H. Luetkens, C. Baines, C. Geibel, and H.-H. Klauss, 2012, Phys. Rev. B **85**, 140406.
Stanley, E., 1971, *Introduction to Phase Transitions and Critical Phenomena* (Oxford University Press, Oxford).
Steiner, M. J., F. Beckers, P. G. Niklowitz, and G. G. Lonzarich, 2003, Physica B (Amsterdam) **329–333**, 1079.
Steppke, A., *et al.*, 2013, Science **339**, 933.
Stewart, G., 2001, Rev. Mod. Phys. **73**, 797.
Stinchcombe, R. B., 1973, J. Phys. C **6**, 2459.
Stingl, C., R. S. Perry, Y. Maeno, and P. Gegenwart, 2011, Phys. Rev. Lett. **107**, 026404.
Stishov, S. M., 2009, Phys. Rev. B **80**, 136401.
Stishov, S. M., A. E. Petrova, S. Khasanov, G. K. Panova, A. A. Shikov, J. C. Lashley, D. Wu, and T. A. Lagrasso, 2007, Phys. Rev. B **76**, 052405.
Stishov, S. M., A. E. Petrova, S. Khasanov, G. K. Panova, A. A. Shikov, J. C. Lashley, D. Wu, and T. A. Lagrasso, 2008, J. Phys. Condens. Matter **20**, 235222.
Stock, C., C. Broholm, F. Demmel, J. Van Duijn, J. W. Taylor, H. J. Kang, R. Hu, and C. Petrovic, 2012, Phys. Rev. Lett. **109**, 127201.
Stockert, O., M. Koza, J. Ferstl, A. Murani, C. Geibel, and F. Steglich, 2006, Physica B (Amsterdam) **378–380**, 157.
Stoner, E. C., 1938, Proc. R. Soc. A **165**, 372.
Strydom, A., P. Khuntia, M. Baenitz, P. Peratheepan, and F. Stegich, 2013, Phys. Status Solidi (b) **250**, 630.
Strydom, A., B. Mhlungu, and A. Thamizhavel, 2008, J. Magn. Magn. Mater. **320**, e453.
Strydom, A. M., and P. Peratheepan, 2010, Phys. Status Solidi RRL **4**, 356.
Subedi, A., and D. J. Singh, 2010, Phys. Rev. B **81**, 024422.
Süllow, S., M. C. Aronson, B. D. Rainford, and P. Haen, 1999, Phys. Rev. Lett. **82**, 2963.
Sung, H. H., H. H. Wu, K. J. Syu, and Y. Y. Chen, 2009, J. Phys. Condens. Matter **21**, 176004.
Sutherland, M., *et al.*, 2012, Phys. Rev. B **85**, 035118.
Suzuki, M., 1976a, Prog. Theor. Phys. **56**, 1454.
Suzuki, M., 1976b, Commun. Math. Phys. **51**, 183.
Svanidze, E., *et al.*, 2015, Phys. Rev. X **5**, 011026.
Svoboda, C., D. Nozadze, F. Hrahsheh, and T. Vojta, 2012, Europhys. Lett. **97**, 20007.

Takashima, S., M. Nohara, H. Ueda, N. Takeshita, C. Terakura, F. Sakai, and H. Takagi, 2007, J. Phys. Soc. Jpn. **76**, 043704.
Takeuchi, T., *et al.*, 2003, Phys. Rev. B **67**, 064403.
Taniguchi, T., H. Morimoto, Y. Miyako, and S. Ramakrishnan, 1998, J. Magn. Magn. Mater. **177–181**, 55.
Tari, A., and B. R. Coles, 1971, J. Phys. F **1**, L69.
Tateiwa, N., T. D. Matsuda, Y. Haga, and Z. Fisk, 2014, Phys. Rev. B **89**, 035127.
Taufour, V., D. Aoki, G. Knebel, and J. Flouquet, 2010, Phys. Rev. Lett. **105**, 217201.
Thill, M. J., and D. A. Huse, 1995, Physica (Amsterdam) **214A**, 321.
Thomson, S. J., F. Krüger, and A. G. Green, 2013, Phys. Rev. B **87**, 224203.
Tompsett, D. A., R. J. Needs, F. M. Grosche, and G. G. Lonzarich, 2010, Phys. Rev. B **82**, 155137.
Torikachvili, M. S., L. Rebelsky, K. Motoya, S. M. Shapiro, Y. Dalichaouch, and M. B. Maple, 1992, Phys. Rev. B **45**, 2262.
Troć, R., and V. H. Tran, 1988, J. Magn. Magn. Mater. **73**, 389.
Trotter, H. F., 1959, Proc. Am. Math. Soc. **10**, 545.
Trovarelli, O., C. Geibel, S. Mederle, C. Langhammer, F. M. Grosche, P. Gegenwart, M. Lang, G. Sparn, and F. Steglich, 2000, Phys. Rev. Lett. **85**, 626.
Trzebiatowski, W., and R. Troć, 1963, Bull. Acad. Polon. Sci. Ser. Sci. Chim. **11**, 661.
Tsui, D. C., H. Stormer, and A. C. Gossard, 1982, Phys. Rev. Lett. **48**, 1559.
Ubaid-Kassis, S., and A. Schroeder, 2008, Physica (Amsterdam) **403B**, 1325.
Ubaid-Kassis, S., T. Vojta, and A. Schroeder, 2010, Phys. Rev. Lett. **104**, 066402.
Uemura, Y. J., *et al.*, 2007, Nat. Phys. **3**, 29.
Uhlarz, M., C. Pfleiderer, and S. M. Hayden, 2004, Phys. Rev. Lett. **93**, 256404.
Vališka, M., J. c. v. Pospíšil, M. Diviš, J. Prokleška, V. Sechovský, and M. M. Abd-Elmeguid, 2015, Phys. Rev. B **92**, 045114.
Varma, C. M., 2010, "What is the Model for Ferromagnetism in Itinerant Fermions?," Journal Club for Condensed Matter Physics Commentary, October 31, 2010, http://www.condmatjournalclub.org/?p=1146, retrieved 8 December 2014.
Veenhuizen, P. A., F. R. de Boer, A. A. Menovsky, V. Sechovsky, and L. Havela, 1988, J. Phys. (Paris), Colloq. **49**, C8-485.
Vojta, T., 2003, Phys. Rev. Lett. **90**, 107202.
Vojta, T., 2009, Phys. Rev. B **80**, 041101.
Vojta, T., 2010, J. Low Temp. Phys. **161**, 299.
Vojta, T., and J. A. Hoyos, 2014, Phys. Rev. Lett. **112**, 075702.
Vojta, T., J. Igo, and J. A. Hoyos, 2014, Phys. Rev. Lett. **112**, 075702.
Vojta, T., and J. Schmalian, 2005, Phys. Rev. B **72**, 045438.
von Klitzing, K., G. Dorda, and M. Pepper, 1980, Phys. Rev. Lett. **45**, 494.
von Löhneysen, H., A. Rosch, M. Vojta, and P. Wölfle, 2007, Rev. Mod. Phys. **79**, 1015.
Wan, X., A. M. Turner, A. Vishwanath, and S. Y. Savrasov, 2011, Phys. Rev. B **83**, 205101.
Wang, L., T. Y. Chen, and C. Leighton, 2004, Phys. Rev. B **69**, 094412.
Wegner, F., 1979, Z. Phys. B **35**, 207.
Wegner, F. J., 1974, J. Phys. C **7**, 2109.
Wegner, F. J., and E. K. Riedel, 1973, Phys. Rev. B **7**, 248.
Weiss, P., 1907, J. Phys. Theor. Appl. **6**, 661.
Westerkamp, T., M. Deppe, R. Kuchler, M. Brando, C. Geibel, P. Gegenwart, A. P. Pikul, and F. Steglich, 2009, Phys. Rev. Lett. **102**, 206404.
Widom, B., 1964, J. Chem. Phys. **41**, 1633.
Wilhelm, H., and D. Jaccard, 1998, Solid State Commun. **106**, 239.
Wilson, K. G., and J. Kogut, 1974, Phys. Rep. **12**, 75.
Winkelmann, H., M. M. Abd-Elmeguid, H. Micklitz, J. P. Sanchez, P. Vulliet, K. Alami-Yadri, and D. Jaccard, 1999, Phys. Rev. B **60**, 3324.
Wiśniewski, P., A. Gukasov, and Z. Henkie, 1999, Phys. Rev. B **60**, 6242.
Wissinger, M., D. Fuchs, L. Dieterle, H. Leiste, R. Schneider, D. Gerthsen, and H. V. Löhneysen, 2011, Phys. Rev. B **83**, 144430.
Wohlfarth, E. P., 1980, J. Phys. Lett. **41**, 563.
Woo, B., *et al.*, 2013, Phys. Rev. B **87**, 125121.
Wu, W., M. S. Kim, K. Park, A. M. Tsvelik, and M. C. Aronson, 2014, Proc. Natl. Acad. Sci. U.S.A. **111**, 14088.
Wu, W., A. McCollam, S. A. Grigera, R. S. Perry, A. P. Mackenzie, and S. R. Julian, 2011, Phys. Rev. B **83**, 045106.
Wulff, M., J. Fournier, A. Delapalme, B. Gillon, A. Sechovsky, L. Havela, and A. Andreev, 1990, Physica (Amsterdam) **163B**, 331.
Wysokiński, M. M., M. Abram, and J. Spałek, 2014, Phys. Rev. B **90**, 081114.
Wysokiński, M. M., M. Abram, and J. Spałek, 2015, Phys. Rev. B **91**, 081108.
Xu, G., H. Weng, Z. Wang, X. Dai, and Z. Fang, 2011, Phys. Rev. Lett. **107**, 186806.
Yamada, H., 1993, Phys. Rev. B **47**, 11211.
Yamada, Y., and A. Sakata, 1988, J. Phys. Soc. Jpn. **57**, 46.
Yamamoto, S. J., and Q. Si, 2010, Proc. Natl. Acad. Sci. U.S.A. **107**, 15704.
Yang, J., B. Chen, H. Ohta, C. Michioka, K. Yoshimura, H. Wang, and M. Fang, 2011, Phys. Rev. B **83**, 134433.
Yaouanc, A., P. Dalmas de Réottier, P. C. M. Gubbens, C. T. Kaiser, A. A. Menovsky, M. Mihalik, and S. P. Cottrell, 2002, Phys. Rev. Lett. **89**, 147001.
Yashima, H., H. Mori, T. Satoh, and K. Kohn, 1982, Solid State Commun. **43**, 193.
Yashima, H., and T. Satoh, 1982, Solid State Commun. **41**, 723.
Yelland, E. A., J. M. Barraclough, W. Wang, K. V. Kamenev, and A. D. Huxley, 2011, Nat. Phys. **7**, 890.
Yelland, E. A., *et al.*, 2005, Phys. Rev. B **72**, 214523.
Yildiz, A., S. B. Lisesivdin, M. Kasap, and M. Bosi, 2009, Solid State Commun. **149**, 337.
Yomo, S., 1979, J. Phys. Soc. Jpn. **47**, 1486.
Yoshimura, K., T. Imai, T. Kiyama, K. R. Thurber, A. W. Hunt, and K. Kosuge, 1999, Phys. Rev. Lett. **83**, 4397.
Young, A. P., 1997, Phys. Rev. B **56**, 11691.
Yuan, H. Q., M. Nicklas, Z. Hossain, C. Geibel, and F. Steglich, 2006, Phys. Rev. B **74**, 212403.
Zhang, H., C.-X. Liu, X.-L. Qi, X. Dai, Z. Fang, and S.-C. Zhang, 2009, Nat. Phys. **5**, 438.
Zhao, G. L., J. Callaway, and M. Hayashibara, 1993, Phys. Rev. B **48**, 15781.
Zhao, J., *et al.*, 2008, Nat. Mater. **7**, 953.
Zhu, L., M. Garst, A. Rosch, and Q. Si, 2003, Phys. Rev. Lett. **91**, 066404.
Zimmer, B. I., W. Jeitschko, J. H. Albering, R. Glaum, and M. Reehuis, 1995, J. Alloys Compd. **229**, 238.
Zinn-Justin, J., 1996, *Quantum Field Theory and Critical Phenomena* (Oxford University Press, Oxford).
Zou, Y., P. Logg, M. Barber, Z. Feng, T. Ebihara, and F. M. Grosche, 2013, Phys. Status Solidi (b) **250**, 529.
Zou, Y., G. Refael, A. Stern, and J. P. Eisenstein, 2010, Phys. Rev. B **81**, 205313.
Zumbusch, M., 1941, Z. Anorg. Allg. Chem. **245**, 402.